Polyploid Cell Cycles Mediate Organ Growth and Regeneration in the *Drosophila* Ejaculatory Duct

by

Navyashree Amruthahalli Ramesh

A dissertation submitted in partial fulfillment
of the requirements for the degree of
Doctor of Philosophy
(Molecular, Cellular, and Developmental Biology)
in the University of Michigan
2025

Doctoral Committee:

Professor Laura Buttitta, Chair
Professor Cunming Duan
Associate Professor Longhua Guo
Professor Tzumin Lee

Navyashree Amruthahalli Ramesh
navyaar@umich.edu

ORCID iD: 0000-0002-6453-7347

© Navyashree A. Ramesh 2025

Dedication

I dedicate this thesis to all my teachers and mentors, whose guidance, encouragement, and wisdom have shaped my journey as a Researcher.

Acknowledgements

I am incredibly thankful to the many people who have helped me gain admission to the PhD program and supported me throughout this incredible journey. My sincere thanks go to all my mentors and teachers for inspiring me to pursue my passion for science and research. I am also grateful to the MCDB Department at the University of Michigan for accepting me as a PhD student.

The most important person on this journey is my PhD mentor, Prof. Dr. Laura Buttitta. Simply saying "thank you" would not be enough to express my gratitude for all you have done. You have guided me through every aspect of my PhD journey, offering invaluable advice, unwavering support, and constant encouragement. You have inspired me to become a passionate and independent researcher and to think critically. Your insight, expertise, and patience have shaped not only this thesis but also my approach to science and problem-solving. You are, and will always be, the best mentor in my life, and I feel truly fortunate to have been your student.

I am sincerely thankful to my thesis committee members Cunming Duan, Tzumin Lee, and Longhua Guo for their constructive feedback, thoughtful discussions, and for challenging me to think more deeply and critically about my work.

I extend my heartfelt thanks to all members of the Buttitta lab for their friendship, technical assistance, and for creating a collaborative and supportive research environment. Every current and past member of the lab has helped me in some way during this journey. I am especially grateful to Liz, Deena, Elli, Allison, Jaimian, Shyama, Lizi, Hailee, and Arpitha for their help with experiments and countless scientific discussions.

A very special thanks to the youngest scientist in the lab, Elise, who has always made me smile during weekends in the lab. I have learned so much from you and feel very fortunate to have known you. I will miss you greatly.

Many other faculty members in MCDB have enriched my graduate education. I thank Mathew Chapman for his support as graduate chair. I am grateful to Gyorgyi Csankovszki and the members of the Csankovszki lab for being wonderful lab neighbors. Special thanks go to Ken

Cadigan, with whom I first interacted in this department, and who made my first rotation smooth and welcoming. Ken has also played many roles during my time here as teacher, chair, and colleague at the fly bench.

I also thank Rich for being my best friend and helping me survive during this journey.

Outside the Department, I thank GRIN (Graduate Rackham International Student Organization) for helping me build my leadership skills. I also thank all my GRIN friends for keeping me sane.

I am deeply grateful to my mom and dad for their endless love, encouragement, and sacrifices throughout my life. Your belief in me has been my greatest source of strength, and without your unwavering support, I would not have been able to reach this milestone. You have always stood by me through every challenge, celebrated every success, and reminded me to keep going when times were tough.

I thank all the male fruit flies who have sacrificed their life for my research.

Finally, I cannot thank my husband, Vishwas enough for his constant love, patience, and support during my PhD journey. You have been my rock, encouraging me on difficult days, celebrating my accomplishments, and making countless personal sacrifices so that I could pursue my dreams. You're understanding and unwavering belief in me have been invaluable, and I am so fortunate to have shared this journey with you by my side.

Table of Contents

Dedication ii

Acknowledgements iii

List of Figures xi

List of Tables xiv

Abstract xv

Chapter 1 Introduction and Literature Review 1

1.1 Using *Drosophila melanogaster* as a model system 1

1.2 Different Inducible systems (RU feeding, Gal80ts) 2

1.3 Lineage tracing tool -GTRACE 4

1.4 The *Drosophila* male reproductive system 5

1.5 The Drosophila Ejaculatory Duct (ED) 7

1.6 The secretory epithelium of the ED also serves as an epithelial barrier 8

1.7 Apical-Basal polarity of ED 9

1.8 High secretory demands on the ED 10

1.9 Genome duplication and the canonical cell cycle 10

1.10 Genome duplication by a variant cell cycle - Endocycling 11

1.11 Advantages of Polyploidy 13

1.12 Regulatory factors involved in Endocycling 15

1.12.1 E2F- Transcriptional activation and repression of cell cycle genes 15

1.12.2 CycE/Cdk2- phosphorylation of G1-S substrates 16

1.12.3 $CRL4^{Cdt2}$- destruction of G1-S phase substrates 17

1.12.4 CKI-Dacapo 17

1.12.5 APC/C Fzr 18

1.12.6 Geminin 19

1.13 Progression of Endocycling 20

1.14 Endoreplication is involved in increased protein synthesis 21

1.15 Signaling pathways involved in the endocycle 21

1.15.1 Juvenile Hormone (JH) Signaling 22

1.15.2 The growth regulatory Pathways 23

1.15.3 The JNK Pathway 24

1.15.4 Myc 25

1.16 Regeneration 26

1.17 Different stem-cell-mediated regeneration 27

1.18 Regeneration by the re-entry of cell division 29

1.19 Key regulators of mitotic re-entry during regeneration 31

1.20 Regeneration in tissues that have permanently exited mitosis 33

1.21 Developmental timing plays an important role in regeneration 34

1.22 Thesis Overview 35

1.23 Bibliography 46

Chapter 2 Post-Eclosion Growth in the *Drosophila* Ejaculatory Duct is Driven by Juvenile Hormone Signaling and is Essential for Male Fertility 63

2.1 Abstract 63

2.2 Introduction 64

2.3 Results 65

2.3.1 Identification of different cell types and their organization in adult Drosophila Ejaculatory duct 65

2.3.2 Endoreplication of secretory cells of the adult Drosophila Ejaculatory duct leads to post-eclosion organ growth. 66

2.3.3 Post eclosion endoreplication and growth of the adult Ejaculatory duct secretory cells are conserved in different species of Drosophila. 67

2.3.4 Drosophila ED secretory cell ploidy correlates with organ shape and size 67

2.3.5 Compromising the endoreplication of ED secretory cells results in reduced ED size and fertility. 68

2.3.6 Inducing extra endoreplication in the ED leads to organ hypertrophy 70

2.3.7 Stabilized Geminin effectively blocks adult endoreplication in the ED 70

2.3.8 Juvenile hormone (JH) signaling promotes post eclosion endoreplication and growth of the ED 71

2.3.9 Juvenile hormone signaling is sufficient to overcome blocked endoreplication in the adult ED 72

2.3.10 JH signaling and the endocycle are required for proper protein synthesis in the adult ED. 72

2.3.11 Protein synthesis in secretory cells of the ED requires mTOR signaling and is coupled to ED growth via the endocycle 73

2.4 Discussion 74

2.4.1 Post-eclosion endoreplication in the secretory cells of the ED is required for organ growth, protein synthesis and male fertility. 74

2.4.2 JH promotes the early adult endoreplication in secretory cells of male Drosophila ED 75

2.4.3 Using the Drosophila ED as a context to study post-mitotic tissue growth. 76

2.5 Materials and Methods 78

2.5.1 Drosophila husbandry 78

2.5.2 Fly strains used 78

2.5.3 ED dissection, fixation, and Immunostaining 79

2.5.4 5-Ethynyl-2-deoxyUridine (EdU) feeding and labeling 81

2.5.5 Confocal imaging 82

2.5.6 Area measurements 82

2.5.7 Juvenile Hormone ex-vivo assay 82

2.5.8 Ploidy/DAPI intensity measurements 83

2.5.9 Fertility Assay 84

2.5.10 Flow Cytometry 84

2.5.11 Protein synthesis O-propargyl-puromycin (OPP) Assay 85

2.5.12 Software and data analysis 85

2.5.13 Acknowledgments 85

2.6 Bibliography 120

Chapter 3 Isolation of Polyploid Nuclei and Measurement of the Ploidy of the *Drosophila* Male Reproductive System Using Flow Cytometry 127

3.1 Abstract 127

3.2 Introduction 127

3.3 Results and discussions 131

3.3.1 Polyploid nuclei Isolation from AG and ED of Drosophila male and ploidy Quantification via Flow Cytometry 131

3.3.2 Flow cytometric ploidy measurements from the frozen and fresh Accessory glands 132

3.3.3 Ploidy measurements of AG and ED under Varying Cell Cycle Conditions and across Drosophila species 133

3.3.4 Isolation of Diploid Nuclei from the Drosophila Male Ejaculatory Duct (ED) and Ploidy Quantification by Flow Cytometry 135

3.4 Materials and Methods 136

3.4.1 Drosophila husbandry 136

3.4.2 Fly strains 136

3.4.3 Dissection and Nuclei isolation from fresh tissues 136

3.4.4 Freezing of the AGs and isolation of the nuclei 138

3.4.5 Thawing Samples 139

3.4.6 Diploid nuclei isolation from the basement membrane 139

3.5 Bibliography 154

Chapter 4 A Window of Cell Cycle Plasticity Enables Imperfect Regeneration of an Adult Postmitotic Organ in *Drosophila* 156

4.1 Abstract 156

4.2 Introduction 156

4.3 Results & Discussion 158

4.3.1 Apoptotic cell loss in the ED occurs through apical extrusion and leads to irreversible cell loss. 158

4.3.2 Recovery from transient damage in the anterior region of the Ejaculatory Duct 160

4.3.3 The ED undergoes compensatory cellular hypertrophy (CCH) in response to cell loss. 162

4.3.4 Cell cycle plasticity is required for ED regeneration. 165

4.4 Materials and methods 166

4.4.1 Drosophila husbandry 166

4.4.2 ED dissection, fixation, and Immunostaining 167

4.4.3 5-Ethynyl-2-deoxyuridine (EdU) feeding and labeling 168

4.4.4 Confocal imaging 168

4.4.5 Area measurements 169

4.4.6 Ploidy/DAPI intensity measurements 169

4.4.7 Fertility Assay 170

4.4.8 Flow cytometry 170

4.4.9 Software and data analysis 171

4.5 Acknowledgements 171

4.6 Bibliography 192

Chapter 5 Conclusions and Future Directions 194

5.1 Conclusions 194

5.2 Future experiments 196

5.2.1 What are the regulatory factors limiting endocycle progression? 196

5.2.2 Can we make cell cycle exit reversible in ED cells? 197

5.2.3 Identifying regional-specific genes in the ED 198

5.2.4 Identifying the downstream targets of Juvenile Hormone signaling 199

5.2.5 Does blocking endoreplication prevent recovery of the ED from cell loss? 201

5.2.6 Can ectopic or prolonged JH signaling activity improve or extend the recovery of the ED from cell loss? 202

5.2.7 What signaling pathways transmit information about organ damage or cell loss to trigger endocycling of the remaining ED cells? 203

5.2.8 Does polyploid mitosis in the ED aid or hinder recovery from cell loss? 205

5.2.9 How does damage and recovery impact nascent protein synthesis in the ED? 205

5.3 Bibliography 208

List of Figures

Figure 1.1: *Drosophila melanogaster* life cycle with the stages of development. 37

Figure 1.2: The GAL4/UAS system for regulating transgene in *Drosophila*. 38

Figure 1.3: (A) Schematic illustrating the temperature-sensitive Gal80^{ts} system. 39

Figure 1.4: The G-TRACE analysis system. 40

Figure 1.5: The adult *Drosophila melanogaster* male reproductive system. 41

Figure 1.6: Confocal micrographs of ED with different fluorescent labeling to differentiate basal and Apical layer. 42

Figure 1.7: Different Cell cycles 43

Figure 1.8: Oscillation of cell cycle regulators during endoreplication 44

Figure 1.9:The titer of Juvenile hormone in both males and females across during development. 45

Figure 2.1: Endoreplication of secretory cells of the adult *Drosophila* Ejaculatory Duct and post-eclosion organ growth. 87

Figure 2.2: Post-eclosion endoreplication and growth of the ED is conserved in different *Drosophila* species. 89

Figure 2.3: The ploidies of *Drosophila* Ejaculatory duct secretory cells correlate with local organ shape and size 91

Figure 2.4: Compromising the endoreplication of ED secretory cells results in reduced ED size and fertility 93

Figure 2.5: Inducing extra endoreplication in secretory cells of ED leads to organ hypertrophy 95

Figure 2.6: Stabilized Geminin effectively blocks the adult endoreplication in the ejaculatory duct 97

Figure 2.7: Juvenile hormone (JH) signaling promotes post-eclosion endoreplication and growth of *Drosophila* ejaculatory duct 99

Figure 2.8: Juvenile hormone signaling is sufficient to induce endoreplication in the adult *Drosophila* ejaculatory duct. 101

Figure 2.9: JH signaling and the endocycle are required for proper protein synthesis in the ED 103

Figure 2.10: Protein Synthesis in the secretory cells of the ED requires mTOR signaling and is coupled via the endocycle 105

Figure 2.11: A model for ED organ growth and protein synthesis driven by endoreplication induced by JH signaling. 107

Figure 2.12: Identification of different cell types in adult *Drosophila* Ejaculatory duct 108

Figure 2.13:EdU and PH3 labeling at different time points in ED and in different tissues of *Drosophila* 110

Figure 2.14:EdU and ploidy quantifications in different species of *Drosophila* 112

Figure 2.15: Luna Gal4 expression and ploidy measurements in different cell cycle conditions in ED 114

Figure 2.16:Supplementary data for the viability of the embryos under different cell cycle conditions 116

Figure 2.17: Measurement of nuclear area 118

Figure 3.1**:** Schematic overview of the nuclei isolation and ploidy measurement workflow for the *Drosophila* male accessory gland (AG) and ejaculatory duct (ED). 141

Figure 3.2: Flow cytometry plots of *Drosophila Canton S* Accessory Gland, Ejaculatory Duct and Ovary nuclei 143

Figure 3.3: Flow cytometry plots of the *Drosophila Canton S* fresh and frozen male Accessory gland polyploid nuclei 145

Figure 3.4: Flow cytometry ploidy peaks of different species of *Drosophila* male AG and ED secretory cell nuclei 147

Figure 3.5: Ploidy peaks of AG and ED nuclei under different cell cycle conditions 149

Figure 3.6: Isolation and flow cytometry plots of diploid cell nuclei of ED basement membrane 151

Figure 3.7: Images of isolated individual nuclei 153

Figure 4.1: Reaper expression induces apoptosis in Drosophila ejaculatory duct (ED) secretory cells. 173

Figure 4.2: Transient Reaper expression using temperature-sensitive Gal80 system enables ablation and recovery of ejaculatory duct (ED) secretory cells in anterior region 175

Figure 4.3: Endoreplication in the ED during recovery restores ploidy, tissue mass and supports functional regeneration 177

Figure 4.4: Inducing damage during the early endoreplication window is essential for optimal recovery of ED secretory cells 180

Figure 4.5: Constitutive expression of Reaper in ED 182

Figure 4.6: Temporal expression of Reaper in ED 184

Figure 4.7: Temporal expression of reaper in ED in the presence of UAS-P35 186

Figure 4.8: Different staining during ED damage and GTRACE expression 188

Figure 4.9: MMP1 is upregulated during ED damage and recovery 190

Figure 5.1: ED labelled with DAPI and PH3 under different cell cycle regulators overexpression to induce mitosis. 207

List of Tables

Table 2.1: List of antibodies and their dilutions used. 80

Table 3.1: Homogenization buffer. 136

Table 4.1: Antibody and the dilutions used. 167

Abstract

Post-mitotic cells have permanently exited the mitotic cell cycle and no longer divide. However, some of these cells can enter a variant cell cycle known as endocycling or endoreplication. Endocycling is a modified cell cycle in which cells undergo DNA synthesis (S phase) without entering mitosis (M phase). These cells alternate between G and S phases, duplicating their genome without chromosome segregation or cell division. As a result, no new cells are formed. Instead, nuclear DNA content increases, leading to polyploidy, where the DNA content exceeds the diploid level (2C), with "C" representing the amount of DNA in a haploid genome. Depending on the number of endocycles, cells can reach ploidy levels of 4C, 8C, 16C, 32C, or higher. Increased ploidy is well-known to correlate with increased cell size, thus the endocycle serves as a mechanism to support postmitotic cellular and tissue growth. Some specialized secretory cells are polyploid, a feature that may enhance capacity for biosynthesis and secretion. The Drosophila ejaculatory duct (ED) is a secretory organ within the somatic male reproductive system. It contributes to fertility and the female post-mating response by producing seminal fluid protein components and ED-specific antimicrobial peptides. Additionally, the ED acts as a conduit for transferring sperm and seminal fluid during copulation. Structurally, it consists of secretory epithelial cells encased in a layer of innervated contractile muscle. Despite its essential role in male reproduction, little was previously known about the cell cycle behavior of ED secretory cells in adult flies.

In Chapter 2 of my thesis, I demonstrate that the secretory cells of the adult Drosophila ED are post-mitotic and enter endocycling during organ maturation. This process drives growth of the ED during the first 24-48 hours after eclosion in young adult males. These secretory cells exit the endocycle by the third day of adulthood, reach ploidy levels ranging from 8C to 32C. When endoreplication is disrupted in this organ, ED growth is halted, protein production is reduced, and male fertility is compromised. I show that Juvenile Hormone (JH) signaling regulates ED growth and endocycling in young adult males and is essential for the reproductive function of

this tissue. This work demonstrates that hormone-mediated endocycling is critical for postmitotic organ growth and function.

Adult tissues and organs can often contain mixtures of cells of various ploidy, a biological feature often overlooked through the prevalence of in vitro cell culture studies, where most animal cells remain diploid. In Chapter 3, we describe an optimized method for isolating nuclei from the secretory cells of the Drosophila male reproductive system to perform quantitative ploidy distribution analysis by flow cytometry. This technique addresses a key methodological gap, offering a reliable tool for sensitive and precise ploidy analysis in the Drosophila male reproductive system. This tool enables future investigations in endocycle regulation and will be compatible with future single-nucleus transcriptomics to integrate changes in ploidy with changes in gene expression.

Polyploid, post-mitotic tissues face specific challenges when responding to cell loss, primarily due to their inability to undergo mitotic division. In Chapter 4, I show that the immature adult ED can recover from substantial cell loss through compensatory endocycles that partially restore tissue mass and organ function. Upon cell loss, the normal time-window for endocycling in the young adult ED is temporarily extended, allowing post-mitotic polyploid cells to undergo additional endocycles that compensate for lost cells. However, as the organ matures and the animal ages, this cell cycle plasticity is lost, and cells lose the ability to undergo additional endocycles and recover from cell loss. Thus, regulatory mechanisms governing endocycle exit and quiescence constrain the ED's regenerative potential. This work shows that cell cycle plasticity during tissue maturation is vital for tissue repair even in a postmitotic context. Further work will be needed to resolve the intersections of hormonal signaling, post-mitotic regeneration, and cell cycle plasticity in this organ.

Chapter 1 Introduction and Literature Review

Mitotic cell division is a fundamental process used by all multicellular organisms for growth and development. In mature tissues, most cells stop dividing, except for stem and progenitor cells. Some of these cells undergo terminal differentiation, permanently exit the mitotic cycle, and no longer divide - these are referred to as post-mitotic cells. To maintain tissue function, post-mitotic cells must preserve their specialized roles throughout the organism's lifespan. Tissues can be exposed to physiological stress or injury, leading to cell loss. In response, the tissue initiates regeneration to replace lost cells and restore function. When post-mitotic cells are damaged, they must recover to support tissue integrity, and during this recovery, they may undergo variant cell cycles.

This thesis uses the *Drosophila* ejaculatory duct (ED) as a model system. The ED is composed of cells that have exited mitosis following terminal differentiation but retain a high demand for protein secretion. This system provides an opportunity to study the variant cell cycle these cells undergo, specifically endocycling, which allows them to increase biosynthetic capacity without mitosis. Additionally, this work investigates how these post-mitotic cells respond to damage and whether they can re-enter growth programs or recover tissue structure and function. In this chapter, I will introduce the key concepts required to understand the canonical cell cycle, its variants, and relevant existing literature. As my research is centered on the *Drosophila* male ejaculatory duct, this chapter will primarily focus on findings from *Drosophila* tissues.

1.1 Using *Drosophila melanogaster* as a model system

Drosophila melanogaster has been a valuable genetic model organism for over a century, and its genome is completely sequenced, which makes it easier for genetic manipulation and examination of conserved cellular processes like the cell cycle (Adams et al., 2000; Follette and O farrell, 1997; Harold Plough and Maurice Strauss, 1923; Charles e. bessey, 1910, Morgan T.H et al., 1910). Compared to mammals, flies have minimal gene redundancy, simplifying functional studies. Mammals have undergone two genome-wide duplications as well as gene-specific duplications,

leading to multiple paralogs for many key cell cycle regulators, which have fewer family members in fruit flies (Dehal and Boore, 2005). Their short lifespan and rapid development at ambient temperatures (about 10-12 days from egg to adult at 22-25°C) make them ideal for experiments involving development and aging. Additionally, flies are inexpensive and easy to maintain. The growth cycle of *Drosophila melanogaster* is rapid and well-characterized process that progresses through four main stages: embryo, larva, pupa, and adult (Figure 1.1)(Basumatary and Deka, 2024; Wolf, 2012; Ashburner, 1989; Prokop, 2008; Allocca, Zola and Bellosta, 2018) Embryogenesis is completed within 24 hours after egg laying, followed by three larval instar stages over the next 4–5 days, during which the organism undergoes significant growth through feeding on food. The larval stage culminates in pupariation, initiating metamorphosis during the pupal stage, which lasts about 4–5 days (Prokop, 2008; Wolf, 2012; Allocca, Zola and Bellosta, 2018). Upon eclosion, the adult fly emerges and becomes fertile within 8–12 hours, although full sexual maturation and optimal fertility may take an additional 2-5 days (Prokop, 2008; Long E. C et al, 1980). The day the adult fly emerges from the pupa is termed the Day of Eclosion (DOE). All the experiments in this thesis were performed using male flies at different time points from the DOE. *Drosophila* has great tools for tissue-specific genetic manipulations discussed below.

1.2 Different Inducible systems (RU feeding, Gal80ts)

There are multiple inducible transgenic expression systems in *Drosophila melanogaster*. We can target transgene expression to specific tissues and at a specific developmental stage. The most used system is the "binary" system of GAL4/UAS, which is often modified by adding a temperature-sensitive Gal80^{ts}. The Gal4/UAS system is a yeast-derived bipartite transcriptional activation system transgenically inserted into flies over 3 decades ago (Brand and Perrimon, 1993). In the GAL4/UAS system, GAL4 is a driver line that expresses the yeast GAL4 transcriptional activator in a specific pattern, which is determined by the chosen promoter/enhancer fused to the Gal4 coding sequence. A separate UAS, which is a responder line, that carries the Upstream Activation Sequence (UAS), the DNA motif to which the GAL4 binds, fused upstream to the coding sequence of a gene of interest (McGuire, Roman and Davis, 2004a). When combined in progeny, tissue specific enhancer/promoter-specific GAL4 protein binds UAS enhancers and activates transcription of the target gene in the GAL4-expression pattern (Figure 1.2). This system allows spatial expression of any gene, cDNA or RNAi construct tagged with UAS. The expression levels can be tuned by UAS copy number or by using stronger activation domains fused to GAL4 (Brand

and Perrimon, 1993; McGuire, Roman and Davis, 2004a). In my research, I have used the Gal4/UAS system to express and knockdown (via RNAi) genes in *Drosophila.*

To make this system temporally inducible it has been modified by incorporating a constitutively expressed temperature-sensitive GAL80 ($Gal80^{TS}$). Gal80 is a natural inhibitor of GAL4 from yeast (McGuire, Roman and Davis, 2004a). Gal80 binds to the activation domain of GAL4 and prevents GAL4 from turning on transcription. The discovery of a temperature-sensitive mutant version of GAL80, which functions normally to repress at low temperatures but becomes inactive at higher temperatures, allows for Gal4 induction to be controlled through temperature shifts. At low temperature (around 18–21°C), a constitutive *tubulin* promoter driven $GAL80^{ts}$ is active everywhere and binds to Gal4 to blocks its activity, preventing the expression of UAS (Monje, Toda and Palmer, 2003). At higher temperatures (around 29-30 °C), the $GAL80^{ts}$ protein is degraded, thus allowing Gal4 to freely bind to UAS and lead to the expression of the transgene (Figure 1.3(A)). This system thus provides temporal control by shifting flies from 18°C (GAL4 OFF) to 29°C (GAL4 ON) for the expression of genes. In Chapters 2 and 3 I use the traditional binary Gal4/UAS system to manipulate gene expression. In Chapter 4 I will use the inducible $Gal80^{TS}$ system to temporally control the expression of transgenes.

GeneSwitch inducible system is an alternate modified GAL4 system that renders GAL4 activity dependent on the presence of the drug RU486 (mifepristone) (Osterwalder et al., 1993a). It is essentially a chimeric protein combining the yeast GAL4 DNA-binding domain with a human progesterone receptor (PR) ligand-binding domain and a minimal activation domain. In the absence of the ligand RU486, the GeneSwitch protein is expressed (in whatever cells its driver is active) but remains transcriptionally inert (Roman et al., 2001; Osterwalder et al., 1993b; McGuire, Roman and Davis, 2004a). When RU486 is provided, it binds to the PR domain of GeneSwitch, causing a conformational change that activates the protein's ability to recruit transcriptional machinery, and GeneSwitch, now ligand-bound, can activate UAS promoters. In practical terms, one uses a GeneSwitch driver line, which is like a GAL4 driver but with the GeneSwitch protein under a tissue-specific promoter. The target gene must still be on a UAS-transgene. Flies are kept on normal food (no drug) until induction is required, and then RU486 is added to the food and within a few hours GeneSwitch will bind RU486 and begin driving UAS-transgene expression. Crucially, RU486 is a steroid hormone analog that can easily penetrate tissues, and it can be delivered by feeding, soaking, or even through yeast paste fed to adults (Roman et al., 2001;

Osterwalder et al., 1993b; McGuire, Roman and Davis, 2004a; Nicholson et al., 2008). Thus, GeneSwitch-driven expression is a powerful inductive tool that is dose-dependent: higher RU486 concentrations up to a saturation point yield higher transgene expression. However, the main limitations of the GeneSwitch system are the necessity for induction via feeding, which does not occur equally among all animals, and our discovery that feeding does not begin until ~6-8h post eclosion in males, missing the earliest timepoints of adult organ maturation (Allison M Box et al., 2024) .

The FLP/FRT system is a genetic tool that enables both spatial and temporal control of transgene expression through the use of the recombinase FLP (flippase) and its corresponding recognition sites, FRT (FLP Recognition Targets). This technique, commonly referred to as FLP-out, involves placing a transcriptional stop cassette flanked by FRT sites in front of a transgene. The stop cassette silences the gene until FLP is expressed, excising the cassette and thereby activating gene expression, as illustrated in Figure 1.3 (B) (Harrison and Perrimon, 1993; Theodosiou A. Nicole and Xu Tian,1998; Del Valle Rodríguez, Didiano and Desplan, 2012). This system can be combined with the GAL4-UAS binary expression system to introduce additional layers of regulation. For instance, a FLP-out cassette can be inserted between a UAS promoter and a transgene. FLP expressions can be temporally controlled using a heat-shock promoter (hs-FLP) or spatially restricted by using a tissue-specific promoter like. This represents an intersectional approach where gene expression occurs only in cells that express both GAL4 and FLP (see Fig. 1b). FLP can also be used in conjunction with GAL80 to repress GAL4 (FLP-in) or to remove GAL80-mediated repression (FLP-out). When combined with the Gal4/UAS system, FLP/FRT can be used for powerful lineage tracing approaches to study organ development and growth.

1.3 Lineage tracing tool -GTRACE

Lineage tracing tools in *Drosophila* can be used to track the developmental origin, fate, and proliferation of cells over time. These tools allow us to mark a group of cells at a specific time and/or location and then observe where those cells or their descendants end up, what types they become, and how gene expression changes during development. There are multiple lineage tracing tools available, such as G-TRACE, MARCM, twin-spot MARCM, TIE-DYE, etc. In this section I will cover the G-TRACE lineage tracing tools, as we will be using this tool in Chapter 4.

The G-TRACE system (GAL4 Technique for Real-time and Clonal Expression) is a genetic lineage tracing tool that simultaneously reveals both current and past gene expression within the

same organism and tissue (Figure 1.4). It combines the GAL4/UAS system with FLP/FRT-mediated recombination and fluorescent reporters. The RFP reporter serves as a real-time indicator of current GAL4 activity, highlighting cells that are actively expressing the gene of interest. The GFP reporter, activated through FLP/FRT recombination under GAL4 control, acts as a permanent lineage marker. In cells where a GAL4 driver is active, GAL4 induces the expression of RFP for real-time visualization and also activates the FLP recombinase, which removes an FRT-flanked STOP cassette to permanently activate GFP expression under a ubiquitous promoter. As a result, once GFP is activated, it is stably expressed in those cells and all of their progeny, even if GAL4 expression ceases (Evans et al., 2009). This system allows cells to display three distinct fluorescence patterns: RFP-only cells indicate current GAL4 activity; GFP-only cells indicate past GAL4 activity with no current expression and cells positive for both RFP and GFP are currently expressing GAL4 and also belong to a lineage that previously expressed GAL4. Cells that have never expressed GAL4 remain unlabeled (RFP^-/GFP^-). By examining the red and green fluorescence patterns within a tissue, researchers can determine which cells are actively expressing the gene of interest and which are descendants of earlier expression domains. Thus, G-TRACE provides a clear visual distinction between ongoing and historical gene expression within the same specimen.

1.4 The *Drosophila* male reproductive system

The ability of reproductive organs to coordinate growth, differentiation, and secretory function is essential for successful reproduction and species survival. Across metazoans, secretory tissues within the male reproductive system play vital roles not only in the storage and transfer of sperm but also in producing complex mixtures of seminal fluid proteins (SFPs) and bioactive molecules that profoundly influence competitive reproductive success (Hopkins et al., 2019; Lung, Kuo and Wolfner, 2001a; Cohen and Moussian, 2016a). The fruit fly *Drosophila melanogaster* has emerged as a powerful genetic model for elucidating the developmental and physiological regulation of reproductive tissues. *Drosophila* are polyandrous, meaning females mate with multiple males. It was discovered that polyandrous females achieve greater reproductive success and longevity compared to those limited to a single mate (Gowaty et al., 2010; Croshaw and Gómez, 2018). Females produced more offspring by laying significantly more eggs over an extended period and had a longer reproductive lifespan than once mated or monogamous females (Gowaty et al., 2010; Croshaw and Gómez, 2018). Multiple mating provides direct fitness advantages likely through

continuous sperm replenishment and additional nutritional contributions from different males, showing polyandry as a beneficial female mating strategy in *Drosophila* (Gowaty et al., 2010; Gowaty, 2012; Pizzari and Wedell, 2013; Croshaw and Gómez, 2018).

Sperm competition is a key component of post-copulatory sexual selection in *Drosophila*. Since female flies are polyandrous and have the ability to store sperm from previous matings internally within the spermatheca, a male's reproductive success depends on how effectively his sperm and seminal fluid competes with that of rivals to fertilize eggs in the female reproductive tract (Price CS et al, 1999; Fiumera, Dumont and Clark, 2005). Sperm competition plays a central role in determining male fertilization success, shaping fertilization dynamics, and driving the evolution of traits such as sperm displacement, storage, and seminal fluid composition. As a result, post-mating sexual selection via sperm competition has been a major force shaping *Drosophila* reproductive biology, influencing both behavior and the molecular architecture of the ejaculate (Price CS et al, 1999; Fiumera, Dumont and Clark, 2005; Yeh, Chan and Ranz, 2013; Bretman et al., 2023). It is therefore crucial for male fitness, enabling adaptations that maximize fertilization success in a competitive reproductive environment. This competitive environment also places great importance on the volume and production of seminal fluid proteins that impact success in sperm competition. Many of these seminal fluid proteins are produced outside of the testes, in organs of the somatic male reproductive tract.

The *Drosophila* male reproductive tract consists of a pair of sperm-producing testes, seminal vesicles that function in the secretion of seminal fluid proteins and temporary storage of sperm until ejaculation, a pair of accessory gland (AG) lobes, the ejaculatory duct (ED), and the ejaculatory bulb (Bertram et al., 1992; Cohen and Moussian, 2016b; Allison M. Box et al., 2024) as illustrated in Figure 1.5. The accessory glands contain two types of secretory cells that produce major SFPs, including the well-known Sex Peptide, a peptide secreted by the AG that helps in post mating response in the mated females discussed further below (Hopkins et al., 2019; Date-Ito et al., 2002). Secretions from the testes, seminal vesicles, and accessory glands converge and are transferred into the ejaculatory duct during copulation via a specialized transition zone known as the anterior ED papillae, which physically connects these structures to the ED (Lung, Kuo and Wolfner, 2001a). Within the ED, sperm and glandular secretions are mixed and propelled toward the ejaculatory bulb, from which they are ultimately transferred to the female reproductive tract during mating.

The *Drosophila* female post-mating response caused by transfer of the seminal fluid proteins, ED and AG secretions, is a physiological and behavioral changes that occur in female flies after mating (Chapman et al., 2003). These changes are triggered by the receipt of sperm and, importantly, seminal fluid proteins (SFPs) that are transferred to the female from the male during copulation. Post-mating responses in females include increased egg laying, reduced receptivity to remating, changes in sperm storage, and altered immune and metabolic activity (Chapman et al., 2003; Sitnik et al., 2016; Newell et al., 2020). Some of the behavioral responses include changes in activity level and preferences for egg-laying sites.

1.5 The Drosophila Ejaculatory Duct (ED)

The ED is a polarized epithelial organ. Basally, the epithelium is surrounded by a layer of collagenous extracellular matrix enveloped by innervated muscles. The apically located epithelium contains large secretory cells that forms a large lumen apically into which all the secretions are released (Figure 1.5). ED cells are derived from the portion of the genital disc arising from the A9 primordium and thus are ectodermal in origin (Ahmad M.S, and Baker S.B, 2002; Cohen and Moussian, 2016c). Proteomic mapping of the ED ejaculate has shown that ED secretes at least 138 peptides, and out of these 63 are known to be SFPs (Takemori and Yamamoto, 2009; Sturm et al., 2021). Peptides secreted from the ED are known to be involved in processes such as lipid modification, immune response mediation, catalysis, hormone-like activity, sperm storage, female post-mating response, cell adhesion, odorant-binding, and cellular metabolism (Takemori and Yamamoto, 2009). Some of the peptides secreted by ED are antimicrobial peptides such as Cecropin A1 and the ED-specific Andropin (Anp), and many more help increase fertility by reducing infections upon mating (Samakoviis et al., 1991; Samakovlis et al., 1991; Lung, Kuo and Wolfner, 2001b; Date-Ito et al., 2002). All the ED secretions, AG secretions, seminal fluid, and sperm from the testis are transferred from the ED lumen by the peristaltic contractions of ED to the Ejaculatory bulb, which is further transferred to the female reproductive system during copulation (Lung, Kuo and Wolfner, 2001b; Cohen and Moussian, 2016c; Wilson et al., 2017). The innervated muscle of ED helps in the peristaltic contractions to transfer the secretions. Additionally, ED is involved in synthesizing and secreting the peptide called Dup99B, which is similar to Sex Peptide (Rexhepaj et al., 2003). DUP99B is involved in post-mating response inside the female reproductive system and helps in oviposition and ovulation in the female reproductive genital tract (Saudan et al., 2002; Rexhepaj et al., 2003).

Structurally, we observed that the ED organ is larger and wider in the anterior end, where the AG, seminal vesicles, and the testis connect to the ED papillae, and it is smaller and tapers towards the posterior end, where the ED connects to the Ejaculatory bulb (Figure 1.5). In Chapter 2 of my thesis, I examine the ploidy of the secretory cells in the different regions of ED. Previous studies provide evidence that the anterior region of the ED is involved in the secretion of esterase 6, which is transferred to females during copulation, where it may induce changes in the female reproductive tract to optimize remating time and reproductive fitness (Pape, Klott and Kreutz, 1971; Ludwig, Tamarina and Richmond, 1993; Saad et al., 1994). This Esterase-6 secreted from ED is also involved in the synthesis of sex pheromones (Takemori and Yamamoto, 2009). The ED also produces Glucose dehydrogenase (Gld) an enzyme that aids in sperm storage in the female reproductive tract after mating (Cavener, 1985; Cox-Foster et al., 1990). Hence, the ED is an important tissue of the male reproductive system because it provides components to optimize male fertility as well as induce changes in the female reproductive tract that support the male's reproductive success, in addition to serving a structural role in transferring seminal fluid. Despite these predicted functions of ED, limited information is known about the development and growth of this tissue. In Chapter 2, I explore the post-eclosion growth and cell cycle dynamics of the secretory cells of the ED.

1.6 The secretory epithelium of the ED also serves as an epithelial barrier

In *Drosophila melanogaster* and other insects, tissues and organs are housed within an open circulatory system, where hemolymph freely bathes the internal organs rather than being confined within blood vessels. Despite this, the internal contents of many tissues, particularly secretory or luminal organs such as the nervous system and reproductive tract, remain well compartmentalized. This spatial separation is achieved through several layered mechanisms, most fundamentally through the presence of a basal membrane (also called basal lamina). The basal membrane is a specialized, sheet-like extracellular matrix (ECM) composed primarily of collagen IV, laminin, etc. The basal membrane forms a continuous sheath around epithelial cells, creating a diffusion barrier that prevents the mixing of tissue-derived proteins, peptides, and secretions with circulating hemolymph (Pastor-Pareja and Xu, 2011; Yurchenco, 2011). This structure physically isolates epithelial tissues, including the ejaculatory duct (ED), accessory glands, gut, testis sheath, and others, from direct contact with the open circulatory system (Pastor-Pareja and Xu, 2011; Yurchenco, 2011) The ED secretory cells are also connected with selectively permeable septate

and cadherin cell-cell junctions. These septate junctions seal the neighboring epithelium cells (Buckley and St Johnston, 2022). Septate junctions are equivalent to the tight junctions in vertebrates in terms of function (Banerjee et al.,2006; Oshima and Fehon, 2011; Buckley and St Johnston, 2022). These junctions form a selectively permeable structure (Banerjee et al.,2006; Buckley and St Johnston, 2022). Both septate and tight junctions in epithelial cells play an important role by preventing paracellular transport between apical and basolateral surfaces (Oshima and Fehon, 2011; Buckley and St Johnston, 2022). In the ED, both the basement membrane and the septate, cadherin cell-cell junctions ensure that secretions such as seminal fluid proteins, pheromones, and antimicrobial peptides are retained within the duct lumen and only released during mating. This basal membrane provides mechanical support and maintains epithelial integrity (Figure 1.6).

1.7 Apical-Basal polarity of ED

The epithelial secretory cells of the ED exhibit basal localization of integrin βPS protein (as shown in chapter 2), which mediates firm adhesion to the basal membrane and supports epithelial integrity during tissue growth, contractile activity, and prevents leakage of secreted factors into hemolymph. This polarity is critical for targeting secretory vesicles apically, toward the lumen, and ensuring that the basal surface does not become a site of unintended efflux (Lemaitre and Miguel-Aliaga, 2013). Additionally, during developmental morphogenesis and post-eclosion tissue expansion, remodeling of the basal lamina is tightly controlled by matrix metalloproteases to preserve tissue containment (Srivastava et al., 2007). Thus, the ED has a large lumen surrounded by apical secretory cells, which are in turn surrounded by basal innervated muscles (Figure 1.6). The presence of septate junction complexes, containing proteins such as such as Fascillin III, DLG (Disc large), between adjacent secretory cells further reinforces compartmentalization of luminal secretions, creating a paracellular barrier that prevents leakage of luminal contents into surrounding tissue and hemolymph. Such epithelial polarization and junctional integrity have been well-characterized in other Drosophila secretory tissues such as the gut (Lemaitre and Miguel-Aliaga, 2013) and follicular epithelium (Tanentzapf et al., 2000), and their extension to the ED underscores a conserved strategy of epithelial cells to maintain specialized secretory compartments despite constant exposure to hemolymph. Together, these features enable the ED to function as a high-capacity secretory tissue without compromising the separation between internal reproductive secretions and systemic hemolymph.

1.8 High secretory demands on the ED

Highly secretory tissues such as the *Drosophila* ejaculatory duct, accessory glands, salivary glands, follicular cells, or fat body, as well as analogous organs in other organisms, face substantial physiological and structural demands to support their function. It is known that ED secretory cells are involved in the secretion of over 100 seminal fluid proteins and antimicrobial peptides. To meet these high demands of the biosynthetic capacity for secretion of these proteins into the lumen, the cells should have increased transcription and translation machinery. If the secretory cells exit the cell cycle permanently and if they suffer any damage or cell loss due to physiological stress or acute injury, the tissue still must recover to meet the high biosynthesis demand. To meet these demands without epithelial barrier-disrupting proliferation, some terminally differentiated secretory cells adopt a variant cell cycle called endocycling (Edgar and Orr-Weaver, 2001a). This strategy enables secretory cells to grow in mass and increase biosynthetic output without undergoing cell division, which requires epithelial cell-cell junction and extracellular matrix remodeling that compromises epithelial barrier integrity (Osswald M, Morais-de-Sá E. 2019). Cells support additional biosynthesis by increasing their DNA content. Some of the *Drosophila* tissues such as larval salivary glands, ovary follicle cells and male adult accessory glands, undergo doubling of their DNA content by undergoing endoreplication which helps in making multiple copies of each gene to meet the high biosynthesis demands of the tissue (Box et al., 2004; Edgar and Orr-Weaver, 2001a; Zielke et al., 2011a; Ren et al., 2020a). This whole genome amplification leads to increased transcriptional capacity, essential for sustained production of mRNAs encoding secreted proteins, metabolic enzymes, and vesicle trafficking components during secretion. In my thesis second chapter I will be exploring how the ED meets these high secretory demands and what happens when this endoreplication is disrupted. In order to duplicate the genome, cells of the ED undergo a specialized cell cycle termed the endocycle. To understand how the endocycle works, we must first review the canonical cell cycle.

1.9 Genome duplication and the canonical cell cycle

The cell cycle is a tightly controlled sequence of events through which a cell grows, duplicates its genetic material, and ultimately divides to form two identical daughter cells. This is a fundamental process to the growth and development of all multicellular organisms. The cell cycle machinery and its regulators in *Drosophila melanogaster* are fundamentally conserved with other eukaryotic organisms, comprising four distinct, ordered phases Gap1 (G1), Synthesis (S), Gap2 (G2), and

Mitosis (M) coordinated by cyclins, cyclin-dependent kinases (Cdks), checkpoint proteins, and transcriptional regulators. In G1 phase the cell grows and prepares for DNA replication followed by an S phase where DNA replication occurs, resulting in duplicated chromosomes. Next G2 phase the cell continues to grow and prepares for mitosis. In M phase the cell undergoes nuclear division (mitosis) and cytoplasmic division (cytokinesis), completing the formation of two daughter cells. When a cell becomes terminally differentiated, it exits the cell cycle and enters a phase of the cell cycle termed G0. This non-cycling phase of G0 can be temporary or permanent, depending on external signals or intrinsic factors. The G0 phase is a resting state/quiescent state where cells are not actively cycling but remain metabolically active. Cells can enter G0 from mitosis or the G1 phase, and they may re-enter the cell cycle depending on the developmental context or environmental cues (Coller, Sang and Roberts, 2006a; Sun D, Buttitta L, 2017; Ruijtenberg S, van den Heuvel S, 2016). In terminally differentiated cells, such as neurons and skeletal muscle fibers, this G0 phase is largely irreversible, reflecting a final exit from the cell cycle (Buttitta and Edgar, 2007a). These terminally differentiated cells that permanently exit mitosis during development are called post-mitotic, as they do not undergo anymore mitosis. In contrast, quiescent adult stem cells and certain somatic cells, like fibroblasts, can re-enter the cell cycle from G0 in response to injury or mitogenic signals, reflecting a reversible arrest (Coller, Sang and Roberts, 2006b; Cheung and Rando, 2013). Although the standard mitotic cell cycle is most commonly associated with tissue and organismal development, it's important to recognize that a variety of alternative cell cycle programs exist throughout the tree of life. One of the variant cell cycles that these post-mitotic cells undergo is called endocycling.

1.10 Genome duplication by a variant cell cycle - Endocycling

During early development, cells may undergo several rounds of canonical mitotic cycles (G1–S–G2–M) to expand the cell population. Upon terminal differentiation or tissue maturation, many of these cells exit the mitotic cycle and adopt variant cycles, such as the endocycle, or enter a quiescent G0-like state if further growth is no longer required (Buttitta and Edgar, 2007; Zielke et al., 2011). Endoreplication, also known as the endocycle, is a modified cell cycle in which cells undergo repeated rounds of DNA synthesis (S phase) without entering mitosis (M phase) (Figure 1.7 B). These cells shuttle between G and S phases, successively duplicating their genomic DNA without chromosome segregation or cell division. As a result, no new cells are formed instead, the nuclear DNA content increases, leading to polyploidy where their DNA content is more than 2C

(C=total ‘chromatin’ value, as a multiple of the haploid genome) (Øvrebø and Edgar, 2018). Depending on the number of endocycles, the ploidy level can reach 4C, 8C, 16C, 32C, or even higher (Figure 1.7 C).

Conversely, some tissues undergo endocycling during development. Endocycling and the resulting polyploidy play important roles in tissue development across a wide range of organisms and are often considered irreversible processes associated with terminal differentiation. Developmental endocycling has been reported in fish, mice, and humans, and is likely present in most mammals (Øvrebø and Edgar, 2018a, Polyploidy atlas). In mammals, endocycling occurs during normal development in several tissues, including the skin, heart, placenta, liver, and blood (Fox and Duronio, 2013a). For instance, placental trophoblast cells undergo endocycling to form a polyploid barrier that separates the maternal blood supply from that of the developing embryo (Rossant and Crossno, 2001). Similarly, megakaryocytes undergo endocycles to become highly polyploid before fragmenting into platelets, which are essential for blood clotting (Ravid et al., 2002). Perhaps most famously, mammalian hepatocytes undergo progressive polyploidization through endomitosis during postnatal liver growth, a process associated with terminal differentiation and cellular aging (Conway at al, 2024). However, certain human tissues may contain as many as 50% to 70% polyploid cells, depending on their type and function (Mollova et al., 2013; Gandarillas and Freije, 2014).

Endoreplication is also widespread among invertebrates, including insects, and has been thoroughly studied in the fruit fly *Drosophila melanogaster* (Edgar and Orr-Weaver, 2001b; Fox, Gall and Spradling, 2010; Zielke et a*l.*, 2011a; Fox and Duronio, 2013b; Edgar, Zielke and Gutierrez, 2014; Fox, Cohen and Smith-Bolton, 2020a). In *Drosophila*, the majority of differentiated larval tissues undergo development through endocycling. This process has been well documented in various tissues, including the salivary glands, fat body, gut, renal (Malpighian) tubules, trachea, and epidermis (Øvrebø and Edgar, 2018b). In contrast, mitotic proliferation is largely restricted to undifferentiated progenitor and stem cell populations, such as the imaginal discs, abdominal histoblasts, cell populating the nervous system, and adult midgut progenitors within the larval gut. In the adult fly, several cell types undergo endocycling and become polyploid, including a subset of neurons, sensory bristle cells, gut enterocytes, and nurse and follicle cells in the ovary, with ploidy levels ranging from 8C to as high as 2,000C (Hammond and Laird, 1985; Unhavaithaya and Orr-Weaver, 2012a). Endocycling is essential for the growth and functional

capacity of these cells. When the ploidy in ovarian nurse cells is compromised, it results in female sterility, highlighting the requirement of endocycles for proper oocyte development (Lilly and Spradling, 1996). Adult *Drosophila* male accessory glands secretory cells are post-mitotic and undergo endocycling (Allison M Box et al., 2024). These cells are also involved in the secretion of many seminal fluid proteins. Thus, most of the cells that undergo this variant cell cycle-endocycles are the cells with higher biosynthesis demand that are essential for the function of the tissues. The outcome of endocycling from all different organisms/tissues is a single, enlarged, polyploid cell capable of enhanced gene expression and biosynthesis. Endoreplication is commonly employed by cells in highly secretory or metabolically active tissues to meet elevated demands for protein production. In Chapter 2, I have discovered that the *Drosophila* ED secretory cells are post-mitotic, and they exit mitosis permanently during growth, but they enter a variant cell cycle called endocycling post-eclosion. I have shown that the endocycling is conserved in secretory cells of ED in different species of *Drosophila*.

1.11 Advantages of Polyploidy

Polyploidy in cells plays a crucial role in supporting high biosynthetic demand, thereby enabling them to produce higher transcriptional output. In *Caenorhabditis elegans*, the intestine plays an important role in cell growth and yolk biosynthesis (Dimov and Maduro, 2019). During normal development, the *C. elegans* intestine undergoes endocycling and becomes polyploid (Dimov and Maduro, 2019). When ploidy in the intestinal cells was compromised, it led to smaller cell size and reduced transcript levels. This reduction in ploidy also resulted in diminished synthesis of yolk proteins and a significantly lower number of offspring (Lessenger et al., 2025). In yeast strains with an increase in DNA copy number, there is an increase in the size of the yeast, and the cell size scales linearly with the ploidy/DNA copies (Cadart and Heald, 2022). Yeast cells with higher ploidy allometrically have higher mRNA and protein compared to cells with haploid DNA content. The yeast strain with tetraploid nuclei had a threefold increase in protein synthesis compared to the strain with haploid nuclei (Galitski T et al, 1999; Yahya et al., 2022). These studies suggest that the ploidy status may lead to an increase in the mRNA and protein synthesis, as often hypothesized (Fox and Duronio, 2013; Øvrebø and Edgar, 2018).

Another advantage of polyploid cells is that they exhibit increased survival in response to DNA damage compared to diploid cells (Herriage et al, 2024). This is true across kingdoms, including plants (Muntzing and Prakken, 1941). In polyploid cells resistance to DNA damage is conferred

by the number of copies of the genome where somatic mutations in one copy of a gene will not greatly impact the capacity of the cell to function, since it will have many other copies of the genome (Edgar and Orr-Weaver, 2001a; Edgar, Zielke and Gutierrez, 2014; Øvrebø and Edgar, 2018a). Protection against DNA damage is being studied in *Drosophila* polyploid cells of fat body, salivary glands, and ovarian follicle cells (Mehrotra *et al.*, 2008). It has also been shown that polyploidy protects against oxidative damage in the *Drosophila* brain (Nandakumar, Grushko and Buttitta, 2020).

As discussed, *Drosophila* polyploidy is common in the salivary glands, fat body, nurse cells, and male accessory glands, often supporting secretion or metabolic activity (Edgar and Orr-Weaver, 2001b; Zielke et al., 2008a, 2011a; Fox and Duronio, 2013c). Some of these polyploid cells are highly secretory and perform epithelial barrier function. When cells that serve as an epithelial barrier undergo mitosis, cell-cell contacts become compromised (Erenpreisa and Cragg, 2001; Lancaster et al., 2013; Orr-Weaver, 2015; Sauer, 1935). This can disrupt their epithelial barrier function. Thus, endocycling and becoming polyploid is a strategy for these cells to grow in size and genome copy number without increasing cell number and without compromising their epithelial barrier functions (Edgar and Orr-Weaver, 2001a). Large, polyploid epithelial cells form tight barriers against mechanical stress, pathogen entry, or osmotic damage by helping with barrier function (Fang et al., 2023). Below are some of the examples of cells that are polyploid with high secretory and maintain the epithelial barrier functions

Drosophila salivary glands have ploidy up to 1000–2000C, and this increased ploidy is required for the large volume of glue protein production during pupariation to affix the animal undergoing metamorphosis to the substrate. In *Drosophila,* polyploidization of the subperineurial glia (SPG) results in increased cell size, which maintains the blood-brain barrier surrounding the growing brain without barrier-compromising proliferation (Unhavaithaya and Orr-Weaver, 2012b). In mammalian hepatocytes and megakaryocytes, polyploidy is involved in liver metabolism and platelet biogenesis, respectively (Ravid et al., 2002; Miyaoka et al., 2012). The epithelial cells of the ED have both secretory and barrier functions. In Chapters 2 and 4 I show how they maintain these functions without undergoing mitosis.

Given the numerous advantages associated with polyploidization, it is unsurprising that diploid cells often adopt this strategy when faced with stress or injury. Extensive research in both *Drosophila* and certain mammalian systems has explored how polyploidization supports tissue

response to wounding and cell loss, as well as its protective role against DNA damage. These studies have significantly deepened our understanding of the function of polyploidy in responding to acute cellular damage. In Chapter 2, I have discovered that ED secretory cells undergo polyploidization as a result of endocycling, and this helps in post-eclosion growth and development of the ED in adult males. There are cell cycle regulatory factors involved in endocycling, and I have utilized these in Chapter 2. Therefore, in the next section, I will briefly discuss these factors.

1.12 Regulatory factors involved in Endocycling

In this section, I will focus specifically on the molecular regulators of endocycling in *Drosophila*, outlining the key pathways and factors that control the transition to endocycles. In endocycling cells, it is the transition from G to S phase that is part of the canonical cell cycle. Thus, most of the factors will be G1 and S-phase cell cycle factors that will help regulate endocycling. An important requirement for endocycling is the sustained suppression of mitotic cyclin-dependent kinase (M-CDK) activity, along with the maintenance of oscillating S-phase CDK activity during the transitions between G and S phases (Edgar, Zielke and Gutierrez, 2014). The key regulators are E2F transcription Factor that promotes expression of hundreds of cell cycle genes and is essential for the endocycle, Rbf (Retinoblastoma-family protein) the main E2F inhibitor, Cyclin E (CycE) the activator of S-phase Cdk activity to promote S-phase entry, APC/C^{Fzr}, a ubiquitin ligase that regulates the stability of DNA replication licensing factors, Geminin, a replication licensing inhibitor, and CRL4Cdt2, a ubiquitin ligase that regulates the stability of many S-phase proteins including the critical E2F transcription factor. The progression of the endocycle is driven by the oscillations of these cell cycle regulatory mechanisms, which ultimately generate pulses of S-CDK to drive alternating S and G phases (Edgar and Orr-Weaver, 2001b; Lee, Davidson and Duronio, 2009; Edgar, Zielke and Gutierrez, 2014; Shu, Row and Deng, 2018).

1.12.1 E2F- Transcriptional activation and repression of cell cycle genes

Unlike mammals, which have multiple E2F and DP proteins, *Drosophila* has a simplified two-component E2F network; E2F1, an activator that promotes the transcription of S-phase genes, and E2F2, that acts as a repressor (Guarner et al., 2017). The DP protein acts as a dimerization partner required for the DNA binding of both E2F1 and E2F2. Binding of DP to E2F promotes the transcription of hundreds of cell cycle genes including most genes required for S and M phases

(Dynlacht et al., 1994; Van Den Heuvel and Dyson, 2008). Both the E2Fs bind similar DNA binding motifs, and it has been proposed that cell cycle exit during the development of certain *Drosophila* tissues is regulated by a switching mechanism between these two factors (Dimova et al., 2003; Korenjak et al., 2014). However, in the absence of the repressive E2F2, E2F1 can take on repressive functions. Inhibitory functions of E2Fs are triggered by binding to Retinoblastoma family members (Rbfs 1 and 2 in *Drosophila*), which convert the E2F/DP transcription factor complex to a repressive complex that suppresses cell cycle gene expression (Dimova et al., 2003; Giacinti and Giordano, 2006; Hoareau M et al., 2024). (Harbour and Dean, 2000; Giacinti and Giordano, 2006). Upon entry into the G1 phase, Rbf is hyperphosphorylated by the growth factor-stimulated Cyclin D (CycD)/Cdk4 complex (Narasimha et al., 2014). This is followed by partial E2F-activation of Cyclin E expression which leads to increased (CycE)/Cdk2 activity in late G1 phase, which also further phosphorylates Rbf proteins (Harbour and Dean, 2000; Dimova et al., 2003; Giacinti and Giordano, 2006). This hyperphosphorylation induces a conformational change in Rbf, leading to the complete release of the E2F1 transcription factor from the repressive complex, thereby activating the transcription of DNA synthesis genes essential for S-phase progression (Harbour and Dean, 2000; Giacinti and Giordano, 2006). E2F transcription factors activate hundreds of cell cycle regulatory factors in addition to Cyclin E, such as Cyclin A, CDK2, DNA polymerase alpha, and PCNA (Proliferating Cell Nuclear Antigen), which plays a key role in DNA replication by enhancing DNA polymerase complex processivity (Duronio and O'farrell, 1995; Herr et al., 2012). However, the function of the proteins encoded by these genes is not solely determined at the transcriptional level, they are further regulated through phosphorylation and ubiquitination, which adds a crucial layer of control to ensure proper cell cycle timing and coordination.

1.12.2 CycE/Cdk2- phosphorylation of G1-S substrates

E2Fs, during late G1 phase, stimulate the transcription of Cyclin E, which in turn activates S-CDK and drives the initiation of S phase (Edgar, Zielke and Gutierrez, 2014). All cyclins and CDKs are not active on their own, their activity is triggered when cyclins dimerize with CDKs (Duronio and O'Farrell, 1995; Lilly and Spradling, 1996). Once activated, cyclin–CDK complexes phosphorylate specific target proteins to facilitate cell cycle transitions. In this context, Cyclin E, transcribed under the control of E2F1, forms a complex with Cdk2. This CycE/Cdk2 complex further hyperphosphorylates Rbf, leading to the release of additional E2F1, which further promotes

the transcription of replication genes. This positive feedback loop ensures the bi-stability of the S-phase triggering process by the Cyclin/Cdk Rbf/E2F complexes (Stallaert et al, 2019). CycE/Cdk2 also phosphorylates and activates DNA pre-replication factors such as Cdc6, which helps recruit the MCM (mini chromosome maintenance) complex to replication origins, cdt1, thereby enabling DNA replication (Duronio and O'farrell, 1995; Lilly and Spradling, 1996; Herr et al., 2012; Fagundes and Teixeira, 2021; Blank, No and Polymenis, 2025). Overall, the CycE/Cdk complex is essential for driving the transition from G1 to S phase during endocycling (Edgar, Zielke and Gutierrez, 2014). Therefore, E2F1 and CycE/Cdk2 represent key rate-limiting regulators of G1/S progression.

1.12.3 CRL4^{Cdt2}- destruction of G1-S phase substrates

E2F1 levels begin to rise just prior to the onset of S phase but are rapidly degraded once DNA replication begins. This degradation is mediated by CRL4^{Cdt2}, a S phase-specific E3 ubiquitin ligase whose activity depends on ongoing DNA synthesis (Arias and Walter, 2006; Shibutani, Swanhart and Duronio, 2007). CRL4^{cdt2} directly binds E2F1 via its PIP box and mediates its destruction. Evidence from *Drosophila* salivary glands supports a model in which E2F1 accumulation during late G phase induces Cyclin E transcription. Cyclin E then activates S-phase CDK (S-CDK) to initiate DNA replication. In turn, the onset of S phase activates CRL4^{Cdt2}, which targets E2F1 for degradation, thereby halting further production of Cyclin E mRNA. The subsequent decline in Cyclin E protein leads to reduced S-CDK activity, allowing the cell to re-enter a G phase, during which pre-replication complexes (preRCs) can be assembled in preparation for the next endocycle (Edgar, Zielke and Gutierrez, 2014; Kim, Santos and Moon, 2021).

1.12.4 CKI-Dacapo

The activity of Cyclins and CDKs is regulated by Cyclin-Dependent Kinase Inhibitors (CKIs), which bind to Cyclin/CDK complexes and inhibit their enzymatic activity (De Nooij, Letendre and Hariharan, 1996). Proper regulation of these complexes is essential for accurate cell cycle progression and timely exit from the cycle. In the context of endocycling, CycE/Cdk2 activity must be oscillatory, requiring the complex to be degraded after the transition from G1 to S phase for the progression of endocycle (De Nooij, Letendre and Hariharan, 1996; Lane et al., 1996). In *Drosophila*, the primary CKI belongs to the p21/p27 family and is known as Dacapo. Dacapo regulates CycE/Cdk2 activity by forming a feedback loop: as Cyclin E levels rise during the late

G1 phase, Dacapo levels also increase. Upon entry into S phase, Dacapo contributes to the inhibition of CycE/Cdk2, thereby reducing S-CDK activity and allowing the cell to return to G phase. This reciprocal regulation between Dacapo and CycE/Cdk2 ensures the oscillatory control necessary for successful endocycle progression (Lane, Sauer and Wallace, 1996; Hong et al., 2007). Dacapo can also inhibit Cyclin E–Cdk2 activity during the late stages of S phase, leading to a shortening of S phase duration. As a result, DNA replication often remains incomplete during typical endocycles, especially in heterochromatic regions of the genome (Hong et al., 2007; Swanson et al., 2015). Dacapo oscillations are required for the proper progression of the endocycling.

1.12.5 APC/C Fzr

The Anaphase-Promoting Complex/Cyclosome (APC/C) is a large, multi-subunit E3 ubiquitin ligase that plays a central role in controlling cell cycle transitions, particularly the exit from mitosis and the regulation of the G1 phase. By targeting specific cell cycle proteins for ubiquitin-mediated degradation, APC/C ensures that cell cycle events occur in the correct order and only once per cycle (Peter,2006; Harper, 2002; Peter, 2022). APC/C is activated by the two proteins with WD repeats Fzy (Fizzy)/cdc20 and Fzr (Fizzy-related)/cdh1(Zur and Brandeis,2002; Raff, Jeffers and Huang, 2002). These activator subunits bind to APC/C, which facilitates the binding of the substrate for ubiqutination. Fzy and Fzr play complementary roles during the cell cycle to target specific proteins during specific phases. Fzy/Cdc20 levels start accumulating in S-phase, peak in mitosis, and its levels are reduced in G1-phase, therefore the APC/C-Fzy complex targets mitotic cyclins and proteins early in the exit from mitosis for ubiquitination (Zur and Brandeis,2002; Pesin and Orr-Weaver, 2008). By contrast, Fzr levels are high during late M-phase and G1, thus the APC/C-Fzr complex targets mitotic cyclins and additional substrates for degradation later in mitotic exit and during G1. Both these complexes (APC/C-Fzy and APC/C-Fzr) bind to the substrate by recognizing the specific sequence on it. APC/C. APC/C-Fzy recognizes and binds to the substrate that has conserved motifs (RxxLxxxxN) called the destruction box (D-box) and further mediates the degradation of the substrate (Pfleger, Lee and Kirschner, 2001; Kapanidou, Curtis and Bolanos-Garcia, 2017). APC/C-Fzr binds to the substrates that have the conserved sequence KEN motifs, called as KEN box, and it can also recognize and bind to D-box and further mediates the degradation of mitotic cyclins in G1 (Pfleger and Kirschner, 2000; Pfleger, Lee and Kirschner, 2001; Michael et al., 2008; Narbonne-Reveau et al., 2008). Thus, the activity of APC/C

is regulated by the binding of activator subunits, which bind to the complex differentially depending on the phase of the cell cycle, as well as confer specificity, targeting proteins for destruction by the 26S proteasome.

As mentioned above, APC/C-Fzr is active in the G1 phase and therefore promotes degradation of Cyclin A, Cyclin B, and Geminin (a DNA replication licensing inhibitor that prevents DNA replication re-initiation, discussed in the next section), to maintain low CDK activity and prevent DNA replication during G1 phase (Dawson, Roth and Artavanis-Tsakonas, 1995; Schaeffer et al., 2004). The activity of APC/C-Fzr is by the S-Cdk, CyclinE/cdk2, which results in a decline of activity for the G1 to S-phase transition. Ultimately these negative inhibitory relationships lead to oscillations of Gap-phase promoting APC/C FZR activity and S-phase promoting CyclinE/cdk2 activity (Acquaviva and Pines, 2006; Narbonne-Reveau et al., 2008; Zielke et al., 2008b; Edgar, Zielke and Gutierrez, 2014). This promotes an alternating G–S–G–S cycle, characteristic of the endocycle. APC/C-Fzr thus acts as a gatekeeper, ensuring that cells do not enter mitosis and can re-license replication origins during each G phase. It has been shown that in *Drosophila* larval salivary glands and nurse cells, when APC/C is knocked down and its activity is compromised, it results in the accumulation of the targets of APC/C and prevents the endocycle (Narbonne-Reveau et al., 2008). APC/C functions to reduce the levels of the mitotic cyclins and Geminin to facilitate the relicensing of DNA replication origins and cell cycle progression (Dawson, Roth and Artavanis-Tsakonas, 1995; Schaeffer et al., 2004; Narbonne-Reveau et al., 2008)

1.12.6 Geminin

Geminin plays a critical role in S-phase DNA synthesis by preventing the formation of pre-replication complexes (pre-RCs) during ongoing DNA replication, thereby inhibiting DNA re-replication (Calvi, Lilly and Spradling, 1998; Lilly and Duronio, 2005). It is essential not only for restricting DNA replication but also for regulating the G2 to M phase transition. During S-phase, DNA replication is initiated when the ORC binds to replication origins. This is followed by the recruitment of the replication initiation factors Cdc6 and Cdt1, which together load the mini chromosome maintenance (MCM) helicase complex onto DNA. MCM proteins unwind the DNA helix, allowing assembly of the full pre-replication complex (pre-RC) and progression through replication (Quinn et al., 2001a; Luo et al., 2007; Zielke et al., 2008b; Hua and Orr-Weaver, 2017) . To prevent re-licensing of replication origins during the same S-phase, the small (~25 kDa) Geminin protein binds to Cdt1, thereby blocking its interaction with MCM and inhibiting MCM

reloading (Luo et al., 2007). This ensures that each segment of the genome is replicated exactly once during one S phase. Geminin levels are kept low during G phase to allow Cdt1-dependent preRC assembly. Geminin levels remain high throughout S-phase to prevent re-replication. At the end of S-phase, during G phase, when cells are preparing for the next round of DNA synthesis, Geminin is degraded via the APC/C. This oscillatory degradation of Geminin is crucial for the alternation between G and S phases in the absence of mitosis and essential for supporting repeated rounds of endoreplication. Structurally, Geminin contains a coiled-coil domain, necessary for its interaction with Cdt1, a destruction box (D-box), and KEN box that is ubiquitinated by APC/C, targeting it for proteasomal degradation (Benjamin et al., 2004). Notably, overexpression of (a stabilized form) Geminin in *Drosophila* salivary gland cells leads to reduced DNA content and inhibition of endoreplication, confirming its central role in replication licensing control (Zielke et al., 2008b).

1.13 Progression of Endocycling

The oscillatory action of endocycling regulatory factors are important for the cells to endocycle (Figure 1.8). These specific cell cycle regulators drive the transition between G phase (growth and licensing) and S phase (DNA synthesis) without entry into mitosis. This oscillation is central to how endoreplicating cells in *Drosophila* such as those in the salivary gland, fat body, and ejaculatory duct achieve polyploidy and maintain tissue growth and biosynthetic output (Edgar and Orr-Weaver, 2001b, 2001a; Lee, Davidson and Duronio, 2009; Fox and Duronio, 2013c, 2013a, 2013b; Shu, Row and Deng, 2018).

Data from *Drosophila* salivary glands reveal a recurring endocycling regulatory cycle in which E2F1 accumulates during late G phase, triggering the expression of Cyclin E and other genes involved in S-phase DNA synthesis. Cyclin E then activates S-CDK, initiating S phase. This phase subsequently activates CRL4Cdt2, which degrades E2F1 and halts further production of Cyclin E mRNA. Once DNA replication begins during S phase, Geminin levels increase, leading to the inhibition of CRL4Cdt2 and thereby preventing re-replication within the same cycle (Quinn et al., 2001a, 2001b; Lee, Davidson and Duronio, 2009; Shu, Row and Deng, 2018). As Cyclin E levels decline, S-CDK activity decreases, allowing the cell to return to G phase and assemble pre-replication complexes for the next round of endocycling. Notably, this feedback loop is directly linked to DNA replication through CRL4Cdt2.

1.14 Endoreplication is involved in increased protein synthesis

Endocycling/Endoreplication, as mentioned earlier, is suggested to play a beneficial role in development of secretory cells to meet their increased biosynthesis demands. But the evidence for whether endocycling directly helps increase protein synthesis is complex. Studies in developing plant seeds have shown that seeds that undergo endocycling show increased endosperm mass and rapid synthesis of starch, suggesting that increasing the genome copy number can assist in maximizing mRNA and protein synthesis (Lee, Davidson and Duronio, 2009; Edgar, Zielke and Gutierrez, 2014; Shu, Row and Deng, 2018). It is widely assumed that increased genome copy numbers produces a larger template for gene expression, to allow for increased transcriptional output (Dimov and Maduro, 2019; Cadart and Heald, 2022; Yahya et al., 2022; Lessenger et al., 2025). Indeed in many highly biosynthetic tissues, extensive polyploidization is pervasive, correlating DNA copy number with high biosynthesis (Lee, Davidson and Duronio, 2009). The mammalian placenta is an excellent example of combining protein synthesis with epithelial barrier function. The Trophoblast giant cells (TGCs) undergo massive amounts of endoreplication to form and maintain a protective barrier between the maternal and embryonic tissues, yet cells must produce large amounts of proteins to build and maintain this growing barrier. and the increased ploidy facilitates cells to fulfill this function (Zybina and Zybina, 2020).

1.15 Signaling pathways involved in the endocycle

Cells rely on well-established signaling pathways to transmit information, allowing specific cues to elicit consistent and predictable responses in target tissues. These pathways play essential roles in coordinating tissue development and cell differentiation, including the regulation of cells that transition into the endocycle. In *Drosophila*, numerous polyploid cell types are influenced by such signaling mechanisms. Moreover, the expression of certain transgenes or mutations can disrupt these pathways, inducing endoreplication in cells that would typically remain diploid. Some of the signaling pathways known to regulate endocycling are Myc, Notch, Insulin/Insulin-like Growth Factor (IIS), and Target of Rapamycin (TOR), Hippo, Ras/MAPK, and c-Jun N-terminal Kinase (JNK) (Almeida Machado Costa et al., 2022) and Juvenile hormone signaling (JH) (Ren, D. et al, 2020). In this section, we will explore some of the signaling pathways that are more relevant to my work, such as Juvenile hormone signaling, JNK pathway, Myc, insulin-like growth factor and mTOR pathways.

1.15.1 Juvenile Hormone (JH) Signaling

Juvenile Hormone (JH) is a family of acyclic sesquiterpenoids released by the endocrine gland Corpus allatum, which plays an important role in insect development and reproduction, including in *Drosophila* (Braun and Wyatt, 1995; Goodman and Cusson, 2011; Jindra, Palli and Riddiford, 2013). The levels of JH fluctuate throughout the growth and development of *Drosophila*. Specifically, JH levels increase during larval development up to the third instar stage, then drop rapidly during metamorphosis, followed by a sharp increase immediately post-eclosion (Figure 1.9) (Bownes and Rembold, 1987; Zhang, Li and Liu, 2022). JH is a master regulator of *Drosophila* metamorphosis, reproduction, and behavior.

In addition, JH plays a significant role in inducing polyploidy in the fat body during vitellogenesis to promote reproduction, primarily by activating the transcription factor E2F1, and by acting on Mcm gene expression levels (Riddiford, 2012; Wu et al., 2018, 2020; Ren et al., 2020b). The nuclear receptors Methoprene-tolerant (Met), Germ-cell expressed (Gce), and the co-activator Taiman (Tai), a member of the transcriptional regulator family, are all required for JH signal transduction. Gce and Met belong to the basic helix-loop-helix (bHLH) transcription factor (TF) family (Abdou et al., 2011). bHLH transcription factors containing proteins are known to be involved in broad functions such as cell proliferation, cellular differentiation, etc. (Heim et al., 2003). Most bHLH transcription factors have two connected sub-regions, the N-terminal basic region directly followed by the HLH (helix-loop-helix) domain, which helps in binding to the DNA and helps in transcription of the target genes (Heim et al., 2003; Qian et al., 2021). JH signal transduction occurs via these nuclear receptors: Met, Gce, and their co-activator Tai. All three Gce, Met, and Tai have been reported to be expressed in the adult *Drosophila* ejaculatory duct (ED), suggesting they may play important roles in this tissue. In the adult male reproductive system, Met and Gce have been shown to be expressed at elevated levels in the ED (Pursley, Ashok, and Wilson, 2000; Wilson, DeMoor and Lei, 2003a; Baumann et al., 2017). Knockdown of these receptors in the male accessory glands leads to reduced protein synthesis and accumulation, diminished secretion of seminal fluid proteins, and lower fertility (Box et al., 2024; Pursley, Ashok and Wilson, 2000; Wilson, DeMoor and Lei, 2003b, 2003a; Baumann et al., 2010b). JH has been implicated in playing a critical role in adult reproduction in many insects, including *Drosophila*, and is essential for proper protein synthesis and growth of the male accessory glands. Furthermore, studies in other insects suggest that JH acts upstream of the cell cycle to promote polyploidy.

Taken together, the observed correlations between tissue size, protein synthesis, and JH-mediated regulation of the cell cycle in other insects suggest that JH may be a key regulator of tissue maturation in the adult *Drosophila* accessory gland.

However, the role and function of these receptors in the adult male ED have not yet been explored. Therefore, in my Chapter 2, I will be investigating whether Juvenile Hormone signaling is involved in endoreplication of secretory cells in the *Drosophila* ejaculatory duct and whether this process contributes to the growth and development of the ED post-eclosion. In the earlier studies, it was found that the levels of JH signaling increase immediately post eclosion, so we wanted to test if this signaling plays any important role in the early endocycling of secretory cells of ED immediately post-eclosion.

1.15.2 The growth regulatory Pathways

The Insulin/Insulin-like Growth Factor (IIS) and Target of Rapamycin (TOR) pathways are evolutionarily conserved and work in tandem to regulate how cells adapt to nutrient availability. These signaling networks suppress endocycle progression under dietary restriction in several *Drosophila* larval tissues, such as the fat body, gut, proventriculus, and salivary glands, where E2F1 translation is modulated in response to nutrient status (Almeida Machado Costa et al., 2022). In ovarian follicle cells, which are poised to transition from mitosis to endocycling (termed the M/E switch), nutritional stress can interfere with Notch signaling through IIS and TOR pathway modulation. During starvation, levels of insulin-like peptides drop, leaving the Insulin-like receptor (InR) unbound. This causes the suppression of the mitotic to endocycle transition. This effectively stalls the M/E switch. However, when food is reintroduced, the process resumes, and the follicle cells initiate endocycling (Jouandin, Ghiglione and Noselli, 2014). Similarly, in the midgut, InR is essential for the differentiation of enterocytes. Loss-of-function mutations in components of the IIS/TOR pathways, such as Pi3K, TOR, or InR halt intestinal stem cell-derived clones in a diploid state. In contrast, boosting InR or Rheb expression in enteroblasts leads to cell enlargement and increased ploidy (Xiang et al., 2017).

There are reports showing that the mammalian TOR pathway serves as a central driver of cellular growth by stimulating cyclin-dependent kinase (CDK) activity and accelerating cell cycle progression. It plays a critical role in facilitating the early G1 phase transition in both yeast and mammalian systems. Emerging research indicates that mTOR also contributes to the initiation of DNA replication by promoting the expression of CDC6, a key factor necessary for assembling the

MCM2–7 helicase complex at replication origins (Petropoulos et al., 2019; Choudhury et al., 2024). When mTOR activity is blocked, there is a marked decline in MCM2 7 complex components and PCNA on chromatin. Both mTOR complexes mTORC1 via S6K1 and mTORC2 appear essential for regulating CDC6 levels (Wu et al., 2019; He et al., 2021). As a result, mTOR supports the recruitment and stability of MCM2–7 on chromatin through its positive effect on CDC6. This link between mTOR signaling and CDC6 deregulation offers potential insights into how the RAS/PI3K-mTOR axis might contribute to genomic instability and cellular diversity commonly observed in cancer (He et al., 2021).

In Chapter 2 I explore the effects on protein synthesis of polyploid secretory cells when we knockdown the some of the components of mTOR signaling.

1.15.3 The JNK Pathway

The JNK (c-Jun N-terminal Kinase) pathway is an evolutionarily conserved signaling cascade that plays crucial roles in regulating apoptosis, immune responses, and cellular responses to DNA damage (Tafesh-Edwards and Eleftherianos, 2020a). It becomes activated under stressful conditions, such as cellular stress or disrupted polarity. When triggered, the TNF ligand Eiger binds to its receptors Wengen or Grindelwald initiating a kinase cascade that ultimately activates the terminal JNK, Basket. Activated Basket phosphorylates various transcription factors that drive the expression of pro-apoptotic genes, including *Reaper* and *head involution defective*, often leading to caspase-mediated cell death (La Marca and Richardson, 2020).

JNK signaling exerts complex and sometimes opposing influences on polyploidy and tumor development, depending on cellular context and interactions with other pathways. JNK also inhibits the mitotic entry regulator String (Cdc25 homolog), thereby blocking faulty mitosis in polyploid cells (Gutierrez et al, 2010). However, this tumor-suppressive action can be counteracted by overexpressing Yorkie (Yki), which activates mitotic gene expression (Gerlach, Eichenlaub and Herranz, 2018).

On the other hand, JNK can also support polyploidization and tumor growth in specific neoplastic settings. In tumors arising from disruptions in endocytic genes like *rab5*, *vps25*, *erupted*, or *avalanche*, as well as in epithelial cancers driven by *RasV12* combined with mutations in *scrib* or *dlg1*, JNK promotes endoreplication. This is achieved by downregulating Cyclin B (CycB), facilitating polyploid cell growth. Simultaneously, JNK cooperates with Yki to enhance Diap1

expression, thereby preventing apoptosis and supporting the survival of these giant polyploid cells (Cong, Ohsawa and Igaki, 2018).

Studies in *Drosophila* epidermis have shown that JNK signaling is activated during Wound Induced Polyploidization, a process where cells polyploidize to compensate for cell loss due to injury. However, unexpectedly, JNK signaling through the AP-1 transcription factor complex appears to limit, rather than stimulate, the level of Yorkie (Yki) activation and polyploidization during this process (Lee and Miura, 2014; Besen-McNally, Gjelsvik and Losick, 2021).

1.15.4 Myc

Drosophila Myc (dMyc), is a bHLH (basic helix-loop-helix) transcription factor. *Drosophila* has only one Myc, unlike mammals which have multiple Myc family members. Like its mammalian homologs, dMyc dimerizes with Max, forming Myc-Max complexes that bind E-box DNA motifs (CACGTG) to activate transcription of growth-promoting genes, and often levels of Myc correlate to levels of several cell cycle regulators such as E2F1 and different cyclins(Bellosta and Gallant, 2010). At the molecular level, *Drosophila* Myc functions as a global regulator of gene expression to promote cellular growth and metabolism. Genomic studies show dMyc influences a broad set of targets involved in protein synthesis, ribosome biogenesis, and metabolic pathways (Johnston et al., 1999).

By globally boosting the protein synthesis capacity of cells, dMyc induces cell growth (mass accumulation) which in turn supports cell cycle progression. Indeed, in imaginal cells, Myc driven growth tends to shorten the G1 phase (cells reach the critical size for S-phase faster) (Johnston et al., 1999; Bellosta and Gallant, 2010; Grifoni and Bellosta, 2015). In endoreplicating polyploid tissues (like larval salivary glands and fat body), Myc's effects on DNA replication are especially pronounced. Myc loss causes reduced endocycle rounds and smaller polyploid nuclei, whereas Myc overexpression triggers excessive endoreplication and greatly enlarged nuclear size in *Drosophila* wing discs (Johnston et al., 1999; Bellosta and Gallant, 2010). Thus, through controlling biosynthesis, *Drosophila* Myc couples growth to the cell cycle, influencing both diploid cell proliferation rates and polyploid cell DNA amplification.

1.16 Regeneration

In normal homeostatic tissues, when exposed to stress or mild injury, cells attempt to adapt to the changing conditions. If adaptation fails, the cells experience injury. When the injury is mild and transient, it leads to reversible damage. However, if the injury is severe or progressive, cells undergo cell death, which may occur through necrosis or apoptosis. In response to injury-induced cell death, a wound-healing or acute damage response is triggered. As a result, when possible the tissue initiates regeneration, a biological process by which damaged or missing cells, tissues, organs, or even entire body parts are renewed, restored, or regrown. Regeneration is a fundamental process observed in many organisms that enables the repair of injuries and the restoration of normal function. Perfect regeneration refers to the complete restoration of damaged tissue to its original structure and full functionality. In contrast, 'imperfect regeneration' results in substantial, but partial organ recovery, often involving significant restoration of organ size, but may include the formation of scar tissue or abnormal growth. Thus imperfect regeneration is characterized by restoration of significant function and size, but not the original organ morphology, cell composition or cell number (Poss et al, 2024). Across the animal kingdom, many species exhibit the ability to regenerate damaged tissues, though the extent of this capability and whether it is perfect or imperfect varies greatly depending on species, organ type, nature of damage, and developmental stage (Xia et al., 2018a; de Morree and Rando, 2023a). Tissue regeneration generally occurs under two main circumstances, homeostatic growth, which involves the routine replacement of aging cells during normal tissue maintenance, and epimorphic and morphallactic regeneration, which is the repair response following trauma such as injury or amputation.

There are three main types of regeneration mechanisms: stem cell-mediated regeneration, regeneration by differentiated cells, and postmitotic cell regeneration. In stem cell-mediated regeneration, damaged or lost cells are replaced through the proliferation and differentiation of stem cells, a process initiated by injury-induced signaling (Lucchetta and Ohlstein, 2017; Xia et al., 2018b; Liu et al., 2019; Seetharaman et al., 2019). These tissues contain pools of stem cells, which have enormous proliferative and self-renewing ability, and which give rise to more than one type of cell. Replicating asymmetrically, each stem cell gives rise to one daughter cell that differentiates and matures and another daughter cell that remains undifferentiated and capable of

beginning another self-renewing cycle. Examples of such tissues include epithelia (such as skin, gastrointestinal epithelium and salivary gland tissue) and hematopoietic tissues.

In regeneration by differentiated cells, tissues that lack a substantial stem cell population rely on existing differentiated cells for repair. These cells, typically in a G0 or quiescent state, are composed of cells that normally exist in a non-dividing state but may re-enter the cell cycle in response to certain stimuli, such as cell injury. Tissues falling into this category include parenchymal cells of the liver, kidney and pancreas, mesenchymal cells such as fibroblasts and smooth muscle cells, endothelial cells and lymphocytes. It should be noted that the liver, unlike other quiescent tissues, has a relatively robust proliferative capacity. When a lobe of the liver is resected for donation, for example, the remaining liver cells proliferate at such a rate that the liver reaches a size similar to that prior to resection. While this process is commonly described as regeneration, it is more accurately viewed as compensatory growth, since the original lobe itself does not regrow.
In postmitotic cell regeneration, cells have irreversibly exited the mitotic cycle during development and possess few or no stem cells. and are therefore unable to proliferate. Tissue repair in these tissues always leaves permanent evidence of injury, such as a scar. These nondividing tissues (or permanent tissues) include cardiac and skeletal muscle (Losick, Fox and Spradling, 2013). Regeneration in such tissues is poorly understood and generally limited, as these cells cannot readily divide.

Even in mammals, various tissues such as the skin, intestinal lining, kidneys, muscles, and parts of the nervous system possess some degree of regenerative potential. While regeneration is a highly orchestrated process, it often begins with a burst of cell division, frequently driven by the formation of a regenerative structure known as a blastema, which later gives rise to specific cell types through differentiation and spatial patterning.

1.17 Different stem-cell-mediated regeneration

In the *Drosophila* digestive system, researchers have identified five distinct types of region- and organ-specific multipotent adult stem cells: intestinal stem cells (ISCs) in the posterior midgut, hindgut intestinal stem cells (HISCs) located at the midgut-hindgut boundary, renal and nephric

stem cells in the Malpighian tubules, type I gastric stem cells at the foregut–midgut junction, and type II gastric stem cells situated in the middle of the midgut. Although these stem cell types are confined to specific digestive organs, they share several molecular markers and regulatory signaling pathways (Jiang and Edgar, 2011; Zeng, Chauhan and Hou, 2013; Ahmed-De-Prado and Baonza, 2018). Among these varieties of *Drosophila* stem cell-mediated regenerative processes across different tissues, most prominently studied is the midgut ISCs. In the adult midgut, ISCs are responsible for maintaining tissue integrity and driving regeneration. ISCs are activated by injury, proliferate, and differentiate to replenish lost or damaged cells, maintaining tissue homeostasis and enabling regeneration. This process involves complex signaling pathways and interactions between stem cells and their surrounding niche. The discovery of somatic stem cells in adult *Drosophila*, ISCs in the midgut, has made it a valuable model organism for exploring stem cell-driven tissue maintenance and regeneration in adults (Jiang and Edgar, 2011; Fox, Cohen and Smith-Bolton, 2020b). In response to tissue injury or stress, signaling pathways such as JNK, Insulin Receptor (InR), JAK-STAT, EGFR, and Wingless (Wg) play key roles in regulating the proliferative activity of intestinal stem cells (ISCs). Additionally, JNK, InR, and JAK-STAT pathways function in coordination with Notch signaling to control ISC self-renewal and differentiation.

In the adult *Drosophila* midgut, regeneration and epithelial homeostasis are maintained through dynamic feedback mechanisms that respond to tissue stress and damage. When mature enterocytes (ECs) are lost—due to pathogenic infection, ingestion of cytotoxic agents such as bleomycin, paraquat, or dextran sodium sulfate (DSS), or through the targeted expression of pro-apoptotic genes like Reaper—the JNK signaling pathway is activated and the Hippo (Hpo) pathway is suppressed within ECs. This shift induces the production of mitogenic cytokines (Upd family) and EGF-like growth factors, including Spitz (spi), Keren (krn), and Vein (vn) (Wang and Spradling, 2022). These signals activate the Jak/Stat and EGFR/Ras/MAPK pathways in progenitor cells, leading to a dramatic 10- to 100-fold increase in ISC proliferation. In parallel, Jak/Stat signaling also promotes enteroblast (EB) differentiation. Newborn EBs, along with pre-existing ones, rapidly mature into enterocytes and enteroendocrine cells, replenishing the epithelium and repairing the damage. This regenerative response is governed by a feedback mechanism, wherein the extent of cell loss is sensed and translated into signals that regulate stem cell proliferation and

differentiation rates. This model enables the midgut to dynamically balance routine tissue turnover with robust regenerative responses following injury, thereby ensuring long-term tissue integrity and function (Jiang and Edgar, 2011; Zeng, Chauhan and Hou, 2013; Ahmed-De-Prado and Baonza, 2018).

Renal stem cells (RSCs) in the adult *Drosophila* Malpighian tubules (MTs) appear to serve a specialized role in tissue remodeling, rather than in routine cell turnover. While *Drosophila* MTs functionally resemble mammalian kidneys, they have a much simpler structure. Under typical physiological conditions, these tubules show minimal cellular turnover but become susceptible to damage under stress. RSCs are specifically located in the stem cell zone (SCZ)—a region encompassing the ureter and lower tubules—where they make up around 66% of the total cell population yet generally remain in a quiescent state. This segment of the tubule is responsible for reabsorbing approximately 30% of the fluid secreted by the upper tubules and is surrounded by visceral muscles, which regulate fluid movement through peristaltic contractions (Singh and Hou, 2009; Wang and Spradling, 2020). Developmentally, RSCs share a common progenitor origin with *Drosophila* intestinal stem cells (ISCs). Both stem cell types arise from the adult midgut progenitor pool, which is known to extensively remodel the larval midgut during metamorphosis. Interestingly, while this remodeling leaves most of the larval MTs intact, it does replace the large principal cells (PCs) in the lower ureter region with smaller adult PCs. RSCs divide asymmetrically through Notch signaling, producing differentiated daughter cells while the stem cell identity is maintained. However, in the absence of tissue damage, RSCs remain in a quiescent, cell cycle-arrested state. Under normal conditions, adult RSCs contribute very little to cell replacement within the MTs, highlighting their context-dependent activation and suggesting a primary role in damage-induced repair or remodeling rather than ongoing tissue maintenance (Wang and Spradling, 2022).

1.18 Regeneration by the re-entry of cell division

The *Drosophila* imaginal discs are larval structures that develop into various adult structures, such as adult wings and eye tissues. During the larval stage, these cells proliferate and differentiate, and then, during pupation, they undergo metamorphosis, elongate, and form these adult structures. Regeneration in *Drosophila* imaginal discs serves as a prime example of regeneration through

mitotic cell division. Most regeneration studies using imaginal discs have been conducted during early larval development, a stage when the tissue is still undergoing developmental cell division (Bosch, Baguñà and Serras, 2008; Smith-Bolton et al., 2009a; Bergantiños, Corominas and Serras, 2010a). This type of regeneration occurs while the tissue remains in its mitotically active phase, before cell cycle exit, terminal differentiation, and the formation of the mature adult wing. In wing regeneration studies, significant research has been conducted by ablating the imaginal discs early during development, specifically in the third instar larval stage, using both physical and genetic ablation systems. In both approaches, they have observed complete regeneration of the adult wing, highlighting that the tissue's regenerative capacity is highly dependent on the timing of the damage. When damage occurs later, after development has progressed and after metamorphosis, the ability to regenerate is lost. An important innovation in wing disc regeneration research is the use of an *in vivo* genetic ablation system to precisely control both the timing and extent of damage to the wing discs. Researchers utilized the Gal4/UAS system to drive the expression of pro-apoptotic genes and induce targeted apoptosis. To achieve spatial and temporal control of this damage, they incorporated a temperature-sensitive Gal80 repressor (Smith-Bolton et al., 2009a; Fox, Cohen and Smith-Bolton, 2020b, 2020a). We have adapted this type of genetic ablation system to induce apoptosis in the ED in Chapter 4.

These regenerative events are governed by distinct signaling pathways and cellular programs that include stem cell activation, cell fate reprogramming, and tissue remodeling. Several signaling pathways are involved in the regeneration of the wing disc, including JNK, JAK/STAT, and Wingless (Wg) pathways. The JNK pathway is initially activated by wounding and promotes cell migration and wound healing. Subsequently, the JAK/STAT pathway, along with Wg, regulates the proliferation of cells forming the blastema, a structure that will regenerate the missing tissue (Katsuyama et al., 2015a). Furthermore, this pathway also modulates the expression of *Drosophila* insulin-like peptide 8 (*dilp8*), a paracrine signal that plays a critical role in delaying pupariation to accommodate tissue repair. Additionally, the Hippo pathway, regulated by Ft, Ds, and Fj, plays a role in controlling growth and pattern formation during regeneration (Smith-Bolton et al., 2009b; Bergantiños, Corominas and Serras, 2010a; Díaz-García and Baonza, 2013; Hariharan and Serras, 2017; Ahmed-de-Prado, Diaz-Garcia and Baonza, 2018a).

Research on *Drosophila* wing disc regeneration has shown that, following tissue development and maturation, enhancer regions for genes such as *Wg*, *MMP1*, and others become silenced or closed. However, when these mature tissues undergo damage and initiate regeneration, the same enhancer regions become reactivated and remain accessible, thereby supporting tissue regeneration. These enhancers, which serve dual functions, are referred to as damage-responsive, maturity-silenced (DRMS) enhancers. Several DRMS enhancers have been specifically identified in wing regeneration, including those regulating *wg*, *Mmp1*, and *apontic*. However, it remains unknown whether these DRMS enhancers also function in the regeneration of post-mitotic tissues following damage (Smith-Bolton et al., 2009a; Harris et al., 2020).

1.19 Key regulators of mitotic re-entry during regeneration

To understand how the cell cycle is regulated in response to cell loss, we have to examine the signaling pathways that are triggered. Some of the signaling pathways that are upregulated during the *Drosophila* tissue regeneration are briefly discussed below.

The Jun N-terminal kinase (JNK)pathway plays a central role in initiating regeneration in response to tissue damage across multiple *Drosophila* tissues, including the wing imaginal disc and midgut. When the extrinsic factors, tumor necrosis factor (TNF)- Egr/TNFα are activated due to stress, cell death they activate the JNK pathway by activating the TNF receptors (Noselli and Agnes,1999). This further activates the cascade of kinases Msn/JNKKKK, dTAK1/JNKKK, Hep/JNKK and Bsk/JNK. Bsk/JNK phosphorylates the AP-1 transcription factor components Kay/Fos and Jra/Jun. Some of the AP-1 target genes include *unpaired* (*upd*), encoding the *Drosophila* interleukin-6 (IL-6) homolog, and *Matrix metalloprotease 1* (*Mmp1*), encoding a protease that degrades the extracellular matrix (Noselli and Agnes,1999; Tafesh-Edwards and Eleftherianos, 2020b; Herrera and Bach, 2021).

Upon injury, JNK is rapidly activated in cells near the wound site, where it activates apoptosis in damaged cells and triggers apoptosis-induced proliferation (AiP) in adjacent surviving cells. JNK activation leads to the induction of mitogenic factors such as wingless (Wg) and decapentaplegic (Dpp), which are critical for regenerative outgrowth and re-patterning (Bergantiños, Corominas and Serras, 2010b; Smith-Bolton, 2016). In the wing disc, this response is essential to stimulate

compensatory cell proliferation and initiate a successful regenerative program. In the midgut, JNK activation in enterocytes promotes the production of cytokines (Upd) and EGFs that stimulate intestinal stem cell (ISC) proliferation. JNK can also activate Jak/STAT signaling (Blanco *et al.*, 2010; Ahmed-de-Prado, Diaz-Garcia and Baonza, 2018b).

Wg/Wnt signaling is essential for both development and regeneration in imaginal discs. Upon damage, Wg is reactivated in the regenerating epithelium and works in coordination with JNK, leads to upregulation of molecules involved in wound healing, such as Mmp1. In the regenerating wing disc, Wg expression is one of the earliest responses to injury, helping establish the regenerative blastema and re-patterning of the tissue (Smith-Bolton et al., 2009b).

The Janus kinase/signal transducer and activator of transcription (JAK/STAT) pathway mediates regeneration by controlling stem cell proliferation and differentiation. The Jak/STAT signaling pathway promotes transcriptional activity in response to growth factors and is known for its quick transcriptional response time. In *Drosophila*, this pathway consists of three ligands (Upd, Upd2, and Upd3) which can bind to a transmembrane receptor (Domeless) and activate the Jak. Jak promotes the translocation of STAT93E, a transcription factor, to the nucleus. This signaling pathway has been implicated in many models of damage-induced proliferation and has been shown to induce mitosis in the intestinal stem cells (Zeidler, Bach and Perrimon, no date; Zeidler and Bausek, 2013; Herrera and Bach, 2019; Cohen et al., 2021). In damaged midguts, Unpaired cytokines secreted by stressed or dying cells activate JAK/STAT pathway in ISCs, leading to rapid tissue renewal. Similarly, in the wing disc, JAK/STAT acts downstream of JNK to promote regenerative proliferation and also controls the expression of Dilp8, which modulates developmental timing in response to tissue stress (Katsuyama et al., 2015a; Ahmed-de-Prado, Diaz-Garcia and Baonza, 2018a).

The Hippo pathway restricts tissue growth by inhibiting Yorkie (Yki), a transcriptional co-activator that drives expression of pro-growth and anti-apoptotic genes. Upon injury, local inactivation of the Hippo pathway allows Yorkie activation, which is required for regenerative proliferation in tissues like the wing disc and midgut. This pathway also interacts with JNK and EGFR signaling to coordinate the regeneration process (Shaw et al., 2010; Besen-McNally, Gjelsvik and Losick, 2021)

1.20 Regeneration in tissues that have permanently exited mitosis

Many tissues respond to stress-induced apoptosis by initiating regenerative programs to restore tissue mass and function. In mitotically active tissues, as discussed earlier involves compensatory cellular proliferation (CCP), where either resident stem cells or surrounding progenitor cells divide to replace the lost cells (Tamori and Deng, 2014; Xia et al., 2018b; de Morree and Rando, 2023b). However, post-mitotic tissues such as the heart, kidneys, cornea, bladder, and brain are composed of cells that have permanently exited the cell cycle during development and possess little to no regenerative stem cell populations. Understanding how these post-mitotic tissues respond to injury, maintain structural integrity, and restore function remains a major challenge in regenerative biology. A significant limitation in addressing this question is the lack of robust post-mitotic model systems that allow experimental manipulation and observation of damage and recovery dynamics. *Drosophila* is an effective model for investigating regenerative processes in tissues that have exited the cell cycle. The ovarian follicular epithelium (FE) in *Drosophila*, which becomes post-mitotic after stage 7, exemplifies such a tissue. Research has shown that even in this non-dividing epithelium, abnormal mutant cells can be selectively removed by surrounding healthy cells through a process known as cell competition. When this competitive mechanism is activated in the post-mitotic FE, the losing cells undergo apoptosis and are cleared after this loss of cells, tissue compensates for cell loss despite the absence of cell proliferation. Interestingly, during this cell competition, neighboring wild-type cells do not divide to replace the eliminated ones. Instead, they undergo compensatory cellular hypertrophy (CCH) a growth response where individual cells enlarge to fill the space. One key regulator of this hypertrophic growth and endoreplication is the Insulin/IGF-like signaling (IIS) pathway. In follicular cells undergoing CCH by endocycles, elevated IIS activity was observed, when IIS signaling was inhibited, it suppressed the endocycling and CCH response (Tamori and Deng, 2013, 2014).

Another example of a *Drosophila* post-mitotic tissue, the adult abdominal epithelium, shows a similar repair mechanism: after being punctured and wounded with a sharp needle, it undergoes tissue repair through cellular hypertrophy during the wound-healing process in the quiescent epithelium. The epithelial integrity was restored in the wound site within 2 days. During the wound healing process, the epithelial cells fused to form a giant syncytium containing many (about 60–120) nuclei that covered the entire region of the wound-induced site. At the same time, within 24 hours after wounding, the quiescent epithelial cells located close to the wound re-entered S phase,

and no increase in epithelial cell number was detected during wound healing. As a result of endocycling cells had increased DNA content. This response to damage was known as wound-induced polyploidization (WIP) (Losick, Fox and Spradling, 2013; Besen-McNally, Gjelsvik and Losick, 2021).

Another example of polyploidy-driven tissue repair in *Drosophila* involves the adult pylorus. In this model, diploid cells that have exited the mitotic cycle respond to injury by entering the endocycle. Notably, the regenerative mechanism employed by the pyloric cells depends on their developmental stage. Prior to full maturation, these cells regenerate through mitotic proliferation. However, once the tissue matures and mitosis is no longer an option, the cells shift to endocycling as a means of regeneration, indicating the presence of a developmental timer that dictates which regenerative strategy is utilized (Cohen, E et al, 2021).

1.21 Developmental timing plays an important role in regeneration

Across the lifespan of most organisms, regenerative capacity tends to shift, often declining with age. As organisms grow older, many tissues experience a gradual loss of homeostasis and regenerative potential, leading to degeneration, impaired function, and disease. There are age-related changes in regenerative ability across different species and in different tissues. In numerous species, regenerative ability diminishes as the organism advances through developmental stages (Yun, 2015). For instance, the hind limbs of the amphibian Xenopus laevis show a gradual reduction in their ability to regenerate following amputation as tadpoles transition into juvenile stages. Similarly, neonatal mice can fully regenerate damaged heart tissue, but this capacity is lost just a week after birth, at which point injuries lead to fibrosis and scarring instead (Porrello *et al.*, 2011, 2013). This marked decline in regenerative potential with increasing maturity is well documented across a variety of mammalian tissues as well as in humans and is also seen in amphibians and invertebrates (Katsuyama *et al.*, 2015b; Harris *et al.*, 2020). Thus, the developmental timing and age play an important role in the ability of the tissue to regenerate. In my thesis, Chapter 4, I will be exploring the hypothesis that increased cell cycle plasticity in younger tissues enables postmitotic ED secretory cells to restore tissue function after ablating a portion of cells.

1.22 Thesis Overview

Previous studies have established that the *Drosophila* ejaculatory duct (ED) plays a central role in producing seminal fluid proteins (SFPs) and antimicrobial peptides, as well as in mixing and transferring sperm and secretions during copulation. In this work, we report for the first time that the secretory cells of the ED, which are responsible for peptide secretion, are post-mitotic and undergo a variant cell cycle known as endocycling. This thesis investigates the development, cellular architecture, regulation of endocycling, and regenerative responses of the ED.

Chapter 2 focuses on the characterization of cell cycle dynamics in ED secretory cells, particularly the early endocycling events occurring during the first three days post-eclosion. This period contributes significantly to tissue growth and development. As a result of this early endocycling, cells reach ploidy levels ranging from 8C to 32C. Through detailed molecular and genetic analysis, this study explores how canonical cell cycle regulators including E2F1, CycE/Cdk2, Dacapo, and Geminin coordinate to promote polyploidization and support the high biosynthetic demand of secretory cells. This variant cell cycle leads to increased cell size and DNA content, which facilitates the elevated protein synthesis required for ED function. Furthermore, this chapter demonstrates that juvenile hormone (JH) signaling plays a critical role in driving this post-eclosion endocycling in ED secretory cells.

Chapter 3 presents the development and optimization of a flow cytometry protocol specifically tailored for isolating and analyzing polyploid and diploid nuclei from the ED and accessory glands (AG). This method improves upon prior DAPI-based imaging by enabling quantitative ploidy analysis across thousands of nuclei with minimal tissue input. It allows precise detection of distinct ploidy states (ranging from 4C to 64C) and their modulation under genetic perturbations, such as CycE/Cdk2 overexpression, stabilized Geminin, or Rbf mutations that affect endocycle progression.

Chapter 4 explores the ED as a genetically tractable model for studying post-mitotic regeneration and cell cycle plasticity. We demonstrate that in response to cell loss, the window for endocycling in the young adult ED is transiently extended, enabling post-mitotic polyploid cells to restore tissue mass through compensatory endocycles and recover fertility function. As the tissue matures, however, this regenerative capacity declines, suggesting that regulators of endocycle exit and quiescence restrict recovery in aged tissues.

Collectively, this thesis establishes the *Drosophila* ED as a robust, physiologically relevant model for dissecting the relationship between polyploidy, secretory function, and regenerative potential. By integrating optimized flow cytometry with powerful *in vivo* genetic tools, this work provides new insights into post-mitotic growth regulation and tissue recovery mechanisms, with broad implications for understanding regeneration in non-proliferative tissues across species.

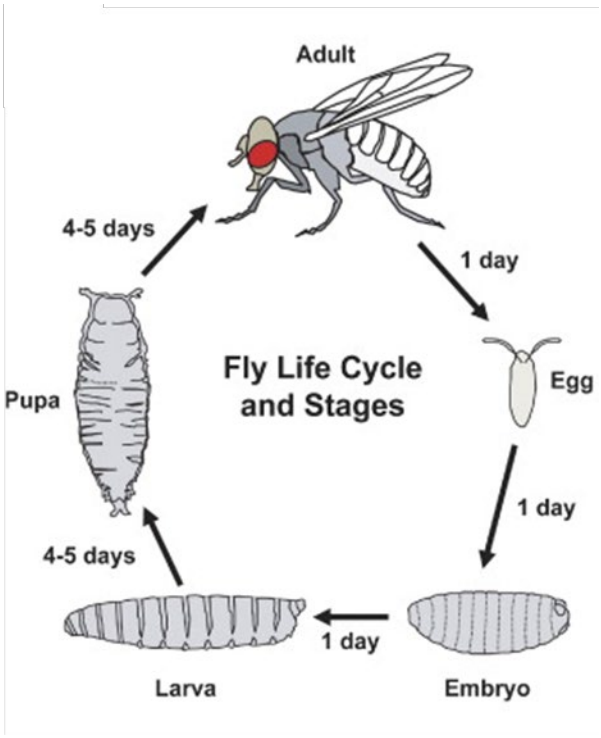


Figure 1.1: *Drosophila melanogaster* life cycle with the stages of development.

Image from: (Wolf, 2012)

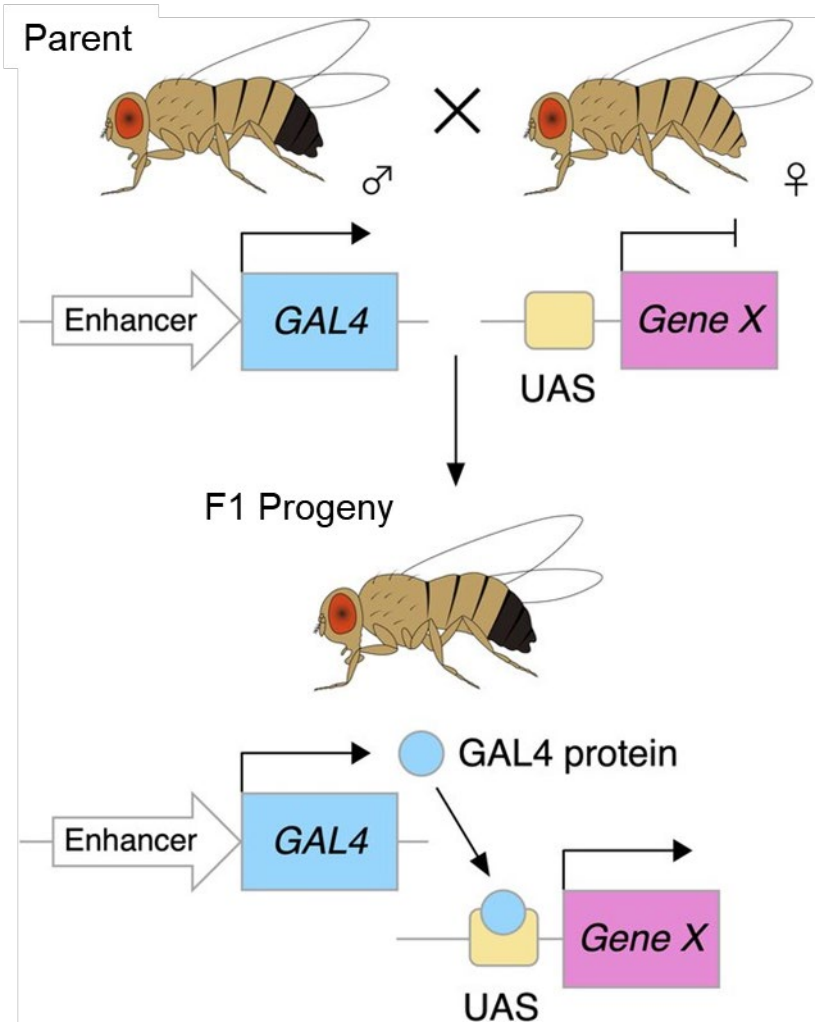


Figure 1.2: The GAL4/UAS system for regulating transgene in *Drosophila*.

This system consists of 2 parts: the yeast transcription factor GAL4, driven by cell type-specific or tissue-specific enhancer/promoter, and its target *UAS*. Crossing parent flies carrying either *Enhancer-GAL4* or *UAS-X* produces F1 offspring with *X* induction specifically in cells or tissues of interest.

Image from: (Yamamura, Ooshio and Sonoshita, 2021)

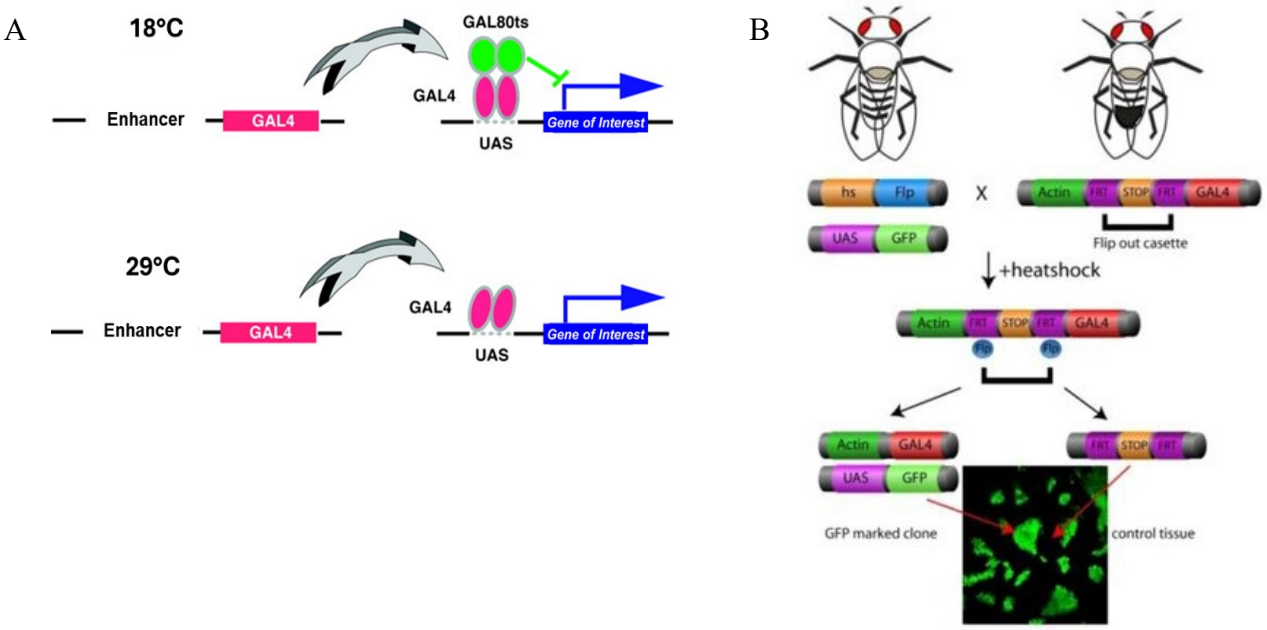


Figure 1.3: (A) Schematic illustrating the temperature-sensitive Gal80^{ts} system.

In the conventional GAL4/UAS system, the GAL4 coding region drives the expression of GAL4 protein in a specific tissue. GAL4 protein then binds to its cognate UAS binding site and activates transcription of the downstream effector gene. At lower temperature of around 18°C Gal80^{ts}, a temperature-sensitive GAL80 protein is expressed ubiquitously and it represses the transcriptional activity of GAL4 at and thus prevents the expression of the UAS-gene of interest but Gal80 becomes inactive at 30°C, allowing GAL4 to drive the expression of the UAS-gene of Interest.

Image modified from (McGuire, Roman and Davis, 2004b)

(B)The FLP/FRTsystem. Heat shock induces FLP expression from hsFlp and this FLP removes the intervening stop sequence from the construct. The actin promoter drives GAL4 for UAS-transgene expression in clones, including UAS-GFP to mark the clone.

Image from : (Amanda Lee *et al.*, 2012)

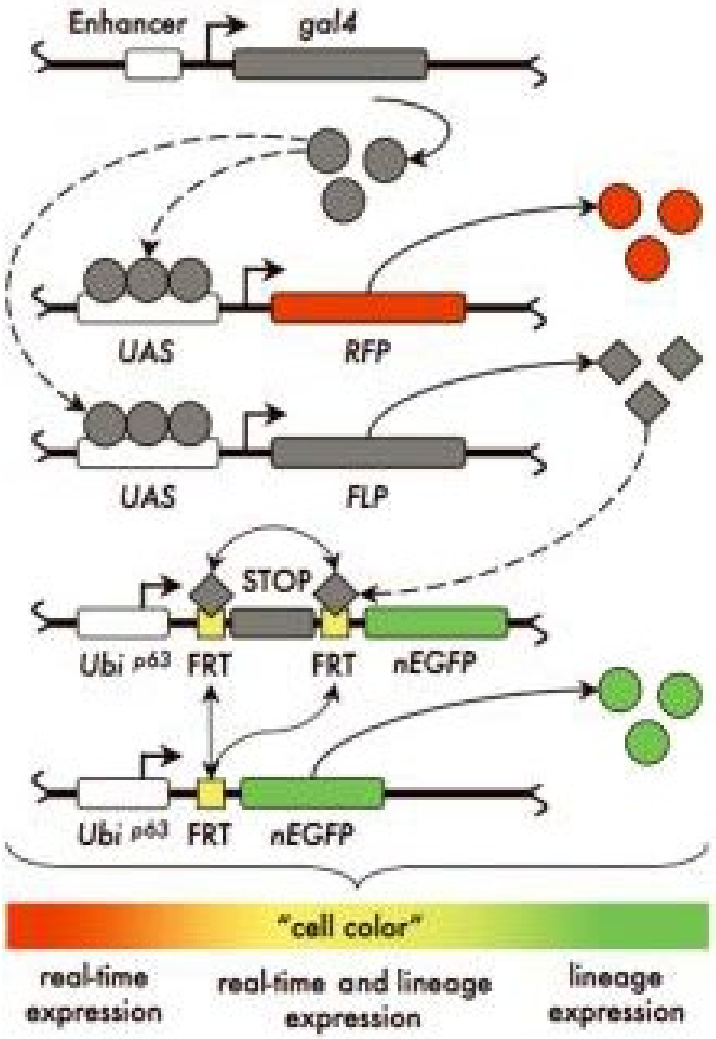


Figure 1.4: The G-TRACE analysis system.

A) Schematic depicting molecular mechanisms underlying the G-TRACE system. Gal4 activates the expression of RFP and FLP recombinase. Cells expressing FLP then excise the FRT-flanked STOP cassette separating the Ubi-p63E promoter and nEGFP open reading frame. This initiates expression of EGFP, which is heritably maintained in all daughter cells. The "cell color" gradient represents the apparent color of cells subsequent to the initiation of Gal4 expression.

Image from: (Evans *et al.*, 2009)

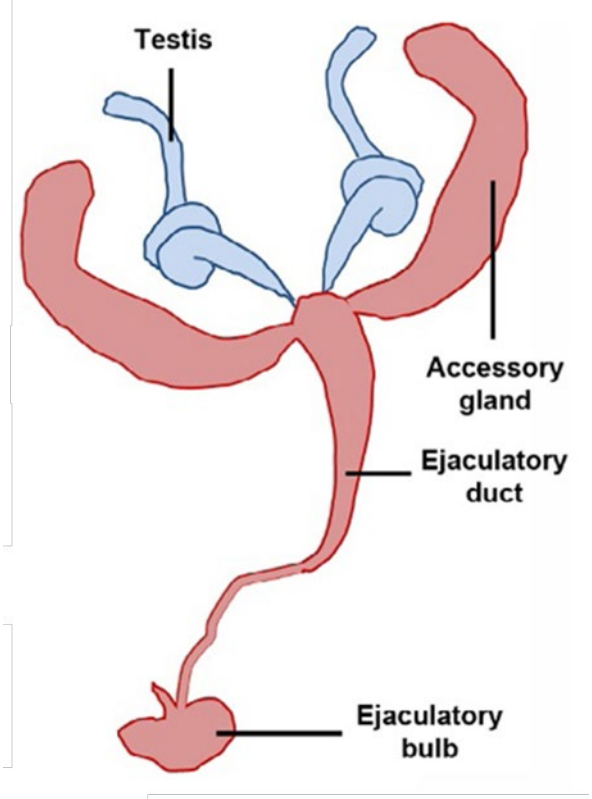


Figure 1.5: The adult *Drosophila melanogaster* male reproductive system.

A cartoon diagram of the *Drosophila* prostate, which includes testis, two accessory gland lobes, the ejaculatory duct, and the ejaculatory bulb. Image From: (Wilson *et al.*, 2017)

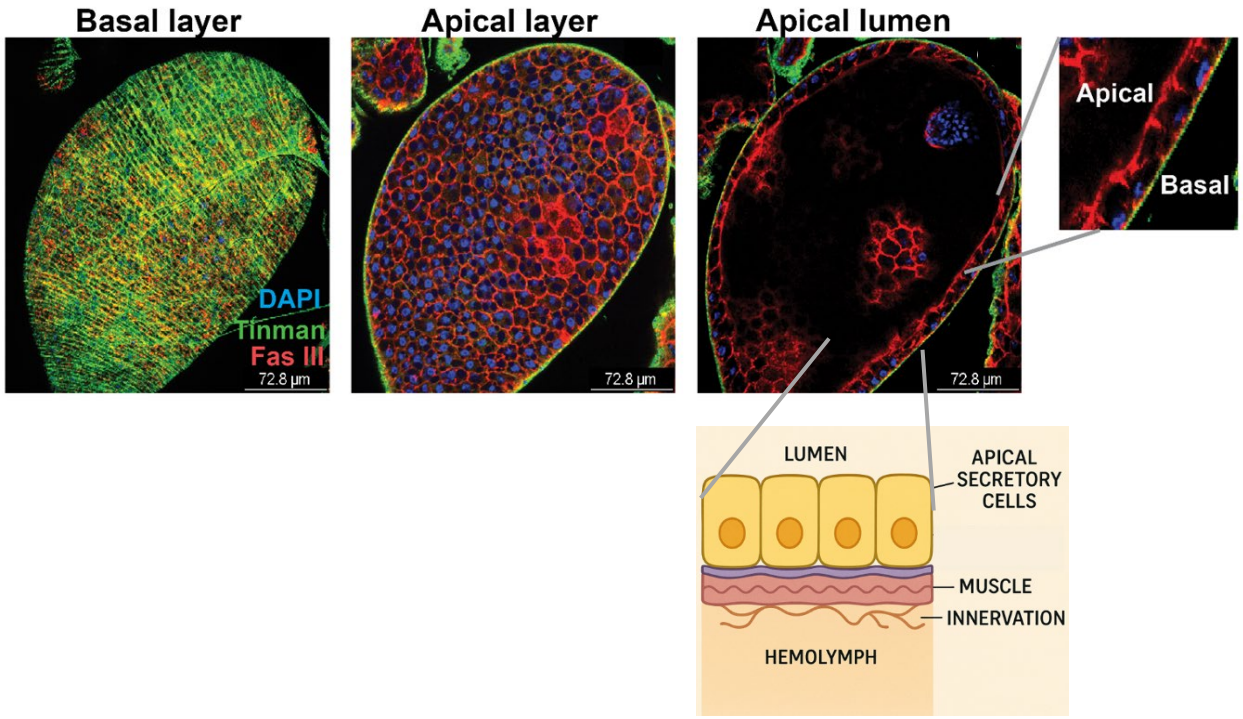


Figure 1.6: Confocal micrographs of ED with different fluorescent labeling to differentiate basal and Apical layer.

ED epithelium is surrounded basally with innervated striated muscles here we have stained with the muscle cell-specific marker Tinman (Green). Apically ED has a monolayer of secretory epithelial cells with larger nuclei expressing the epithelial cell-cell junction marker Fasciclin III (FasIII in Red), forming a lumen apically. Nuclei is stained with DAPI (Blue). Zoomed in image showing the apical and basal side of ED. A cartoon is a representation of ED Basal, apical membrane and lumen and the tissue externally exposed to Hemolymph.

Image source. (Ramesh, Box and Buttitta, 2025)

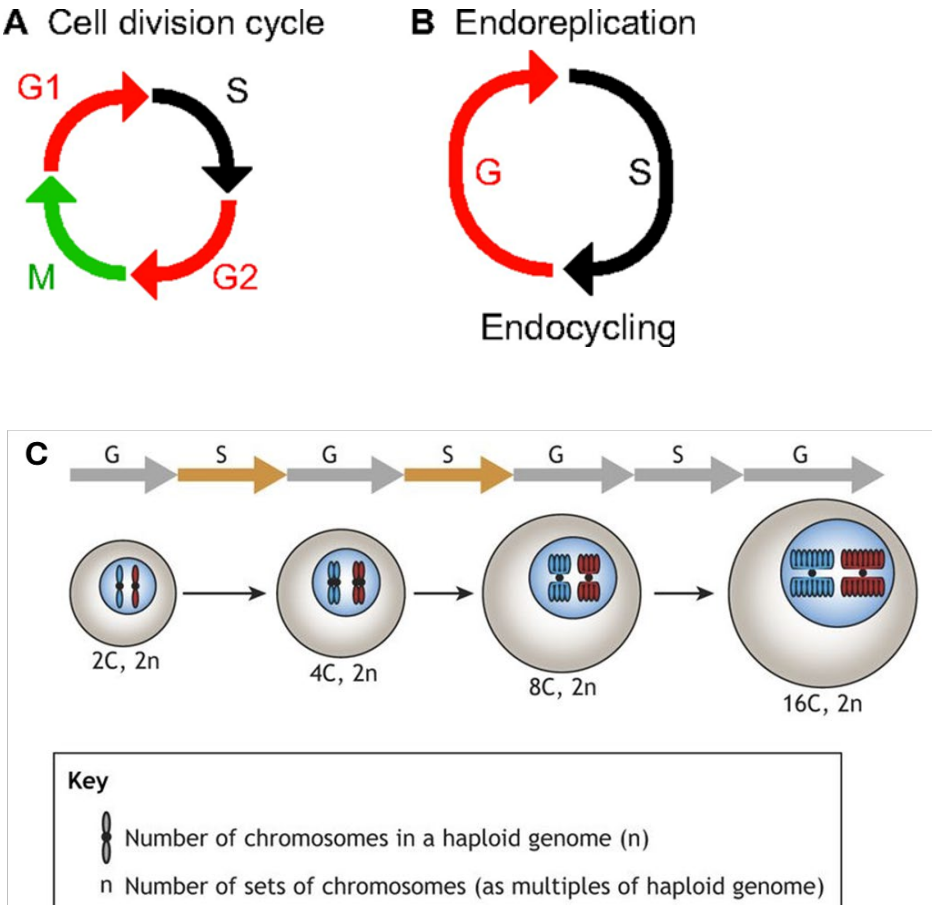


Figure 1.7: Different Cell cycles

(**A**) A canonical cell division cycle consists of four distinct phases. Chromosomes are duplicated during S phase and segregated to daughter cells during M phase. (**B**) Endoreplication or endocycling in which periods of S and G phase alternate with no cell division. Image from:(Fox and Duronio, 2013b)

(C) Endocycling cells lack M phase altogether, resulting in a two-phase cell cycle consisting of alternating G and S phases. Based on number of multiple rounds of endocycling they will have respective copies of DNA.

Image from: (Øvrebø and Edgar, 2018b)

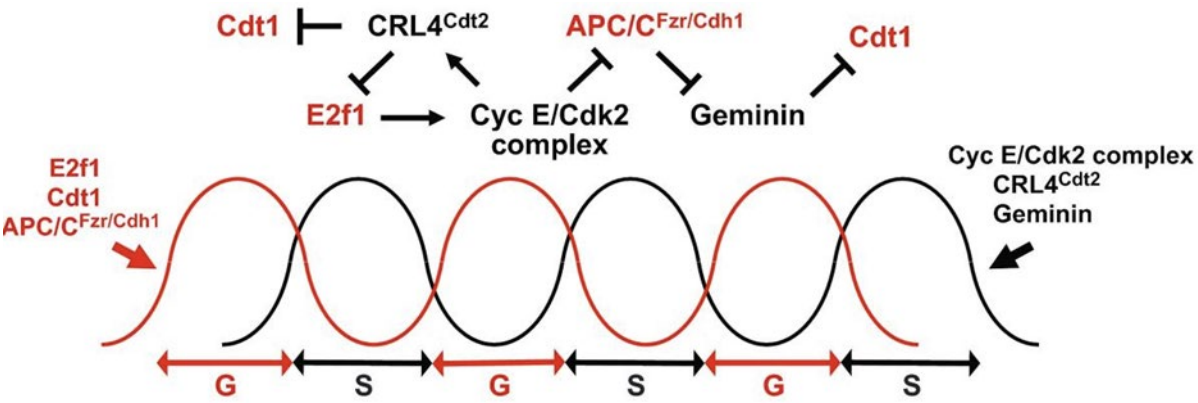


Figure 1.8: Oscillation of cell cycle regulators during endoreplication

The core regulatory relationships between E2f1, Cyclin E and CRL4Cdt2 (top) give rise to out-of-phase oscillations in the activity of key regulatory proteins controlling S phase (bottom). E2f1, APCFzr/Cdh1 and Cdt1 (red) are active during G phase, whereas the Cyclin E/Cdk2 complex, CRL4Cdt2 and Geminin (black) are active during S phase. Note that CRL4Cdt2 activity is dependent on DNA replication, which is triggered by the Cyclin E/Cdk2 complex, and that Cdt1 is inhibited both by Geminin binding and CRL4Cdt2-mediated destruction.

Image from: (Fox and Duronio, 2013b)

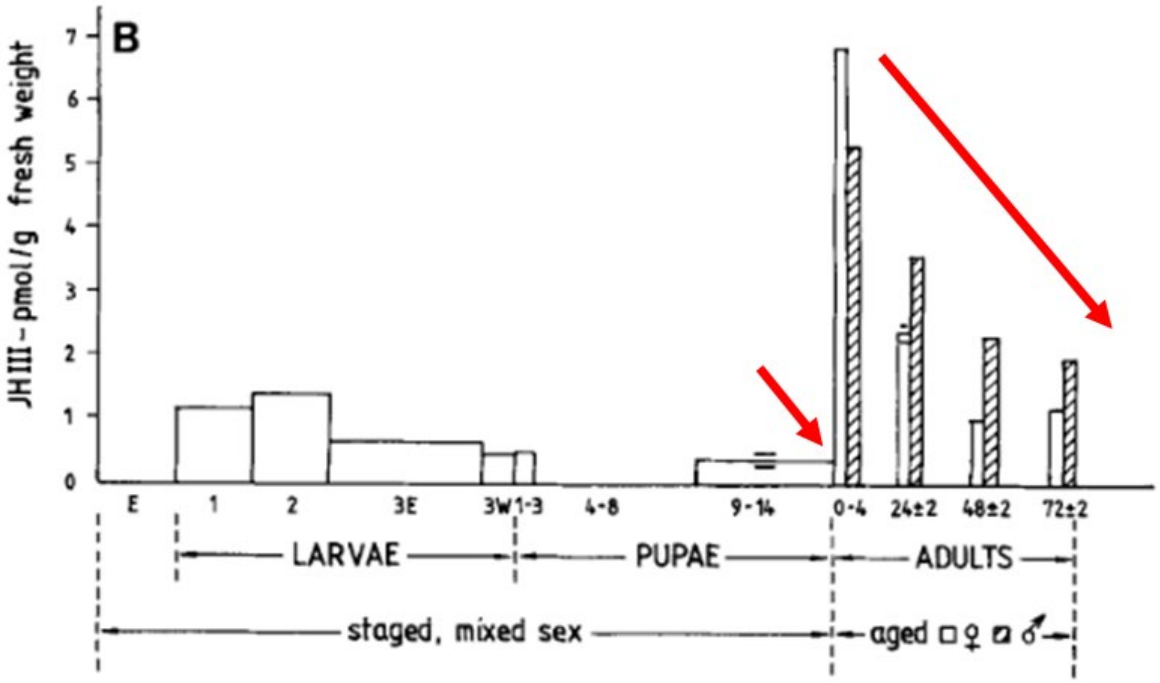


Figure 1.9:The titer of Juvenile hormone in both males and females across during development. On the day of eclosion the level of JH is higher in both male and female flies (Shown in small red arrow). JH levels decrease after 24 hrs post eclosion of flies.

Image from: (BOWNES and REMBOLD, 1987)

1.23 Bibliography

Abdou, M.A. *et al.* (2011) 'Drosophila Met and Gce are partially redundant in transducing juvenile hormone action', *Insect Biochemistry and Molecular Biology*, 41(12), pp. 938–945. Available at: https://doi.org/10.1016/j.ibmb.2011.09.003.

Acquaviva, C. and Pines, J. (2006) 'The anaphase-promoting complex/cyclosome: APC/C', *Journal of Cell Science*, 119(12), pp. 2401–2404. Available at: https://doi.org/10.1242/jcs.02937.

Adams, M.D. *et al.* (no date) *The Genome Sequence of Drosophila melanogaster*. Available at: https://www.science.org.

Ahmed-De-Prado, S. and Baonza, A. (2018) 'Drosophila as a model system to study cell signaling in organ regeneration', *BioMed Research International*. Hindawi Limited. Available at: https://doi.org/10.1155/2018/7359267.

Ahmed-de-Prado, S., Diaz-Garcia, S. and Baonza, A. (2018a) 'JNK and JAK/STAT signalling are required for inducing loss of cell fate specification during imaginal wing discs regeneration in Drosophila melanogaster', *Developmental Biology*, 441(1), pp. 31–41. Available at: https://doi.org/10.1016/j.ydbio.2018.05.021.

Ahmed-de-Prado, S., Diaz-Garcia, S. and Baonza, A. (2018b) 'JNK and JAK/STAT signalling are required for inducing loss of cell fate specification during imaginal wing discs regeneration in Drosophila melanogaster', *Developmental Biology*, 441(1), pp. 31–41. Available at: https://doi.org/10.1016/j.ydbio.2018.05.021.

Allocca, M., Zola, S. and Bellosta, P. (2018) 'The Fruit Fly, Drosophila melanogaster: The Making of a Model (Part I)', in *Drosophila melanogaster - Model for Recent Advances in Genetics and Therapeutics*. InTech. Available at: https://doi.org/10.5772/intechopen.72832.

Almeida Machado Costa, C. *et al.* (2022) 'Polyploidy in development and tumor models in Drosophila', *Seminars in Cancer Biology*. Academic Press, pp. 106–118. Available at: https://doi.org/10.1016/j.semcancer.2021.09.011.

Amanda Lee, J.E. *et al.* (2012) 'Genetic systems to investigate regulation of oncogenes and tumour suppressor genes in Drosophila', *Cells*. MDPI, pp. 1183–1196. Available at: https://doi.org/10.3390/cells1041182.

Arias, E.E. and Walter, J.C. (2006) 'PCNA functions as a molecular platform to trigger Cdt1 destruction and prevent re-replication', *Nature Cell Biology*, 8(1), pp. 84–90. Available at: https://doi.org/10.1038/ncb1346.

Ashburner M, (1989) 'Drosophila; A laboratory handbook', *Cold Spring Harbor Press*.

Atwood, C.S. and Bowen, R.L. (2015) 'The endocrine dyscrasia that accompanies menopause and andropause induces aberrant cell cycle signaling that triggers re-entry of post-mitotic neurons into the cell cycle, neurodysfunction, neurodegeneration and cognitive disease', *Hormones and Behavior*. Academic Press Inc., pp. 63–80. Available at: https://doi.org/10.1016/j.yhbeh.2015.06.021.

Basumatary, D. and Deka, N. (2024) 'Comprehensive study on the life cycle, morphology, and culturing techniques of Drosophila melanogaster in laboratory conditions', *International Journal of Entomology Research*. Available at: www.entomologyjournals.com.

Baumann, A. *et al.* (2010a) 'Paralogous genes involved in juvenile hormone action in Drosophila melanogaster', *Genetics*, 185(4), pp. 1327–1336. Available at: https://doi.org/10.1534/genetics.110.116962.

Baumann, A. *et al.* (2010b) 'Paralogous genes involved in juvenile hormone action in Drosophila melanogaster', *Genetics*, 185(4), pp. 1327–1336. Available at: https://doi.org/10.1534/genetics.110.116962.

Baumann, A.A. *et al.* (2017) 'Genetic tools to study juvenile hormone action in Drosophila', *Scientific Reports*, 7(1). Available at: https://doi.org/10.1038/s41598-017-02264-4.

Bellosta, P. and Gallant, P. (2010) 'Myc function in Drosophila', *Genes and Cancer*. SAGE Publications Inc., pp. 542–546. Available at: https://doi.org/10.1177/1947601910377490.

Benjamin, J.M. *et al.* (2004) 'Geminin has dimerization, Cdt1-binding, and destruction domains that are required for biological activity', *Journal of Biological Chemistry*, 279(44), pp. 45957–45968. Available at: https://doi.org/10.1074/jbc.M407726200.

Bergantiños, C., Corominas, M. and Serras, F. (2010a) 'Cell death-induced regeneration in wing imaginal discs requires JNK signalling', *Development*, 137(7), pp. 1169–1179. Available at: https://doi.org/10.1242/dev.045559.

Bergantiños, C., Corominas, M. and Serras, F. (2010b) 'Cell death-induced regeneration in wing imaginal discs requires JNK signalling', *Development*, 137(7), pp. 1169–1179. Available at: https://doi.org/10.1242/dev.045559.

Bertram, M.J. *et al.* (1992) *Cell type-specific gene expression in the Drosophila melanogaster male accessory gland*, *Mechanisms of Development*.

Besen-McNally, R., Gjelsvik, K.J. and Losick, V.P. (2021) 'Wound-induced polyploidization is dependent on Integrin-Yki signaling', *Biology Open*, 10(1). Available at: https://doi.org/10.1242/bio.055996.

Blanco, E. *et al.* (2010) 'Gene expression following induction of regeneration in Drosophila wing imaginal discs. Expression profile of regenerating wing discs', *BMC Developmental Biology*, 10. Available at: https://doi.org/10.1186/1471-213X-10-94.

Blank, H.M., No, E.G. and Polymenis, M. (2025) 'Cdk activation by phosphorylation: linking growth signals to cell cycle control', *Biochemical Society transactions*. Available at: https://doi.org/10.1042/BST20253004.

Bosch, M., Baguñà, J. and Serras, F. (2008) 'Origin and proliferation of blastema cells during regeneration of Drosophila wing imaginal discs', *International Journal of Developmental Biology*, 52(8), pp. 1043–1050. Available at: https://doi.org/10.1387/ijdb.082608mb.

BOWNES, M. and REMBOLD, H. (1987) 'The titre of juvenile hormone during the pupal and adult stages of the life cycle of Drosophila melanogaster', *European Journal of Biochemistry*, 164(3), pp. 709–712. Available at: https://doi.org/10.1111/j.1432-1033.1987.tb11184.x.

Box, Allison M *et al.* (2024) ‘Cell cycle variants during *Drosophila* male accessory gland development’, *G3: Genes, Genomes, Genetics* [Preprint]. Available at: https://doi.org/10.1093/g3journal/jkae089.

Box, Allison M. *et al.* (2024) ‘Cell cycle variants during Drosophila male accessory gland development’, *G3: Genes, Genomes, Genetics*, 14(7). Available at: https://doi.org/10.1093/g3journal/jkae089.

Brand, H. and Perrimon, N. (1993) ‘Targeted gene expression as a means of altering cell fates and generating dominant phenotypes’, *Development*, 118(2):401-15. Available at: https://doi.org/10.1242/dev.118.2.401

Braun, R.P. and Wyatt, G.R. (1995) ‘Growth of the Male Accessory Gland in Adult locusts: Roles of Juvenile Hormone, JH Esterase, and JH Binding Proteins’, *Archives of Insect Biochemistry and Physiology.*

Bretman, A. *et al.* (2023) ‘Playing to the crowd: Using Drosophila to dissect mechanisms underlying plastic male strategies in sperm competition games’, in *Advances in the Study of Behavior*. Academic Press Inc., pp. 1–35. Available at: https://doi.org/10.1016/bs.asb.2022.11.001.

Buckley, C.E. and St Johnston, D. (2022) ‘Apical–basal polarity and the control of epithelial form and function’, *Nature Reviews Molecular Cell Biology*. Nature Research, pp. 559–577. Available at: https://doi.org/10.1038/s41580-022-00465-y.

Buttitta, L.A. and Edgar, B.A. (2007a) ‘Mechanisms controlling cell cycle exit upon terminal differentiation’, *Current Opinion in Cell Biology*, pp. 697–704. Available at: https://doi.org/10.1016/j.ceb.2007.10.004.

Buttitta, L.A. and Edgar, B.A. (2007b) ‘Mechanisms controlling cell cycle exit upon terminal differentiation’, *Current Opinion in Cell Biology*, pp. 697–704. Available at: https://doi.org/10.1016/j.ceb.2007.10.004.

Cadart, C. and Heald, R. (2022) ‘Scaling of biosynthesis and metabolism with cell size’, *Molecular Biology of the Cell*, 33(9). Available at: https://doi.org/10.1091/mbc.E21-12-0627.

Calvi, B.R., Lilly, M.A. and Spradling, A.C. (1998) *Cell cycle control of chorion gene amplification*. Available at: www.genesdev.org.

Cao, Y. *et al.* (2022) ‘Identification of enhancer regulatory elements that direct epicardial gene expression during zebrafish heart regeneration’, *Development (Cambridge)*, 149(4). Available at: https://doi.org/10.1242/dev.200133.

Cavener, D.R. (1985) ‘Coevolution of the Glucose Dehydrogenase Gene and the Ejaculatory Duct in the Genus *Drosophila’*. *Mol Biol Evol*. Available at: https://academic.oup.com/mbe/article/2/2/141/1220396.

Banerjee S. *et al* (2006) ‘Organization and Function of Septate Junctions’. *Cell Biochemistry and Biophysics*

Chapman, T. *et al.* (2003) *The sex peptide of Drosophila melanogaster: Female post-mating responses analyzed by using RNA interference*. Available at: www.pnas.orgcgidoi10.

Cheung, T.H. and Rando, T.A. (2013) ‘Molecular regulation of stem cell quiescence’, *Nature Reviews Molecular Cell Biology*, pp. 329–340. Available at: https://doi.org/10.1038/nrm3591.

Choudhury, D. *et al.* (2024) ‘Polyploidy and mTOR signaling: a possible molecular link’, *Cell Communication and Signaling* . BioMed Central Ltd. Available at: https://doi.org/10.1186/s12964-024-01526-9.

Church, S.J. *et al.* (2025) ‘Evidence for Transcriptomic Conservation Between the Main Cells of the *Drosophila* Prostate-Like Accessory Gland and Basal Cells of the Mammalian Prostate’. Available at: https://doi.org/10.1101/2025.06.05.658085.

Cohen, E. *et al.* (2021) ‘Accelerated cell cycles enable organ regeneration under developmental time constraints in the Drosophila hindgut’, *Developmental Cell*, 56(14), pp. 2059-2072.e3. Available at: https://doi.org/10.1016/j.devcel.2021.04.029.

Cohen, E. and Moussian, B. (2016a) *Extracellular composite matrices in arthropods*, *Extracellular Composite Matrices in Arthropods*. Springer International Publishing. Available at: https://doi.org/10.1007/978-3-319-40740-1.

Cohen, E. and Moussian, B. (2016b) *Extracellular composite matrices in arthropods*, *Extracellular Composite Matrices in Arthropods*. Springer International Publishing. Available at: https://doi.org/10.1007/978-3-319-40740-1.

Cohen, E. and Moussian, B. (2016c) *Extracellular composite matrices in arthropods*, *Extracellular Composite Matrices in Arthropods*. Springer International Publishing. Available at: https://doi.org/10.1007/978-3-319-40740-1.

Coller, H.A., Sang, L. and Roberts, J.M. (2006a) ‘A new description of cellular quiescence’, *PLoS Biology*, 4(3), pp. 0329–0349. Available at: https://doi.org/10.1371/journal.pbio.0040083.

Coller, H.A., Sang, L. and Roberts, J.M. (2006b) ‘A new description of cellular quiescence’, *PLoS Biology*, 4(3), pp. 0329–0349. Available at: https://doi.org/10.1371/journal.pbio.0040083.

Cong, B., Ohsawa, S. and Igaki, T. (2018) ‘JNK and Yorkie drive tumor progression by generating polyploid giant cells in Drosophila’, *Oncogene*, 37(23), pp. 3088–3097. Available at: https://doi.org/10.1038/s41388-018-0201-8.

Cox-Foster, D.L. *et al.* (1990) *Developmental Expression of the Glucose Dehydrogenase Gene in Drosophila melanogaster*.

Conway PJ, Dao J, Kovalskyy D, Mahadevan D, Dray E. (2004) ‘Polyploidy in Cancer: Causal Mechanisms, Cancer-Specific Consequences, and Emerging Treatments’, *Mol Cancer Ther*, 2;23(5):638-647.

Croshaw, D.A. and Gómez, M. (2018) ‘Polyandrous mating increases offspring production and lifespan in female Drosophila arizonae’, *Behavioral Ecology and Sociobiology*, 72(11). Available at: https://doi.org/10.1007/s00265-018-2589-0.

Dahal, P and Boore, J L. (2005) ‘Two rounds of whole genome duplication in the ancestral vertebrate’, *Plos Biology*, 3(10): e314. Available at: https://doi.org/10.1371/journal.pbio.0030314.

Date-Ito, A. *et al.* (2002) ‘Rapid evolution of the male-specific antibacterial protein Andropin gene in Drosophila’, *Journal of Molecular Evolution*, 54(5), pp. 665–670. Available at: https://doi.org/10.1007/s00239-001-0062-5.

Dawson, I.A., Roth, S. and Artavanis-Tsakonas, S. (1995) 'The *Drosophila* Cell Cycle Gene fizzy Is Required for Normal Degradation of Cyclins A and B During Mitosis and Has Homology to the CDC20 Gene of Saccharomyces cerevisiae'. *Journal of Cell Bio*, 129(3):725-37.

Díaz-García, S. and Baonza, A. (2013) 'Pattern reorganization occurs independently of cell division during Drosophila wing disc regeneration in situ', *Proceedings of the National Academy of Sciences of the United States of America*, 110(32), pp. 13032–13037. Available at: https://doi.org/10.1073/pnas.1220543110.

Dimov, I. and Maduro, M.F. (2019) 'The C. elegans intestine: organogenesis, digestion, and physiology', *Cell and Tissue Research*. Springer Verlag, pp. 383–396. Available at: https://doi.org/10.1007/s00441-019-03036-4.

Dimova, D.K. *et al.* (2003) 'Cell cycle-dependent and cell cycle-independent control of transcription by the Drosophila E2F/RB pathway', *Genes and Development*, 17(18), pp. 2308–2320. Available at: https://doi.org/10.1101/gad.1116703.

Duronio, R.J. and O'farrell, P.H. (1995) 'Developmental control of the G1 to S transition in Drosophila: cyclin E is a limiting downstream target of E2F',*Genes and Development*, pp.1456-1468.

Dynlacht, B.D. *et al.* (1994) *DNA-binding and trans-activation properties of Drosophila E2F and DP proteins*, *Cell Biology*.

Edgar, B. *et al.* (2018) 'Fizzy-Related dictates A cell cycle switch during organ repair and tissue growth responses in the Drosophila hindgut'. Available at: https://doi.org/10.7554/eLife.38327.001.

Edgar, B.A. and Orr-Weaver, T.L. (2001a) *Endoreplication Cell Cycles: Review More for Less*, *Cell*.

Edgar, B.A. and Orr-Weaver, T.L. (2001b) *Endoreplication Cell Cycles: Review More for Less*, *Cell*.

Edgar, B.A., Zielke, N. and Gutierrez, C. (2014) 'Endocycles: A recurrent evolutionary innovation for post-mitotic cell growth', *Nature Reviews Molecular Cell Biology*, pp. 197–210. Available at: https://doi.org/10.1038/nrm3756.

Evans, C.J. *et al.* (2009) 'G-TRACE: Rapid Gal4-based cell lineage analysis in Drosophila', *Nature Methods*, 6(8), pp. 603–605. Available at: https://doi.org/10.1038/nmeth.1356.

Fagundes, R. and Teixeira, L.K. (2021) 'Cyclin E/CDK2: DNA Replication, Replication Stress and Genomic Instability', *Frontiers in Cell and Developmental Biology*. Frontiers Media S.A. Available at: https://doi.org/10.3389/fcell.2021.774845.

Fang, J. *et al.* (2023) 'Cellular polyploidy in organ homeostasis and regeneration', *Protein and Cell*. Oxford University Press, pp. 560–578. Available at: https://doi.org/10.1093/procel/pwac064.

Fiumera, A.C., Dumont, B.L. and Clark, A.G. (2005) 'Sperm competitive ability in Drosophila melanogaster associated with variation in male reproductive proteins', *Genetics*, 169(1), pp. 243–257. Available at: https://doi.org/10.1534/genetics.104.032870.

Theodosiou A.N., Xu Tian. (1998). 'Use of FLP/FRT System to study *Drosophila* Development', *Methods: A companion to methods in Enzymology*, pp. 355-365.

Follette, P.J. and O'farrell, P.H. (1997) 'Cdks and the Drosophila cell cycle', *Current Opinion in Genetics & Development*, Vol 7(1), pp. 17-22. Available at: https://doi.org/10.1016/S0959-437X(97)80104-9

Fox, D.T., Cohen, E. and Smith-Bolton, R. (2020a) 'Model systems for regeneration: Drosophila', *Development (Cambridge)*, 147(7). Available at: https://doi.org/10.1242/dev.173781.

Fox, D.T., Cohen, E. and Smith-Bolton, R. (2020b) 'Model systems for regeneration: Drosophila', *Development (Cambridge)*, 147(7). Available at: https://doi.org/10.1242/dev.173781.

Fox, D.T. and Duronio, R.J. (2013a) 'Endoreplication and polyploidy: Insights into development and disease', *Development (Cambridge)*, 140(1), pp. 3–12. Available at: https://doi.org/10.1242/dev.080531.

Fox, D.T. and Duronio, R.J. (2013b) 'Endoreplication and polyploidy: Insights into development and disease', *Development (Cambridge)*, 140(1), pp. 3–12. Available at: https://doi.org/10.1242/dev.080531.

Fox, D.T. and Duronio, R.J. (2013c) 'Endoreplication and polyploidy: Insights into development and disease', *Development (Cambridge)*, 140(1), pp. 3–12. Available at: https://doi.org/10.1242/dev.080531.

Fox, D.T., Gall, J.G. and Spradling, A.C. (2010) 'Error-prone polyploid mitosis during normal Drosophila development', *Genes and Development*, 24(20), pp. 2294–2302. Available at: https://doi.org/10.1101/gad.1952710.

Gandarillas, A. and Freije, A. (2014) 'Cycling up the epidermis: Reconciling 100 years of debate', *Experimental Dermatology*, 23(2), pp. 87–91. Available at: https://doi.org/10.1111/exd.12287.

Gandarillas, A., Molinuevo, R. and Sanz-Gómez, N. (2018) 'Mammalian endoreplication emerges to reveal a potential developmental timer', *Cell Death and Differentiation*. Nature Publishing Group, pp. 471–476. Available at: https://doi.org/10.1038/s41418-017-0040-0.

Gerlach, S.U., Eichenlaub, T. and Herranz, H. (2018) 'Yorkie and JNK Control Tumorigenesis in Drosophila Cells with Cytokinesis Failure', *Cell Reports*, 23(5), pp. 1491–1503. Available at: https://doi.org/10.1016/j.celrep.2018.04.006.

Giacinti, C. and Giordano, A. (2006) 'RB and cell cycle progression', *Oncogene*, pp. 5220–5227. Available at: https://doi.org/10.1038/sj.onc.1209615.

Goodman, W.G. and Cusson, M. (2011) 'The Juvenile Hormones', in *Insect Endocrinology*. Elsevier, pp. 310–365. Available at: https://doi.org/10.1016/B978-0-12-384749-2.10008-1.

Gowaty, P.A. *et al.* (2010) 'Polyandry increases offspring viability and mother productivity but does not decrease mother survival in Drosophila pseudoobscura', *Proceedings of the National Academy of Sciences of the United States of America*, 107(31), pp. 13771–13776. Available at: https://doi.org/10.1073/pnas.1006174107.

Gowaty, P.A. (2012) 'The evolution of multiple mating: Costs and benefits of polyandry to females and of polygyny to males', *Fly*, 6(1), pp. 3–11. Available at: https://doi.org/10.4161/fly.18330.

Grifoni, D. and Bellosta, P. (2015) 'Drosophila Myc: A master regulator of cellular performance', *Biochimica et Biophysica Acta - Gene Regulatory Mechanisms*. Elsevier, pp. 570–581. Available at: https://doi.org/10.1016/j.bbagrm.2014.06.021.

Guarner, A. *et al.* (2017) 'E2F/DP Prevents Cell-Cycle Progression in Endocycling Fat Body Cells by Suppressing dATM Expression', *Developmental Cell*, 43(6), pp. 689-703.e5. Available at: https://doi.org/10.1016/j.devcel.2017.11.008.

Gutierrez GJ, Tsuji T, Cross JV, Davis RJ, Templeton DJ, Jiang W, Ronai ZA. (2010) 'JNK-mediated phosphorylation of Cdc25C regulates cell cycle entry and G(2)/M DNA damage checkpoint'. *J Biol Chem*. 7;285(19):14217-28. doi: 10.1074/jbc.M110.121848.

Galitski. T. *et al.* (1999) 'Ploidy Regulation of Gene Expression', *Science*, Vol 285.

Hammond, M.P. and Laird, C.D. (1985) 'Control of DNA replication and spatial distribution of defined DNA sequences in salivary gland cells of *Drosophila melanogaster*', *Chromosoma (Bet1) (1985) 91:279-286* .

Harbour, J.W. and Dean, D.C. (2000) 'The Rb/E2F pathway: Expanding roles and emerging paradigms', *Genes and Development*, pp. 2393–2409. Available at: https://doi.org/10.1101/gad.813200.

Hariharan, I.K. and Serras, F. (2017) 'Imaginal disc regeneration takes flight', *Current Opinion in Cell Biology*. Elsevier Ltd, pp. 10–16. Available at: https://doi.org/10.1016/j.ceb.2017.03.005.

Harold Plough Ai, B.H. and Maurice Strauss, -d B (no date) *E X P E R I M E N T S ON TOLERATION OF T E M P E R A T U R E BY DROSOPHILA. The Journal of General Physiology*.

Harris, R.E. *et al.* (2020) 'Damage-responsive, maturity-silenced enhancers regulate multiple genes that direct regeneration in Drosophila', *eLife*, 9, pp. 1–26. Available at: https://doi.org/10.7554/eLife.58305.

Harrison, D.A. and Perrimon, N. (1993) 'Simple and efficient generation of marked clones in *Drosophila'. Current Biology,* pp.425-433

Harper JW, Burton JL, Solomon MJ. (2002) 'The anaphase-promoting complex: it's not just for mitosis any more', *Genes Dev*. 1;16(17):2179-206.

He, Z. *et al.* (2021) 'Regulation of DNA duplication by the mTOR signaling pathway', *Cell Cycle*. Bellwether Publishing, Ltd., pp. 742–751. Available at: https://doi.org/10.1080/15384101.2021.1897271.

Heim, M.A. *et al.* (2003) 'The basic helix-loop-helix transcription factor family in plants: A genome-wide study of protein structure and functional diversity', *Molecular Biology and Evolution*, 20(5), pp. 735–747. Available at: https://doi.org/10.1093/molbev/msg088.

Herr, A. *et al.* (2012) 'Identification of E2F target genes that are rate limiting for dE2F1-dependent cell proliferation', *Developmental Dynamics*, 241(11), pp. 1695–1707. Available at: https://doi.org/10.1002/dvdy.23857.

Herrera, S.C. and Bach, E.A. (2019) 'JAK/STAT signaling in stem cells and regeneration: From Drosophila to vertebrates', *Development (Cambridge)*, 146(2). Available at: https://doi.org/10.1242/dev.167643.

Herrera, S.C. and Bach, E.A. (2021) 'The emerging roles of jnk signaling in Drosophila stem cell homeostasis', *International Journal of Molecular Sciences*, 22(11). Available at: https://doi.org/10.3390/ijms22115519.

Herriage HC, Huang YT, Calvi BR. (2024) 'The antagonistic relationship between apoptosis and polyploidy in development and cancer'. *Semin Cell Dev Biol*,15;156:35-43.

Hoareau M, Rincheval-Arnold A, Gaumer S, Guénal I. (2024) 'DREAM a little dREAM of DRM: Model organisms and conservation of DREAM-like complexes: Model organisms uncover the mechanisms of DREAM-mediated transcription regulation', *Bioessays*.

Van Den Heuvel, S. and Dyson, N.J. (2008) 'Conserved functions of the pRB and E2F families', *Nature Reviews Molecular Cell Biology*, pp. 713–724. Available at: https://doi.org/10.1038/nrm2469.

Hong, A. *et al.* (2007) 'The cyclin-dependent kinase inhibitor Dacapo promotes replication licensing during Drosophila endocycles', *EMBO Journal*, 26(8), pp. 2071–2082. Available at: https://doi.org/10.1038/sj.emboj.7601648.

Hopkins, B.R. *et al.* (2019) 'BMP signaling inhibition in Drosophila secondary cells remodels the seminal proteome and self and rival ejaculate functions',*PNAS*. Available at: https://doi.org/10.5287/bodleian:nb20wgNw8.

Hua, B.L. and Orr-Weaver, T.L. (2017) 'DNA replication control during Drosophila development: Insights into the onset of S phase, replication initiation, and fork progression', *Genetics*, 207(1), pp. 29–47. Available at: https://doi.org/10.1534/genetics.115.186627.

Jiang, H. and Edgar, B.A. (2011) 'Intestinal stem cells in the adult Drosophila midgut', *Experimental Cell Research*. Academic Press Inc., pp. 2780–2788. Available at: https://doi.org/10.1016/j.yexcr.2011.07.020.

Jindra, M., Palli, S.R. and Riddiford, L.M. (2013) 'The juvenile hormone signaling pathway in insect development', *Annual Review of Entomology*, pp. 181–204. Available at: https://doi.org/10.1146/annurev-ento-120811-153700.

Johnston, L.A. *et al.* (1999) 'Drosophila myc regulates cellular growth during development', *Cell*, 98(6), pp. 779–790. Available at: https://doi.org/10.1016/S0092-8674(00)81512-3.

Jouandin, P., Ghiglione, C. and Noselli, S. (2014) 'Starvation induces FoxO-dependent mitotic-to-endocycle switch pausing during Drosophila oogenesis', *Development (Cambridge)*, 141(15), pp. 3013–3021. Available at: https://doi.org/10.1242/dev.108399.

Kapanidou, M., Curtis, N.L. and Bolanos-Garcia, V.M. (2017) 'Cdc20: At the Crossroads between Chromosome Segregation and Mitotic Exit', *Trends in Biochemical Sciences*. Elsevier Ltd, pp. 193–205. Available at: https://doi.org/10.1016/j.tibs.2016.12.001.

Katsuyama, T. *et al.* (2015a) 'During Drosophila disc regeneration, JAK/STAT coordinates cell proliferation with Dilp8-mediated developmental delay', *Proceedings of the National Academy of Sciences of the United States of America*, 112(18), pp. E2327–E2336. Available at: https://doi.org/10.1073/pnas.1423074112.

Katsuyama, T. *et al.* (2015b) 'During Drosophila disc regeneration, JAK/STAT coordinates cell proliferation with Dilp8-mediated developmental delay', *Proceedings of the National Academy of Sciences of the United States of America*, 112(18), pp. E2327–E2336. Available at: https://doi.org/10.1073/pnas.1423074112.

Kim, M., Santos, K.D. and Moon, N.S. (2021) 'Proper CycE-Cdk2 activity in endocycling tissues requires regulation of the cyclin-dependent kinase inhibitor Dacapo by dE2F1b in Drosophila', *Genetics*, 217(1). Available at: https://doi.org/10.1093/GENETICS/IYAA029.

Korenjak, M. *et al.* (2014) 'DREAM co-operates with insulator-binding proteins and regulates expression at divergently paired genes', *Nucleic Acids Research*, 42(14), pp. 8939–8953. Available at: https://doi.org/10.1093/nar/gku609.

Lane, M.E. *et al.* (1996) 'Dacapo, a cyclin-dependent kinase inhibitor, stops cell proliferation during Drosophila development', *Cell*, 87(7), pp. 1225–1235. Available at: https://doi.org/10.1016/S0092-8674(00)81818-8.

Lane, M.E., Sauer, K. and Wallace, K. (1996) *Dacapo, a Cyclin-Dependent Kinase Inhibitor, Stops Cell Proliferation during Drosophila Development*, *Cell*.

Lee, H.O., Davidson, J.M. and Duronio, R.J. (2009) 'Endoreplication: Polyploidy with purpose', *Genes and Development*, pp. 2461–2477. Available at: https://doi.org/10.1101/gad.1829209.

Lee, W.J. and Miura, M. (2014) 'Mechanisms of Systemic Wound Response in Drosophila', in *Current Topics in Developmental Biology*. Academic Press Inc., pp. 153–183. Available at: https://doi.org/10.1016/B978-0-12-391498-9.00001-2.

Lemaitre, B. and Miguel-Aliaga, I. (2013) 'The digestive tract of Drosophila melanogaster', *Annual Review of Genetics*. Annual Reviews Inc., pp. 377–404. Available at: https://doi.org/10.1146/annurev-genet-111212-133343.

Lessenger, A.T. *et al.* (2025) 'Somatic polyploidy supports biosynthesis and tissue function by increasing transcriptional output', *The Journal of cell biology*, 224(3). Available at: https://doi.org/10.1083/jcb.202403154.

Li, K., Jia, Q.Q. and Li, S. (2019) 'Juvenile hormone signaling – a mini review', *Insect Science*. Blackwell Publishing Ltd, pp. 600–606. Available at: https://doi.org/10.1111/1744-7917.12614.

Lilly, M.A. and Duronio, R.J. (2005) 'New insights into cell cycle control from the Drosophila endocycle', *Oncogene*, pp. 2765–2775. Available at: https://doi.org/10.1038/sj.onc.1208610.

Lilly, M.A. and Spradling, A.C. (1996) *The Drosophila endocycle is controlled by Cy.clin E and lacks a checkpoint ensuring S-phase completion*.

Lilly, M.A. and Sptadling, A.C. (1996) 'The Drosophila endocycle is controlled by cyclin E and lacks a checkpoint ensuring S-phase completion', *Genes and Development*, 10(19), pp. 2514–2526. Available at: https://doi.org/10.1101/gad.10.19.2514.

Liu, Q. *et al.* (2019) 'Lung regeneration by multipotent stem cells residing at the bronchioalveolar-duct junction', *Nature Genetics*, 51(4), pp. 728–738. Available at: https://doi.org/10.1038/s41588-019-0346-6.

Losick, V.P., Fox, D.T. and Spradling, A.C. (2013) 'Polyploidization and cell fusion contribute to wound healing in the adult Drosophila epithelium', *Current Biology*, 23(22), pp. 2224–2232. Available at: https://doi.org/10.1016/j.cub.2013.09.029.

Lucchetta, E.M. and Ohlstein, B. (2017) 'Amitosis of Polyploid Cells Regenerates Functional Stem Cells in the Drosophila Intestine', *Cell Stem Cell*, 20(5), pp. 609-620.e6. Available at: https://doi.org/10.1016/j.stem.2017.02.012.

Ludwig, M.Z., Tamarina, N.A. and Richmond, R.C. (1993) *Localization of sequences controlling the spatial, temporal, and sex-specific expression of the esterase 6 locus in Drosophila melanogaster adults (gene regulation/evolution)*. Available at: https://www.pnas.org.

Lung, O., Kuo, L. and Wolfner, M.F. (2001a) *Drosophila males transfer antibacterial proteins from their accessory gland and ejaculatory duct to their mates*, *Journal of Insect Physiology*. Available at: www.elsevier.com/locate/jinsphys.

Lung, O., Kuo, L. and Wolfner, M.F. (2001b) *Drosophila males transfer antibacterial proteins from their accessory gland and ejaculatory duct to their mates*, *Journal of Insect Physiology*. Available at: www.elsevier.com/locate/jinsphys.

Luo, L. *et al.* (2007) 'Regulation of Geminin Functions by Cell Cycle-Dependent Nuclear-Cytoplasmic Shuttling', *Molecular and Cellular Biology*, 27(13), pp. 4737–4744. Available at: https://doi.org/10.1128/mcb.00123-07.

La Marca, J.E. and Richardson, H.E. (2020) 'Two-Faced: Roles of JNK Signalling During Tumourigenesis in the Drosophila Model', *Frontiers in Cell and Developmental Biology*. Frontiers Media S.A. Available at: https://doi.org/10.3389/fcell.2020.00042.

Long E. Cruz, Markow A. Therese, Yaeger (1980) 'Relative male age, fertility, and competitive mating success in *Drosophila melanogaster*', *Behavior Genetics,* pp.163-170. Available at: https://doi.org/10.1007/BF01066266.

Mazzi, S. *et al.* (2018) 'Megakaryocyte and polyploidization', *Experimental Hematology*. Elsevier Inc., pp. 1–13. Available at: https://doi.org/10.1016/j.exphem.2017.10.001.

McGuire, S.E., Roman, G. and Davis, R.L. (2004a) 'Gene expression systems in Drosophila: A synthesis of time and space', *Trends in Genetics*, pp. 384–391. Available at: https://doi.org/10.1016/j.tig.2004.06.012.

McGuire, S.E., Roman, G. and Davis, R.L. (2004b) 'Gene expression systems in Drosophila: A synthesis of time and space', *Trends in Genetics*, pp. 384–391. Available at: https://doi.org/10.1016/j.tig.2004.06.012.

Mehrotra, S. *et al.* (2008) 'Endocycling cells do not apoptose in response to DNA rereplication genotoxic stress', *Genes and Development*, 22(22), pp. 3158–3171. Available at: https://doi.org/10.1101/gad.1710208.

Michael, S. *et al.* (2008) 'Discovery of candidate KEN-box motifs using Cell Cycle keyword enrichment combined with native disorder prediction and motif conservation', *Bioinformatics*, 24(4), pp. 453–457. Available at: https://doi.org/10.1093/bioinformatics/btm624.

Miyaoka, Y. *et al.* (2012) 'Hypertrophy and unconventional cell division of hepatocytes underlie liver regeneration.', *Current biology : CB*, 22(13), pp. 1166–1175. Available at: https://doi.org/10.1016/j.cub.2012.05.016.

Mollova, M. *et al.* (2013) 'Cardiomyocyte proliferation contributes to heart growth in young humans', *Proceedings of the National Academy of Sciences of the United States of America*, 110(4), pp. 1446–1451. Available at: https://doi.org/10.1073/pnas.1214608110.

Monje, M.L., Toda, H. and Palmer, T.D. (2003) 'Inflammatory Blockade Restores Adult Hippocampal Neurogenesis', *Science*, 302(5651), pp. 1760–1765. Available at: https://doi.org/10.1126/science.1088417.

Morgan, T.H. (1910) 'Sex Limited Inheritance in *Drosophila*', *Science* 32(812), pp. 120-122. Availabe at: https://doi/10.1126/science.32.812.120

de Morree, A. and Rando, T.A. (2023a) ‘Regulation of adult stem cell quiescence and its functions in the maintenance of tissue integrity’, *Nature Reviews Molecular Cell Biology* [Preprint]. Nature Research. Available at: https://doi.org/10.1038/s41580-022-00568-6.

de Morree, A. and Rando, T.A. (2023b) ‘Regulation of adult stem cell quiescence and its functions in the maintenance of tissue integrity’, *Nature Reviews Molecular Cell Biology*. Nature Research, pp. 334–354. Available at: https://doi.org/10.1038/s41580-022-00568-6.

MUNTZING, A. and PRAKKEN, R. (1941) ‘CHROMOSOMAL ABERRATIONS IN RYE POPULATIONS’, *Hereditas*, 27(3–4), pp. 273–308. Available at: https://doi.org/10.1111/j.1601-5223.1941.tb03261.x.

Nandakumar, S., Grushko, O. and Buttitta, L.A. (2020) ‘Polyploidy in the adult Drosophila brain’, *eLife*, 9, pp. 1–25. Available at: https://doi.org/10.7554/ELIFE.54385.

Narasimha, A.M. *et al.* (2014) ‘Cyclin D activates the Rb tumor suppressor by mono-phosphorylation’, *eLife*, 3. Available at: https://doi.org/10.7554/elife.02872.

Narbonne-Reveau, K. *et al.* (2008) ‘APC/CFzr/Cdh1 promotes cell cycle progression during the Drosophila endocycle’, *Development*, 135(8), pp. 1451–1461. Available at: https://doi.org/10.1242/dev.016295.

Newell, N.R. *et al.* (2020) ‘The Drosophila post-mating response: Gene expression and behavioral changes reveal perdurance and variation in cross-tissue interactions’, *G3: Genes, Genomes, Genetics*, 10(3), pp. 967–983. Available at: https://doi.org/10.1534/g3.119.400963.

Nicholson, L. *et al.* (2008) ‘Spatial and temporal control of gene expression in Drosophila using the inducible geneSwitch GAL4 system. I. Screen for larval nervous system drivers’, *Genetics*, 178(1), pp. 215–234. Available at: https://doi.org/10.1534/genetics.107.081968.

Noselli, S and Agnes, F. (1999) ‘Roles of the JNK signaling pathway in *Drosophila* morphogenesis’, *Current Opinion in genetics an Development*, pp.466-472. Available at:https://doi.org/10.1016/S0959-437X(99)80071-9.

De Nooij, J.C., Letendre, M.A. and Hariharan, I.K. (1996) ‘A cyclin-dependent kinase inhibitor, dacapo, is necessary for timely exit from the cell cycle during Drosophila embryogenesis’, *Cell*, 87(7), pp. 1237–1247. Available at: https://doi.org/10.1016/S0092-8674(00)81819-X.

Oshima, K. and Fehon, R.G. (2011) ‘Analysis of protein dynamics within the septate junction reveals a highly stable core protein complex that does not include the basolateral polarity protein Discs large’, *Journal of Cell Science*, 124(16), pp. 2861–2871. Available at: https://doi.org/10.1242/jcs.087700.

Osterwalder, T. *et al.* (1993a) *A conditional tissue-specific transgene expression system using inducible GAL4*. Available at: www.pnas.org.

Osterwalder, T. *et al.* (1993b) *A conditional tissue-specific transgene expression system using inducible GAL4*. Available at: www.pnas.org.

Osswald M, Morais-de-Sá E. (2019) ‘Dealing with apical-basal polarity and intercellular junctions: a multidimensional challenge for epithelial cell division’. *Curr Opin Cell Biol*. 60:75-83. Available at: 10.1016/j.ceb.2019.04.006.

Øvrebø, J.I. and Edgar, B.A. (2018a) 'Polyploidy in tissue homeostasis and regeneration', *Development (Cambridge)*. Company of Biologists Ltd. Available at: https://doi.org/10.1242/dev.156034.

Øvrebø, J.I. and Edgar, B.A. (2018b) 'Polyploidy in tissue homeostasis and regeneration', *Development (Cambridge)*. Company of Biologists Ltd. Available at: https://doi.org/10.1242/dev.156034.

Pape, E.H., Klott, K. and Kreutz, W. (1971) *References and Notes 1. M*, *Proc. Natl. Acad. Sci. U.S.A*. Available at: https://www.science.org.

Park, J.H. *et al.* (2019) 'Role of p53 isoforms in the DNA damage response during Drosophila oogenesis', *Scientific Reports*, 9(1). Available at: https://doi.org/10.1038/s41598-019-47913-y.

Pastor-Pareja, J.C. and Xu, T. (2011) 'Shaping Cells and Organs in Drosophila by Opposing Roles of Fat Body-Secreted Collagen IV and Perlecan', *Developmental Cell*, 21(2), pp. 245–256. Available at: https://doi.org/10.1016/j.devcel.2011.06.026.

Pesin, J.A. and Orr-Weaver, T.L. (2008) 'Regulation of APC/C activators in mitosis and meiosis', *Annual Review of Cell and Developmental Biology*, pp. 475–499. Available at: https://doi.org/10.1146/annurev.cellbio.041408.115949.

Petropoulos, M. *et al.* (2019) 'Replication Licensing Aberrations, Replication Stress, and Genomic Instability', *Trends in Biochemical Sciences*. Elsevier Ltd, pp. 752–764. Available at: https://doi.org/10.1016/j.tibs.2019.03.011.

Peters JM. (2006) 'The anaphase promoting complex/cyclosome: a machine designed to destroy'. *Nat Rev Mol Cell Biol*,7(9):644-56.

Peters, J.-M. (2002). 'The anaphase-promoting complex: proteolysis in mitosis and beyond'. *Mol. Cell* 9, 931–943.

Pfleger, C.M. and Kirschner, M.W. (2000) *The KEN box: an APC recognition signal distinct from the D box targeted by Cdh1*. Available at: www.genesdev.org.

Pfleger, C.M., Lee, E. and Kirschner, M.W. (2001) 'Substrate recognition by the Cdc20 and Cdh1 components of the anaphase-promoting complex', *Genes and Development*, 15(18), pp. 2396–2407. Available at: https://doi.org/10.1101/gad.918201.

Pizzari, T. and Wedell, N. (2013) 'The polyandry revolution', *Philosophical Transactions of the Royal Society B: Biological Sciences*, 368(1613). Available at: https://doi.org/10.1098/rstb.2012.0041.

Polyploidy atlas, Available at :https://sites.google.com/umich.edu/polyploidyatlas/home?authuser=0

Porrello, E.R. *et al.* (2011) 'Transient regenerative potential of the neonatal mouse heart', *Science*, 331(6020), pp. 1078–1080. Available at: https://doi.org/10.1126/science.1200708.

Porrello, E.R. *et al.* (2013) 'Regulation of neonatal and adult mammalian heart regeneration by the miR-15 family', *Proceedings of the National Academy of Sciences of the United States of America*, 110(1), pp. 187–192. Available at: https://doi.org/10.1073/pnas.1208863110.

Price CS, Dyer KA, Coyne JA. (1999) 'Sperm competition between Drosophila males involves both displacement and incapacitation'. *Nature*. 400(6743):449-52.

Prokop (2008) 'A. Prokop-A rough guide to Drosophila mating schemes A rough guide to Drosophila mating schemes (version 2.2) 1'. Available at: https://doi.org/10.6084/m9.figshare.106631.

Pursley, S., Ashok, M. and Wilson, T.G. (2000) *Intracellular localization and tissue specificity of the Methoprene-tolerant (Met) gene product in Drosophila melanogaster*, *Insect Biochemistry and Molecular Biology*. Available at: www.elsevier.com/locate/ibmb.

Qian, Y. *et al.* (2021) 'Regulatory Mechanisms of bHLH Transcription Factors in Plant Adaptive Responses to Various Abiotic Stresses', *Frontiers in Plant Science*. Frontiers Media S.A. Available at: https://doi.org/10.3389/fpls.2021.677611.

Quinn, L.M. *et al.* (2001a) 'The Drosophila Geminin homolog: Roles for Geminin in limiting DNA replication, in anaphase and in neurogenesis', *Genes and Development*, 15(20), pp. 2741–2754. Available at: https://doi.org/10.1101/gad.916201.

Quinn, L.M. *et al.* (2001b) 'The Drosophila Geminin homolog: Roles for Geminin in limiting DNA replication, in anaphase and in neurogenesis', *Genes and Development*, 15(20), pp. 2741–2754. Available at: https://doi.org/10.1101/gad.916201.

Raff, J.W., Jeffers, K. and Huang, J.Y. (2002) 'The roles of Fzy/Cdc20 and Fzr/Cdh1 in regulating the destruction of cyclin B in space and time', *Journal of Cell Biology*, 157(7), pp. 1139–1149. Available at: https://doi.org/10.1083/jcb.200203035.

Ramesh, N.A., Box, A.M. and Buttitta, L.A. (2025) 'Post-eclosion growth in the Drosophila ejaculatory duct is driven by Juvenile hormone signaling and is essential for male fertility', *Developmental Biology*, 519, pp. 122–141. Available at: https://doi.org/10.1016/j.ydbio.2024.12.010.

Ravid, K. *et al.* (2002) 'Roads to polyploidy: The megakaryocyte example', *Journal of Cellular Physiology*, pp. 7–20. Available at: https://doi.org/10.1002/jcp.10035.

Ren, D. *et al.* (2020a) 'Regulatory Mechanisms of Cell Polyploidy in Insects', *Frontiers in Cell and Developmental Biology*. Frontiers Media S.A. Available at: https://doi.org/10.3389/fcell.2020.00361.

Ren, D. *et al.* (2020b) 'Regulatory Mechanisms of Cell Polyploidy in Insects', *Frontiers in Cell and Developmental Biology*. Frontiers Media S.A. Available at: https://doi.org/10.3389/fcell.2020.00361.

Rexhepaj, A. *et al.* (2003) 'The sex-peptide DUP99B is expressed in the male ejaculatory duct and in the cardia of both sexes', *European Journal of Biochemistry*, 270(21), pp. 4306–4314. Available at: https://doi.org/10.1046/j.1432-1033.2003.03823.x.

Riddiford, L.M. (2012) 'How does juvenile hormone control insect metamorphosis and reproduction?', *General and Comparative Endocrinology*. Academic Press Inc., pp. 477–484. Available at: https://doi.org/10.1016/j.ygcen.2012.06.001.

Roman, G. *et al.* (2001) 'P{Switch}, a system for spatial and temporal control of gene expression in *Drosophila melanogaster*'. Available at: www.pnas.orgycgiydoiy10.1073ypnas.221303998.

Rossant J and Cross C.J. (2001) "Placental development: lessons from mouse mutants' *Nature Reviews Genetics*. pp. 538-548.

Ruijtenberg S, van den Heuvel S. (2016) 'Coordinating cell proliferation and differentiation: Antagonism between cell cycle regulators and cell type-specific gene expression', *Cell Cycle*, 15(2):196-212. Available at: 10.1080/15384101.2015.1120925

Saad, M. *et al.* (1994) *Associations of esterase 6 allozyme and activity variation with reproductive fitness in Drosophila melanogaster*, *Genetica*. Kluwer Academic Publishers.

Samakoviis, C. *et al.* (1991) *The Andropin gene and its product, a male-specific antibacterial peptide in Drosophila melanogaster*, *The EMBO Journal*.

Samakovlis, C. *et al.* (1991) 'The andropin gene and its product, a male-specific antibacterial peptide in Drosophila melanogaster.', *The EMBO Journal*, 10(1), pp. 163–169. Available at: https://doi.org/10.1002/j.1460-2075.1991.tb07932.x.

Saudan, P. *et al.* (2002) 'Ductus ejaculatorius peptide 99B (DUP99B), a novel Drosophila melanogaster sex-peptide pheromone', *European Journal of Biochemistry*, 269(3), pp. 989–997. Available at: https://doi.org/10.1046/j.0014-2956.2001.02733.x.

Schaeffer, V. *et al.* (2004) 'Notch-Dependent Fizzy-Related/Hec1/Cdh1 Expression Is Required for the Mitotic-to-Endocycle Transition in Drosophila Follicle Cells Overexpression of string Is Not Enough to Induce Efficient Mitosis in Follicle Cells after Stage 6 String encodes the Drosophila homolog of the yeast cell cycle regulator Cdc25, a phosphatase whose role is to activate the Cdk-cyclin complex at the G2/M transition', *Current Biology*, 14, pp. 630–636. Available at: https://doi.org/10.1016/j.

Seetharaman, R. *et al.* (2019) 'An Overview on Stem Cells in Tissue Regeneration', *Current Pharmaceutical Design*, 25(18), pp. 2086–2098. Available at: https://doi.org/10.2174/1381612825666190705211705.

Ahmad M.S and Baker S.B. (2002) 'Sex-Specific Deployment of FGF Signaling in *Drosophila* Recruits Mesodermal Cells into the Male Genital Imaginal Disc', *Cell,* 109, pp. 651-661.

Shaw, R.L. *et al.* (2010) 'The Hippo pathway regulates intestinal stem cell proliferation during Drosophila adult midgut regeneration', *Development*, 137(24), pp. 4147–4158. Available at: https://doi.org/10.1242/dev.052506.

Shibutani, S., Swanhart, L.M. and Duronio, R.J. (2007) 'Rbf1-independent termination of E2f1-target gene expression during early Drosophila embryogenesis', *Development*, 134(3), pp. 467–478. Available at: https://doi.org/10.1242/dev.02738.

Shu, Z., Row, S. and Deng, W.M. (2018) 'Endoreplication: The Good, the Bad, and the Ugly', *Trends in Cell Biology*. Elsevier Ltd, pp. 465–474. Available at: https://doi.org/10.1016/j.tcb.2018.02.006.

Singh, S.R. and Hou, S.X. (2009) 'Multipotent stem cells in the Malpighian tubules of adult Drosophila melanogaster', *Journal of Experimental Biology*, pp. 413–423. Available at: https://doi.org/10.1242/jeb.024216.

Sitnik, J. *et al.* (2016) 'The female post-mating response requires genes expressed in the secondary cells of the male accessory gland in Drosophila melanogaster', *Genetics*, 202(3), pp. 1029–1041. Available at: https://doi.org/10.1534/genetics.115.181644.

Smith-Bolton, R. (2016) 'Drosophila Imaginal Discs as a Model of Epithelial Wound Repair and Regeneration', *Advances in Wound Care*. Mary Ann Liebert Inc., pp. 251–261. Available at: https://doi.org/10.1089/wound.2014.0547.

Smith-Bolton, R.K. *et al.* (2009a) 'Regenerative Growth in Drosophila Imaginal Discs Is Regulated by Wingless and Myc', *Developmental Cell*, 16(6), pp. 797–809. Available at: https://doi.org/10.1016/j.devcel.2009.04.015.

Smith-Bolton, R.K. *et al.* (2009b) 'Regenerative Growth in Drosophila Imaginal Discs Is Regulated by Wingless and Myc', *Developmental Cell*, 16(6), pp. 797–809. Available at: https://doi.org/10.1016/j.devcel.2009.04.015.

Srivastava, A. *et al.* (2007) *Basement membrane remodeling is essential for Drosophila disc eversion and tumor invasion*. Available at: www.pnas.org/cgi/content/full/.

Sturm, S. *et al.* (2021) 'Mass spectrometric characterisation of the major peptides of the male ejaculatory duct, including a glycopeptide with an unusual zwitterionic glycosylation', *Journal of Proteomics*, 246. Available at: https://doi.org/10.1016/j.jprot.2021.104307.

Swanson, C.I. *et al.* (2015) 'Expression of an S phase-stabilized version of the CDK inhibitor Dacapo can alter endoreplication', *Development (Cambridge)*, 142(24), pp. 4288–4298. Available at: https://doi.org/10.1242/dev.115006.

Tafesh-Edwards, G. and Eleftherianos, I. (2020a) 'JNK signaling in Drosophila immunity and homeostasis', *Immunology Letters*. Elsevier B.V., pp. 7–11. Available at: https://doi.org/10.1016/j.imlet.2020.06.017.

Tafesh-Edwards, G. and Eleftherianos, I. (2020b) 'JNK signaling in Drosophila immunity and homeostasis', *Immunology Letters*. Elsevier B.V., pp. 7–11. Available at: https://doi.org/10.1016/j.imlet.2020.06.017.

Takemori, N. and Yamamoto, M.T. (2009) 'Proteome mapping of the Drosophila melanogaster male reproductive system', *Proteomics*, 9(9), pp. 2484–2493. Available at: https://doi.org/10.1002/pmic.200800795.

Tamori, Y. and Deng, W.M. (2013) 'Tissue Repair through Cell Competition and Compensatory Cellular Hypertrophy in Postmitotic Epithelia', *Developmental Cell*, 25(4), pp. 350–363. Available at: https://doi.org/10.1016/j.devcel.2013.04.013.

Tamori, Y. and Deng, W.M. (2014) 'Compensatory cellular hypertrophy: The other strategy for tissue homeostasis', *Trends in Cell Biology*. Elsevier Ltd, pp. 230–237. Available at: https://doi.org/10.1016/j.tcb.2013.10.005.

Tanentzapf, G. *et al.* (2000) *Apical, Lateral, and Basal Polarization Cues Contribute to the Development of the Follicular Epithelium during Drosophila Oogenesis*, *The Journal of Cell Biology*. Available at: http://www.jcb.org/cgi/content/full/151/4/891.

Unhavaithaya, Y. and Orr-Weaver, T.L. (2012a) 'Polyploidization of glia in neural development links tissue growth to blood-brain barrier integrity', *Genes and Development*, 26(1), pp. 31–36. Available at: https://doi.org/10.1101/gad.177436.111.

Unhavaithaya, Y. and Orr-Weaver, T.L. (2012b) 'Polyploidization of glia in neural development links tissue growth to blood-brain barrier integrity', *Genes and Development*, 26(1), pp. 31–36. Available at: https://doi.org/10.1101/gad.177436.111.

Del Valle Rodríguez, A., Didiano, D. and Desplan, C. (2012) 'Power tools for gene expression and clonal analysis in Drosophila', *Nature Methods*. Nature Publishing Group, pp. 47–55. Available at: https://doi.org/10.1038/nmeth.1800.

Wang, C. and Spradling, A.C. (2020) ‘An abundant quiescent stem cell population in Drosophila malpighian tubules protects principal cells from kidney stones’, *eLife*, 9. Available at: https://doi.org/10.7554/eLife.54096.

Wang, C. and Spradling, A.C. (2022) *Drosophila renal stem cells enhance fitness by delayed remodeling of adult Malpighian tubules*. Available at: https://www.science.org.

Wilson, C. *et al.* (2017) ‘The Drosophila Accessory Gland as a Model for Prostate Cancer and Other Pathologies’, in *Current Topics in Developmental Biology*. Academic Press Inc., pp. 339–375. Available at: https://doi.org/10.1016/bs.ctdb.2016.06.001.

Wilson, T.G., DeMoor, S. and Lei, J. (2003a) ‘Juvenile hormone involvement in Drosophila melanogaster male reproduction as suggested by the Methoprene-tolerant27 mutant phenotype’, *Insect Biochemistry and Molecular Biology*, 33(12), pp. 1167–1175. Available at: https://doi.org/10.1016/j.ibmb.2003.06.007.

Wilson, T.G., DeMoor, S. and Lei, J. (2003b) ‘Juvenile hormone involvement in Drosophila melanogaster male reproduction as suggested by the Methoprene-tolerant27 mutant phenotype’, *Insect Biochemistry and Molecular Biology*, 33(12), pp. 1167–1175. Available at: https://doi.org/10.1016/j.ibmb.2003.06.007.

Wolf, M.J. (2012) *Modeling Dilated Cardiomyopathies in Drosophila*. Available at: http://flystocks.

Wu, X. *et al.* (2019) ‘mTOR Signaling Upregulates CDC6 via Suppressing miR-3178 and Promotes the Loading of DNA Replication Helicase’, *Scientific Reports*, 9(1). Available at: https://doi.org/10.1038/s41598-019-46052-8.

Wu, Z. *et al.* (2018) ‘Juvenile hormone promotes locust fat body cell polyploidization and vitellogenesis by activating the transcription of Cdk6 and E2f1’, *Insect Biochemistry and Molecular Biology*, 102, pp. 1–10. Available at: https://doi.org/10.1016/j.ibmb.2018.09.002.

Wu, Z. *et al.* (2020) ‘Juvenile hormone acts through FoxO to promote Cdc2 and Orc5 transcription for polyploidy-dependent vitellogenesis’, *Development (Cambridge)*, 147(18). Available at: https://doi.org/10.1242/dev.188813.

-wwxx (1910) *SOIENOE 121*. Available at: https://www.science.org.

Xia, H. *et al.* (2018a) ‘Tissue repair and regeneration with endogenous stem cells’, *Nature Reviews Materials*. Nature Publishing Group, pp. 174–193. Available at: https://doi.org/10.1038/s41578-018-0027-6.

Xia, H. *et al.* (2018b) ‘Tissue repair and regeneration with endogenous stem cells’, *Nature Reviews Materials*. Nature Publishing Group, pp. 174–193. Available at: https://doi.org/10.1038/s41578-018-0027-6.

Xiang, J. *et al.* (2017) ‘EGFR-dependent TOR-independent endocycles support Drosophila gut epithelial regeneration’, *Nature Communications*, 8. Available at: https://doi.org/10.1038/ncomms15125.

Yahya, G. *et al.* (2022) ‘Sublinear scaling of the cellular proteome with ploidy’, *Nature Communications*, 13(1). Available at: https://doi.org/10.1038/s41467-022-33904-7.

Yamamura, R., Ooshio, T. and Sonoshita, M. (2021) ‘Tiny Drosophila makes giant strides in cancer research’, *Cancer Science*. Blackwell Publishing Ltd, pp. 505–514. Available at: https://doi.org/10.1111/cas.14747.

Yeh, S.D., Chan, C. and Ranz, J.M. (2013) 'Assessing differences in sperm competitive ability in Drosophila', *Journal of visualized experiments : JoVE*, (78), p. e50547. Available at: https://doi.org/10.3791/50547.

Yun, M.H. (2015) 'Changes in regenerative capacity through lifespan', *International Journal of Molecular Sciences*. MDPI AG, pp. 25392–25432. Available at: https://doi.org/10.3390/ijms161025392.

Yurchenco, P.D. (2011) 'Basement membranes: Cell scaffoldings and signaling platforms', *Cold Spring Harbor Perspectives in Biology*, 3(2), pp. 1–27. Available at: https://doi.org/10.1101/cshperspect.a004911.

Zeidler, M.P., Bach, E.A. and Perrimon, N. (no date) *The roles of the Drosophila JAK/STAT pathway*. Available at: www.nature.com/onc.

Zeidler, M.P. and Bausek, N. (2013) ' The Drosophila JAK-STAT pathway ', *JAK-STAT*, 2(3), p. e25353. Available at: https://doi.org/10.4161/jkst.25353.

Zeng, X., Chauhan, C. and Hou, S.X. (2013) 'Stem Cells in the Drosophila Digestive System', in, pp. 63–78. Available at: https://doi.org/10.1007/978-94-007-6621-1_5.

Zhang, B. *et al.* (2014) 'Low Levels of p53 Protein and Chromatin Silencing of p53 Target Genes Repress Apoptosis in Drosophila Endocycling Cells', *PLoS Genetics*, 10(9). Available at: https://doi.org/10.1371/journal.pgen.1004581.

Zhang, X., Li, S. and Liu, S. (2022) 'Juvenile Hormone Studies in Drosophila melanogaster', *Frontiers in Physiology*. Frontiers Media S.A. Available at: https://doi.org/10.3389/fphys.2021.785320.

Zielke, N. *et al.* (2008a) 'The anaphase-promoting complex/cyclosome (APC/C) is required for rereplication control in endoreplication cycles', *Genes and Development*, 22(12), pp. 1690–1703. Available at: https://doi.org/10.1101/gad.469108.

Zielke, N. *et al.* (2008b) 'The anaphase-promoting complex/cyclosome (APC/C) is required for rereplication control in endoreplication cycles', *Genes and Development*, 22(12), pp. 1690–1703. Available at: https://doi.org/10.1101/gad.469108.

Zielke, N. *et al.* (2011a) 'Control of Drosophila endocycles by E2F and CRL4 CDT2', *Nature*, 480(7375), pp. 123–127. Available at: https://doi.org/10.1038/nature10579.

Zielke, N. *et al.* (2011b) 'Control of Drosophila endocycles by E2F and CRL4 CDT2', *Nature*, 480(7375), pp. 123–127. Available at: https://doi.org/10.1038/nature10579.

Zybina, T.G. and Zybina, E. V. (2020) 'Role of cell cycling and polyploidy in placental trophoblast of different mammalian species', *Reproduction in Domestic Animals*. Blackwell Publishing Ltd, pp. 895–904. Available at: https://doi.org/10.1111/rda.13732.

Chapter 2 Post-Eclosion Growth in the *Drosophila* Ejaculatory Duct is Driven by Juvenile Hormone Signaling and is Essential for Male Fertility

Contributions
Navyashree A Ramesh- Performed all experiments and wrote the original draft, contributed to review & editing, conceptualization, and revisions.
Allison M Box- Contributed to the identification of the Luna Gal4 driver.

2.1 Abstract

The *Drosophila* Ejaculatory duct (ED) is a secretory tissue of the somatic male reproductive system. The ED is involved in the secretion of seminal fluid components and ED-specific antimicrobial peptides that aid in fertility and the female post-mating response. The ED is composed of secretory epithelial cells surrounded by a layer of innervated contractile muscle. The ED grows in young adult males during the first 24 h post-eclosion, but the cell cycle status of the ED secretory cells and the role of post-eclosion ED growth have been unexplored. Here, we show that secretory cells of the adult *Drosophila* ED undergo variant cell cycles lacking mitosis called the endocycle, that lead to an increase in the cell and organ size of the ED post eclosion. The cells largely exit the endocycle by day 3 of adulthood, when the growth of the ED ceases, resulting in tissue containing cells of ploidies ranging from 8C to 32C. The size of the ED directly correlates with the ploidy of the secretory cells, with additional ectopic endocycles increasing organ size. When endoreplication is compromised in ED secretory cells, it leads to reduced organ size, reduced protein synthesis and compromised fertility. We provide evidence that the growth and endocycling in the young adult male ED is dependent on Juvenile hormone (JH) signaling and we suggest that hormone-induced early adult endocycling is required for optimal fertility and function of the ED tissue. We propose to use the ED as a post-mitotic tissue model to study the role of polyploidy in regulating secretory tissue growth and function.

2.2 Introduction

The *Drosophila* male reproductive tract consists of a pair of sperm-producing testes connected to seminal vesicles, which along with a pair of accessory gland lobes, empty into an organ called the Ejaculatory Duct (ED). The ED is a site of sperm and seminal fluid mixing prior to transfer to the Ejaculatory bulb for female insemination during mating (Avila et al., 2016; Bertram et al., 1992; Hopkins et al., 2019) and these secretions are transferred into the ejaculatory duct during copulation through a transition zone called the anterior ED papillae (Bairati, 1968). ED cells are derived from the portion of the genital disc arising from the A9 primordium, and thus are ectodermal in origin (Ahmad and Baker, 2002; Avila et al., 2016) The ED also produces seminal fluid components, and by proteomic analysis of ED tissue, 138 peptides have been identified, of which 63 were proposed to be seminal fluid proteins (SFPs) (Sturm et al., 2021; Takemori and Yamamoto, 2009). Peptides secreted by the ED are involved in processes of lipid modification, immune response, catalysis, hormone-like activity, sperm storage, cell adhesion, odorant-binding proteins, and cellular metabolism (Takemori and Yamamoto, 2009). Contents from the ED are transferred to the Ejaculatory bulb and then to the female reproductive system via contractions of muscle, which surround the ED (Avila et al., 2016; Lung et al., 2001; Wilson et al., 2017). ED-produced antimicrobial peptides such as Cecropin A1 and the ED-specific Andropin (Anp) may increase fertility by reducing infections upon mating (Date-Ito et al., 2002; Lung et al., 2001; Samakovlis et al., 1991). Other SFPs are thought to promote male fertility through multiple mechanisms that impact sperm storage and female post-mating response. For example, the ED produces a pheromone peptide termed Ductus ejaculatorius peptide (Dup) Dup99B, which has homology to Sex Peptide (Accessory gland protein, Acp70), and like Sex Peptide, can elicit the female post-mating responses of increased egg laying and reduced sexual receptivity (Rexhepaj et al., 2003; Saudan et al., 2002). The anterior ED produces Esterase 6 (Est-6) a carboxylesterase transferred to females during copulation, which is a pheromone and odorant degrading enzyme that influences female sperm storage, sperm usage and re-mating (Chertemps et al., 2012; Ludwig et al., 1993; Richmond et al., 1980; Saad et al., 1994). Esterase-6 is also involved in the synthesis of sex pheromones (Takemori and Yamamoto, 2009). The ED also produces Glucose dehydrogenase (Gld) an enzyme that aids in sperm storage in the female reproductive tract after mating (Cavener, 1985; Cox-Foster et al., 1990; Iida and Cavener, 2004). The ED is therefore an

important tissue of the male reproductive system that provides components to optimize male fertility, in addition to serving a structural role in transferring seminal fluid.

Despite important predicted functions for the ED in males, little is known about the development and growth of this tissue. Flies lacking the protein tyrosine kinase 7 Wnt co-receptors off-track (otk) and off-track 2 (otk2) are viable but were reported to be male sterile due to defective morphogenesis of the ED (Linnemannstons et al., 2014). In these mutants, it is unclear whether the ED defects leading to infertility were structural due to defects in the muscle layer, or defects in the secretory cells, or both. Here, we examine the post-eclosion growth and cell cycle dynamics in the secretory epithelium of the ED. We show that this tissue undergoes additional cell cycles lacking M-phase that increase cellular ploidy, resulting in increased cell and tissue size, which supports a high level of protein synthesis that promotes male fertility. Post-eclosion endocycles in the ED are conserved in different species of *Drosophila*, and we show that compromising early adult endocycles in the ED reduces tissue growth, protein synthesis and male fertility. Juvenile hormone (JH) signaling is required for reproduction in *Drosophila* males (Baumann et al., 2017; Zhang et al., 2021), and here we show an essential role for JH signaling in promoting early post-eclosion endocycling of the secretory cells of the ED.

2.3 Results

2.3.1 Identification of different cell types and their organization in adult Drosophila Ejaculatory duct

The male adult *Drosophila* Ejaculatory duct is known to be involved in peristaltic motion to transfer sperm from the testes and seminal vesicles as well as seminal fluid containing fertility factors, enzymes, hormones and antimicrobial peptides to females (Avila et al., 2016; Bertram et al., 1992; Lung et al., 2001; Norville et al., 2010; Wilson et al., 2017). Little is known about the cell types in this tissue and their organization. To explore the different cell types in the ED we stained the tissue with cell type-specific antibodies to examine epithelial cells, neurons and muscle. Similar to a previous report (Susic-Jung et al., 2012), we observed that the ED epithelium is surrounded basally with striated muscles revealed by actin and myosin staining as well as staining with the muscle cell-specific marker Tinman (Liu et al., 2009; Zaffran et al., 2006) (Fig. 12A–C). We observed a monolayer of secretory epithelial cells with larger nuclei expressing the epithelial

cell-cell junction marker Fasciclin III (FasIII), forming a lumen apically (Fig. 12C). The basal surface of these large epithelial cells contains Integrin βps, an extracellular matrix receptor (Fig. 12D). The peristaltic contraction of the ED suggests the muscle should be innervated. We identified the ED neurons using the neuronal markers Fustch and Elav (Fig. 12E and F). This revealed the neuronal network overlying the basal muscle layer and labeled the smaller diploid nuclei of the ED. We noted that all diploid nuclei we could find using DAPI labeling in the ED are Elav positive, suggesting the muscle nuclei also express Elav (Fig. 12F). This tissue organization demonstrates the secretory ED epithelium contains enlarged cells forming a lumen surrounded by an ECM layer attached to innervated muscle.

2.3.2 Endoreplication of secretory cells of the adult Drosophila Ejaculatory duct leads to post-eclosion organ growth.

We recently described a post-eclosion wave of endocycling that occurs in the male accessory gland that promotes gland growth and function in male fertility (Box et al., 2024). During those studies, we also observed that the ED grows post-eclosion. We measured the area of ED on the day of eclosion (DOE) and at several time points post-eclosion (PE). The area of the ED increases until day 5 and then remains constant without any further increases all the way to day 55 of adulthood (Fig. 1A and B, Fig. 13A). We also observed that the area of ED secretory cell nuclei significantly increased by day 10 PE compared to DOE (Fig. 1C). To assay for DNA replication/synthesis we labeled live tissues with the S-phase DNA synthesis marker 5-Ethynyl-2′-deoxyuridine (EdU) (Flomerfelt and Gress, 2016). We observed widespread DNA replication on the day of eclosion in this tissue, which we also confirmed with EdU feeding assays in vivo (Fig. 1D and E). However, we did not observe any evidence of cells undergoing mitosis (Fig. 1D). To ensure we did not miss any mitotic events, we stained adult EDs with the mitotic marker phospho-serine 10 Histone H3 (PH3) and labeled ex-vivo with EdU at 1-h intervals throughout the day of eclosion. We observed DNA synthesis during each hour across 24 h, but no mitotic labeling (Fig. 13C). These results suggest that the secretory cells of adult *Drosophila* ED are postmitotic but not quiescent and enter an endocycle.

To determine when the endocycle ceases in the adult ED, we performed EdU feeding assays at 24-h intervals up to day 6 post eclosion. Endocycling of ED secretory cells slowly decreases from day

2 with almost no cells continuing to endocycle by day 5 post-eclosion (Fig. 1E–G). We also looked for any mitotic events up to day 5 post eclosion but observed no evidence of cell proliferation (Fig. 1H). This suggests the post eclosion growth of the ED is driven in part by endoreplication of the secretory cells.

2.3.3 Post eclosion endoreplication and growth of the adult Ejaculatory duct secretory cells are conserved in different species of Drosophila

We recently showed that the post eclosion wave of endocycling in the accessory gland is conserved in other *Drosophila* species. During the course of those studies, we also discovered that the post-eclosion endoreplication of the secretory cells of the adult ED is conserved in other *Drosophila* species. *D. simulans*, and *D. yakuba*, are sister species of melanogaster (Markow and O'Grady, 2006), while *D. pseudoodscura* and *D. willistoni* belong to the sophophora group (Takashima et al., 2023). We observed post eclosion endocycling in all of these species, including the outgroup *D. virilis*, which exhibits slower developmental timing and therefore was assessed 16 h post eclosion (Fig. 2A–C, Fig. 14A). Of note, the two species with the least post eclosion growth of the ED, *D. pseudoodscura* and *D. willistoni*, also exhibited the smallest number of endocycling cells post-eclosion (Fig. 2C and D). Post-eclosion endoreplication of the ED secretory cells is therefore conserved in *Drosophila* and correlates with post eclosion organ growth.

2.3.4 Drosophila ED secretory cell ploidy correlates with organ shape and size

Recent work in the *Drosophila* heart demonstrated that cellular ploidy and regulation of endoreplication can influence tissue morphogenesis and function in a contractile organ (Chakraborty et al., 2023). The anterior portion of the ED where the accessory glands and seminal vesicles meet with the anterior ED papillae is larger and the organ tapers and thins towards the posterior end, where it connects to the ejaculatory bulb (Fig. 3A). We therefore measured nuclear areas in the anterior, middle and posterior regions of the mature tissue on day 10 and observed that nuclei towards the anterior are larger compared to the nuclei of the secretory cells towards the anterior mid and posterior end as shown in Fig. 3A. We further confirmed the differences in ploidy by quantifying integrated DAPI intensities for the nuclei of the secretory cells, normalized to the diploid Elav + cells of the organ (Fig. 3B). The cells in the anterior region have a DNA content of 16C and 32C, while the cells in the anterior middle have a DNA content of 8C and 16C, and the

cells in the posterior end have a DNA content of 4C and 8C (Fig. 3B). These different regions of ED may be involved in providing different secretions or different amounts of secretions (Sturm et al., 2021). Thus, like the *Drosophila* heart, the ED exhibits regional-specific polyploidy of the tissue, which correlates with the tissue size and organ morphogenesis.

To confirm our image-based ploidy measurements and understand how these ploidies arise, we developed a flow cytometry assay to isolate nuclei from the adult EDs and measure DNA content by flow cytometry at timepoints post-eclosion. As a control we used ovaries of age and genotype matched females, which have a known ploidy distribution and serve as a control to accurately assign DNA content peaks (Bosco et al., 2007). On the day of eclosion, ED secretory cells exhibit ploidies of primarily 8C and 16C (Fig. 3C), with some intermediate ploidies consistent with their replicating EdU + status. By day 10, we observed a large population with 32C DNA content, as well as populations with 16C, and 8C (Fig. 3D). Consistent with their EdU-negative non-cycling status, by day 10, we observe very few nuclei with intermediate ploidies. With the flow cytometry confirmation of our DAPI imaging measurements, we quantified the ED ploidy distribution using DAPI imaging in adults from young males (day 2 post eclosion) to aged males (day 55) (Fig. 3E). We observed consistent ploidy measurements from day 15–55 in aged D. melanogaster virgin males suggesting additional endoreplication in aged virgin adults is rare under physiological conditions.

We noted differences in ED endocycling across *Drosophila* species correlated with post eclosion ED growth. However, our longer-term EdU labeling for 10 days revealed differences in nuclear areas across species (Figs. 14B–D). To examine this in more detail we performed flow cytometry measurements of *D. simulans*, *D. yakuba* and *D. virilis* at day 10 using the species-matched female ovary to normalize DNA content measurements to the species genome size (Bosco et al., 2007) (Fig. 14E-G). Consistent with our EdU labeling and DAPI imaging quantifications (Fig. 3F) we observe higher ploidies in *D. simulans* and *D. yakuba* compared with *D. virilis*. We also observe more cells of lower ploidies (<16C or less) in species with smaller, thinner EDs such as *D. pseudoobscura, D. willistoni and D. virilis* (Fig. 3F, Fig. 14B).

2.3.5 Compromising the endoreplication of ED secretory cells results in reduced ED size and fertility

To manipulate the secretory cells of the ED, we performed a Gal4 screen to identify an ED-Gal4 driver. We screened through ~100 Gal4 lines predicted to express in the male accessory glands and/or ED based on RNAseq data and identified Luna-Gal4 (InSite line BDSC 63746) as specific to the ED in the male reproductive system. We verified the Gal4 expression in the polyploid secretory cells of the ED using a Gal-4 responsive Upstream Activating Sequence (UAS) driving a nuclear localized RFP (UAS-RFPnls). We did not observe any expression in the muscle or neuronal layer of the ED, or any other parts of the male reproductive system including the accessory glands and ejaculatory bulb (Fig. 4A, Fig. 13F). We did not find the expression of Luna-Gal4 in any other adult *Drosophila* tissues except cardia (Fig. 13F). Luna-Gal4 expression in the ED begins prior to eclosion (96 h APF) and continues into adulthood. By combining the Luna-Gal4, with a UAS-GFPnls with a temperature-sensitive Gal80 that represses Gal4 (Gal80ts) (McGuire et al., 2004) we used temperature shifts to limit Luna-Gal4 expression to the adult stages and confirmed that Luna Gal4 continues to express Gal4 in the secretory cells of ED throughout adulthood in virgin males, until day 70 post-eclosion (Fig. 15A).

We next used the Luna-Gal4 driver to express transgenes to inhibit or slow the endocycle in the ED. Oscillations of the core cell cycle transcription factor complex E2F have been shown to drive the endocycle (Weng et al., 2003; Zielke et al., 2011), therefore we knocked down the two *Drosophila* E2F transcription factors E2F1 and E2F2 or overexpressed a constitutively active form of the E2F repressor, the Retinoblastoma family protein (Rbf280) (Xin et al., 2002) to limit S-phase entry and performed EdU labeling on the day of eclosion. All three approaches effectively reduced EdU labeling and nuclear ploidy in the ED on the day of eclosion, demonstrating they reduced or slowed post-eclosion S-phases. Rbf280 expression and E2F1 RNAi also effectively reduced adult ED size on the day of eclosion (Fig. 4B–E). We next overexpressed the G1-S CyclinE/Cdk2 inhibitor Dacapo, which acts to limit G1/S entry and therefore also slows or blocks endoreplication when expressed at high levels (Swanson et al., 2015). As expected, Dacapo overexpression severely limited endocycling in the ED on the day of eclosion, resulting in reduced nuclear ploidies and reduced organ size (Fig. 4B–E).

We next examined tissues on day 10, several days after ED cells normally have ceased endocycling. Consistent with the reduced or blocked endocycling observed on the day of eclosion, by day 10 the EDs with inhibited endocycling exhibit reduced organ size, reduced nuclear size and

reduced ploidies, demonstrating that these genetic cell cycle manipulations do not simply delay or slow the endocycle but instead effectively limit it (Fig. 4F–I, Fig. 15B). These results strongly suggest that the early endoreplication in secretory cells of ED post-eclosion is required for the growth of the ED. To test whether reduced ED size and ploidy may impact fertility, we crossed the males with reduced or inhibited endocycling to wild-type Canton-S females at a male-to-female ratio of 1:8 for individual male fertility assays. We observed significantly reduced offspring from males with reduced ploidy in the ED (Fig. 4J), suggesting the smaller organ size and reduced DNA content may lead to reduced secretion of essential ED-specific factors. We confirmed the compromised male fertility was not due to reduced offspring viability by performing counts of embryos, pupae and adult offspring, confirming >90% viability of the progeny (Fig. 16C).

2.3.6 Inducing extra endoreplication in the ED leads to organ hypertrophy

We next asked whether genetic manipulations expected to promote S-phase entry and increase or prolong endocycling would impact ED size and function. Overexpression of the G1-S Cyclin/Cdk complexes including CyclinE/Cdk2 and CyclinD/Cdk4 in *Drosophila* male accessory glands leads to increased endoreplication, as does knockdown of the E2F inhibitor Rbf with RNAi (Box et al., 2024). On the day of eclosion, we observed mild increases in EdU incorporation and organ size with these manipulations (Fig. 5A–C), but by day 10 of adulthood we observed significant increases in organ size, nuclear area and ploidy (Fig. 5D–G, Fig. 15C and D), suggesting that growth and endocycling are already maximally activated on the day of eclosion and that our manipulations led to additional endocycles resulting in higher ploidies, with many cells containing 64C DNA content, a state normally never observed in the ED. These results were further confirmed by knocking down the DNA replication licensing inhibitor Geminin (Diffley, 2004), which also led to a small increase in nuclei with 64C DNA content (Fig. 5A–G). Despite the increased organ size and DNA content, we observed no significant increases in male fertility (Fig. 5H).

2.3.7 Stabilized Geminin effectively blocks adult endoreplication in the ED

Geminin is a DNA replication licensing inhibitor that is targeted for degradation during the cell cycle by the Anaphase Promoting Complex/Cyclosome (APC/C) ubiquitin ligase (Diffley, 2004; Zielke et al., 2008). A stabilized form of geminin lacking the “Destruction Box” site for APC/C-dependent ubiquitination dominantly blocks S-phase entry when overexpressed in *Drosophila*

tissues. To rigorously test whether endocycling is required in the ED we expressed stabilized Geminin using the Luna-Gal4 driver. EdU incorporation on the day of eclosion is nearly completely blocked by stabilized Geminin. EDs that normally exhibit >150 EdU + nuclei exhibit at most 17 EdU + nuclei when stabilized Geminin is expressed (Fig. 6A–C). Blocking the endocycle led to a significant reduction in the area of the ED on DOE (Fig. 6D) and a mild reduction in ploidy (Fig. 6E). By day 10, EDs expressing stabilized Geminin still had not endocycled, indicating a nearly complete block, resulting in dramatically smaller organs (Fig. 6F–G), cells with severely compromised ploidies (Fig. 6 H, Fig. 15E) and severely compromised male fertility (Fig. 6I). This suggests the post eclosion endocycles in the ED are required for proper male organ function and fertility.

2.3.8 Juvenile hormone (JH) signaling promotes post eclosion endoreplication and growth of the ED

JH is a family of acyclic sesquiterpenoids released by the endocrine gland Corpus allatum, which plays an important role in ***D*** development and reproduction (Flatt et al., 2005; Jindra et al., 2013). A pulse of JH is released immediately post-eclosion (Bownes and Rembold, 1987; Zhang et al., 2021) and in females JH has been shown to play an important role in inducing polyploidy in the fat body during vitellogenesis to promote reproduction (Ren et al., 2020; Riddiford, 2012; Wu et al., 2018, 2020). The well-studied nuclear effectors of JH signaling include methoprene-tolerant (Met), germ-cell expressed (gce), and their co-factor taiman (tai) (Baumann et al., 2010; Li et al., 2019). We recently showed that JH receptors Met and Gce are required for post-eclosion endocycling in the accessory gland (Box et al., 2024). We therefore wondered whether this pathway may also mediate post-eclosion endocycling in the ED. We knocked down Met, gce, and tai via UAS-RNAi using Luna-Gal4. We observed reduced EdU incorporation on the day of eclosion in all three knockdowns compared to the control mCherry RNAi (Fig. 7A and B). Consistent with partially redundant functions, knocking down both Gce and Met together resulted in a more dramatic reduction of endoreplication on the day of eclosion (Figs. 16A and B). The area of the ED was also reduced on the day of eclosion and significant reductions in organ size and ploidy were observed at day 10 with JH receptor knockdowns, indicating the endocycles were not simply delayed (Fig. 7C–F). Male fertility was also reduced compared to the control when JH receptors were knocked-down (Fig. 7G). Compromised male fertility was not due to reduced

offspring viability, as shown by embryo counts and counts of adult offspring confirming >90% viability of the progeny (Fig. 16D). These results suggest that JH signaling through gce, Met, and tai is required for post-eclosion ED growth via endocycles and optimal male fertility.

2.3.9 Juvenile hormone signaling is sufficient to overcome blocked endoreplication in the adult ED

We recently showed that ectopic JH was sufficient to promote additional endocycling in post-eclosion accessory glands (Box et al., 2024). We tested this in the ED, but the level of endocycling on the day of eclosion in the ED is already so high under control conditions, we found it difficult to assess whether ectopic JH could further increase it (Fig. 16E). Therefore, we overexpressed stabilized Geminin or Dacapo-GFP, both of which nearly completely block endocycling in the ED (Fig. 4, Fig. 6A), to ask whether ectopic JH may be sufficient to restore some endocycles in the ED on the day of eclosion. Strikingly, ectopic JH was sufficient to restore EdU labeling in EDs expressing either stabilized Geminin or Dacapo-GFP, with half of the samples exhibiting >60 EdU positive cells Figure 8A-E. Since Geminin is a replication licensing inhibitor, this suggests JH acts somehow to either reduce the levels of stabilized Geminin in this context, or to promote DNA replication in parallel to or downstream of replication licensing. We confirmed that treatment with JH did not alter or reduce the levels of Luna-Gal4 driven UAS-RFPnls expression suggesting levels of stabilized UAS-driven Geminin should be similar among samples treated with vehicle (acetone) vs. JH (Fig. 4F). We further confirmed this by measuring levels of Dacapo-GFP expression in EDs treated with vehicle vs. JH, which also did not change (Fig. 15G). JH treatment did not lead to any detectable mitoses, as measured by PH3 staining (Fig. 16E). Thus, we favor the hypothesis that JH signaling activates targets in parallel to or downstream of the replication licensing complex to promote endocycling in the adult ED. Indeed, previous work on JH signaling in the female adult fat body of locusts suggests the replication licensing factor Cdc6 and components of the replication complex MCMs 4 and 7 are transcriptional targets of JH signaling to promote endocycling (Guo et al., 2014; Wu et al., 2016).

2.3.10 JH signaling and the endocycle are required for proper protein synthesis in the adult ED.

Polyploidy is often correlated with increased biosynthetic capacity for secretory cells (Edgar and Orr-Weaver, 2001). To resolve the biological function of the post eclosion endocycles in the ED driven by JH signaling, we examined whether JH signaling altered the level of nascent protein synthesis in the ED. To test this, we used a well-established puromycin-Click-IT based labeling assay that fluorescently labels nascent proteins (Deliu et al., 2017). When we use Luna-Gal4 to drive RNAis to tai, gce or Mmet, we observe significant reductions in protein synthesis in the ED compared to mCherry RNAi controls, when normalized to the total area of the ED. (Fig. 9A and B). JH signaling has been proposed to promote protein synthesis as well as promote the endocycle (Braun and Wyatt, 1995; Wilson et al., 2003; Wolfner et al., 1997; Wu et al., 2018, 2020; Yamamoto et al., 1988), so we next examined whether preventing the post eclosion endocycles could reduce protein synthesis in the adult ED, independent of JH signaling. Indeed, inhibition of the endocycle effectively reduced protein synthesis in the adult ED. We observed significantly reduced nascent protein synthesis in the ED when we knocked down E2F1 or E2F2, or overexpressed Rbf280, stabilized Geminin or Dacapo-GFP using Luna-Gal4 (Fig. 9C–F). Protein synthesis is high in the secretory adult ED but could be further increased by manipulations that increased the endocycling in the ED, such as overexpression of the G1-S Cyclin/Cdk complexes CyclinE/Cdk2 and CyclinD/Cdk4 using Luna-Gal4 (Fig. 9G and H). These results show that the JH-induced post eclosion endocycling in the ED is required for the proper levels of protein synthesis in the secretory cells of the growing ED.

2.3.11 Protein synthesis in secretory cells of the ED requires mTOR signaling and is coupled to ED growth via the endocycle

The conserved mTOR signaling pathway is a key regulator of protein synthesis (Grewal, 2009; Yang et al., 2022). To test whether protein synthesis in the ED is modulated by mTOR signaling we manipulated components of the pathway, including overexpressing the mTOR activating GTPase Rheb, and inhibiting core pathway components such as mTOR and the mTOR Complex 1 (mTORC1) target, ribosomal S6 Kinase (S6K), by RNAi. Rheb overexpression using Luna-Gal4 was sufficient to increase protein synthesis in the secretory cells of the ED, without promoting significant additional endocycling or organ growth. (Fig. 10 A, B, E, F). By contrast, we observed significantly reduced protein synthesis when we knocked down S6K and mTOR using Luna-Gal4 (Fig. 10C and D). We observed a mild reduction in the percentage of 32C cells with the S6K

knockdown, although this did not affect organ growth, whereas mTOR knockdown significantly reduced ploidy and ED size (Fig. 10E and F). This demonstrates that proper protein synthesis in the secretory cells of the ED requires mTOR signaling and that severe mTOR inhibition can reduce ED endocycling to impact organ growth. We suggest that modulation of mTOR signaling sufficient to alter protein synthesis levels but not the endocycle, does not impact organ growth, while severe inhibition of mTOR does reduce endocycling, which reduces organ growth.

2.4 Discussion

In this work, we demonstrate that the ploidy of the secretory cells of the *Drosophila* male ED impact organ growth and function. Our data suggests this organ is shaped in part through regulated endocycling, which is required for proper protein synthesis levels and organ growth to support male fertility. The growth and endoreplication in the young adult male ED is dependent on Juvenile Hormone signaling post eclosion, and ectopic JH is sufficient to drive additional endocycling in the early adult tissue. The *Drosophila* ED is an important post-mitotic tissue, essential for male fertility, where hormonal signaling, cell growth pathways and cell cycle regulation intersect to impact tissue morphogenesis and function (Fig. 11).

2.4.1 Post-eclosion endoreplication in the secretory cells of the ED is required for organ growth, protein synthesis and male fertility.

Here we show that the secretory cells of the male ED undergo endoreplication in young adults, leading to increases in organ size and ploidy. The cells largely exit from endoreplication by day 3 and reach a maximum ploidy state with the mature organ composed of largely 16C and 32C cells, that are maintained throughout adulthood. When we directly manipulate core cell cycle machinery, ED size, protein synthesis and fertility are affected. While we do not see significant increases in fertility when organ growth is driven through additional endocycling, we do see significant decreases in fertility when endocycles are compromised. Many secretory cells require cell cycle variants that lead to the production of additional copies of genes to support uniquely high biosynthetic requirements for specialized cells (Edgar and Orr-Weaver, 2001). Perhaps the most striking examples are the cell cycle alterations that lead to the amplification of specific genes, such as that observed in the *Drosophila* follicle cells of the ovary preparing to secrete the chorion for the egg (Orr-Weaver, 1991) or the trophoblast giant cells of the mammalian placenta (Hannibal

and Baker, 2016). Extensive endoreplication and polyploidization is also seen in the highly secretory cells of the *Drosophila* larval salivary gland, which secrete extensive amounts of glue proteins and components required for pupal adhesion during metamorphosis (Chung et al., 2014). The male *Drosophila* ED, is made up of about 500 cells, yet is required to synthesize a significant amount of seminal fluid components to support male fertility. Our protein synthesis assays in this tissue show that this process is highly active in these cells, modulated by growth and hormonal signaling, and highly responsive to alterations in cellular ploidy.

The normal ploidy distribution in the ED is highly reproducible from animal to animal, suggesting it is tightly regulated. We only observe ploidies higher than 32C with strong direct cell cycle manipulations, such as direct activation of G1-S cell cycle regulators or inhibition of cell cycle checkpoint regulators such as the G1-S inhibitor Rbf or the replication licensing inhibitor Geminin. Even under these strong cell cycle manipulations, the maximum DNA content observed in the ED is 64C across adult timepoints, suggesting the ED cells are only capable of limited extra rounds of endoreplication. Further work will be needed to understand the additional mechanisms promoting cell cycle exit in these cells that limit their ability to endoreplicate further.

2.4.2 JH promotes the early adult endoreplication in secretory cells of male Drosophila ED

JH signaling is involved in multiple aspects of *Drosophila* male fertility (Braun and Wyatt, 1995; Wilson et al., 2003). While the use of JH transcriptional response reporters suggest signaling levels are high in the seminal vesicles, and lower in the accessory glands and ED, there are notable differences between reporters using a JH response element from mosquitos vs a JH response element from the *Drosophila melanogaster* JH target gene Kr-h1 (Kurogi et al., 2024). We recently showed that JH signaling is required for an early post-eclosion endocycle in the adult male *Drosophila* accessory gland (Box et al., 2024), and here we show that JH performs a similar function in the adult ED. Work from the Riddiford lab has shown JH receptors Gce and Met are strongly expressed in the accessory gland and ED (Baumann et al., 2017), and when we examine gene expression in the Luna positive ED cells of the single cell Fly Cell Atlas (Li et al., 2022), we see overlapping expression of JH targets Kr-h1 and E75 (Dubrovsky et al., 2004). JH signaling has been shown to promote polyploidization by activating the transcription of the genes involved in regulating S-phase and DNA synthesis (Guo et al., 2014; Wu et al., 2016, 2020) and may also

suppress mitosis indirectly through upregulating replication licensing factors, or through other mechanisms (Truman et al., 2024). While we do not yet know the direct targets of JH signaling in the male accessory gland or ED, our finding that JH is sufficient to drive additional endocycling in tissues where the endocycle is blocked by stabilized Geminin, suggests the critical targets are likely to be downstream of the typical G1-S cell cycle regulators and may act at the level of DNA replication licensing and replication. Provocatively, JH receptors Gce and Met have been shown to activate components of the DNA replication complex such as Mcm4 and Mcm7, and the DNA replication licensing factor Cdc6, by binding to an E-box region of their promoters in female locust fat body (Guo et al., 2014; Wu et al., 2016, 2020). Further work will be needed to identify the targets of JH signaling that drive endoreplication in the secretory cells of the male reproductive system.

2.4.3 Using the Drosophila ED as a context to study post-mitotic tissue growth

Studies of the ED have been limited to descriptive approaches such as transcriptomics and proteomics due to the lack of a tissue-specific Gal4 driver to permit inducible genetic manipulations. Here we show that a specific Luna-Gal4 driver can be effectively used to manipulate pathways regulating hormonal signaling, protein synthesis and the cell cycle in the adult ED. The driver turns on in the late pupal stages a few hours prior to eclosion and maintains expression throughout adulthood, independent of mating status. Using this driver we show that the mTOR signaling pathway intersects with the cell cycle pathway, such that severe inhibition of mTOR signaling leads to a reduction in endocycling and cellular ploidy. This intersection may be through mTOR regulation of E2F1 protein production (Ovrebo et al., 2022), as E2F1 is required for proper endocycling in this tissue (Fig. 4) and across other endocycling tissues (Zielke et al., 2011). While severe inhibition of mTOR signaling limits endocycling, increased mTOR signaling is sufficient to increase protein synthesis without significantly increasing endocycling in this tissue. Thus, milder manipulations of mTOR signaling allow us to separate out the effects of altering protein synthesis from effects on the endocycle that more strongly impact organ size. JH signaling has been shown to promote both protein synthesis for reproduction and the endocycle (Guo et al., 2014; Wu et al., 2016, 2018, 2020; Yamamoto et al., 1988). Here, because these pathways are linked through mTOR, we cannot rigorously discern whether JH acts through one or both of these pathways in the ED. But our data strongly suggests the impact of JH on the endocycle

is likely to be the major effector of its impact on postmitotic ED growth. Additional work will be needed to discern the targets of JH signaling in this tissue, to allow for manipulations of specific outputs of the hormonal growth response.

The similar response of the accessory glands and ED to the post eclosion JH pulse suggests that these two secretory, polyploid tissues are physically linked, as well as linked in function and hormonal response. Since these tissues are involved in producing and secreting seminal fluid components required for male fertility, we suggest that together these tissues can be considered to compose the *Drosophila* prostate-like organ. The mouse prostate is made up of multiple lobes connected to the urethra, while in humans the prostate is made up of multiple zones (Wang et al., 2018). We suggest the *Drosophila* prostate-like organ is made up of two tissues, the accessory glands and the ED, connected via a transition zone made up of the anterior ED papillae. Further work will be needed to examine the cell cycle status of the anterior ED papillae, and we note that accessory gland drivers such as Paired-Gal4 and the ED driver Luna-Gal4 described here, do not drive expression in the transition zone.

A major regulator of mammalian prostate growth and function is the steroid hormone Androgen (Banerjee et al., 2018; Massie et al., 2011). Androgen signaling in the mammalian prostate intersects with cell cycle regulation and is a major regulatory axis in mammalian prostate regeneration and cancer (Balk and Knudsen, 2008; Schiewer et al., 2012). Steroid hormone signaling via the ecdysone pathway has been shown to play a role in regulating growth and the endocycle in the male *Drosophila* accessory gland (Leiblich et al., 2019; Sekar et al., 2023; Sharma et al., 2017), but whether ecdysone impacts the ED remains unknown. This question can now be addressed using the ED Gal4 driver we discovered. Our work on JH signaling in the accessory gland has shown that steroid hormone signaling via ecdysone is not the only hormone signaling axis regulating the accessory gland endocycles. Similarly, we expect that JH will not be the only hormonal signaling pathway regulating endocycling and growth in the ED. JH and ecdysone signaling often act in opposition to each other and can converge on shared targets. Future work will be needed to discern whether there is an interplay between JH and ecdysone signaling pathways in these reproductive tissues.

2.5 Materials and Methods

2.5.1 Drosophila husbandry

All the flies used in this paper were housed at room temperature (23°C) on a Bloomington Cornmeal food without crowding (less than 50 animals per vial). For all the day of eclosion (DOE) experiments males were collected immediately post-eclosion (0-4hrs) in a fresh media vial. All the male flies used in all the experiments are virgins except for those used in fertility assays. For day 10 experiments the males were collected on DOE and transferred 5 to 8 flies per vial all males, aged until day 10 with flipping into fresh media vials at an interval of 2-3 days and housed at room temperature.

2.5.2 Fly strains used

Canton S

The following *Drosophila* species were kindly provided by the P. Wittkopp Lab (U. Michigan)
D. simulans

D. yakuba

D. pseudoobscura

D. willistoni

D. virilis

Other lines used for the study are as follows:

Luna-Gal4 (BDSC#63746).

Luna-Gal4 recombined with UAS-nlsRFP

mcherry-RNAi (BDSC #35785).

E2f1-RNAi (BDSC #27564).

E2f2-RNAi (BDSC #36674).

UAS-Rbf280 (BDSC #50748).

Dacapo-OE: UAS-Dacapo-GFP (BDSC #83337).

CycE-Cdk2-OE: y,w, hs-flp; +; UAS-CycE,UAS-Cdk2/TM6B (Buttitta et al., 2007).

CycD-Cdk4-OE: y,w,hs-flp; UAS CycD, UAS-Cdk4 (Datar et al., 2000).

Geminin-RNAi (BDSC #30929).

Rbf-RNAi: (VDRC v10696).

Gce-RNAi (BDSC #26323 or #61852 in Fig. 16) (Rahman et al., 2017).

Tai-RNAi (BDSC #32885) This TRiP HMS00673 line is effective for Tai knockdown but results in hypomorphic phenotypes (Zhang et al., 2015).

Met-RNAi (BDSC #26205).

Stabilized Geminin: UAS-Gem DeltaD/DeltaKEN (BDSC #59069).

mTOR-RNAi (BDSC #33951).

Rheb OE: UAS-Rheb on 3 (BDSC #9689).

S6K-RNAi (BDSC #41702).

2.5.3 ED dissection, fixation, and Immunostaining

Drosophila male EDs were dissected in 1X Phosphate Buffered Saline (PBS). The dissected EDs were immediately transferred to an Eppendorf containing 1ml of 4% Paraformaldehyde (PFA) in 1X PBS to fix the tissues for 30 minutes under continuous rocking. Fixed EDs were rinsed twice using 0.1% Triton-X +1× PBS for 10 minutes each wash. Fixed EDs were permeabilized with 1% Triton-X+1X PBS for 30 minutes on a rocker. Permeabilized tissues were blocked with PAT (1X PBS, 0.1% Triton X-100, 1% BSA) for 10 min. Once tissues settled and PAT removed, tissues were resuspended in primary antibody freshly diluted into PAT at the indicated concentration (table below) and incubated overnight at 4ºC on a rocker. Tissues were washed with 1XPBS 0.1% Triton X-100, 3 times 10 min. Tissues were blocked with 2% Normal Goat Serum in PBT-X (1× PBS + 0.1% bovine serum albumin + 0.3% Triton-X (PBT)-X) for 10 min at room temperature. Secondary antibodies were diluted 1:2,000 in 2% Normal Goat Serum in PBT-X and incubated for

4 hours under continuous rocking at room temperature. EDs were washed thrice with 1X PBS 0.1% Triton-X prior to incubation with DAPI 1µg/ml for 15 minutes and subsequent mounting. For actin staining we added 2 drops of Actin Red 555 in 1ml of PBS and incubated the EDs for 30 mins and washed twice prior to mounting. Tissues were mounted in Vectashield (Vector Labs). using spacers between the slides and coverslip with double-sided tape or one layer of clear nail polish. The list of antibodies used is in the following table with their dilutions.

Table 2.1: List of antibodies and their dilutions used

Antibody	**Source**	**Catalog numbers**	**Dilutions Used**
Mouse Anti-Myosin	Developmental Studies Hybridoma Bank	MF 20	1:500
Actin Red 555	Thermo Fisher Scientific	R37112	2 drops/ml
Mouse Anti-Fas III	Developmental Studies Hybridoma Bank	7G10	1:500
Rabbit Anti-Tinman	Developmental Studies Hybridoma Bank	Tinman	1:500
Mouse Anti-Integrin Beta PS	Developmental Studies Hybridoma Bank	CF.611	1:200
Mouse Anti-Futsch	Developmental Studies Hybridoma Bank	22C10	1:200

Rat Anti-Elav	Developmental Studies Hybridoma Bank	7E8A10	1:100
Mouse Anti- Discs large (DLG)	Developmental Studies Hybridoma Bank	4F3	1:500
Rabbit Anti-Phospho Histone3 Serine 10 (PH3)	Millipore	06-570	1:500
DAPI-DNA Dye	Sigma-Aldrich	D9542	1:1000
Alexa Fluor Goat 488 anti-mouse	Invitrogen	A11029	1:2000
Alexa Fluor 568 goat anti-mouse	Invitrogen	A11031	1:2000
Alexa Fluor 568 goat anti-rat	Invitrogen	A11077	1:2000
Alexa Fluor Goat 633 anti-mouse	Invitrogen	A21052	1:2000

2.5.4 5-Ethynyl-2-deoxyUridine (EdU) feeding and labeling

Two different parameters were used to label DNA synthesis using EdU. For EdU labeling on the day of eclosion (DOE) we dissected the EDs in *Drosophila* Ringer's solution (Sullivan and Hawley, 2000) and incubated the dissected live EDs in 0.1 mM of EdU in Ringers Solution for 1

h at room temperature (23 °C) on a rotator with medium speed. After 1-h EdU incubation, EDs were fixed in 4% PFA/PBS, permeabilized as described above performed the Click-it reaction for Alexa-Fluor 488 or Alexa Fluor 555 (Thermofisher EdU Click-IT Plus C10638) as described by the manufacturer. For prolonged labeling of endoreplication, we fed animals an EdU solution made with 1 mM EdU, 10% Sucrose in PBS, and blue food coloring (5 µl/ml) on Whatman paper. We confirmed uptake of the EdU solution by detection of blue food dye in the animals prior to dissection. For the experiments in Fig. 1E–G we fed the animals with EdU for a 24hr interval prior to dissection. For the experiments in Fig. 2A and C we fed the animals with EdU from the day of eclosion until Day 10 post eclosion. For long term multi day labeling, Whatman paper with freshly made EdU solution to was added to vials every other day. To quantify the median fluorescence intensity (MFI) of the EdU, we imaged the EDs at 10X magnification on a Leica confocal, keeping the detector gain and laser power the same across all the samples for comparison. Using ImageJ (Fiji) we quantified the intensity of EdU per unit area of ED. We repeated EdU experiments in three independent trials, with at least 3 EDs in each trial.

2.5.5 Confocal imaging

EDs (except for EdU) were imaged using a Leica SP8 Confocal microscope with 40X objective. Some images (as indicated) were taken at 10X and 20X magnification using a Leica SP5 Confocal microscope or Leica DMI6000B epifluorescence system with ImageQuant Deconvolution.

2.5.6 Area measurements

A complete ED image was captured in one frame using a Leica SP5 Confocal microscope with 10X objective. The images were opened in Fiji ImageJ software and obtained the maximum Z projection of the stacks of the image. Manually using the free hand selection tool, the area around the ED was drawn from the anterior end of the ED where the AG and seminal vesicles are connected to the posterior end of the ED where it connects to the EB. The area around the ED was measured by clicking Analyze and then Measure. These area values were plotted using the GraphPad Prism.

2.5.7 Juvenile Hormone ex-vivo assay

Juvenile Hormone III (Sigma Aldrich #J2000) was reconstituted in acetone to generate a stock concentration of 10 mg/ml. We used a final concentration of 0.1 µg/ml diluted in Ringer's solution for all the JH ex-vivo experiments. Tissues were dissected in Ringer's solution immediately after eclosion and incubated in JH III or acetone vehicle along with 0.1 mM of EdU to assess the endoreplication levels in the presence and absence of JH III for 1 h under continuous rotation at room temperature. After the 1-h incubation of vehicle or JH III and EdU, the tissues were fixed, permeabilized, and stained as described above. We repeated JH experiments in three independent trials, with at least n = 3 samples in each trial (n therefore = at least 9 in total, except for controls in Fig. 8 with vehicle only, where n = at least 4).

2.5.8 Ploidy/DAPI intensity measurements

DAPI images were obtained with a Leica SP8 confocal microscope, taking care not to underexpose or saturate the DAPI intensity. Images were exported in Tiff format and opened in Fiji Imagej. The maximum projection of the stacks of DAPI-stained images was obtained. We observed that the basally located nuclei in the external muscle layer of the ED are diploid by flow cytometry. We therefore used these diploid nuclei to normalize the measurements of ED secretory cells and to calculate the haploid nuclei intensity. We subtracted the background intensity by drawing regions of interest (ROI) in the background region of the images and subtracting the background MFI. ROIs were manually drawn around the DAPI-stained nuclei of diploid and polyploid secretory cells. We also performed tests using *Luna-Gal4* driven *UAS-RFP$_{NLS}$* fluorescence to segment nuclei, and obtained similar results across multiple experiments. The raw integrated density of diploid and secretory were measured for at least 30 secretory cell polyploid nuclei and 10 diploid nuclei from multiple EDs. We calculated the corrected fluorescence intensity from each nucleus raw integrated intensity, by subtracting the average background intensity. The intensity of the haploid nuclei DNA was calculated by taking the average of the diploid nuclei intensity and dividing it by half, we used this as a reference of haploid nuclei with DNA content of 1C. Based on these haploid nuclei we estimated the DNA content of polyploid secretory cell nuclei. For Figure 4F, we directly scored the DNA content without binning. For all other DNA content/ploidy measurements, we plotted after the following binning-2N (1.9-2.9), 4N (3.0-6.9), 8N (7-12.9), 16N (13.0-24.9), 32N (>24.9).

2.5.9 Fertility Assay

Virgin males were used to set up the fertility assay in all the genotypes mentioned in the figures. We used 2-3-day-old virgin Canton S females to cross the males of each genotype. We used a ratio of 1:8 (one Male: eight Females in a vial) to set up the fertility assay in each vial and allowed them to mate for 3 days in a 25°C incubator. The total number of the embryos laid, pupae and the eclosed offspring were counted and plotted. For each genotype, we performed the fertility assay for at least 5 males in three independent trials therefore, n= at least 15 males.

2.5.10 Flow Cytometry

Nuclei from were isolated from EDs at the indicated time points. Nuclear preps were performed in S2 media (Thermofisher #21720024) with 10%Fetal Bovine Serum (Cytiva # SH30396.02HI) and 1% Pen-strep antibiotic solution. The EDs were dissected in Ice-cold S2 media+10%FBS+1% Pen-strep with 25-30 EDs for the nuclear extraction per sample. We briefly spun the tissues to allow them to settle, removed the S2 media, and added 1ml of Lysis Buffer (10mM Tris HCl-pH 7.4, 10mM NaCl, 3mM MgCl2, 0.1% NP40) for transfer to a Dounce homogenizer placed on ice. To release the nuclei, tissues were homogenized with 20 strokes of the loose Dounce pestle followed by a rest on ice for 5 minutes. Next, homogenization was performed with a tight Dounce pestle for 40 strokes. Tissue was triturated with a silanized fire-polished glass Pasteur pipette (BrainBits). The resulting homogenate was filtered through a 100 micron filter mesh, followed by filtering through a 40 micron filter mesh to remove debris and unlysed tissue. To this filtered homogenate, 100µl of S2 media was added to stop the lysis reaction. This filtrate was centrifuged at 800 rcf for eight minutes at 4°C to pellet nuclei. Supernatant was removed, and 200µl of S2 media was added to the pelleted nuclei with incubation on ice for 5 minutes. After incubation, an additional 800µl of S2 media was added and centrifuged for eight minutes at 800 rcf, 4°C. Supernatant was removed and the pellet was resuspended in 200µl S2 media with Vybrant DyeCyle Violet (Invitrogen #V35003) at a ratio of 1:100 and allowed to incubate on ice for 5 minutes. After the incubation, 800µl of S2 media was added and centrifuged at 800rcf for eight minutes at 4°C. The supernatant was removed, and the pellet was resuspended in 1ml of S2 media, gently vortexed, and run on an Attune Flow Cytometer. We used ovaries as a positive control for

ploidies beyond 4C, to overlay the ED peaks. We followed the same steps to isolate the nuclei from the ovaries and stained them with the same protocol. For flow cytometry on different Drosophila species, we overlaid the ED ploidy plot with ovaries from the matching species. All flow cytometry experiments were repeated at least three times with at least 25 EDs combined in each trial. One representative example from the three trials is shown.

2.5.11 Protein synthesis O-propargyl-puromycin (OPP) Assay

We performed the OPP assay in S2 Media (invitrogen) that has been reconstituted with 10%FBS and 1% Pen-strep. Tissues were dissected in S2 media and incubated with 20 μM of OPP (O-Propargyl Puromycin, Thermofisher) in S2 media for 10 minutes. The tissues were immediately fixed in 4% paraformaldehyde made with 1XPBS for 30 minutes. Fixed EDs were rinsed twice using 0.1% Triton-X +1× PBS for 10 minutes each wash. Fixed EDs were permeabilized with 1% Triton-X+1X PBS for 30 minutes on a rocker. The click-it reaction was performed according to the manufacturer's protocol (Thermofisher #C10456). After labeling, the tissues were washed twice with 0.1% Triton-X-1XPBS for 10 minutes each wash, stained with DAPI as described above, and mounted using Vectashield as described above. OPP assays were repeated three times, with at least 3 EDs in each trial. Damaged or folded samples were removed from quantification. We quantified the Mean Fluorescence Intensity (MFI) of OPP fluorescence by normalizing the integrated intensity of OPP signal to the area of the ED.

2.5.12 Software and data analysis

We used Fiji ImageJ to analyze all the imaging data. We used GraphPad Prism software to plot values and perform statistical tests. The specific tests and parameters used to determine significance are mentioned in the figure legends.

2.5.13 Acknowledgments

We thank Dr. P. Wittkopp and the Wittkopp Lab for providing *Drosophila* of various species. We thank S.J. Church for contributions to developing the flow cytometry protocol for the ED. We thank Buttitta Lab members for valuable discussions and suggestions on this project. Funding for this work was provided by the National Cancer Institute (P01CA093900) and the National Institute of General Medical Sciences of the National Institutes of Health (R01GM127367 and

R35GM149273). A. Box was supported in part by the University of Michigan Organogenesis Predoctoral Training Grant (NIH T32 HD007505) and the Eunice Kennedy Shriver National Institute of Child Health and Human Development of the National Institutes of Health (NIH F31HD103430). The authors have no conflicts of interest to disclose.

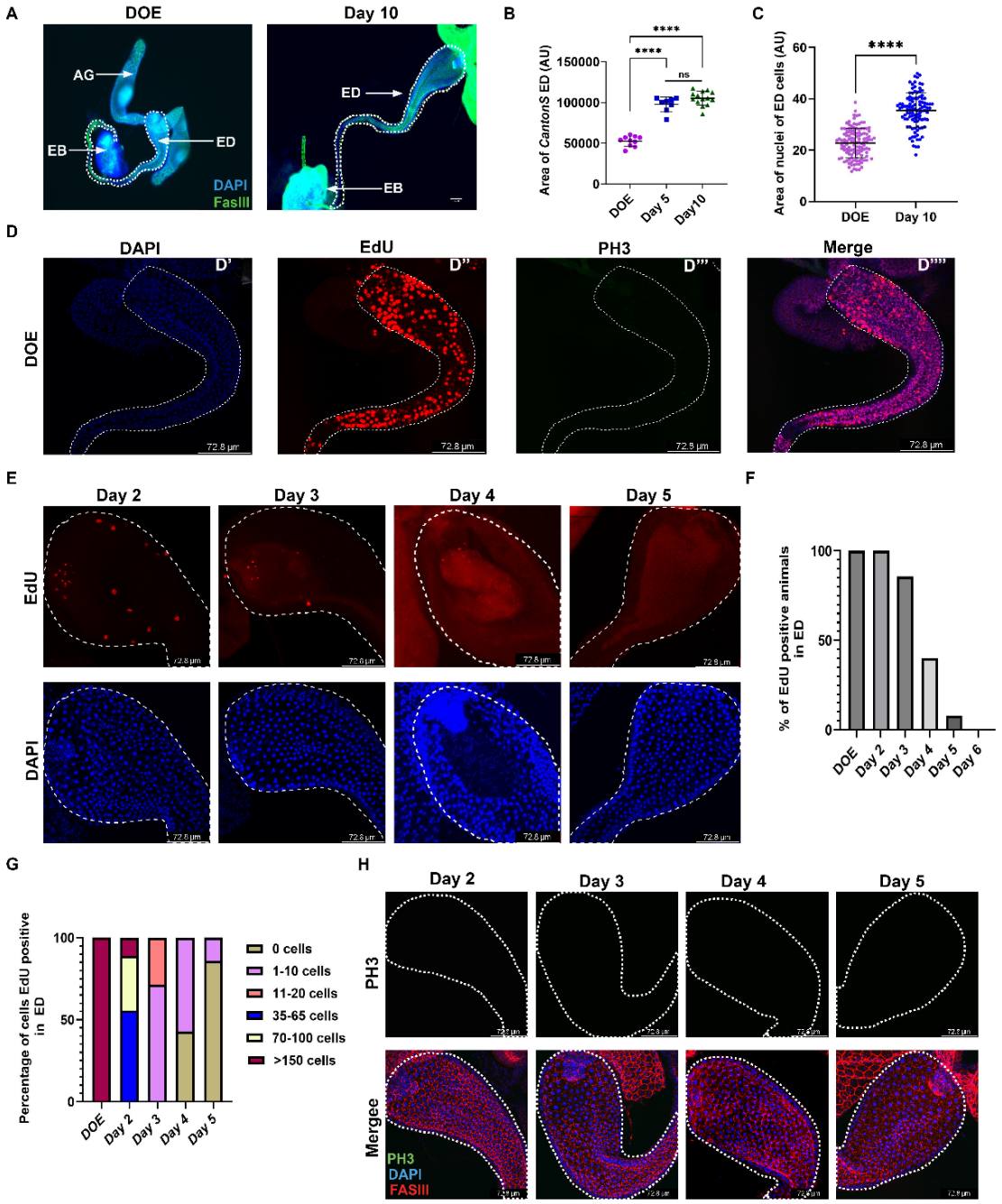


Figure 2.1: Endoreplication of secretory cells of the adult *Drosophila* Ejaculatory Duct and post-eclosion organ growth.

A. Images of adult ejaculatory duct (ED) on the day of eclosion (DOE) and day 10 showing an increase in the tissue size on Day 10. The ED is outlined with a dotted line. The tissue is labeled with Fas III antibody. The images were captured at 10X magnification. Scale bar: 70µm
B. Quantification of the area of ED on DOE, Day 5, and Day 10 post-eclosion shows that the size of the ED increases from DOE to Day 5 and the growth ceases after Day 5 post-

eclosion. Each dot represents the area of one ED from each male fly (n=at least 9 across 3 independent experiments).

C. Quantification of the area of the nuclei of the secretory cells of the ED on DOE and Day 10 post-eclosion showing the increase in nuclear size. (n=9 with 10 nuclei from each animal measured.)
D. Confocal micrographs of the ED on DOE (0-2hrs post-eclosion) with EdU incorporation in secretory cells of ED with no mitotic PH3 positive cells. EdU incorporation was performed with an *ex vivo* exposure for 1 hour. D'-DAPI, D''- EdU staining, D'''- mitosis marker PH3 antibody staining. D''''- Merge with FasIII staining of ED. (n= at least 9)
E. Confocal micrographs of ED with EdU incorporation that was done by feeding the adult animals with EdU for 24hrs prior to time points on Day 2, Day 3, Day 4, and Day 5. Nuclei were labeled with DAPI. (n= at least 9 for each timepoint)
F. Quantification of the percentage of males that are EdU positive on DOE, Day 2, Day 3, Day 4, and Day 5 post-eclosion.
G. Quantification of the percentage of cells that are EdU positive in each ED on DOE, Day 2, Day 3, Day 4, and Day 5 post-eclosion. We classified the total EdU-positive cells into multiple groups: 0 cells, 1-10 cells, 11-20 cells, 35-65 cells, 70-100 cells, and>150 cells that are EdU-positive.
H. Micrographs of ED stained with the mitotic marker Phosphohistone H3 Ser10 (PH3) on Day 2, Day 3, Day 4, and Day 5. We did not observe any cells undergoing mitosis at any adult time points. (n= at least 9 for each timepoint).

Statistical analysis performed for Figure 2 B-C, Two-tailed unpaired t-test. $P<0.0001$ ****

Scale bar for panels D, E, H – 72.8 μm.

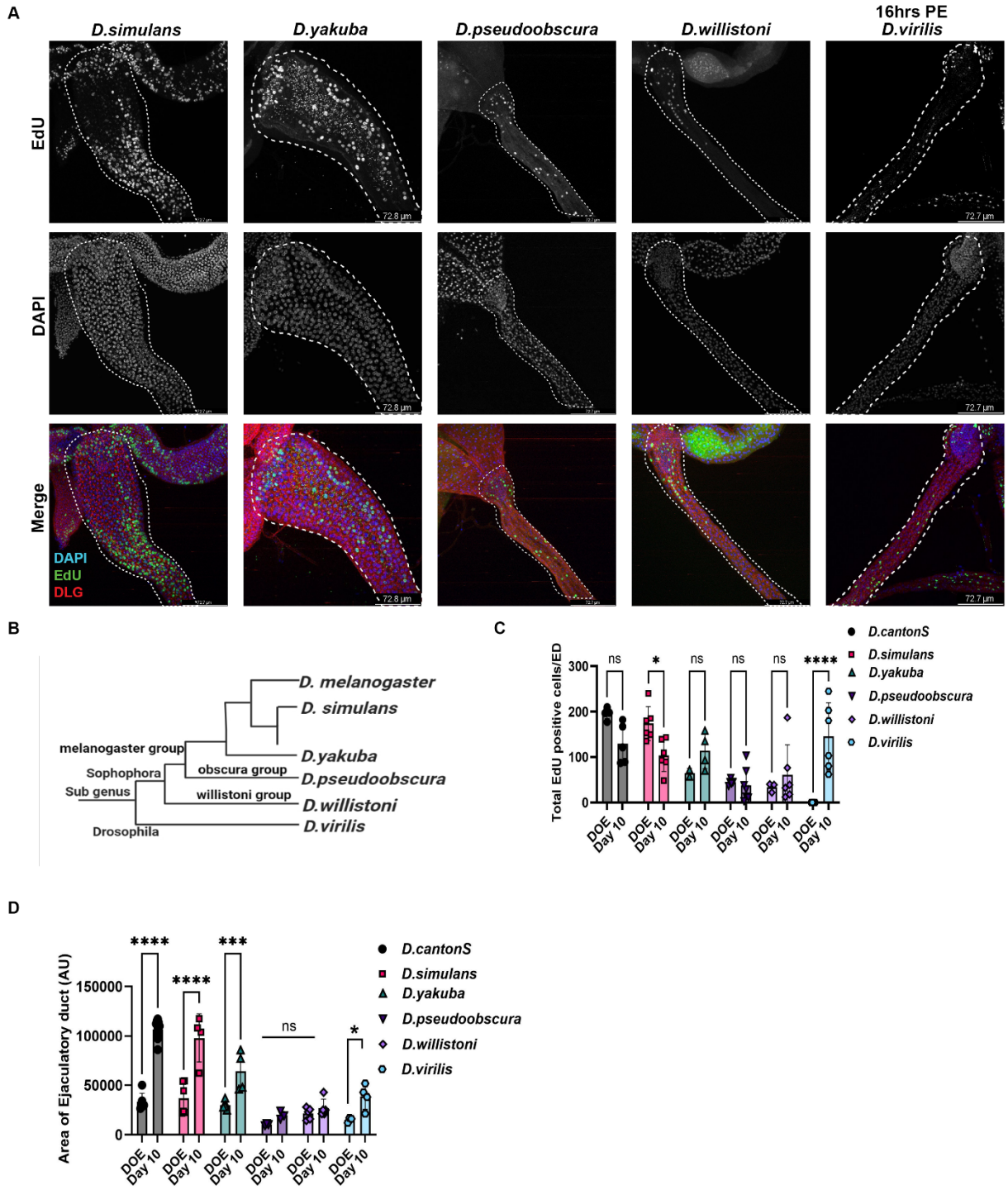


Figure 2.2: Post-eclosion endoreplication and growth of the ED is conserved in different *Drosophila* species.

A. Confocal micrographs of EDs from different *Drosophila* species labeled for 1 hour *ex vivo* with EdU on DOE (0-2hrs post-eclosion). Nuclei are labeled with DAPI, and the cell junctions of the secretory cells are labeled with anti-discs large (DLG). (n= at least 3 for each species) Scale bar:72.8 µm

B. A phylogeny tree for subgroups of the different *Drosophila* species examined.
C. Quantification of total EdU positive cells in different species on DOE performed with *ex vivo* EdU incorporation within 0-4 hrs post-eclosion. For day 10 EdU quantification we fed animals EdU until Day 10 and quantified the EdU incorporation on Day 10 (Male feeding begins ~6h post eclosion). (n= at least 3 for each species)
D. Quantification of the area of the ED on DOE (0-2hrs PE) and Day 10. (n= at least 7 for each species)

Statistical test performed: Two-way ANOVA with multiple comparisons between DOE and Day 10 for respective species. $P<0.0001$ ****

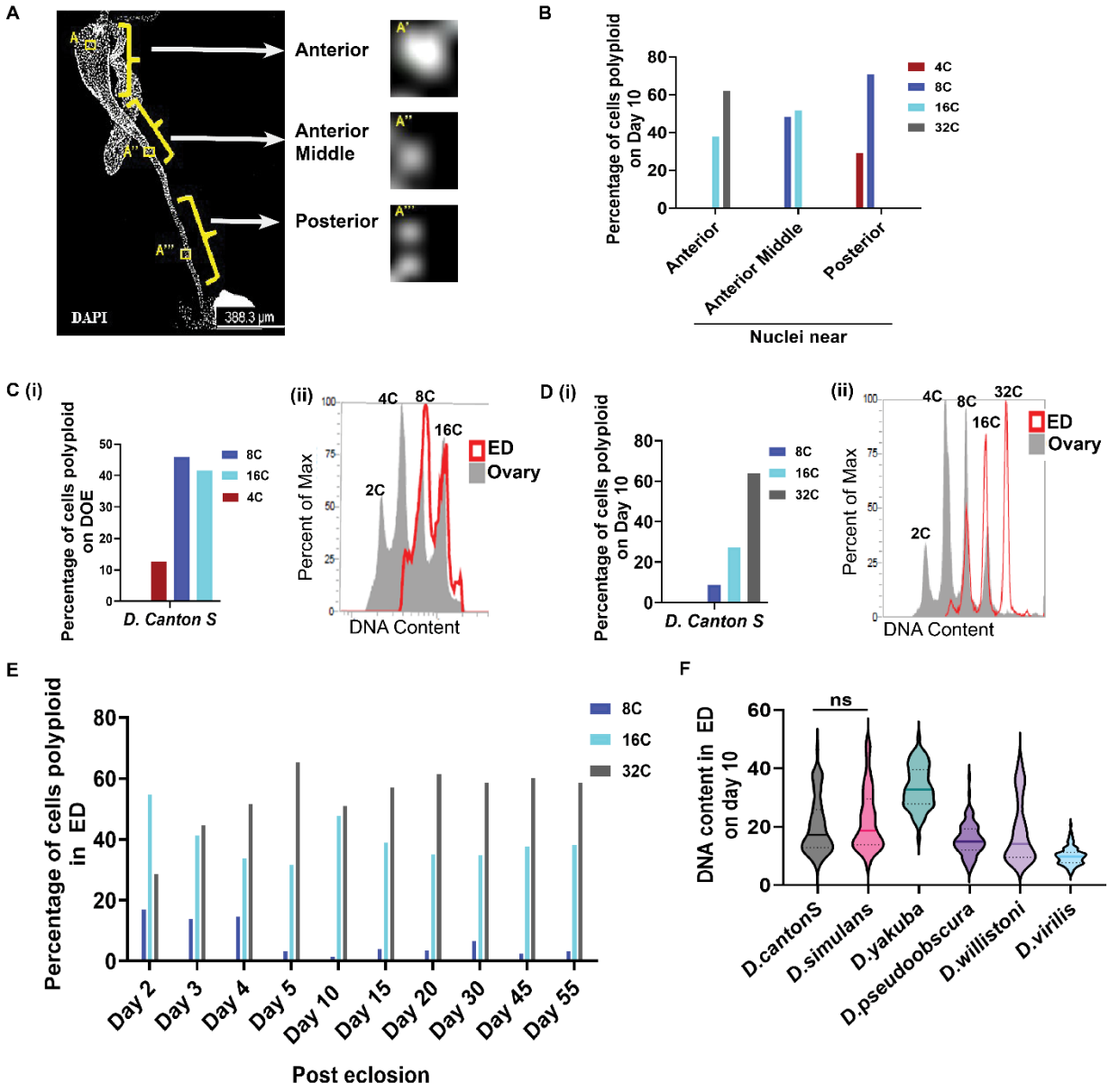


Figure 2.3: The ploidies of *Drosophila* Ejaculatory duct secretory cells correlate with local organ shape and size

A. Image of a whole ED, showing that the volume of the duct reduces from the anterior to posterior end. Based on this, we classified ED secretory nuclei into three zones, anterior, anterior-mid, and posterior. Zoomed images A', A'', A''' shows the nuclei of secretory cells from these respective regions of ED. Scale bar:388.3µm
B. Quantification of the DNA content/ploidy from the nuclei of the secretory cells from the anterior, anterior-mid, and posterior regions of the ED. We quantified the ploidy from males at 10 days by measuring the DAPI intensity, normalized to the muscle-layer diploid cells from that specific region. (n= at least 9, repeated in three independent trials)

C. (i) Quantification of the DNA content/ploidy on DOE by measuring images of the DAPI intensity, the endocycling secretory cells have ploidies of 4C, 8C, and 16C on DOE. (ii) Quantification of the ploidy of the secretory cells of ED by flow cytometry performed by isolating the nuclei from ED on DOE. The peak shaded in grey is from female ovaries which contains cells of known ploidies, and the ED is shown in red. Flow cytometry was performed three times, with a representative example shown.

D. (i) Quantification of the DNA content/ploidy from the secretory cells of the ED on Day 10 post-eclosion by measuring the DAPI intensity from images. (ii) Quantification of the ploidy from the secretory cells of the ED by flow cytometry performed by isolating the nuclei from males on Day 10 post-eclosion. The peak shaded in grey is from female ovaries which contains cells of known ploidies, and the ED is shown in red. Flow cytometry was performed three times, with a representative example shown.

E. Quantification of the DNA content/ploidies of secretory cells of the ED performed by measuring the DAPI intensity on different days post-eclosion showing that the ploidy distribution is unchanged and constant after Day 5. (n=7, From each animal we have quantified 30 nuclei)

F. Quantification of the DNA content/ploidy of the secretory cells by measuring the DAPI intensity in different species, showing that the secretory cells of EDs of different *Drosophila* species we used are polyploid. (n= at least 9, from each animal we quantified 30 nuclei)

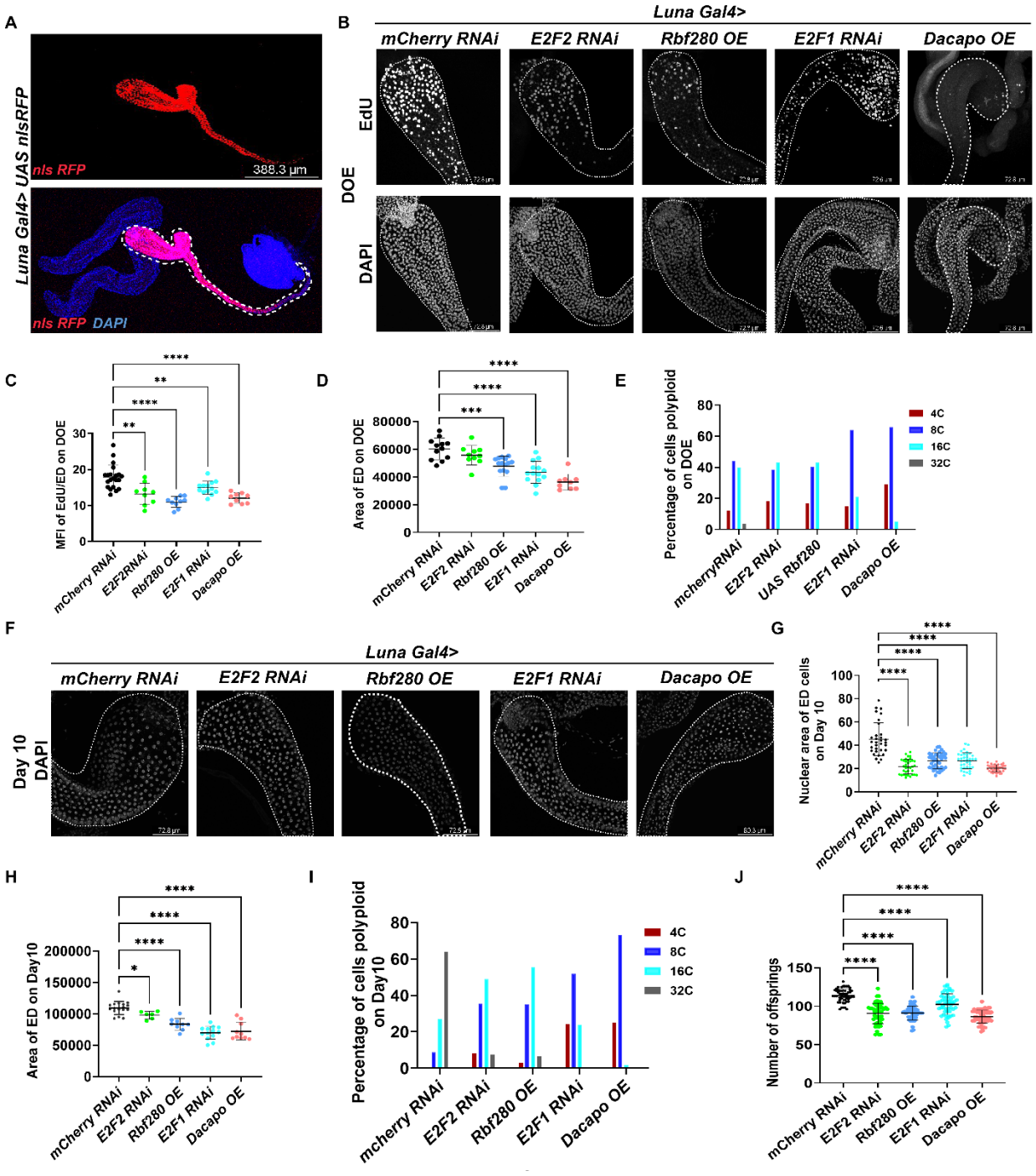


Figure 2.4: Compromising the endoreplication of ED secretory cells results in reduced ED size and fertility

A. Confocal micrograph of *Drosophila* male reproductive system showing the expression of *Luna Gal4* specifically in ED secretory cells verified with the expression of *UAS-nls-RFP* in the ED cells. Scale bar: 388.3µm

B. Confocal micrographs of ED on DOE with knockdown of *E2F1, E2F2* using RNAi, Overexpression of *Rbf280,* and *Dacapo-GFP* using *Luna Gal4*. The upper panel is the EdU labeling on DOE with *ex-vivo* incubation in the background of all these manipulations in ED secretory cells. We stained the nuclei with DAPI to measure the DNA content. N= at last 9 for each genotype. Scale bar:72.8 μm
C. Quantification of the Mean fluorescence intensity of EdU on DOE with knockdown of *E2F1, E2F2* using RNAi, Overexpression of *Rbf280*, and *dacapo GFP* using *Luna Gal4.*
D. Quantification of the area of the ED on DOE with knockdown of *E2F1*, and *E2F2* using RNAi, Overexpression of *Rbf280*, and *Dacapo-GFP* using *Luna Gal4.* N= at last 9 for each genotype.
E. Quantification of the DNA content/ploidy on DOE measured using the DAPI intensities in all the different backgrounds of Overexpression and knockdowns in secretory cells.
F. Confocal micrographs of the ED on Day 10 post-eclosion labeled with DAPI show that the nuclei are smaller in *E2F1 RNAi, E2F2 RNAi, Rbf 280*, and *Dacapo-GFP* overexpression. Scale bar:72.8 μm
G. Quantification of the nuclear area of the secretory cells of the ED on Day 10 post-eclosion showing reduced nuclear size in *E2F1 RNAi, E2F2 RNAi, Rbf 280*, and *Dacapo-GFP* overexpression conditions.
H. Quantification of the Area of the ED on Day 10 post-eclosion showing reduced area of ED in *E2F1* RNAi, *E2F2* RNAi, *Rbf 280*, and *Dacapo-GFP* overexpression conditions.
I. Quantification of the DNA content/ploidy of the secretory cells of the ED on Day 10 post-eclosion showing reduced ploidy in *E2F1* RNAi, *E2F2* RNAi, *Rbf 280*, and *Dacapo-GFP* overexpression conditions compared to the control. (N= at least 9 for each genotype, with ploidies measured from 30 nuclei in each ED).
J. Quantification of fertility for males with reduced DNA content in the ED.

MFI: Mean Fluorescence Intensity

Statistical Analysis: Two-way ANOVA with multiple comparisons between control and Different knockdown and overexpression conditions. $P<0.0001$ ****

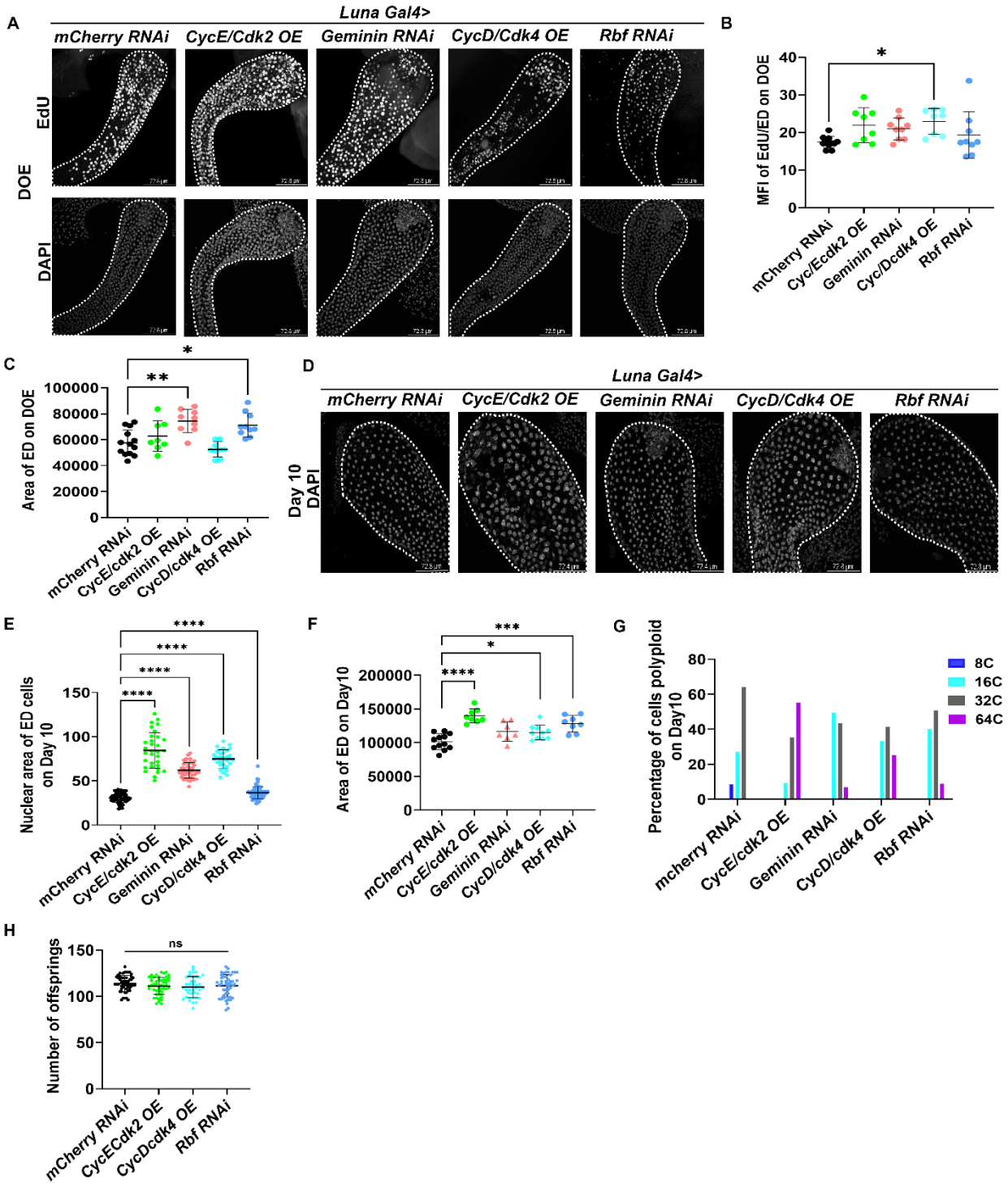


Figure 2.5: Inducing extra endoreplication in secretory cells of ED leads to organ hypertrophy

A. Confocal micrographs of EDs on DOE with overexpression of *CycE-Cdk2, CycD-Cdk4*, and knockdown of *Geminin, or Rbf* with RNAi using *Luna Gal4*. The upper panel is the EdU labeling performed by *ex-vivo* incubation on DOE, the lower panel is nuclei labeled

with DAPI to measure the DNA content. N= at least 9 for each genotype. Scale bar:72.8 µm

B. Quantification of the Mean fluorescence intensity of EdU on DOE in the condition with overexpression of *CycE-Cdk2, CycD-Cdk4*, and *Geminin or Rbf* with RNAi driven by *Luna Gal4.*
C. Quantification of the area of the ED with overexpression of *CycE-Cdk2, CycD-Cdk4,* and *Geminin or Rbf* with RNAi driven by *Luna Gal4.*
D. Confocal micrographs of the ED on Day 10 post-eclosion labeled with DAPI show that the nuclei and the ED are larger with overexpression of *CycE-Cdk2, CycD-Cdk4,* and knockdown of *Geminin* or *Rbf* with RNAi using *Luna Gal4*. Scale bar:72.8 µm
E. Quantification of the nuclear area of the secretory cells of ED on Day 10 post-eclosion with the indicated transgenes. (N= at least 9, with 10 nuclei quantified from each ED)

F. Quantification of the area of the ED on Day 10 post-eclosion expressing the indicated transgenes.
G. Quantification of the DNA content/ploidy of the secretory cells of ED on Day 10 post-eclosion using DAPI measurements showing increased ploidy with overexpression of *CycE-Cdk2, CycD-Cdk4*, and knockdown of *Geminin or Rbf* with RNAi using *Luna Gal4* compared to the control.
H. Quantification of male fertility for animals expressing the indicated transgenes driven by *Luna-Gal4*. The animals with increased ED DNA content do not have significant differences in the number of offspring.

MFI: Mean Fluorescence Intensity

Statistical Analysis: Two-way ANOVA with multiple comparisons between control and Different knockdown and overexpression conditions. $P<0.0001$ ****

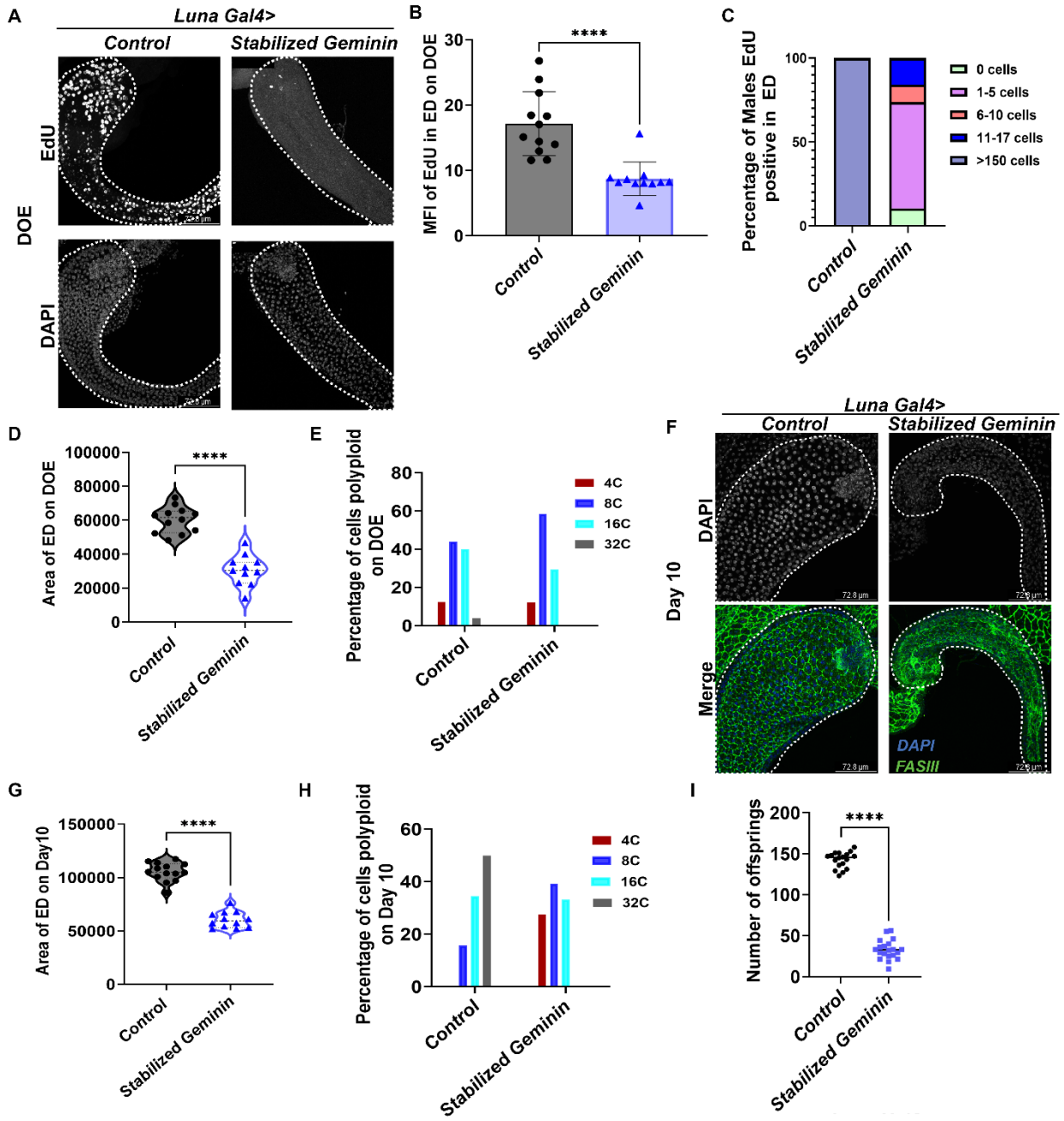


Figure 2.6: Stabilized Geminin effectively blocks the adult endoreplication in the ejaculatory duct

A. Confocal micrograph of the ED on DOE (0-2hrs) with EdU labeling performed ex vivo. A nearly complete block of endocycling is observed when stabilized *Geminin* is expressed. Nuclei are labeled with DAPI. Scale bar:72.8 µm
B. Quantification of the mean fluorescence intensity of the EdU incorporated on DOE shows significantly reduced EdU with stabilized *Geminin* expression compared to the control. N=at least 11 per sample.

C. Quantification of the percentage of cells that are EdU positive on DOE in each ED performed with *ex vivo* EdU incorporation. We classified the total EdU-positive cells into multiple groups: 0 cells, 1-5 cells, 6- 10 cells, 11-17 cells, and>150 cells that are EdU-positive in each ED of control and stabilized Geminin.
D. Quantification of the area of ED on DOE with the indicated transgenes driven by *Luna Gal4*.
E. Quantification of the DNA content/ploidy of the secretory cells on DOE with the indicated transgenes driven by *Luna Gal4*.
F. Confocal micrographs of the ED on Day 10 post-eclosion labeled with DAPI and cell junction marker Fas III show that the nuclei are smaller with overexpression of stabilized *Geminin* compared to the control.
G. Quantification of the area of ED on Day 10 with the indicated transgenes driven by *Luna Gal4*.
H. Quantification of the DNA content/ploidy of the secretory cells of ED on Day 10 post-eclosion showing reduced ploidy in stabilized *Geminin* overexpression conditions compared to the control.
I. Quantification of male fertility for animals with the indicated transgenes driven by *Luna Gal4*. The animals with *stabilized Geminin* overexpression have significantly reduced offspring compared to the control.

Statistical Analysis: unpaired Two-tailed t-test. P<0.0001 ****

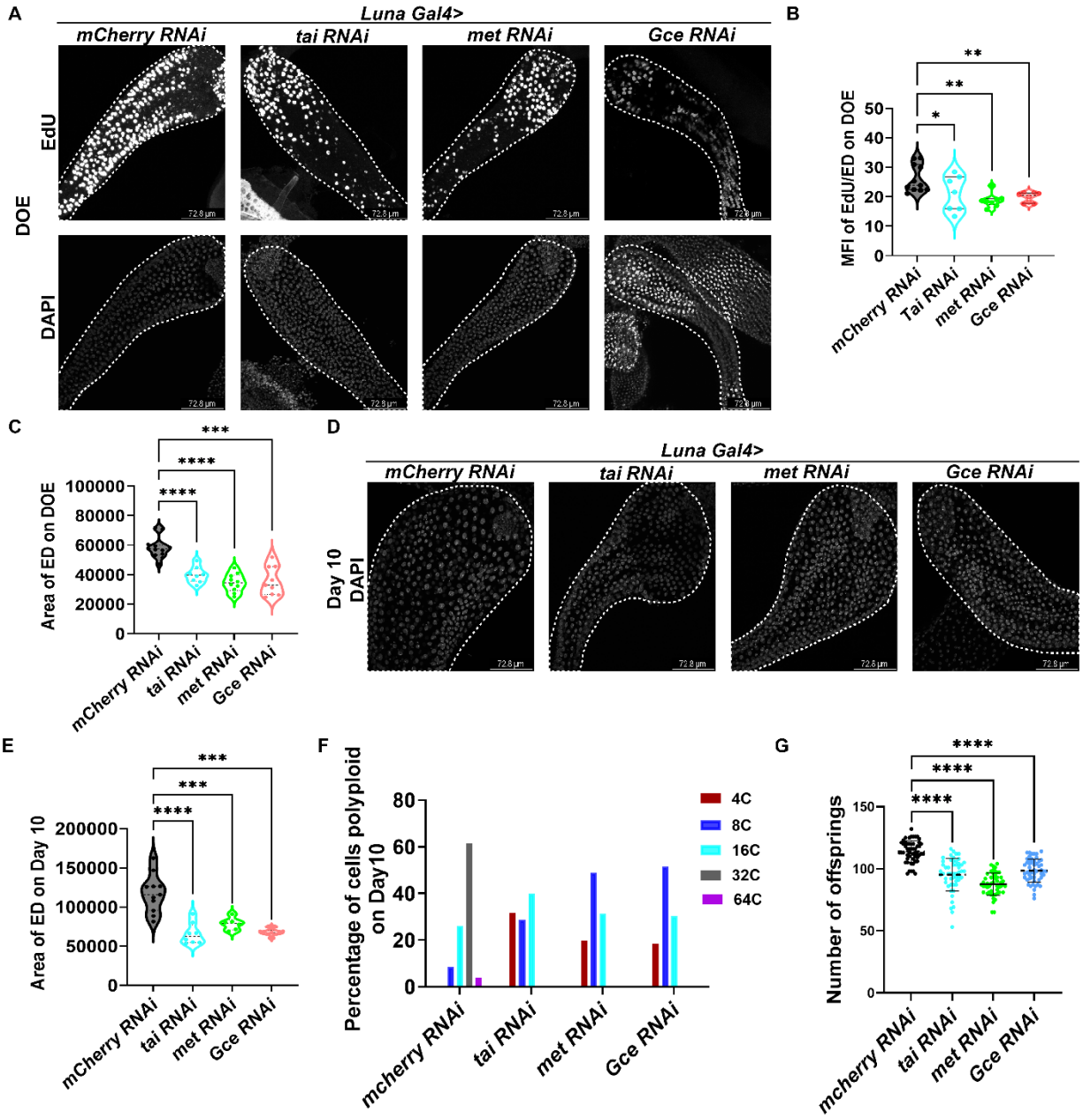


Figure 2.7: Juvenile hormone (JH) signaling promotes post-eclosion endoreplication and growth of *Drosophila* ejaculatory duct

A. Confocal micrographs of ED on DOE with knockdown of Juvenile hormone receptors *Gce, Met*, and transcription factor *tai* with RNAi using *Luna Gal4.* The control expresses *mCherry* RNAi driven by *Luna Gal4*. The upper panel is the EdU labeling on DOE. Nuclei are labeled with DAPI (lower panels) to measure the DNA content. Scale bar:72.8 µm
B. Quantification of EdU incorporated on DOE shows reduced EdU with knockdown of *Gce*, *Met,* and *tai* with RNAi using *Luna Gal4*. N= at least 9 per genotype.

C. Quantification of the area of ED on DOE with the indicated transgenes driven by *Luna Gal4*. (n= at least 9 per genotype)
D. Confocal micrographs of the ED on Day 10 post-eclosion labeled with DAPI for the indicated transgenes driven by Luna Gal4. Nuclei are smaller with knockdown of *Gce, met, or tai* compared to the control.
E. Quantification of the area of the ED on Day 10 post-eclosion for the indicated transgenes driven by Luna Gal4.(n= at least 7 per genotype, overlapping or damaged tissues were removed from analysis)
F. Quantification of the DNA content/ploidy of the secretory cells of ED on Day 10 post-eclosion for the indicated transgenes driven by Luna Gal4. Reduced ploidy is observed for knockdown of *Gce, met or tai*.
G. Quantification of male fertility for animals expressing the indicated transgenes driven by Luna Gal4. Fertility is reduced with the knockdown of *Gce, met or tai.*

Statistical Analysis: Two-way ANOVA with multiple comparisons between control and Different knockdown and overexpression conditions. $P<0.0001$ ****

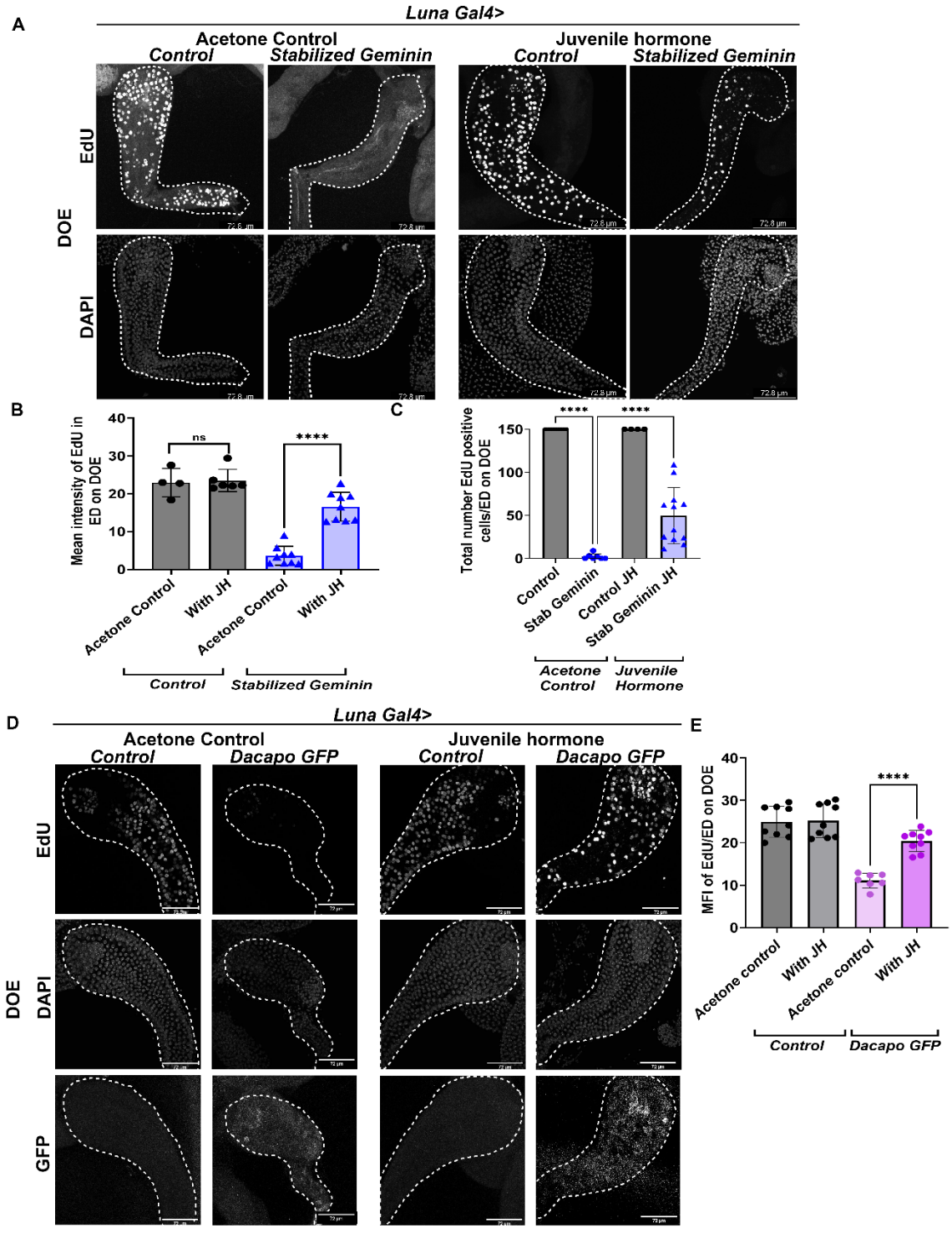


Figure 2.8: Juvenile hormone signaling is sufficient to induce endoreplication in the adult *Drosophila* ejaculatory duct.

A. Confocal micrograph of EdU incorporation on DOE (0-2 hrs PE) with vehicle only control (acetone, A', A'') or Juvenile hormone (JH) III with 1-hour *ex-vivo* incubation (A''', A'''') control EDs or EDs expressing stabilized *Geminin* to block the endocycle. Top panel EdU, bottom panel DAPI staining. Scale bar:72.8 μm
B. Quantification of the Mean fluorescence intensity (MFI) of the EdU signal per ED. N= at least 4 per genotype and treatment.
C. Quantification of the percentage of cells that are EdU positive with *ex vivo* acetone and JH III incubation on DOE for EDs expressing the indicated transgenes. Controls express *Luna-Gal4* only. We classified the total EdU-positive cells into multiple groups: 0 cells, 1-10 cells, 11- 20 cells, 20-50 cells, 60- 100, and>150 cells that are EdU-positive in each ED of control and stabilized Geminin.
D. Confocal micrograph of EdU incorporation in ED on DOE (0-2 hrs PE) with Acetone control (No JH) and JH III with 1-hour *ex-vivo* incubation along with the EdU in controls and EDs expressing *Dacapo-GFP* to block the endocycle. The top panel EdU, middle panel is DAPI staining, and the bottom panel is the expression of *Dacapo GFP*. Scale bar:72.8 μm.
E. Quantification of the MFI of EdU per ED in both Dacapo GFP and controls incubated with JHIII or vehicle only (No JH, acetone). (N= at least 7 per genotype and treatment)

Statistical Analysis: Unpaired t-test, P< 0.0001 ****

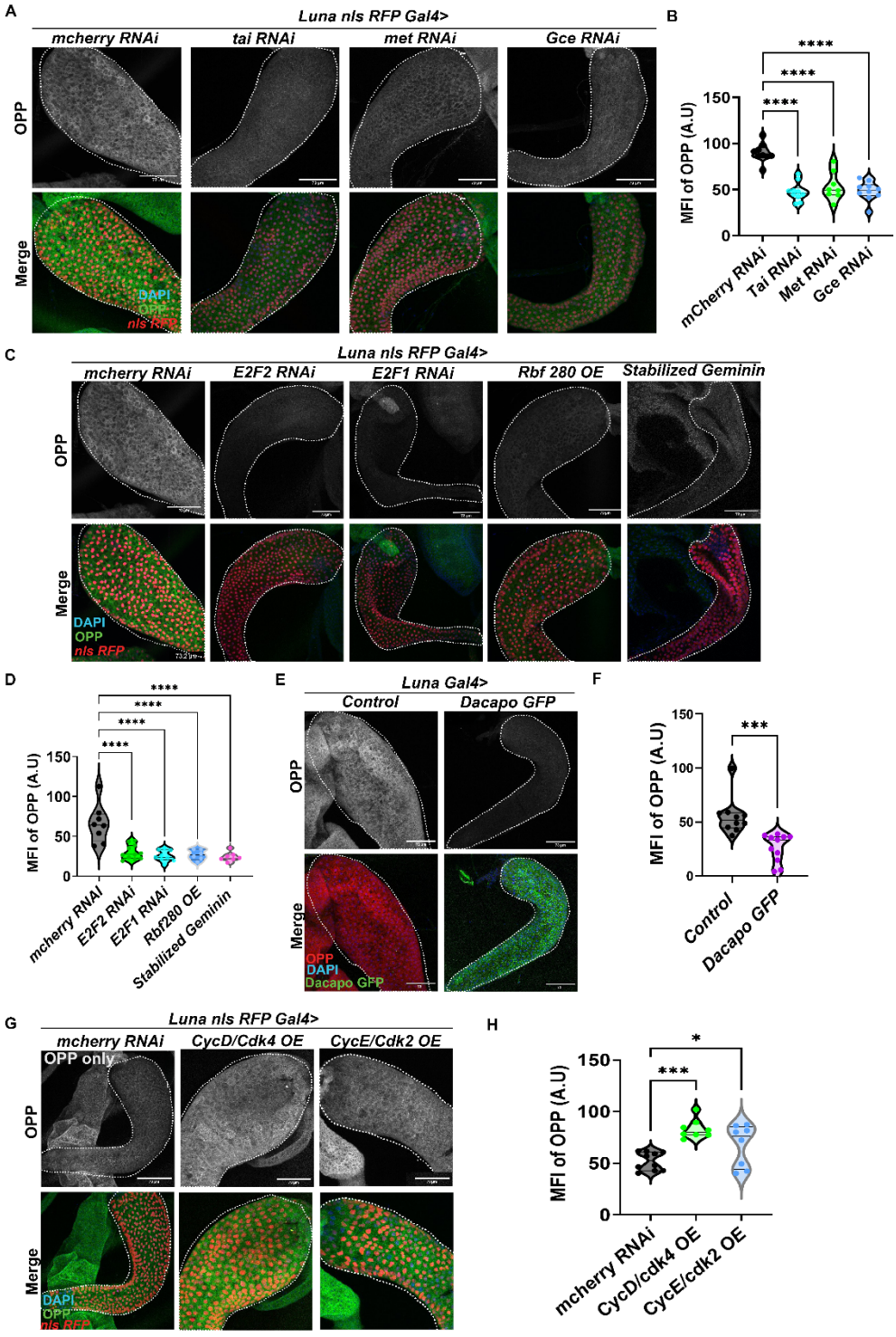


Figure 2.9: JH signaling and the endocycle are required for proper protein synthesis in the ED

A. Confocal images of ED after OPP nascent protein synthesis assay for 10 minutes on Day 10 with the indicated transgenes driven by *Luna-Gal4, with UAS-nls RFP.* The top panel shows OPP incorporation, the bottom panel is a merge with OPP in Green, *UAS-nlsRFP* in red and DAPI in blue. Scale Bar:73µm

B. Quantification of the Mean Fluorescence Intensity of OPP in ED on Day 10 with *mcherry RNAi, tai RNAi*, *Gce RNAi*, or *met* RNAi, driven using *LunaGal4nls RFP.* OPP intensity is normalized to the total area of the ED. N= at least 9 EDs per genotype.
C. Confocal images of ED after OPP nascent protein synthesis assay for 10 minutes on Day 10 with *mcherry, E2F1* or *E2F2* RNAis, or overexpression of *Rbf280* or stabilized *Geminin* driven using *LunaGal4nls RFP.* The top panel shows OPP incorporation, the bottom panel is the merged image with OPP in green, *UAS-nlsRFP* in red and DAPI in blue. Scale Bar:73.2µm
D. Quantification of the Mean fluorescence intensity of OPP from panel C that is normalized to the area of the ED. N= at least 7 EDs per genotype.
E. Confocal images of EDs after OPP nascent protein synthesis assay for 10 minutes on Day 10 in controls or overexpression of *dacapo-GFP* driven by *LunaGal4.* The top panel is the images of OPP incorporation, the bottom panel is the merge with OPP in red, *dacapo-GFP* expression in green, and DAPI in blue. Scale Bar:73µm
F. Quantification of the Mean fluorescence intensity of OPP from panel E that is normalized to the area of the ED. N= at least 9 EDs per genotype.
G. Confocal images of EDs after OPP nascent protein synthesis assay for 10 minutes on Day 10 with the indicated transgenes driven by *Luna-Gal4 with UAS-nlsRFP.* The top panel is the images of OPP incorporation, the bottom panel is the merge with OPP in green, *nls RFP* expression in red, and DAPI in blue. Scale Bar:73µm
H. Quantification of the Mean fluorescence intensity of OPP from panel G that is normalized to the area of the ED. N= at least 8 EDs per genotype.

Statistical Analysis: Two-way ANOVA with multiple comparisons between control and Different knockdown, overexpression conditions. $P<0.0001$ ****

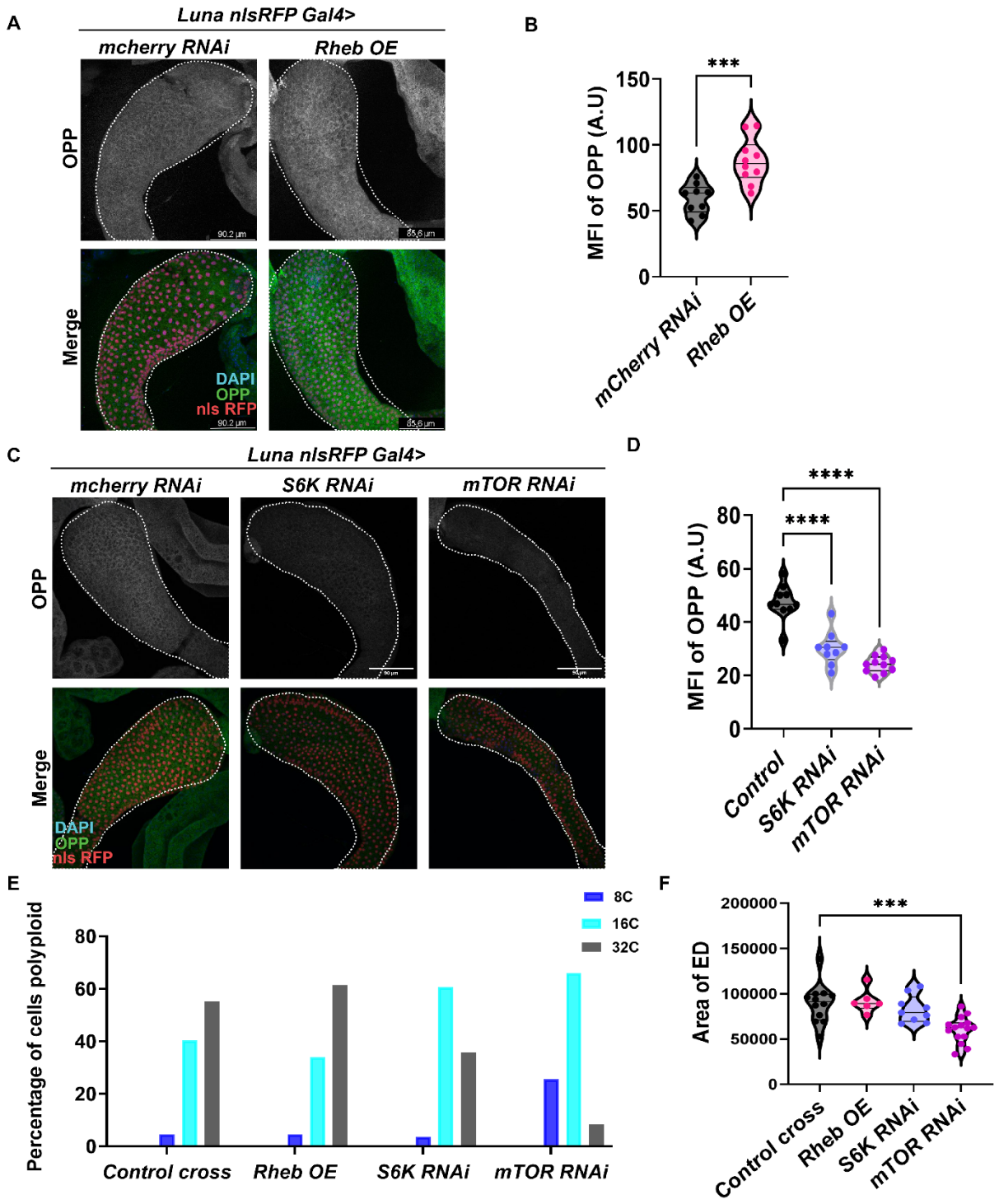


Figure 2.10: Protein Synthesis in the secretory cells of the ED requires mTOR signaling and is coupled via the endocycle

A. Confocal images of EDs after OPP nascent protein synthesis assay for 10 minutes on Day 10 with *mCherry RNAi* or overexpression of *Rheb* driven by *LunaGal4* with *UAS-nls RFP.*

The top panel is the images of OPP incorporation in the ED, the bottom panel is the merge with OPP in green, *nlsRFP* in red, and DAPI in blue. Scale Bar:90.2µm

B. Quantification of the Mean Fluorescence Intensity (MFI) of the OPP signal on from panel A, OPP intensity is normalized to the area of the ED. N= at least 9 EDs per genotype.
C. Confocal images of EDs after OPP nascent protein synthesis assay for 10 minutes on Day 10 with *mCherry, S6K*, or *mTOR* RNAis, driven by *LunaGal4* with *UAS-nls RFP.* The top panel is the images of OPP incorporation, the bottom panel is the merge with OPP in green, *nlsRFP* in red, and DAPI in blue. Scale Bar:90µm
D. Quantification of the Mean Fluorescence Intensity (MFI) of the OPP on Day 10 from panel C, OPP intensity is normalized to the area of the ED. N= at least 9 EDs per genotype.
E. Quantification of the DNA content/ploidy of the secretory cells of ED on Day 10 post-eclosion for controls expressing *mCherry RNAi*, versus *Rheb* overexpression, knockdown of *S6K* or *mTOR* by RNAi. Reduced ploidy is observed in *S6K* or *mTOR* knockdown conditions.
F. Quantification of the area of the ED on Day 10 post-eclosion with overexpression of *Rheb*, or knockdown of *S6K* or *mTOR* with RNAi driven by *Luna Gal4 with UAS-nls RFP.* N= at least 6 EDs per genotype.

Statistical Analysis: Figure 10B: Two-tailed unpaired t-test. P<0.0001 ****. Figure 10D, F: Unpaired Two-way ANOVA with multiple comparisons between control and Different knockdown and overexpression conditions. P<0.0001 ****

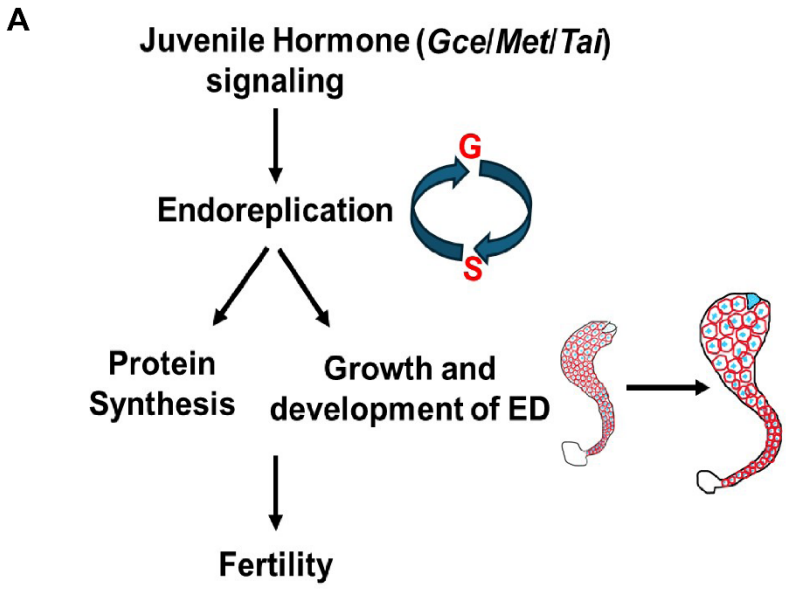


Figure 2.11: A model for ED organ growth and protein synthesis driven by endoreplication induced by JH signaling.

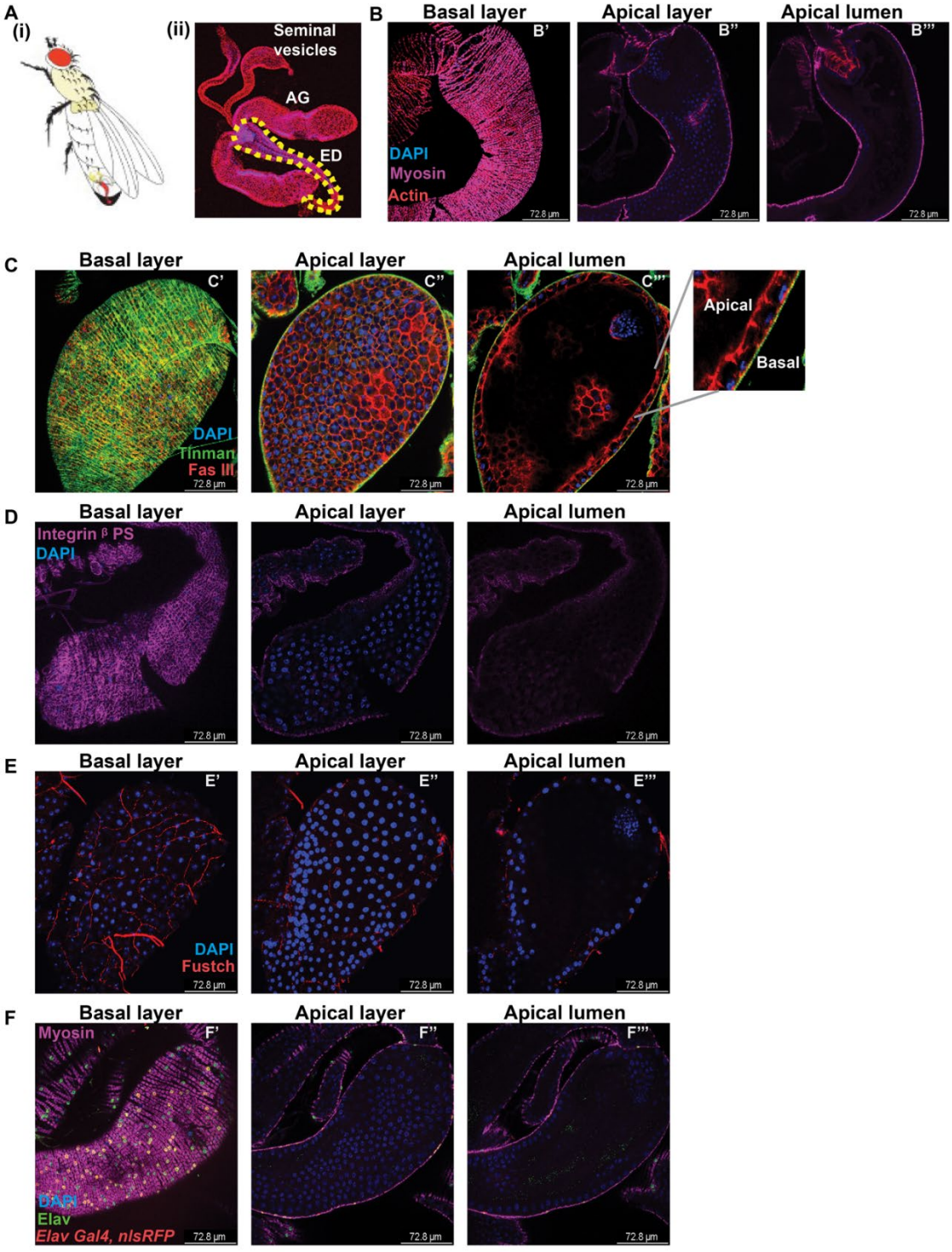


Figure 2.12: Identification of different cell types in adult *Drosophila* Ejaculatory duct

A. (i) Cartoon of the *Drosophila* male reproductive system (ii) Micrograph of male reproductive system stained with cell junction marker DLG and nuclear staining DAPI with yellow dotted line highlighting the ED.

B. Confocal micrographs of Myosin, actin, and DAPI staining in different apico-basal planes of the ED, B’ is the outer basal layer, B’’ is the inner Apical layer, and B’’’ is the Inner apical layer of cells that is exposed to the hollow lumen.
C. Confocal micrographs of Tinman staining in the basal layer of ED (C’) and the Apical secretory cells are labeled with cell junction protein Fas III (C’’) with nuclei labeled with DAPI. Zoomed in image of C’’’ showing the apical and basal side of ED.
D. Confocal micrographs of ED stained with Integrin βps antibody which labels an extracellular matrix receptor, and Dapi staining in the apical secretory cells.
E. Confocal micrographs of ED Basal (E’), Apical (E”), and Apical lumen (E’’’) showing the axonal projections that are stained with the Fustch antibody, and nuclei labeled with DAPI.
F. Confocal micrographs of ED showing the Elav staining (green), and the same cells labeled with Elav Gal4 expressing nlsRFP. Muscles are stained with anti-Myosin (magenta). The staining shows that the ED muscles are innervated with neurons and are present on the exterior basal layer. The nuclei are labeled with DAPI. Scale bar: 72.8 microns

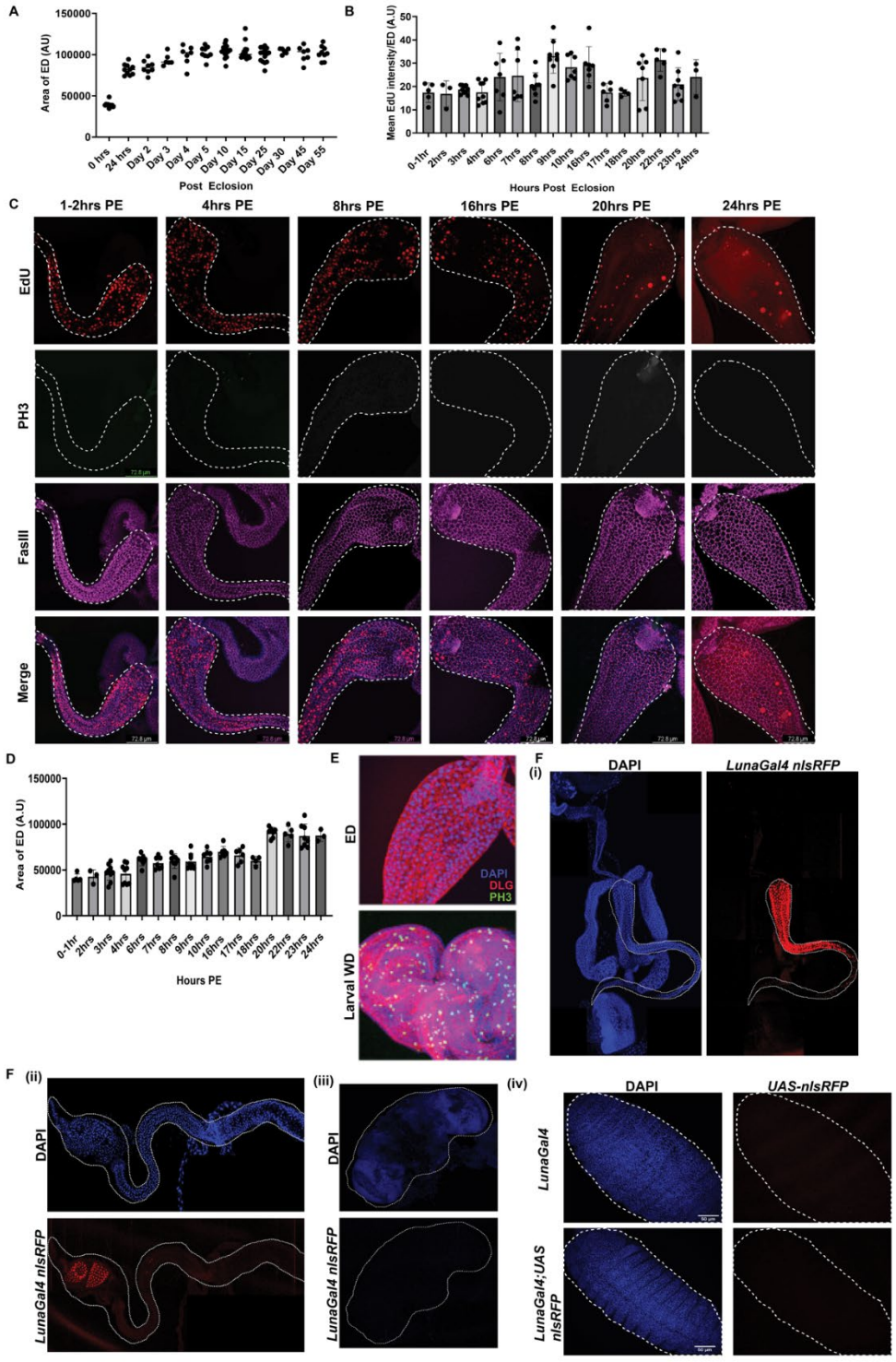


Figure 2.13:EdU and PH3 labeling at different time points in ED and in different tissues of *Drosophila*

A. Area of adult EDs at indicated time points post-eclosion. The ED grows from Day of eclosion (DOE) to Day 5 with significant growth ceasing after day 5. Each point is the measurement of the area of one ED.

B. Quantification of the intensity of EdU labeling in EDs exposed to EdU for one hour intervals post eclosion up to 24hrs. The intensity is normalized to the area of the ED at each time point.
C. Confocal images of EDs labeled with EdU at 1-2hrs, 4hrs, 8hrs, 16hrs, 20hrs, 24hrs post-eclosion performed with *ex vivo* incubation. Top panel in red is the EdU incorporation in ED, next is Phospho histone H3 (PH3) staining in green showing no mitotic cells, next panel is cell-cell junctions labeled with FasIII in Magenta. The bottom panel is the merge of EdU (red), PH3 (green) FasIII (magenta), and DAPI (blue). Scale Bar:50μm
D. Measurement of the area of ED at an interval of every hour post-eclosion to 24 hrs. ED area increases until 24 hrs post eclosion.
E. Confocal images of EDs and larval imaginal discs stained with PH3 in green, with cell junctions labeled by Discs Large (DLG) (red), and nuclei stained by DAPI (blue). Note larval and adult tissues were stained in the same tube, confirming the mitotic labeling worked.
F. Testing *Luna Gal4* expression in different tissues using *UAS-nls RFP* with nuclei counter-stained with DAPI (i) Confocal image of male reproductive system with *Luna Gal4* expression in only ED. (ii) Confocal image of the gastrointestinal tract with *Luna-Gal4* expression only in the cardia. (iii) Confocal images of the brain showing the absence of *Luna Gal4* expression. Scale bar: 333.3 μm. (iv) Confocal images of the Embryo showing the absence of *Luna Gal4* expression. Scale bar: 156.6 μm

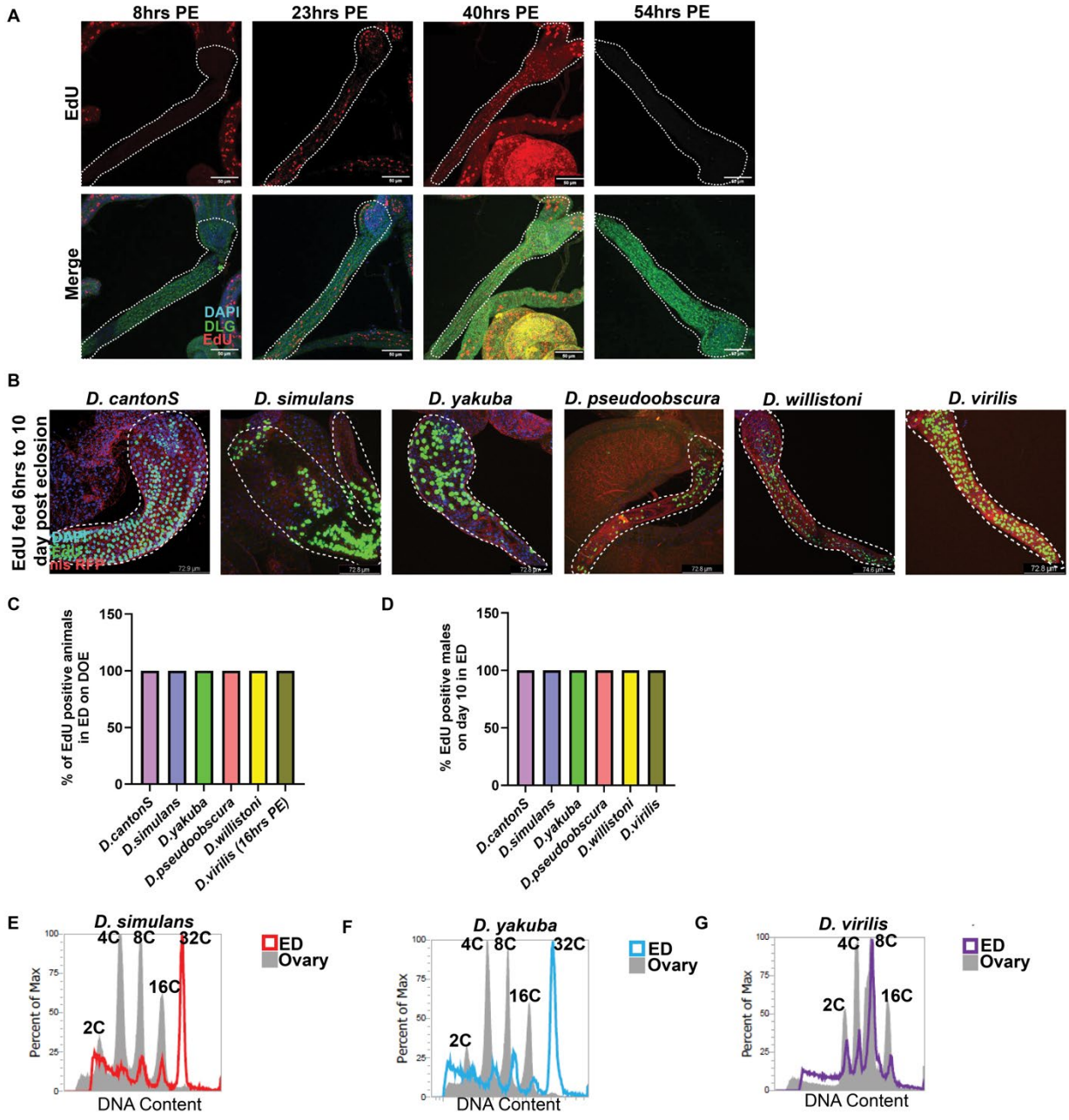


Figure 2.14:EdU and ploidy quantifications in different species of *Drosophila*

A. Confocal images of EdU labeling in *D.virilis* to identify the time point when the ED starts endocycling post-eclosion (PE) by soaking the tissue *ex vivo* in EdU for 1hr. Endocycling is absent at 8hrs PE but starts by 16hrs PE, continues for 40-50hrs PE and cell cycle exit occurs by 60 hrs. The top panel is EdU (red) labeling and the bottom panel is the merged image of DAPI (blue), and cell junction marker Discs Large (DLG, green).
B. Confocal images of different species of *Drosophila* fed with EdU from 6hrs to Day 10 PE and dissected on Day 10 and imaged to observe the EdU labeling in secretory cells of ED. DLG (red), EdU (green), DAPI (blue).

C. Quantification of the EdU labeling on day of eclosion (DOE) in different *Drosophila* species. Data shown as the percentage of animals that are positively labeled with EdU during a 1 hour *ex vivo* labeling on DOE.
D. Quantification of EdU labeling on Day 10 in different *Drosophila* species. Data shown as the percentage of animals that are positively labeled with EdU over a 10 day feeding.
E. -G: Flow cytometry histograms of nuclear DNA content of ED secretory cells on Day 10 in *D. simulans, yakuba and virilis* species respectively. Gray shaded peaks in all the three plots are species-matched ovary nuclei to assign correct ploidy peaks for each species genome size.

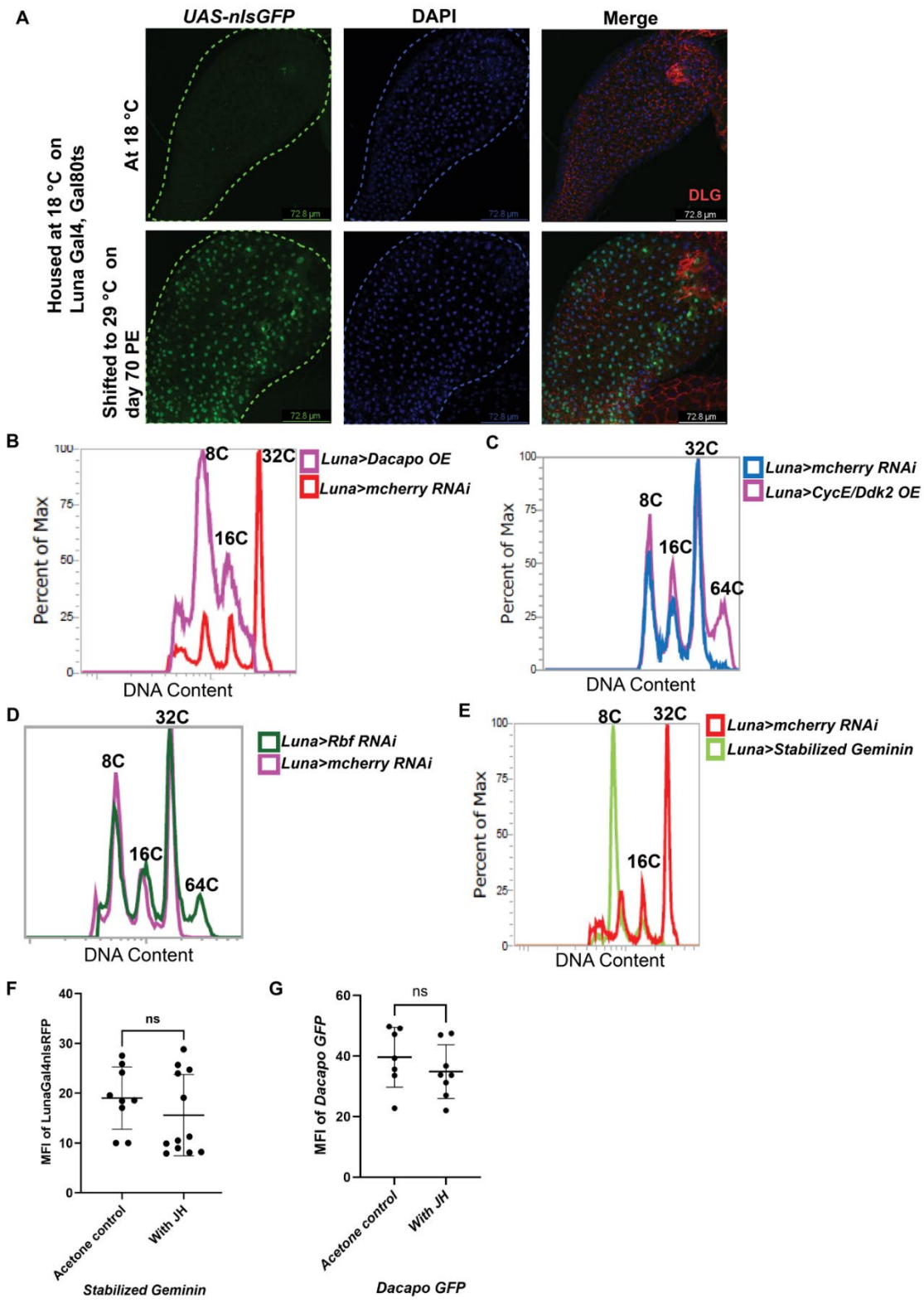


Figure 2.15: Luna Gal4 expression and ploidy measurements in different cell cycle conditions in ED

A. Confocal images of EDs showing expression of *Luna Gal4* on Day 70 post-eclosion (PE) using *UAS-nls RFP.* Scale bar: 72.8μm. Note that day 70 at 18°C is roughly equal to day 39-40 at room temp.
B. Flow cytometry histogram of nuclear DNA content of ED secretory cells on Day 10 with *Dacapo-GFP* Overexpression and control *mcherry RNAi.* For panels B-E, Each sample contains at least 25 dissected EDs pooled for nuclear isolation and flow cytometry. One representative example is shown.
C. Flow cytometry histogram of nuclear DNA content of ED secretory cells on Day 10 with *CycE/Cdk2* overexpression vs. control *mcherry RNAi.*
D. Flow cytometry histogram of nuclear DNA content of ED secretory cells on Day 10 with *Rbf RNAi* vs. control *mcherry RNAi.*
E. Flow cytometry histogram of nuclear DNA content of ED secretory cells on Day 10 with stabilized *Geminin* overexpression vs. control *mcherry RNAi.*
F. Quantification of the Mean Fluorescence Intensity (MFI) of *UAS-nls RFP* expression in EDs driven by *Luna Gal4* with expression of *Stabilized Geminin* in JH and Acetone (vehicle only). JH treatment does not alter the expression level of Luna-Gal4 driven *UAS-nls RFP.*

G. Quantification of MFI of UAS-*Dacapo-GFP* levels driven by *Luna Gal4* in JH and Acetone (vehicle only) incubation. JH treatment does not alter the expression level of Luna-Gal4 driven *UAS-Dacapo-GFP*.

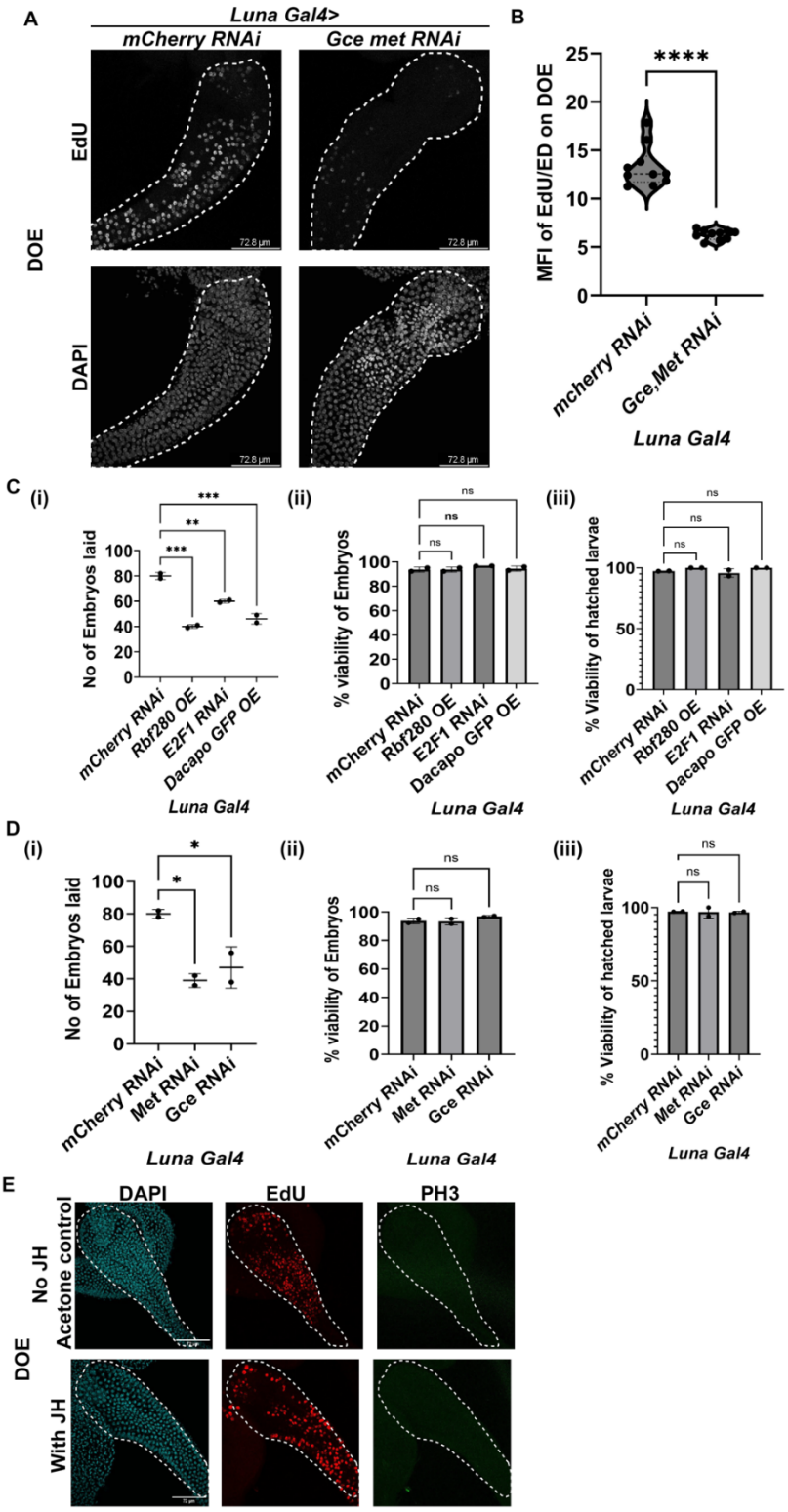


Figure 2.16:Supplementary data for the viability of the embryos under different cell cycle conditions

A. Confocal micrographs of EDs on day of eclosion (DOE) with simultaneous knockdown of Juvenile hormone receptors *Gce and Met* using *Luna Gal4.* The control expresses *mCherry* RNAi driven by *Luna Gal4*. The upper panel is EdU labeling on DOE. Nuclei are labeled with DAPI (lower panels). Scale bar:72.8 μm
B. Quantification of the Mean Fluorescence Intensity (MFI) of EdU on DOE in EDs with *Gce+ Met* RNAi driven by *Luna Gal4.* The control expresses *mCherry* RNAi driven by *Luna Gal4*. N= at least 9 per genotype.
C. Viability assay for the genotypes with reduced ploidy and fertility (i) Number of embryos laid, (ii) percentage viability of the embryos laid (measured as number of embryos that pupariate), (iii) Percentage viability of the hatched larvae to the adult fly stage (measured as the number of pupa that give rise to viable adults).
D. Viability assay for the *Gce* and *Met* RNAi genotypes (i) Number of embryos laid, (ii) percentage viability of the embryos laid (measured as number of embryos that pupariate), (iii) Percentage viability of the hatched larvae to the adult fly stage (measured as the number of pupa that give rise to viable adults).
E. Confocal micrographs of *Canton-S* EDs on the day of eclosion (DOE) with 1hr JH incubation vs acetone vehicle control (No JH). Samples were labeled with EdU, and stained with Phosphohistone H3 (PH3) to label mitotic events. No mitoses are observed with or without JH.

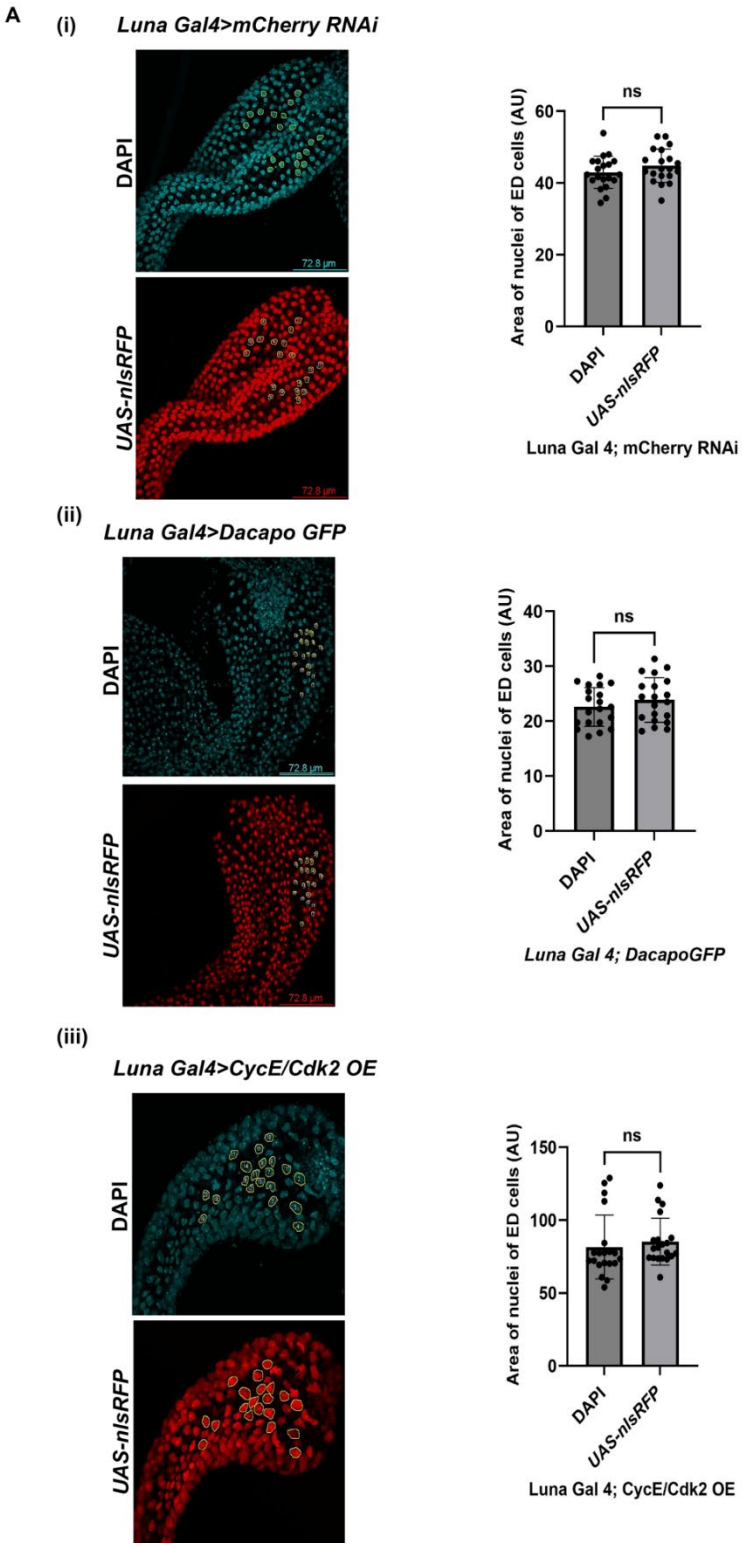


Figure 2.17: Measurement of nuclear area

Representative confocal micrographs of EDs on day 10 expressing the indicated transgenes driven by *Luna-Gal4* with *UAS-RFPnls*. We measured nuclear area using both Dapi to segment nuclei

and the nuclear-localized marker *UAS-RFPnls*. Nuclear area measurements were similar with both approaches, whether nuclear size was decreased (e.g. ii *UAS-Dacapo-GFP* expression) or increased (e.g. iii *UAS-CycE/Cdk2* expression).

2.6 Bibliography

Ahmad SM, Baker BS, (2002). Sex-specific deployment of FGF signaling in Drosophila recruits mesodermal cells into the male genital imaginal disc. Cell 109, 651–661. [PubMed: 12062107]

Alyagor I, Berkun V, Keren-Shaul H, Marmor-Kollet N, David E, Mayseless O, Issman-Zecharya N, Amit I, Schuldiner O, (2018). Combining Developmental and Perturbation-Seq Uncovers Transcriptional Modules Orchestrating Neuronal Remodeling. Dev Cell 47, 38–52 e36. [PubMed: 30300589]

Avila FW, Sánchez-López JA, McGlaughon JL, Raman S, Wolfner MF, Heifetz Y, (2016). Nature and Functions of Glands and Ducts in the Drosophila Reproductive Tract, in: Cohen E, Moussian B (Eds.), Extracellular Composite Matrices in Arthropods. Springer International Publishing, Cham, pp. 411–444.

Bairati A, (1968). STRUCTURE AND ULTRASTRUCTURE OF THE MALE REPRODUCTIVE SYSTEM IN DROSOPHILA MELANOGASTER MEIG. Monitore Zoologico Italiano - Italian Journal of Zoology 2:3–4, 105–182
Ahmad, S.M., Baker, B.S., 2002. Sex-specific deployment of FGF signaling in Drosophila recruits mesodermal cells into the male genital imaginal disc. Cell 109, 651-661.

Avila, F.W., Sánchez-López, J.A., McGlaughon, J.L., Raman, S., Wolfner, M.F., Heifetz, Y., 2016. Nature and Functions of Glands and Ducts in the Drosophila Reproductive Tract, in: Cohen, E., Moussian, B. (Eds.), Extracellular Composite Matrices in Arthropods. Springer International Publishing, Cham, pp. 411-444.

Bairati, A., 1968. Structure and ultrastructure of the male reproductive system in *Drosophila* melanogaster meig. Monitore Zoologico Italiano - Italian Journal of Zoology 2:3-4, 105-182.

Balk, S.P., Knudsen, K.E., 2008. AR, the cell cycle, and prostate cancer. Nucl Recept Signal 6, e001.

Banerjee, P.P., Banerjee, S., Brown, T.R., Zirkin, B.R., 2018. Androgen action in prostate function and disease. Am J Clin Exp Urol 6, 62-77.

Baumann, A., Barry, J., Wang, S., Fujiwara, Y., Wilson, T.G., 2010. Paralogous genes involved in juvenile hormone action in Drosophila melanogaster. Genetics 185, 1327-1336.

Baumann, A.A., Texada, M.J., Chen, H.M., Etheredge, J.N., Miller, D.L., Picard, S., Warner, R., Truman, J.W., Riddiford, L.M., 2017. Genetic tools to study juvenile hormone action in Drosophila. Sci Rep 7, 2132.

Bertram, M.J., Akerkar, G.A., Ard, R.L., Gonzalez, C., Wolfner, M.F., 1992. Cell type-specific gene expression in the Drosophila melanogaster male accessory gland. Mech Dev 38, 33-40.

Bosco, G., Campbell, P., Leiva-Neto, J.T., Markow, T.A., 2007. Analysis of Drosophila species genome size and satellite DNA content reveals significant differences among strains as well as between species. Genetics 177, 1277-1290.

Bownes, M., Rembold, H., 1987. The titre of juvenile hormone during the pupal and adult stages of the life cycle of Drosophila melanogaster. Eur J Biochem 164, 709-712.

Box, A.M., Ramesh, N.A., Nandakumar, S., Church, S.J., Prasad, D., Afrakhteh, A., Taichman, R.S., Buttitta, L., 2024. Cell cycle variants during Drosophila male accessory gland development. G3 (Bethesda). Jul 8;14(7):jkae089. doi: 10.1093/g3journal/jkae089

Braun, R.P., Wyatt, G.R., 1995. Growth of the male accessory gland in adult locusts: Roles of juvenile hormone, JH esterase, and JH binding proteins. Archives of Insect Biochemistry and Physiology 30, 383-400.

Buttitta, L.A., Katzaroff, A.J., Perez, C.L., de la Cruz, A., Edgar, B.A., 2007. A double-assurance mechanism controls cell cycle exit upon terminal differentiation in Drosophila. Dev Cell 12, 631-643.

Cavener, D.R., 1985. Coevolution of the glucose dehydrogenase gene and the ejaculatory duct in the genus Drosophila. Mol Biol Evol 2, 141-149.

Chakraborty, A., Peterson, N.G., King, J.S., Gross, R.T., Pla, M.M., Thennavan, A., Zhou, K.C., DeLuca, S., Bursac, N., Bowles, D.E., Wolf, M.J., Fox, D.T., 2023. Conserved chamber-specific polyploidy maintains heart function in Drosophila. Development 150. Aug 15;150(16):dev201896. doi: 10.1242/dev.201896.

Chertemps, T., Francois, A., Durand, N., Rosell, G., Dekker, T., Lucas, P., Maibeche-Coisne, M., 2012. A carboxylesterase, Esterase-6, modulates sensory physiological and behavioral response dynamics to pheromone in Drosophila. BMC Biol 10, 56.

Chung, S., Hanlon, C.D., Andrew, D.J., 2014. Building and specializing epithelial tubular organs: the Drosophila salivary gland as a model system for revealing how epithelial organs are specified, form and specialize. Wiley Interdiscip Rev Dev Biol 3, 281-300.

Cox-Foster, D.L., Schonbaum, C.P., Murtha, M.T., Cavener, D.R., 1990. Developmental expression of the glucose dehydrogenase gene in Drosophila melanogaster. Genetics 124, 873-880.

Datar, S.A., Jacobs, H.W., de la Cruz, A.F., Lehner, C.F., Edgar, B.A., 2000. The Drosophila cyclin D-Cdk4 complex promotes cellular growth. Embo J 19, 4543-4554.

Date-Ito, A., Kasahara, K., Sawai, H., Chigusa, S.I., 2002. Rapid evolution of the male-specific antibacterial protein andropin gene in Drosophila. J Mol Evol 54, 665-670.

Deliu, L.P., Ghosh, A., Grewal, S.S., 2017. Investigation of protein synthesis in Drosophila larvae using puromycin labelling. Biol Open 6, 1229-1234.

Diffley, J.F., 2004. Regulation of early events in chromosome replication. Curr Biol 14, R778-786.

Edgar, B.A., Orr-Weaver, T.L., 2001. Endoreplication cell cycles: more for less. Cell 105, 297-306.

Flatt, T., Tu, M.P., Tatar, M., 2005. Hormonal pleiotropy and the juvenile hormone regulation of Drosophila development and life history. Bioessays 27, 999-1010.

Flomerfelt, F.A., Gress, R.E., 2016. Analysis of Cell Proliferation and Homeostasis Using EdU Labeling. Methods Mol Biol 1323, 211-220.

Guo, W., Wu, Z., Song, J., Jiang, F., Wang, Z., Deng, S., Walker, V.K., Zhou, S., 2014. Juvenile hormone-receptor complex acts on mcm4 and mcm7 to promote polyploidy and vitellogenesis in the migratory locust. PLoS Genet 10, e1004702.

Hannibal, R.L., Baker, J.C., 2016. Selective Amplification of the Genome Surrounding Key Placental Genes in Trophoblast Giant Cells. Curr Biol 26, 230-236.

Hopkins, B.R., Sepil, I., Bonham, S., Miller, T., Charles, P.D., Fischer, R., Kessler, B.M., Wilson, C., Wigby, S., 2019. BMP signaling inhibition in Drosophila secondary cells remodels the seminal proteome and self and rival ejaculate functions. Proc Natl Acad Sci U S A 116, 24719-24728.

Iida, K., Cavener, D.R., 2004. Glucose dehydrogenase is required for normal sperm storage and utilization in female Drosophila melanogaster. J Exp Biol 207, 675-681.

Jindra, M., Palli, S.R., Riddiford, L.M., 2013. The juvenile hormone signaling pathway in insect development. Annu Rev Entomol 58, 181-204.

Kurogi, Y., Mizuno, Y., Okamoto, N., Barton, L., Niwa, R., 2024. The seminal vesicle is a juvenile hormone-responsive tissue in adult male Drosophila melanogaster. bioRxiv. Mar 23:2024.03.20.585833. doi: 10.1101/2024.03.20.585833

Leiblich, A., Hellberg, J., Sekar, A., Gandy, C., Mendes, C.C., Redhai, S., Mason, J., Wainwright, M., Marie, P., Goberdhan, D.C.I., Hamdy, F.C., Wilson, C., 2019. Mating induces switch from hormone-dependent to hormone-independent steroid receptor-mediated growth in Drosophila secondary cells. PLoS Biol 17, e3000145.

Li, K., Jia, Q.Q., Li, S., 2019. Juvenile hormone signaling - a mini review. Insect Sci 26, 600-606.

Linnemannstons, K., Ripp, C., Honemann-Capito, M., Brechtel-Curth, K., Hedderich, M., Wodarz, A., 2014. The PTK7-related transmembrane proteins off-track and off-track 2 are co-receptors for Drosophila Wnt2 required for male fertility. PLoS Genet 10, e1004443.

Liu, Y.H., Jakobsen, J.S., Valentin, G., Amarantos, I., Gilmour, D.T., Furlong, E.E., 2009. A systematic analysis of Tinman function reveals Eya and JAK-STAT signaling as essential regulators of muscle development. Dev Cell 16, 280-291.

Ludwig, M.Z., Tamarina, N.A., Richmond, R.C., 1993. Localization of sequences controlling the spatial, temporal, and sex-specific expression of the esterase 6 locus in Drosophila melanogaster adults. Proc Natl Acad Sci U S A 90, 6233-6237.

Lung, O., Kuo, L., Wolfner, M.F., 2001. Drosophila males transfer antibacterial proteins from their accessory gland and ejaculatory duct to their mates. J Insect Physiol 47, 617-622.

Markow, T.A., O'Grady, P.M., 2006. Drosophila : a guide to species identification and use. London, UK ; Burlington, MA : Elsevier Academic Press.

Massie, C.E., Lynch, A., Ramos-Montoya, A., Boren, J., Stark, R., Fazli, L., Warren, A., Scott, H., Madhu, B., Sharma, N., Bon, H., Zecchini, V., Smith, D.M., Denicola, G.M., Mathews, N., Osborne, M., Hadfield, J., Macarthur, S., Adryan, B., Lyons, S.K., Brindle, K.M., Griffiths, J., Gleave, M.E., Rennie, P.S., Neal, D.E., Mills, I.G., 2011. The androgen receptor fuels prostate cancer by regulating central metabolism and biosynthesis. EMBO J 30, 2719-2733.

McGuire, S.E., Mao, Z., Davis, R.L., 2004. Spatiotemporal gene expression targeting with the TARGET and gene-switch systems in Drosophila. Sci STKE 2004, pl6.

Norville, K., Sweeney, S.T., Elliott, C.J., 2010. Postmating change in physiology of male Drosophila mediated by serotonin (5-HT). J Neurogenet 24, 27-32.

Orr-Weaver, T.L., 1991. Drosophila chorion genes: cracking the eggshell's secrets. Bioessays 13, 97-105.

Ovrebo, J.I., Bradley-Gill, M.R., Zielke, N., Kim, M., Marchetti, M., Bohlen, J., Lewis, M., van Straaten, M., Moon, N.S., Edgar, B.A., 2022. Translational control of E2f1 regulates the Drosophila cell cycle. Proc Natl Acad Sci U S A 119.

Ren, D., Song, J., Ni, M., Kang, L., Guo, W., 2020. Regulatory Mechanisms of Cell Polyploidy in Insects. Front Cell Dev Biol 8, 361.

Rexhepaj, A., Liu, H., Peng, J., Choffat, Y., Kubli, E., 2003. The sex-peptide DUP99B is expressed in the male ejaculatory duct and in the cardia of both sexes. Eur J Biochem 270, 4306-4314.

Richmond, R.C., Gilbert, D.G., Sheehan, K.B., Gromko, M.H., Butterworth, F.M., 1980. Esterase 6 and reproduction in Drosophila melanogaster. Science 207, 1483-1485.

Riddiford, L.M., 2012. How does juvenile hormone control insect metamorphosis and reproduction? Gen Comp Endocrinol 179, 477-484.

Saad, M., Game, A.Y., Healy, M.J., Oakeshott, J.G., 1994. Associations of esterase 6 allozyme and activity variation with reproductive fitness in Drosophila melanogaster. Genetica 94, 43-56.

Samakovlis, C., Kylsten, P., Kimbrell, D.A., Engstrom, A., Hultmark, D., 1991. The andropin gene and its product, a male-specific antibacterial peptide in Drosophila melanogaster. EMBO J 10, 163-169.

Saudan, P., Hauck, K., Soller, M., Choffat, Y., Ottiger, M., Sporri, M., Ding, Z., Hess, D., Gehrig, P.M., Klauser, S., Hunziker, P., Kubli, E., 2002. Ductus ejaculatorius peptide 99B (DUP99B), a novel Drosophila melanogaster sex-peptide pheromone. Eur J Biochem 269, 989-997.

Schiewer, M.J., Augello, M.A., Knudsen, K.E., 2012. The AR dependent cell cycle: mechanisms and cancer relevance. Mol Cell Endocrinol 352, 34-45.

Sekar, A., Leiblich, A., Wainwright, S.M., Mendes, C.C., Sarma, D., Hellberg, J., Gandy, C., Goberdhan, D.C.I., Hamdy, F.C., Wilson, C., 2023. Rbf/E2F1 control growth and endoreplication via steroid-independent Ecdysone Receptor signalling in Drosophila prostate-like secondary cells. PLoS Genet 19, e1010815.

Sharma, V., Pandey, A.K., Kumar, A., Misra, S., Gupta, H.P.K., Gupta, S., Singh, A., Buehner, N.A., Ravi Ram, K., 2017. Functional male accessory glands and fertility in Drosophila require novel ecdysone receptor. PLoS Genet 13, e1006788.

Sturm, S., Dowle, A., Audsley, N., Isaac, R.E., 2021. Mass spectrometric characterisation of the major peptides of the male ejaculatory duct, including a glycopeptide with an unusual zwitterionic glycosylation. J Proteomics 246, 104307.

Stallaert W, Kedziora KM, Chao HX, Purvis JE. (2019) ‘Bistable switches as integrators and actuators during cell cycle progression’. *FEBS Lett*. 593(20):2805-2816.

Sullivan, W.A., M; Hawley, RS, 2000. Drosophila Protocols. Cold Spring Harbor Press.

Susic-Jung, L., Hornbruch-Freitag, C., Kuckwa, J., Rexer, K.H., Lammel, U., Renkawitz-Pohl, R., 2012. Multinucleated smooth muscles and mononucleated as well as multinucleated striated muscles develop during establishment of the male reproductive organs of Drosophila melanogaster. Dev Biol 370, 86-97.

Swanson, C.I., Meserve, J.H., McCarter, P.C., Thieme, A., Mathew, T., Elston, T.C., Duronio, R.J., 2015. Expression of an S phase-stabilized version of the CDK inhibitor Dacapo can alter endoreplication. Development 142, 4288-4298.

Takashima, Y.A., Majane, A.C., Begun, D.J., 2023. Evolution of secondary cell number and position in the Drosophila accessory gland. PLoS One 18, e0278811.

Takemori, N., Yamamoto, M.T., 2009. Proteome mapping of the Drosophila melanogaster male reproductive system. Proteomics 9, 2484-2493.

Wang, G., Zhao, D., Spring, D.J., DePinho, R.A., 2018. Genetics and biology of prostate cancer. Genes Dev 32, 1105-1140.

Weng, L., Zhu, C., Xu, J., Du, W., 2003. Critical role of active repression by E2F and Rb proteins in endoreplication during Drosophila development. Embo J 22, 3865-3875.

Wilson, C., Leiblich, A., Goberdhan, D.C., Hamdy, F., 2017. The Drosophila Accessory Gland as a Model for Prostate Cancer and Other Pathologies. Curr Top Dev Biol 121, 339-375.

Wilson, T.G., DeMoor, S., Lei, J., 2003. Juvenile hormone involvement in Drosophila melanogaster male reproduction as suggested by the Methoprene-tolerant(27) mutant phenotype. Insect Biochem Mol Biol 33, 1167-1175.

Wu, Z., Guo, W., Xie, Y., Zhou, S., 2016. Juvenile Hormone Activates the Transcription of Cell-division-cycle 6 (Cdc6) for Polyploidy-dependent Insect Vitellogenesis and Oogenesis. J Biol Chem 291, 5418-5427.

Wu, Z., Guo, W., Yang, L., He, Q., Zhou, S., 2018. Juvenile hormone promotes locust fat body cell polyploidization and vitellogenesis by activating the transcription of Cdk6 and E2f1. Insect Biochem Mol Biol 102, 1-10.

Wu, Z., He, Q., Zeng, B., Zhou, H., Zhou, S., 2020. Juvenile hormone acts through FoxO to promote Cdc2 and Orc5 transcription for polyploidy-dependent vitellogenesis. Development 147.

Xin, S., Weng, L., Xu, J., Du, W., 2002. The role of RBF in developmentally regulated cell proliferation in the eye disc and in Cyclin D/Cdk4 induced cellular growth. Development 129, 1345-1356.

Yamamoto, K., Chadarevian, A., Pellegrini, M., 1988. Juvenile Hormone Action Mediated in Male Accessory Glands of Drosophila by Calcium and Kinase C. Science 239, 916-919.

Yang, M., Lu, Y., Piao, W., Jin, H., 2022. The Translational Regulation in mTOR Pathway. Biomolecules. Jun 8;12(6):802. doi: 10.3390/biom12060802.

Zaffran, S., Reim, I., Qian, L., Lo, P.C., Bodmer, R., Frasch, M., 2006. Cardioblast-intrinsic Tinman activity controls proper diversification and differentiation of myocardial cells in Drosophila. Development 133, 4073-4083.

Zhang, X., Li, S., Liu, S., 2021. Juvenile Hormone Studies in Drosophila melanogaster. Front Physiol 12, 785320.

Zielke, N., Kim, K.J., Tran, V., Shibutani, S.T., Bravo, M.J., Nagarajan, S., van Straaten, M., Woods, B., von Dassow, G., Rottig, C., Lehner, C.F., Grewal, S.S., Duronio, R.J., Edgar, B.A., 2011. Control of Drosophila endocycles by E2F and CRL4(CDT2). Nature 480, 123-127.

Zielke, N., Querings, S., Rottig, C., Lehner, C., Sprenger, F., 2008. The anaphase-promoting complex/cyclosome (APC/C) is required for rereplication control in endoreplication cycles. Genes Dev 22, 1690-1703.

Chapter 3 Isolation of Polyploid Nuclei and Measurement of the Ploidy of the *Drosophila* Male Reproductive System Using Flow Cytometry

3.1 Abstract

Polyploidy in the *Drosophila melanogaster* male reproductive system plays an essential role in supporting the high secretory demands of the accessory glands (AG) and ejaculatory duct (ED), which are critical for male fertility. Polyploidy in these tissues is both spatially and temporally regulated. Traditional ploidy measurements using microscopy-based nuclear DNA staining are low-throughput. Here, we present an optimized, scalable novel nuclei isolation method and flow cytometry protocol that enables robust, high-throughput quantification of DNA content in polyploid nuclei from the secretory cells of the AG and ED. This method is also suitable for nuclear isolations for future molecular genomics analysis. This method combines tissue homogenization, DNA staining with DyeCycle Violet, and rigorous gating strategies to accurately resolve distinct ploidy populations. We demonstrate its versatility by applying it across multiple *Drosophila* species and validating its sensitivity to detect ploidy changes under genetic perturbations that reduce and increase nuclear ploidy. Additionally, we show that this approach remains effective for pooled frozen tissues, enabling experiments where fresh tissues are limited. Beyond the polyploid nuclei, we extend our approach to include a trypsin-based dissociation and genetic labeling strategy to isolate and quantify diploid nuclei from the ED's innervated muscle layer populations not previously analyzed by flow cytometry in this tissue. Together, this work fills a key methodological gap by providing a reliable tool for accurate ploidy measurements in the *Drosophila* male reproductive system, with potential future applications in studying endoreplication, tissue regeneration, single-cell sequencing, and spatial transcriptomics.

3.2 Introduction

The *Drosophila* male reproductive tract consists of a pair of sperm-producing testes connected to seminal vesicles, which secrete seminal fluid proteins (SFPs) and temporarily store sperm until

ejaculation. It also includes a pair of accessory gland (AG) lobes, the ejaculatory duct (ED), and ejaculatory bulb (Hopkins et al.,2019). The two large AG lobes are functionally analogous to the mammalian prostate and seminal vesicles, with key roles in secreting Sex Peptide and other proteins which impact female post-mating responses, antimicrobial peptides, and seminal fluid proteins (Susic-Jung et al., 2012). The ED secretes additional SFPs as well as ED-specific antimicrobial peptides such as Andropin and Cecropin, and it also serves as the site where sperm from the testis and seminal fluids from the seminal vesicles and AG mix before being transferred to the ejaculatory bulb and ultimately to the female during mating (Takemori & Yamamoto, 2009). Secretions from the testes, seminal vesicles and AGs are transferred to ED through an organ transition zone with a small opening called the anterior ED papillae (Lung et al., 2001). Secretions from both the AG and ED are crucial for inducing post-mating responses in the female reproductive system and ensuring successful fertility (Cohen & Moussian, 2016). The epithelial secretory cells are the main source of these secretions in both the AG and ED. These secretory cells are polyploid, which likely helps meet the high secretion demands of these tissues (Box et al., 2024; Ramesh et al., 2025a). Mature AG secretory cells are binucleate with a ploidy of 8C per nucleus (16C per cell), whereas mature ED secretory cells have ploidy levels that range from 8C to 32C. We have recently shown that reducing ploidy levels in the AG and ED leads to decreased fertility and, for the ED, results in a lower nascent protein synthesis rate (Ramesh et al., 2025a). Thus, normal ploidy levels in AG and ED secretory cells are essential for optimal fertility.

The anterior portion of the ED, where it interfaces with the accessory glands and seminal vesicles at the ED papillae, is wider and gradually tapers toward the posterior end, connecting to the ejaculatory bulb. We have shown that cells in the anterior region of the ED are larger and contain nuclei with DNA contents of 16C and 32C, while cells in the anterior middle region are smaller and have nuclei with DNA contents of 8C and 16C. Cells at the posterior end are the smallest and have nuclei with DNA contents of 4C and 8C (Ramesh et al., 2025). These different regions of the ED may produce distinct secretions or vary in the amount of secretion they provide (Sturm et al., 2021). Currently, there are no known region-specific or ploidy-specific promoters for the ED. Therefore, nuclei could be isolated from this tissue and separated based on ploidy in order to identify region and ploidy-specific ED genes and their promoters.

Accurately measuring ploidy levels in this tissue is essential for studying its cell cycle dynamics and functional roles. Despite the biological importance of polyploidy in these reproductive tissues, quantitative assessment has historically relied on microscopy-based DNA staining methods such as DAPI fluorescence intensity measurements (Edgar & Orr-Weaver, 2001; Fox & Duronio, 2013). While informative, these techniques are labor-intensive, low-throughput, and can be sensitive to aneuploidy under different genetic or environmental conditions. Image-based ploidy measurement is time-consuming if we want to quantify in 1000s of nuclei compared to flow cytometry, where we can quantify more nuclei fewer at a time. In this methods study, we introduce a novel methodological framework for flow cytometry analysis of nuclei within the *Drosophila* melanogaster reproductive system. A gold standard methodology for cell cycle dynamics is the flow cytometer. Flow cytometry offers a powerful alternative for rapid, high-throughput measurement of nuclear DNA content, with proven applications in analyzing endoreplication and polyploidy in various Drosophila tissues such as salivary glands, follicle cells, and imaginal discs (Stormo and Fox, 2016; Lilly & Spradling, 1996). Established methods typically involve isolating intact nuclei/isolating cells from freshly dissected tissues, staining with DNA-specific fluorophores like propidium iodide or DyeCycle Violet, and using internal standards or controls to calibrate ploidy peaks. We cannot perform flow cytometry on isolated AG cells because they are difficult to dissociate, as the cells are connected by ring canals, making it impossible to separate them using conventional tissue dissociation methods (Box et al., 2024). Additionally, AG cells are binucleate, which can complicate flow cytometric measurements of DNA content so we must isolate individual nuclei instead. However, published protocols have largely focused on larval or female reproductive tissues, leaving comparable high-throughput methods for the male AG and ED underdeveloped.

To address this gap, we developed and optimized a reliable nuclei isolation and flow cytometry protocol specifically for the *Drosophila* male AG and ED. Our approach combines mechanical tissue homogenization with dual pestles to break the surrounding muscle layer and efficiently release polyploid secretory cell nuclei. By staining with DyeCycle Violet and applying robust gating strategies to remove doublets, we can resolve distinct ploidy populations with high accuracy, using well-established follicle cell nuclei as an internal control (Lilly & Duronio, 2005). The method achieves a good recovery of the secretory cells nuclei from AG and ED. We have also shown that this method is compatible with tissue freezing, enabling pooling of samples across

multiple dissections when the desired genotypes are scarce, an important advantage over protocols that require immediate fresh tissue processing. Our optimized nuclei isolation protocol can be used to build a single-cell sequencing atlas of ED cells with spatial resolution. We can also use this protocol of polyploid nuclei isolation to do any ATAC sequencing on these cells.

Beyond standard polyploid nuclei isolation, we expanded this workflow to study ploidy dynamics under genetic perturbations known to modulate endocycle progression, such as stabilized Geminin overexpression (Quinn et al., 2001), CycE/Cdk2 overexpression (Edgar & Orr-Weaver, 2001), and Rbf^{120} hypomorphic mutants (Buttitta et al., 2007). These experiments confirmed the sensitivity of our protocol to detect expected ploidy shifts. This method allows for the high-throughput, quantitative analysis of nuclear properties and provides unprecedented insights into the cell cycle states of these tissues. This allows researchers to study the cell cycle dynamics of these essential organs at a higher resolution than previously published methods. Additionally, by introducing a trypsin-based dissociation step and a genetic labeling strategy (Elav-Gal4 > UAS-RFPnls), we demonstrated that this pipeline can also isolate and quantify diploid nuclei from the innervated muscle layer of the basement membrane, a population not previously characterized for ploidy by flow cytometry.

We used the Attune NxT Flow Cytometer, a state-of-the-art instrument known for its precision and versatility in flow cytometry analysis. The Attune Flow Cytometer is particularly well-suited for our study due to its acoustic focusing technology, which allows for a higher throughput of samples without compromising the accuracy and quality of data. This feature is crucial when dealing with the small size of *Drosophila* nuclei. By utilizing the Attune Flow Cytometer, we significantly enhanced the resolution and sensitivity of the current assay for nuclei measurement in the *Drosophila* male reproductive system, enabling the detection of subtle differences in nuclear properties that were previously undetectable with conventional methods. This increased sensitivity is instrumental in identifying distinct cell cycle phases within the accessory glands and the ejaculatory duct, thereby providing a more nuanced understanding of the cell cycle dynamics in these tissues. This technology not only facilitated a more detailed and accurate analysis but also opened new avenues for exploring the intricate processes governing reproduction in Drosophila melanogaster.

Taken together, this method bridges a technical gap by providing a robust, versatile, and scalable approach for high-resolution ploidy analysis in the *Drosophila* male reproductive system. It complements and extends previous flow cytometry methods designed for other Drosophila tissues (Lee et al., 2009; Wu et al., 2022) and lays a foundation for future applications in single-cell polyploid sequencing, spatial transcriptomics, and regenerative biology

3.3 Results and discussions

3.3.1 Polyploid nuclei Isolation from AG and ED of Drosophila male and ploidy Quantification via Flow Cytometry

Anatomically, the *Drosophila* male accessory gland (AG) and ejaculatory duct (ED) are enclosed by a basement membrane of an innervated muscle layer, and an apical layer of polarized epithelium composed of a layer of large secretory cells (Church et al., 2025; Ramesh et al., 2025b; Susic-Jung et al., 2012). These secretory cells face a central lumen, into which they release their contents along with fluids from the reproductive tract. The secretory cells of the AG are binucleate and polyploid, with each nucleus containing a DNA content of 8C (Box et al., 2024b). In contrast, ED secretory cells are mononucleate and polyploid, with ploidy levels ranging from 8C to 32C (Ramesh et al., 2025b). To extract polyploid nuclei from both the accessory gland (AG) and the ejaculatory duct (ED), the outer basal muscle layer was disrupted by homogenizing the tissues in homogenization buffer using a loose pestle, thereby releasing the basal secretory cells. These cells were then further homogenized with a tight pestle to release the polyploid nuclei (Figure 1). We optimized this protocol to enable efficient isolation of individual polyploid nuclei from both the AG and ED (Fig. 7A). The isolated nuclei were washed and stained with DyeCycle Violet, a DNA-binding dye with an excitation wavelength of 360 nm.

Ploidy analysis of AG and ED nuclei was performed using the Attune NxT flow cytometer. To accurately overlay the ploidy peaks of AG and ED, we used *Drosophila* (*Canton-S*) ovarian follicle cell nuclei as a positive control, due to their well-established ploidy levels (Bosco et al., 2007). Since doublet nuclei can significantly skew results and lead to inaccurate conclusions, a forward scatter height (FSC-H) versus forward scatter area (FSC-A) density plot was used to exclude doublets.

As a reference, isolated and stained ovarian nuclei were first analyzed using the same protocol. We observed four distinct ploidy populations of follicle cell nuclei, gated in R1 (Figure 2A(i)).

These populations were further resolved based on Violet fluorescence in gate R2 (Figure 2A(ii)). Single-parameter histograms enabled the separation of nuclei with 2C, 4C, 8C, and 16C DNA content (Figure 2A(iii)). The same gating strategy and intensity settings were consistently applied for the analysis of ovary, AG, and ED nuclei. AG and ED tissues were dissected from 10-day-old virgin males, at which point endoreplication is known to have ceased in both tissues. In AG samples, forward scatter profiles revealed three distinct nuclear populations, which corresponded to three ploidy peaks in the histograms (Figure 2B). We used AGs from 20 males, totaling 40 AG lobes, and isolated approximately 28,000 nuclei. Using this method, we achieved a recovery rate of approximately 66% for AG nuclei. Overlaying these with the ovary control histogram showed that most AG nuclei had a ploidy of 8C, with a small proportion at 4C and 16C (Figure 2D(i)). Recovery of the 16C nuclei is lower compared to the 8C nuclei of AG. In ED samples, forward scatter profiles revealed four nuclear populations. Using DyeCycle Violet fluorescence alone, we identified four distinct ploidy peaks in the histogram (Figure 2C). Overlay with ovary control histograms confirmed the presence of nuclei with 4C, 8C, 16C, and 32C DNA content in the ED, with the majority being 32C (Figure 2D(ii)). Using this protocol, we isolated approximately 9,500 nuclei from the EDs of 20 males. These results of ploidies are consistent with DAPI intensity quantification from confocal micrographs of AG and ED tissues (Box et al., 2024b; Ramesh et al., 2025b). This protocol can be used to separate nuclei based on ploidy under different cell cycle regulation conditions. It can also be applied to isolate distinct ploidy populations for single-cell polyploid sequencing. Additionally, the nuclei isolated from the AG and ED using this method can be used for spatial transcriptomic gene expression analysis. Ideally, for the tissues where the ploidy correlates with the size of the tissue (Ramesh et al., 2025b).

3.3.2 Flow cytometric ploidy measurements from the frozen and fresh Accessory glands

Most ploidy measurements by flow cytometry are performed on nuclei isolated immediately after tissue dissection. However, in cases where only a small number of offspring with the desired genotype are available at a given time, or when tissues need to be pooled from different days for age- or time-matched experiments, obtaining a sufficient number of AGs can be challenging. To address this, we optimized a freezing protocol for AGs post-dissection. This allowed us to freeze AGs from multiple time points in liquid nitrogen and later pool them for nuclear isolation using the same extraction protocol that we used to extract the nuclei from the freshly dissected tissue.

To validate the freezing method, we compared ploidy profiles from frozen and freshly dissected AGs. We dissected 40 males for each condition. In fresh AG nuclei, flow cytometry revealed a distinct 8C ploidy peak, first separated by forward scatter, followed by Violet fluorescence (Figure 3A). For frozen AG nuclei, we used FSC-H vs. FSC-A gating and observed two distinct ploidy populations (Figure 2). Single-parameter histograms showed two clear peaks, comparable to those observed in fresh AG samples (Figure 3B(iii)). To confirm the exact ploidy of the observed peaks, we overlaid the histograms of nuclei extracted from both fresh and frozen AGs with the ploidy profile of ovarian follicle cell nuclei (Figure 3C). Notably, freezing the AGs immediately after dissection resulted in improved recovery of 16C polyploid nuclei compared to fresh AGs. Thus, freezing AGs post-dissection enhances the yield and recovery of polyploid nuclei for downstream analysis.

3.3.3 Ploidy measurements of AG and ED under Varying Cell Cycle Conditions and across Drosophila species

We performed ploidy measurements from the AG and ED under different cell cycle regulatory conditions and across multiple *Drosophila* species to assess conserved and divergent patterns of polyploidy, using flow cytometry. Specifically, we tested the applicability of our nuclei isolation and ploidy analysis protocol in *D. simulans*, *D. yakuba*, and *D. virilis* species. Among these, *D. simulans* and *D. yakuba* are closely related to *D. melanogaster*, while *D. virilis* is more distantly related. Previous findings from our lab have shown that *D. virilis* exhibit delayed developmental timing compared to the other species. All ploidy measurements were conducted using AGs and EDs dissected from 10-day-old virgin males. For each species, we used ovaries from the same species as an internal control to overlay and assign ploidy levels.

In *D. simulans*, the AG nuclei displayed a dominant ploidy of 8C, with a small population of 16C nuclei, as confirmed by overlay with *D. simulans* ovarian follicle cell nuclei (Figure 4A(i)). In contrast, *D. simulans* EDs exhibited a wide range of ploidy levels, from 2C to 32C, similar to what we observed in *D. melanogaster* EDs (Figure 4A(ii)). Likewise, *D. yakuba* AGs primarily showed an 8C ploidy peak, with a minor population at 16C (Figure 4B(i)), while the ED nuclei displayed a broader range of ploidy levels, from 4C to 32C (Figure 4B(ii)). In the more distantly related species *D. virilis*, AG nuclei exhibited a broad ploidy distribution between 8C and 16C, which may reflect under-replication. The ED nuclei from *D. virilis* displayed lower ploidy levels overall, with the majority at 8C, and smaller populations at 2C, 4C, and 16C (Figure 4C). These flow

cytometry-based ploidy measurements are consistent with our previous DAPI intensity quantifications from confocal micrographs from these different species of *Drosophila* AG and ED, validating the robustness of this method across species.

The cell cycle dynamics within this tissue have so far been examined only to a limited extent using staining methods and DAPI intensity measurements. Here, we aimed to apply our optimized protocol to measure cell cycle dynamics under different cell cycle conditions in the AG and ED using flow cytometry. Previous studies have shown that while the ED is post-mitotic, it does undergo endoreplication (Ramesh et al., 2025b). Geminin functions as an inhibitor of DNA replication licensing and is normally degraded during the cell cycle by the Anaphase Promoting Complex/Cyclosome (APC/C) ubiquitin ligase. A variant of Geminin that is stable can dominantly inhibit entry of cells into S-phase when overexpressed in *Drosophila* ED and other tissues (Diffley, 2004; Ramesh et al., 2025b; Zielke et al., 2008). We observed a similar reduction in 16C and 32C nuclei when measuring ED ploidy under stabilized-Geminin conditions compared to the control (Figure 5A). It is well established that CycE/Cdk2 plays a key role in driving endocycle progression through its oscillations during the cell cycle (Box et al., 2024; Ramesh et al., 2025a). When CycE/Cdk2 was overexpressed in the ED using the ED-specific Luna-Gal4 driver, it induced additional endocycles, resulting in higher ploidy levels in ED secretory cells (Ramesh et al., 2025a). Many of these cells reached a ploidy of 64C, a state not normally seen in the ED. Using our nuclei isolation and flow cytometry protocol, we captured this increase in ploidy, clearly detecting a 64C ploidy peak in CycE/Cdk2-overexpressing EDs compared to controls (Figure 5B). To further validate the accuracy of our nuclei isolation and flow cytometry method for measuring the ploidy of ED and AG secretory cells, we used *Rbf120* hypomorphic mutant flies, which have reduced Rbf function. This results in decreased degradation of E2F, leading to increased DNA synthesis. In these mutants, both the AG and ED undergo additional rounds of endoreplication, resulting in higher ploidy levels. Using our protocol, we detected elevated ploidy in the ED, with nuclei reaching the ploidy of 64C compared to the control (*Canton-S*) ED (Figure 5C). Similarly, we isolated and observed increased ploidy in the AG, with DNA content reaching 16C in *Rbf120* mutants compared to *Canton-S* AG (Figure 5D). Together, these results highlight the significant advantages of our optimized nuclei isolation and flow cytometry protocol for accurately measuring ploidy in the Drosophila male AG and ED. Unlike traditional methods that rely solely on DAPI staining and microscopy, this approach enables rapid, high-throughput quantification of ploidy

across thousands of nuclei with minimal tissue input. It is sensitive enough to detect subtle shifts in ploidy under various genetic manipulations. Overall, this method provides a robust, scalable tool for investigating cell cycle dynamics, endoreplication, and polyploidy in reproductive tissues, with potential applications in single-cell sequencing and spatial gene expression analyses.

3.3.4 Isolation of Diploid Nuclei from the Drosophila Male Ejaculatory Duct (ED) and Ploidy Quantification by Flow Cytometry

The polyploid nuclei extraction protocol described above is specific for isolating polyploid nuclei from the secretory cells of the AG and ED. To extract nuclei from the innervated muscle layer located on the basement membrane of these tissues, we used a trypsin-based dissociation method, which releases nuclei from the external basement membrane (Figure 6B). The ploidy levels of these innervated muscle nuclei in the ED are not known. Using this modified nuclei extraction method and our flow cytometry protocol, we aimed to determine their ploidy. To specifically label these basement membrane nuclei, we used the pan-neuronal *Drosophila* driver *Elav-Gal4* to express a nuclear-localized RFP (UAS-RFPnls) under the control of a Gal4-responsive upstream activating sequence (UAS). We observed that all nuclei in the basement membrane were RFP-positive, with no RFP-positive nuclei detected in the ED secretory cells (Figure 6A). Using the modified extraction protocol, we successfully isolated these nls-RFP–positive nuclei and analyzed them with the Attune NxT flow cytometer. First, we separated the nuclei using Yellow Light-Height (FSC-H) versus Violet Light-Area (FSC-A) plots to exclude doublets (Figure 6C(i)). Next, we gated the R1 population and further resolved it using Yellow Light-Height versus Violet Light-Height plots (Figure 6C(ii)). We then gated the R2 population, which was positive for both RFP and DyeCycle Violet, and analyzed it with a single-parameter histogram, where we observed a single distinct nuclear peak (Figure 6C(iii)). We then overlaid this peak with the ovary control peak and confirmed that the RFP and DyeCycle Violet–positive nuclei were diploid (Figure 6D). Thus, using this modified protocol, we can isolate diploid nuclei from the basement membrane of the *Drosophila* male reproductive system. This demonstrates that the protocol reliably isolates diploid nuclei from the basement membrane, complementing the standard method for extracting polyploid secretory cell nuclei.

3.4 Materials and Methods

3.4.1 Drosophila husbandry

All the flies are housed at room temperature (23°C) on a Bloomington Cornmeal food without crowding, all the flow cytometry experiments were performed with male virgin flies of 10 days old post-eclosion. For the day 10 experiments, the males were collected on DOE and transferred 5 to 8 flies per vial, aged till day 10 from DOE/Day 1 flipping into fresh media vials at an interval of 2-3 days and housed at room temperature.

3.4.2 Fly strains

Canton S

Different species of flies were Gift from Patricia Wittkopp Lab

D. simulans

D. yakuba

D. virilis

Luna-Gal4 (BL#63746): w[1118]; PBac{w[+mC]=IT.GAL4}luna[0689-G4]/CyO

mcherry-RNAi (BL#35785): [1] sc[*] v[1] sev[21]; P{y[+t7.7] v[+t1.8]=VALIUM20-mCherry}attP2

Rbf120 (BL#81612): Rbf[120a]/FM7i, P{w[+mC]=ActGFP}JMR3

CycE-Cdk2-OE: y,w, hs-flp; +; UAS-CycE,UAS-Cdk2/TM6B

Stabilized Geminin (BL#59069): w[*]; Kr[If-1]/CyO, P{ry[+t7.2]=en1}wg[en11]; P{w+mC]=UAS geminin.DeltaD.DeltaKEN}M7

3.4.3 Dissection and Nuclei isolation from fresh tissues

Table 3.1: Homogenization Buffer

Reagent	**Amount**	**Final concentration**	**Storage**
milli-Q	400 mL	Final volume 500 mL	RT
Tris-HCl pH 7.4	0.788 g	10 mM	RT
NaCl (Sigma S9888)	0.292.2 g	10 mM	RT

Reagent	Amount	Final concentration	Storage
$MgCl_2$ (Sigma M8266)	0.142.8 g	3 mM	RT
NP40 (Sigma 9002-93-1)	50 µL	0.1%	RT

Schneider's *Drosophila* Medium (Gibco 21720024), Fetal Bovine Serum (FBS Cytiva # SH30396.02HI), Dounce Tissue Grinder, 7 mL (WHEATON 357542), 100µm strainer(Corning 431752), 40µm-strainer (Fisherbrand 22363547), Glass Pasteur pipette (BrainBits FPP, NC0319875), Vybrant Dye Cycle Violet (Invitrogen V35003), glass dissection dish, Dissection forceps (FST #5SF)

Rinse all plasticware and glassware with water, then sterilize by rinsing with 70% ethanol, and finally rinse with Schneider's *Drosophila* Medium containing 10% FBS before use. All steps should be performed on ice or at 4 °C. Schneider's medium with 10% FBS and 1% penstrep is used for all dissections, and washing steps should be kept ice cold. Dissect the Drosophila male reproductive system in prepared S2 medium. Separate the AGs and EDs and transfer them into separate 1.5 mL Eppendorf tubes containing S2 medium. Dissect approximately 20 males to obtain 40 pairs of AGs, and 25 males to obtain 25 EDs. All dissections should be completed within 20–30 minutes per sample. To allow the tissues to settle, briefly spin down the tubes, remove the S2 medium, and add 1000 µL of homogenization buffer. Transfer the tissues with homogenization buffer to an ice-cold Dounce tissue grinder and incubate on ice for 5 minutes, vortexing intermittently at low speed.

To remove the external basement membrane, homogenize the tissues using the loose-fit Dounce pestle with 20 strokes on ice. Incubate for an additional 10 minutes, vortexing intermittently at low speed. Next, homogenize with 40 strokes using the tight-fit Dounce pestle on ice to release the nuclei from the secretory cells. Avoid creating bubbles while homogenizing. Add 500 µL of prepared S2 medium through a filter to stop the lysis reaction. Triturate the tissue 15 times using a silanized fire-polished glass Pasteur pipette. Filter the homogenate through a 100 µm strainer into Falcon round-bottom polystyrene tubes or 1.5 mL Eppendorf tubes to remove tissue debris and unlysed tissue, then filter again through a 40 µm strainer to remove any remaining small debris. Rinse with an additional 100 µL of S2 medium through the filter afterward.

Centrifuge the filtrate at 500 rcf for 8 minutes at 4 °C to pellet the nuclei. Discard the supernatant and resuspend the pellet in 200 µL of prepared S2 medium to wash away excess homogenization

buffer and incubate on ice for 5 minutes. After incubation, add 800 µL of S2 medium and centrifuge again at 500 rcf for 8 minutes at 4 °C. Remove the supernatant and resuspend the pellet in 200 µL of S2 medium containing 10 µg/mL Vybrant DyeCycle Violet stain, incubate for 5 minutes on ice (use 1 µL DyeCycle Violet per 100 µL S2 medium). For multiple samples, prepare a master mix of S2 medium with Vybrant DyeCycle Violet. Resuspend the pellet and mix with an additional 800 µL of S2 medium, then perform a final centrifugation at 500 rcf for 8 minutes at 4 °C. Remove the supernatant and resuspend the pellet in 1100 µL of S2 medium. The nuclei sample is now ready for flow cytometry.

We used ovaries from *Canton-S* flies as a positive control for ploidies greater than 4C to overlay with the ED peaks. The same protocol was used to isolate nuclei from the ovaries, and they were stained using DyeCycle Violet following identical steps. For flow cytometry experiments involving different *Drosophila* species, we used ovaries from the respective species. All flow cytometry experiments were repeated at least three times, with a minimum of 25 EDs pooled per trial. One representative example from the three trials is shown. Our flow cytometry was performed using an Attune NxT at a flow rate of 100 µL/min.

3.4.4 Freezing of the AGs and isolation of the nuclei

Four Dissection dishes, Liquid nitrogen (LN_2), Cryotubes, Dissection forceps, Schneider's Drosophila Medium with 10% FBS + 1% penstrep, Phosphate Buffered Saline (PBS), 70% ethanol, Pipettes and pipette tips

Label cryotubes with sample information (date, genotype, experimental condition, etc.). Prepare the dissection dishes as follows:

- Dish 1: 70% ethanol — for disinfecting flies
- Dish 2: PBS — for rinsing off ethanol
- Dish 3: Schneider's medium — for dissecting accessory glands
- Dish 4: Fresh Schneider's medium — for temporary storage of dissected glands before freezing

Anesthetize flies as needed. Transfer flies to Dish 1 (70% ethanol) briefly for surface sterilization. Rinse flies in Dish 2 (PBS) to remove ethanol. Move flies to Dish 3 (Schneider's medium). Dissect accessory glands under a stereomicroscope, transferring dissected glands into

Dish 4 (fresh Schneider's medium). Limit the dissection phase to 20 minutes to preserve tissue quality before freezing.

After 20 minutes of dissection, transfer the accessory glands from Dish 4 into a labeled cryotube using a pipette.

Tip: Before transferring samples, pre-wet the pipette tip with Schneider's medium to reduce glands sticking to the tip. Add approximately 200 µL of Schneider's medium to the cryotube containing the glands. Securely close the lid of the cryotube. Wearing liquid nitrogen gloves and using long forceps, plunge the cryotube into liquid nitrogen and hold it submerged for at least 30 seconds. It is important to hold the tube fully below the surface, as it will otherwise float.

Transfer frozen cryotubes to a -80 °C freezer for long-term storage.

3.4.5 Thawing Samples

To thaw frozen samples, place cryotubes in an ice bucket with ice for approximately 45 minutes, allowing the medium to thaw completely. Briefly spin down the samples (about 30 seconds) in Schneider's medium using a mini benchtop centrifuge.

Once thawed, pool the samples and transfer the medium with the tissues to a 1.5 mL Eppendorf tube. Spin to pellet the tissues. Remove the S2 medium, add 1 mL of homogenization buffer, and proceed directly with the nuclear extraction protocol as described above.

3.4.6 Diploid nuclei isolation from the basement membrane

Staining solution (1mL):

900uL 10X Trypsin, 100uL 10X Phosphate Buffered Saline (PBS) pH 7.2, 2 µL DyeCycle Violet. This solution is aliquoted and stored in -20°C to minimize freeze/thaw cycles.

Dissect the *Drosophila* male reproductive system in 1X PBS. Separate the ED from the surrounding tissue. We used 20 EDs to extract diploid nuclei. Dissections should be completed within 20 minutes to limit cell death. In a 1.5 mL Eppendorf tube cap, add 100 µL of staining solution. Using forceps, transfer the dissected EDs into the Eppendorf cap containing the staining solution and incubate for 20 minutes at room temperature.

Using a plastic P200 pipette tip pressed against the side of the cap, gently triturate the tissue to dissociate the ED and release the nuclei from the innervated muscle layer surrounding the basement membrane. Transfer the 100 µL from the cap containing the cells to the remaining 400 µL of staining solution in the Eppendorf tube, bringing the total volume to 500 µL. Incubate

the sample in the dark (without mixing or vortexing) for 45–50 minutes to allow proper staining of the diploid nuclei. *(*Note: Incubating for less than 45 minutes may cause DNA under staining and smearing artifacts in FACS analysis, while incubating for more than 1 hour may result in overdigestion and excessive cell death.

Add 500 µL of 1X PBS to stop the trypsinization and dilute the sample. Do not pipette to mix, as cells can adhere to the pipette tip at this stage. The addition of PBS will gently mix the sample and adjust the concentration to optimize the passage of individual nuclei through the laser. Gently vortex the sample. Run the sample on the flow cytometer, drawing 800 µL at a rate of 200–500 µL/min, within 10 minutes of adding the PBS solution.

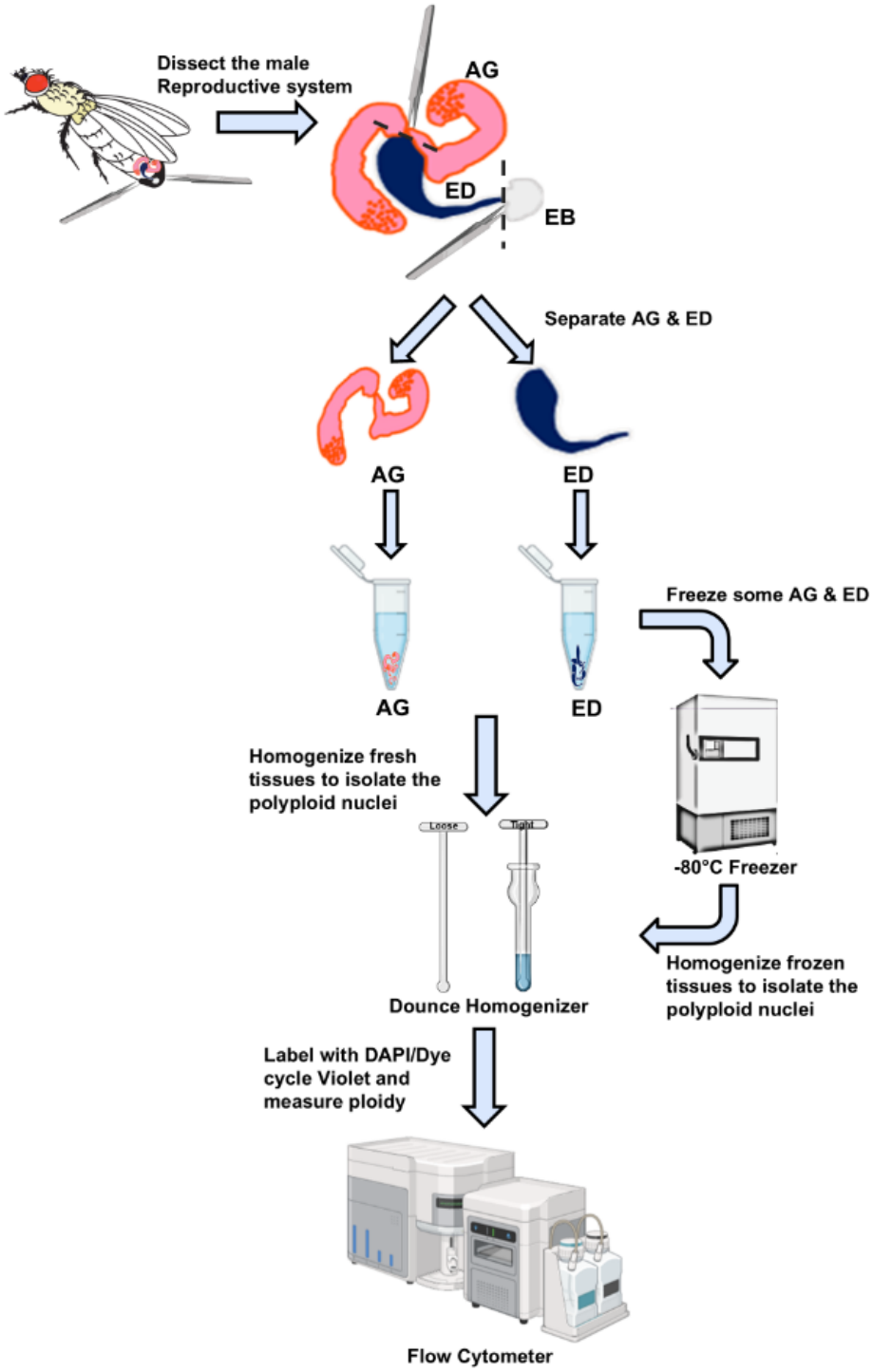


Figure 3.1**:** Schematic overview of the nuclei isolation and ploidy measurement workflow for the *Drosophila* male accessory gland (AG) and ejaculatory duct (ED).

Adult virgin *Drosophila* males are dissected to isolate the male reproductive system, from which the AG and ED are separated. Fresh tissues can be processed immediately to isolate polyploid nuclei, while additional AG and ED samples can be frozen at –80 °C for pooling and later

extraction. Tissues are homogenized using a Dounce homogenizer with loose and tight pestles to release nuclei. Isolated nuclei are stained with DAPI or DyeCycle Violet to label DNA content. Flow cytometry is then performed to measure nuclear ploidy and analyze cell cycle dynamics in AG and ED tissues.

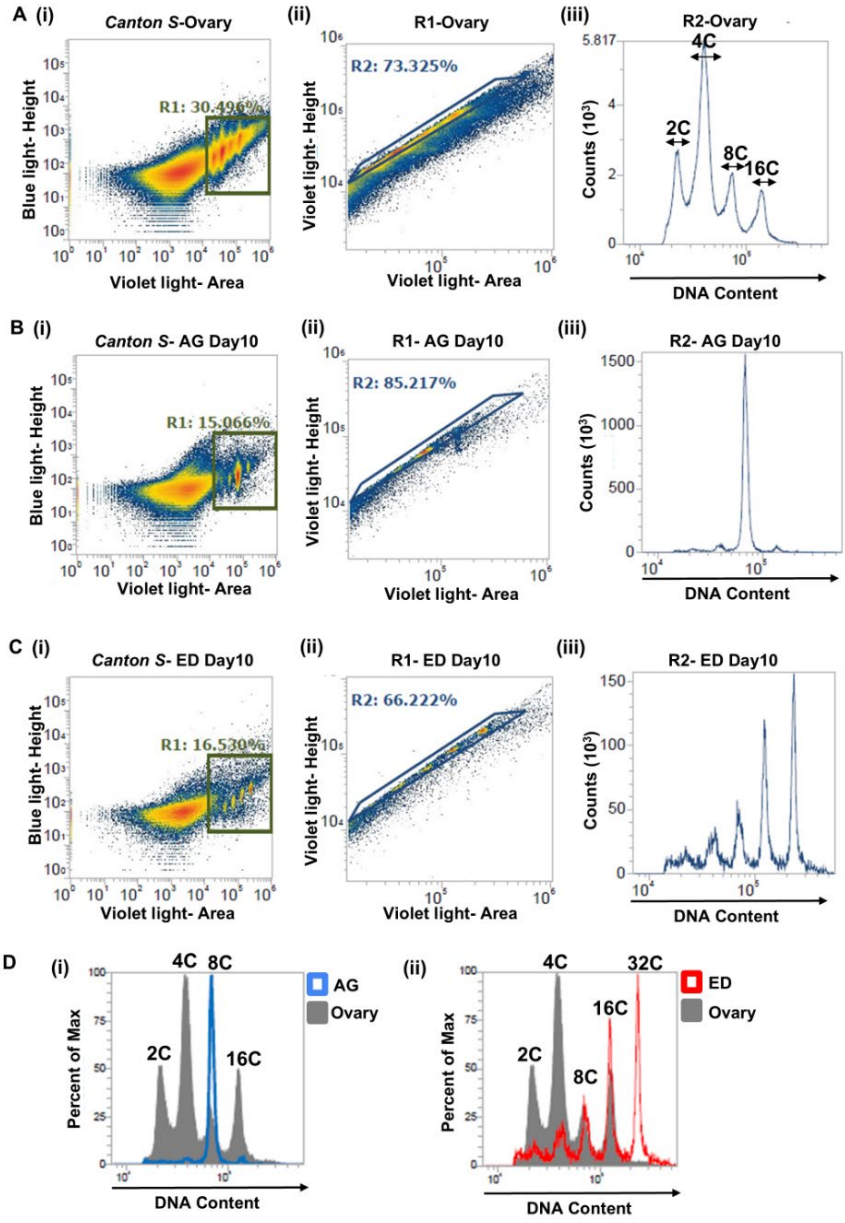


Figure 3.2: Flow cytometry plots of *Drosophila Canton S* Accessory Gland, Ejaculatory Duct and Ovary nuclei

A representative Flow cytometer workspace containing densityt plots and histograms with the same intensity settings for Ovary follicle cells, and Day 10 virgin male AG and ED cells (**A)** (i) Density plot of Ovary Follicle cell nuclei using the Forward scattering (Blue light) Height and area with Gate R1 to exclude doublets and clumps. (ii) Density plot of the R1 gated population resolved using the violet light to separate based on Dye cycle violet staining. (iii) Histogram of the separated populations of follicular cell nuclei in gate R2 using the single parameter to separate the nuclei

with 2C, 4C, 8C, and 16C DNA content. (B) (i)Density plot of AG secretory cell nuclei using the Forward scattering (Blue light) Height and area with Gate R1 to exclude doublets and clumps. (ii) Density plot of the R1 gated population of AG nuclei resolved using the violet light to separate based on Dye cycle violet staining. (iii) Histogram of the separated populations of AG secretory cell nuclei using the single parameter to separate the nuclei with DNA content. (**C)** (i)Density plot of ED secretory cell nuclei using the Forward scattering (Blue light) Height and area with Gate R1 to exclude doublets and clumps. (ii) Density plot of the R1 gated population of ED nuclei resolved using the violet light to separate based on Dye cycle violet staining. (iii) Histogram of the separated populations of ED secretory cell nuclei using the single parameter to separate the nuclei with DNA content. (D) Overlay of Ovary Follicular cell nuclei histogram ploidy peak with the (i) AG secretory cell nuclei ploidy peaks and (ii) ED secretory cell nuclei ploidy peaks.

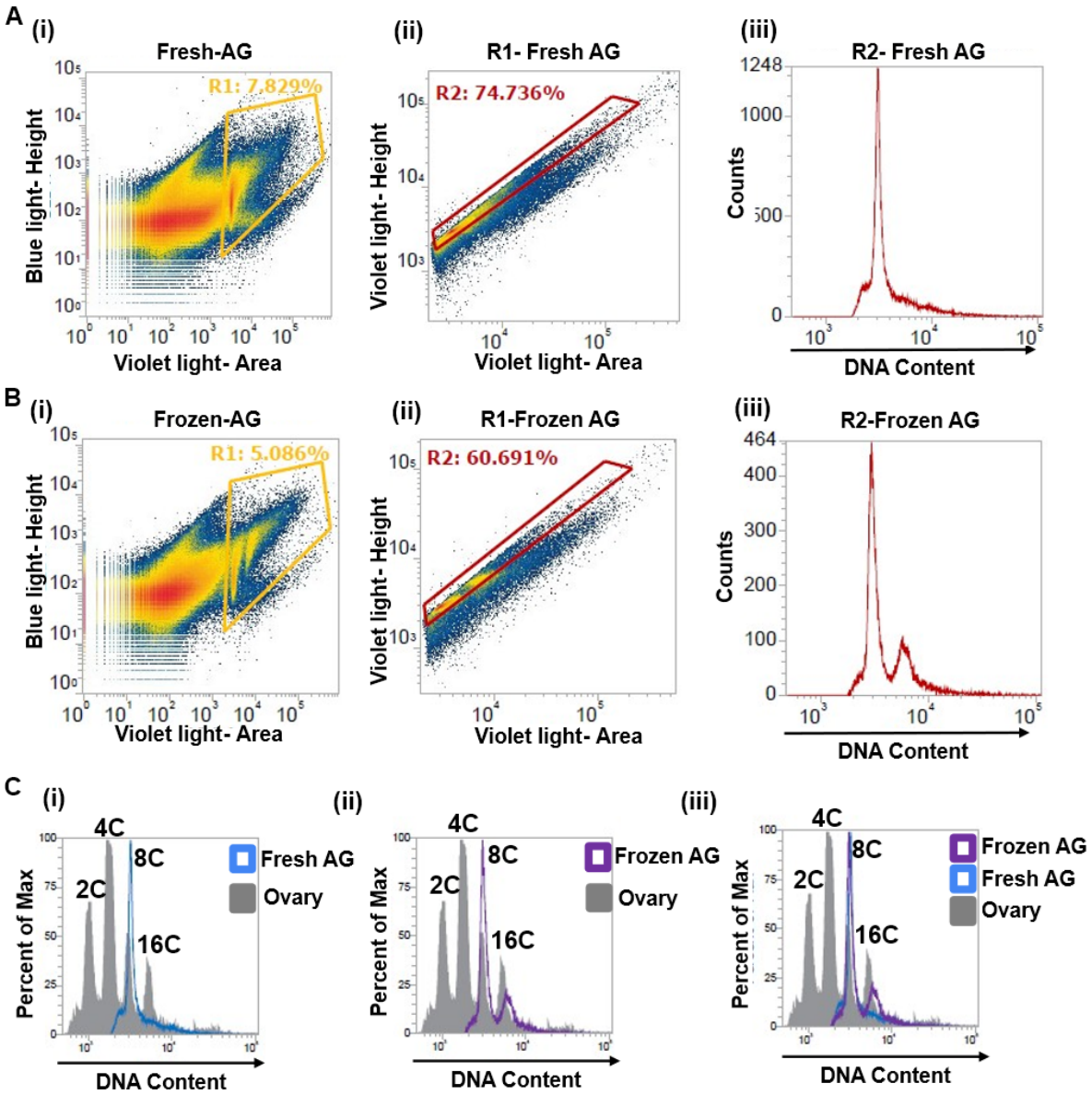


Figure 3.3: Flow cytometry plots of the *Drosophila Canton S* fresh and frozen male Accessory gland polyploid nuclei

(A**)** (i)Density plot of freshly isolated-AG secretory cell nuclei using the Forward scattering (Blue light) Height and area with Gate R1 to exclude doublets and clumps. (ii) Density plot of the R1 gated population of freshly isolated AG nuclei resolved using the violet light to separate based on Dye cycle violet staining. (iii) Histogram of the separated populations of freshly AG secretory cell nuclei using the single parameter to separate the nuclei with DNA content. (B) (i)Density plot of nuclei isolated from AG secretory cell after freezing the AGs using the Forward scattering (Blue light) Height and area with Gate R1 to exclude doublets and

clumps. (ii) Density plot of the R1 gated population of AG nuclei isolated after freezing the AGs resolved using the violet light to separate based on Dye cycle violet staining. (iii) Histogram of the separated populations of AG secretory cell nuclei using the single parameter to separate the nuclei with DNA content.

(C) Overlay of Ovary Follicular cell nuclei histogram ploidy peak with the (i) Fresh AG secretory cell nuclei ploidy peaks and (ii) Frozen AG extracted secretory cell nuclei.

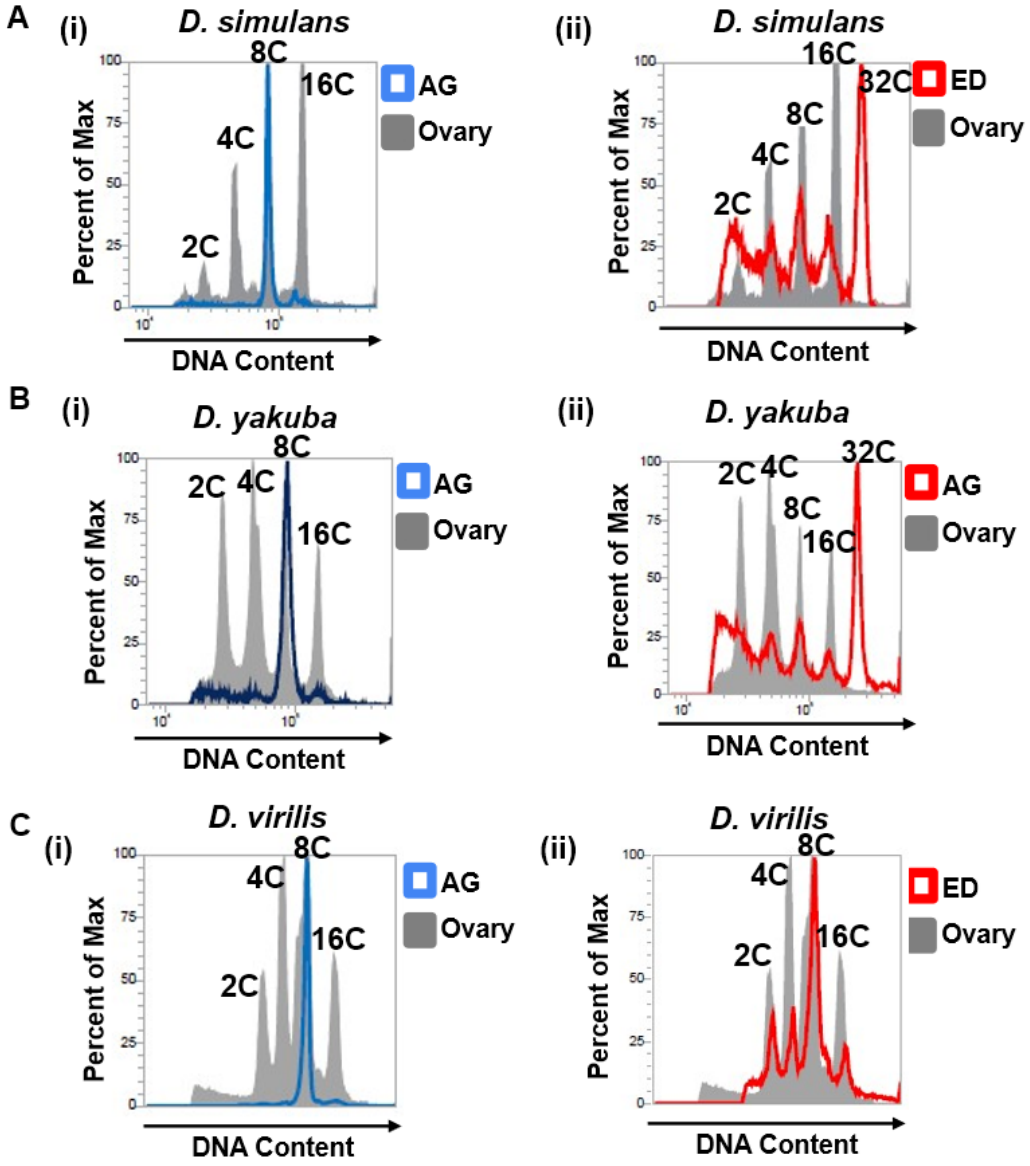


Figure 3.4: Flow cytometry ploidy peaks of different species of *Drosophila* male AG and ED secretory cell nuclei

(A) Flow cytometry histograms of nuclear DNA content of AG secretory cells(i) and ED secretory cells (ii) on Day 10 *D. simulans* overlaid with the Ovary follicle cells. Gray shaded peaks is ovary nuclei of *D. simulans* to assign correct ploidy peaks of AG and ED. (B) Flow cytometry histograms of nuclear DNA content of AG secretory cells(i) and ED secretory cells (ii) on Day 10 *D. yakuba* overlaid with the Ovary follicle cells. Gray shaded peaks is ovary nuclei of *D. yakuba* to assign correct ploidy peaks of AG and ED. (C) Flow cytometry

histograms of nuclear DNA content of ED secretory cells(i) and AG secretory cells (ii) on Day 10 *D. virilis* overlaid with the Ovary follicle cells. Gray shaded peaks is ovary nuclei of *D. virilis* to assign correct ploidy peaks of AG and ED.

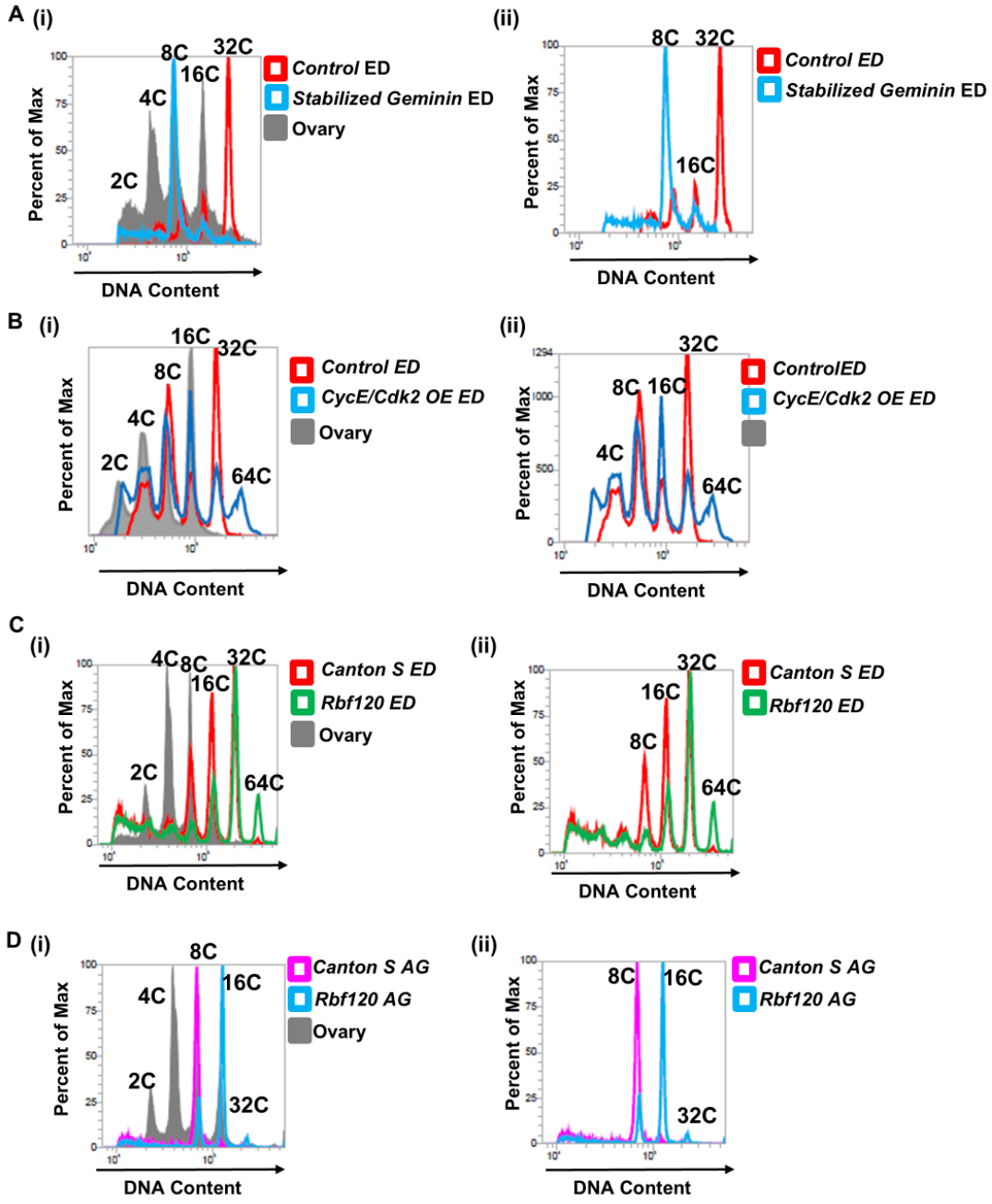


Figure 3.5: Ploidy peaks of AG and ED nuclei under different cell cycle conditions

(A) (i) Flow cytometry histogram of nuclear DNA content of ED secretory cells on Day 10 with stabilized Geminin overexpression vs. control ED and overlaid with the Ovaru follicle cell nuclei. (B) Flow cytometry histogram of nuclear DNA content of ED secretory cells on Day 10 with CycE/Cdk2 overexpression vs. control and overlaid with the Follicle cell nuclei of the ovary. (C) Flow cytometry histogram of nuclear DNA content of ED secretory cells on Day 10

with Rbf 120 hypomorphic mutant RNAi vs. *Canton s* and overlaid with the ovary follicle cell nuclei.(C) Flow cytometry histogram of nuclear DNA content of AG secretory cells on Day 10 with Rbf 120 hypomorphic mutant RNAi vs. *Canton s* and overlaid with the ovary follicle cell nuclei.

Each sample contains at least 25 dissected EDs pooled for nuclear isolation and flow cytometry.

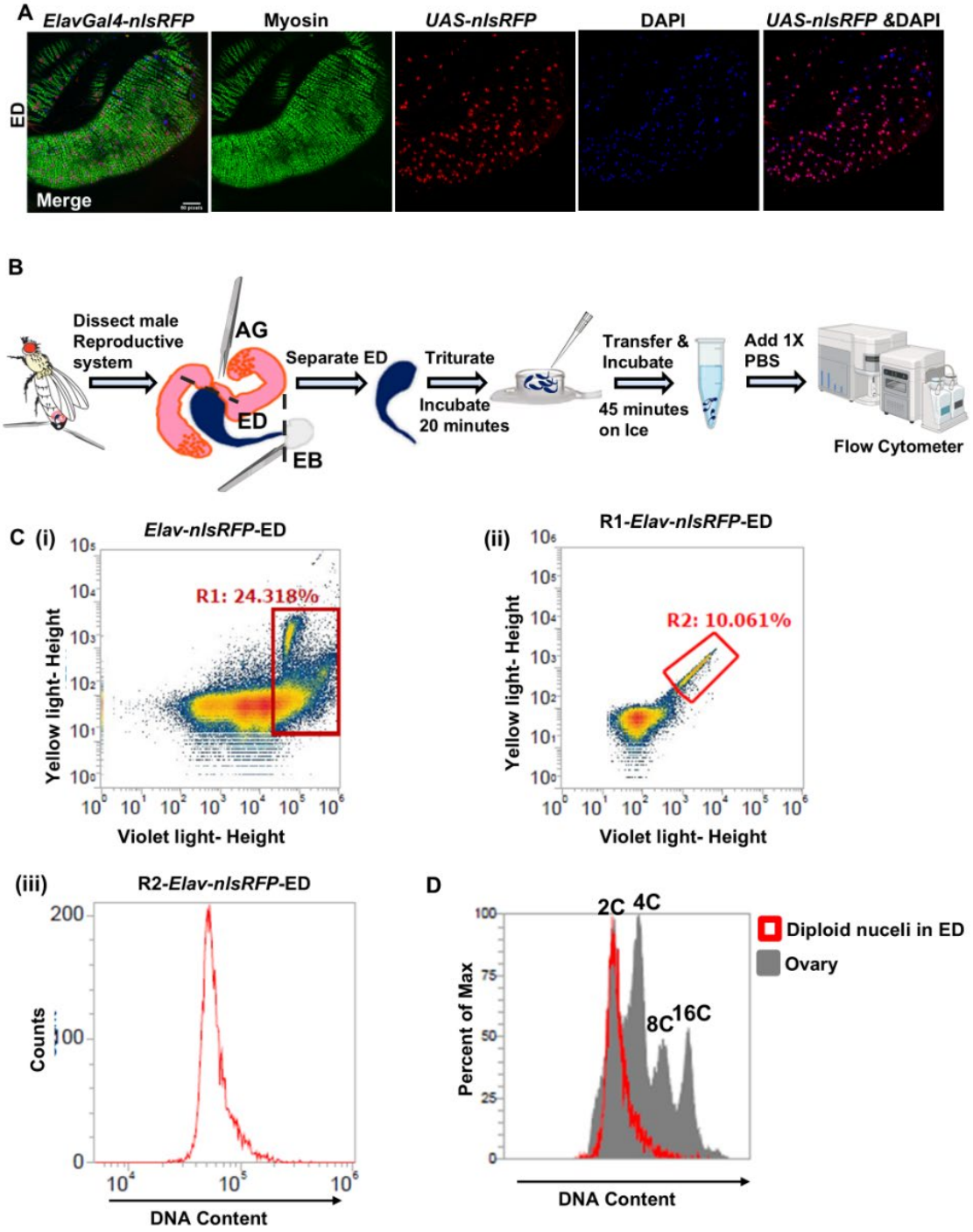


Figure 3.6: Isolation and flow cytometry plots of diploid cell nuclei of ED basement membrane

(A) Confocal micrographs of ED labelled with Elav Gal4 expressing nuclear localization signal (nls) tagged with reporter Red fluorescence protein(RFP) expressing in the innervated muscle cell nuclei which overlaps with the DAPI staining, Muscles are stained with Myosin-Green. (B) Schematic overview of the nuclei isolation and ploidy measurement workflow for the *Drosophila*

ejaculatory duct (ED) basement membrane diploid cell. (C) Separation of the nuclei using Yellow Light-Height (FSC-H) versus Violet Light-Area (FSC-A) plots to exclude doublets with the gating R1 and R2 (i, ii). (iii)Analyzed both both RFP and DyeCycle Violet positive R2 population with a single-parameter histogram, where a single distinct nuclear peak is observed. (iv)Overlay of iii peak with the ovary control peak and confirmed that the RFP and DyeCycle Violet–positive nuclei were diploid.

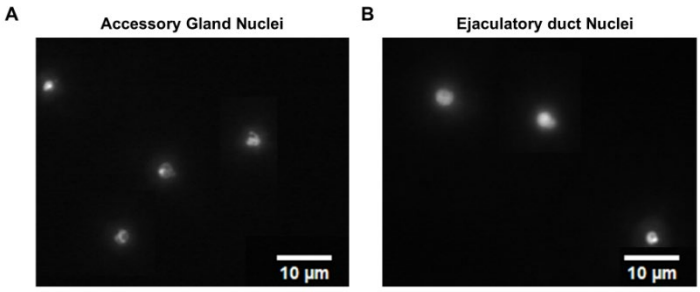


Figure 3.7: Images of isolated individual nuclei

(A) Micrographs of Accessory gland polyploid individual nuclei after nuclear isolation labelled with DAPI. (B) Ejaculatory Duct nuclei after the nuclei isolation from the ED.

3.5 Bibliography

Benjamin M Stormo, Donald T Fox (2016) Distinct responses to reduplicated chromosomes require distinct Mad2 responses. *eLife,* 5:e15204.

Bosco, G., Campbell, P., Leiva-Neto, J. T., & Markow, T. A. (2007). Analysis of Drosophila species genome size and satellite DNA content reveals significant differences among strains as well as between species. *Genetics*, *177*(3), 1277–1290.

Box, A. M., Ramesh, N. A., Nandakumar, S., Church, S. J., Prasad, D., Afrakhteh, A., Taichman, R. S., & Buttitta, L. (2024a). Cell cycle variants during *Drosophila* male accessory gland development. *G3: Genes, Genomes, Genetics*.

Box, A. M., Ramesh, N. A., Nandakumar, S., Church, S. J., Prasad, D., Afrakhteh, A., Taichman, R. S., & Buttitta, L. (2024b). Cell cycle variants during Drosophila male accessory gland development. *G3: Genes, Genomes, Genetics*, *14*(7).

Buttitta, L. A., Katzaroff, A. J., Perez, C. L., de la Cruz, A., & Edgar, B. A. (2007). A Double-Assurance Mechanism Controls Cell Cycle Exit upon Terminal Differentiation in Drosophila. *Developmental Cell*, *12*(4), 631–643.

Church, S. J., Pulianmackal, A. J., Dixon, J. A., Loftus, L. V., Amend, S. R., Pienta, K., Cackowski, F. C., & Buttitta, L. A. (2025). Oncogenic signaling in the Drosophila prostate-like accessory gland activates a pro-tumorigenic program in the absence of proliferation. *DMM Disease Models and Mechanisms*, *18*(4).

Cohen, E., & Moussian, B. (2016). Extracellular composite matrices in arthropods. In *Extracellular Composite Matrices in Arthropods*. Springer International Publishing.

Diffley, J. F. X. (2004). Regulation of early events in chromosome replication. In *Current Biology* (Vol. 14, Issue 18).

Edgar, B. A., & Orr-Weaver, T. L. (2001). Endoreplication Cell Cycles: Review More for Less. In *Cell* (Vol. 105).

Fox, D. T., & Duronio, R. J. (2013). Endoreplication and polyploidy: Insights into development and disease. *Development (Cambridge)*, *140*(1), 3–12.

Hopkins, B. R., Sepil, I., Bonham, S., Miller, T., Charles, P. D., Fischer, R., Kessler, B. M., Wilson, C., & Wigby, S. (2019). *BMP signaling inhibition in Drosophila secondary cells remodels the seminal proteome and self and rival ejaculate functions*.

Lee, H. O., Davidson, J. M., & Duronio, R. J. (2009). Endoreplication: Polyploidy with purpose. In *Genes and Development* (Vol. 23, Issue 21, pp. 2461–2477).

Lilly, M. A., & Duronio, R. J. (2005). New insights into cell cycle control from the Drosophila endocycle. In *Oncogene* (Vol. 24, Issue 17, pp. 2765–2775).

Lilly, M. A., & Spradling, A. C. (1996). *The Drosophila endocycle is controlled by Cy.clin E and lacks a checkpoint ensuring S-phase completion*.

Lung, O., Kuo, L., & Wolfner, M. F. (2001). Drosophila males transfer antibacterial proteins from their accessory gland and ejaculatory duct to their mates. In *Journal of Insect Physiology* (Vol. 47).

Quinn, L. M., Herr, A., McGarry, T. J., & Richardson, H. (2001). The Drosophila Geminin homolog: Roles for Geminin in limiting DNA replication, in anaphase and in neurogenesis. *Genes and Development*, *15*(20), 2741–2754.

Ramesh, N. A., Box, A. M., & Buttitta, L. A. (2025b). Post-eclosion growth in the Drosophila ejaculatory duct is driven by Juvenile hormone signaling and is essential for male fertility. *Developmental Biology*, *519*, 122–141.

Sturm, S., Dowle, A., Audsley, N., & Isaac, R. E. (2021). Mass spectrometric characterisation of the major peptides of the male ejaculatory duct, including a glycopeptide with an unusual zwitterionic glycosylation. *Journal of Proteomics*, *246*.

Susic-Jung, L., Hornbruch-Freitag, C., Kuckwa, J., Rexer, K. H., Lammel, U., & Renkawitz-Pohl, R. (2012). Multinucleated smooth muscles and mononucleated as well as multinucleated striated muscles develop during establishment of the male reproductive organs of Drosophila melanogaster. *Developmental Biology*, *370*(1), 86–97.

Takemori, N., & Yamamoto, M. T. (2009). Proteome mapping of the Drosophila melanogaster male reproductive system. *Proteomics*, *9*(9), 2484–2493.

Wu, C.-S., Lu, W.-H., Hung, M.-C., Huang, Y.-S., & Chao, H.-W. (2022). *From polyploidy to polyploidy reversal: its role in normal and disease states*.

Zielke, N., Querings, S., Rottig, C., Lehner, C., & Sprenger, F. (2008). The anaphase-promoting complex/cyclosome (APC/C) is required for rereplication control in endoreplication cycles. *Genes and Development*, *22*(12), 1690–1703.

Chapter 4 A Window of Cell Cycle Plasticity Enables Imperfect Regeneration of an Adult Postmitotic Organ in *Drosophila*

4.1 Abstract

The *Drosophila* ejaculatory duct (ED) is a secretory tissue of the male somatic reproductive system responsible for producing components of the seminal fluid which support fertility, serve antimicrobial functions and influence the physiological changes in the female after mating. The ED is a simple organ made up of secretory epithelial cells that are encased by extracellular matrix and a layer of innervated contractile muscle. These secretory cells are post-mitotic and lack known stem cells or progenitors in the adult, but they are not fully quiescent, as they undergo a variant cell cycle called endoreplication immediately post-eclosion to increase organ size and protein synthesis capacity. Polyploid and post-mitotic tissues often face unique challenges in response to cell loss due to their inability to proliferate. Here, we show that the adult ED is capable of significant recovery after cell loss due to a combination of increased nuclear and cellular hypertrophy that partially restores tissue mass and organ function. The early cell cycle plasticity of this adult tissue is critical for this recovery, as older tissues that have few or no endocycles exhibit reduced capacity for recovery after cell loss. Together, our findings establish the *Drosophila* ED as a model to study post-mitotic polyploid tissue repair and highlight a combination of endocycles and hypertrophy as a key mechanism for functional regeneration in the absence of mitosis.

4.2 Introduction

The *Drosophila* male ejaculatory duct (ED) serves as a conduit for mixing sperm from the testes, seminal fluid from the seminal vesicles, and secretions from the accessory glands prior to transfer to the female via the ejaculatory bulb. In addition to its transport function, the ED itself is a

secretory organ, producing a substantial number of seminal fluid proteins (SFPs) (Imamura et al., 1998; Lung et al., 2001; Richmond et al., 1980). Of approximately 138 peptides identified from the ED, at least 63 have been classified as SFPs (Sturm et al., 2021; Takemori and Yamamoto, 2009). Among the secreted molecules are antimicrobial peptides such as Andropin and Cecropin A1, which are thought to prevent microbial infections and enhance fertility (Date-Ito et al., 2002; Lung et al., 2001). Other ED-derived peptides are involved in a range of reproductive functions, including sperm storage, cell metabolism, lipid modifications, and female post-mating responses potentially influencing sperm storage and other reproductive outcomes (Takemori and Yamamoto, 2009). Anatomically, the ED is composed of a basal muscular layer innervated by neurons and an apical layer of large, polyploid secretory cells (Ramesh et al., 2025; Susic-Jung et al., 2012). These secretory cells are the primary source of ED-derived fertility factors which are released into an apical lumen where mixing with other reproductive tract fluids takes place.

ED secretory cells of the newly eclosed adult are post-mitotic, but not fully quiescent (Ramesh et al., 2025). Hours after eclosion, secretory cells of the ED undergo a variant cell cycle known as endocycling (Edgar et al., 2014). In this process, cells alternate between G1 and S phases without undergoing mitosis, resulting in polyploid mononuclear cells with DNA contents ranging from 8C to 32C (Ramesh et al., 2025). The post eclosion endocycles are essential in the secretory cells for post-eclosion growth of the ED and full male fertility (Ramesh et al., 2025). The endocycling activity of the secretory ED cells slows after 48-72h and fully ceases by Day 4 post-eclosion, after which the cells remain fully quiescent. This tissue contains no known stem or progenitor cell population and thus is thought to have very limited to no regenerative capability.

Many tissues respond to stress-induced apoptosis by initiating regenerative programs to restore tissue mass and function. In mitotically active tissues, this typically involves compensatory cellular proliferation (CCP), where either resident stem cells or surrounding progenitor cells divide to replace the lost cells (de Morree and Rando, 2023; Xia et al., 2018). However, largely post-mitotic tissues such as the heart, kidneys, cornea, bladder, and brain are mostly composed of cells that have permanently exited the cell cycle during development and possess relatively few or no regenerative stem cell populations (Lavecchia et al., 2022; Losick, 2016; Shu et al., 2018). Understanding how these largely post-mitotic tissues respond to injury, to maintain structural integrity and partially restore function remains a major challenge in regenerative biology.

Here, we show that the secretory cells of the young adult male ED retain a surprising capacity to restore tissue morphological integrity and recover fertility function after genetically-driven partial organ ablation. In response to cell loss, the window for endocycling in the ED is extended temporarily, providing an opportunity for postmitotic polyploid cells to restore tissue mass in part through compensatory endocycles. As the tissue matures and cell cycle plasticity is lost, the regenerative capacity of this tissues declines, suggesting that the regulators of endocycle exit and entry into quiescence limit this organ's recovery after damage. We propose the ED can be a genetically tractable model to study postmitotic regeneration and cell cycle plasticity in a terminally differentiated adult tissue.

4.3 Results & Discussion

4.3.1 Apoptotic cell loss in the ED occurs through apical extrusion and leads to irreversible cell loss.

Secretory cells of the ejaculatory duct (ED) play an important role in the growth and development of the ED. These cells are post-mitotic and polyploid, with ploidy levels ranging from 8-32C. Although these cells are post-mitotic and no longer divide prior to eclosion, in newly eclosed males they undergo a variant cell cycle called endoreplication, in which they replicate their DNA without entering mitosis, thereby increasing cellular ploidy. We previously showed that post-eclosion endocycles in this tissue are essential for full male fertility (Ramesh et al., 2025). However direct studies of secretory cell loss in the ED have not been performed. We genetically ablated all the secretory cells of the adult ED by expressing the IAP antagonist *Reaper* in these cells to trigger caspase-mediated programmed cell death (Ryoo et al., 2002; Sandu et al., 2010). We used an ED-secretory cell specific *Luna-Gal4,* to induce Reaper-mediated cell death in secretory cells (Figure 1A).

When we expressed the pro-apoptotic gene *Reaper* in the ED, we observed secretory cells with pyknotic nuclei, indicating that the cells were undergoing apoptosis-induced cell death, as shown in Figure 1B with DAPI staining. To validate the expression of Gal4 in secretory cells, we expressed a transgenic reporter, RFP tagged with a nuclear localization signal (*UAS-nls-RFP*), as shown in Figure 1B, Figure 5A. Upon *Reaper* expression, the nls-RFP signal was degraded due to apoptosis. In this condition, we observed disruption of epithelial cell-cell contacts, such as septate

junctions labeled with Fasciclin III (Fas III). Following nearly complete ablation of secretory cells, only muscle/neuronal nuclei, which were Elav-positive, remained in the ED (Figure 5A).

The ejaculatory duct (ED) is basally surrounded by an innervated muscle sheath, with the monolayer of large, polyploid secretory cells forming an apical fluid-filled lumen. We observed that, upon *Reaper* expression, secretory cells undergo apical extrusion, with apoptotic cells being eliminated into the lumen (Figure 1C). The images in Figure 1C show single Z-sections through the lumen, confirming apical extrusion in *UAS-Reaper* samples, compared to control samples where the lumen remains empty. These apoptotic cells are further expelled through the ejaculatory bulb, as shown in Figure 5 B. Despite the loss of most secretory cells, the external basal muscle layer remained largely unaffected, as confirmed by Myosin staining (Figure 5C). However, complete loss of secretory cells led to noticeable organ shrinkage, resulting in a significantly reduced ED area in *UAS-Reaper* samples compared to controls (Figure 1D). That ED secretory cells are essential for the early growth and development of the organ from the day of eclosion (DOE) to 10 days post-eclosion. Consistent with this, the quantification of ED area following secretory cell ablation showed a significant reduction at both DOE and day 10, indicating a loss of the secretory epithelium leads compromises ED growth during this period (Figure 1E). To determine whether epithelial cell loss triggered proliferation or cell cycles within the diploid cells of the muscle layer or adjacent non-Luna Gal4 expressing tissues, such as the diploid anterior ED papillae, we fed the animals 5-Ethynyl-2′-deoxyuridine (EdU) to label S-phases and stained for phospho-Histone H3 (PH3 Ser10) to visualize mitotic activity. We observed no evidence of cell cycles in the muscle layer or nearby ED papillae in response to the loss of the secretory cells (Figure 1F). We also did not observe any evidence of multinucleated cells that would result from cell fusion.

Our previous study revealed that disrupting post-eclosion endoreplication in ED secretory cells led to reduced fertility and fewer offspring (Ramesh et al., 2025). In line with this, nearly complete ablation of secretory cells severely affects fertility. In individual male fertility assays with 5-day-old males and *Canton-S* virgin females at a male-to-female ratio of 1:8, males with ED secretory cells expressing *UAS-Reaper* were near-sterile or completely sterile (Figure 1G). We confirmed that males expressing *UAS-Reaper* performed mating behaviors and mating attempts at the same frequency and rate as control males without tissue damage.

At the conclusion of the fertility assay, we dissected the EDs and observed that sperm becomes entrapped within the lumen when the secretory layer is severely disrupted. This contrasts with mating males without *UAS-Reaper*, where retained sperm is very rarely observed in the duct (Figure 5D). Together with the quantification of offspring, these findings strongly support that ED secretory cells are essential for male fertility. It is likely that these cells secrete factors required for the effective transfer of sperm, seminal fluid proteins, and other peptides to the female reproductive tract. Overall, these results reinforce the essential role of the ED as a key functional component of the *Drosophila* male reproductive system.

4.3.2 Recovery from transient damage in the anterior region of the Ejaculatory Duct

To investigate whether the secretory epithelium can recover following transient damage, we employed a conditional approach using the *Gal4/UAS-Reaper* system in combination with a temperature-sensitive *Gal80* repressor (*Gal80^{ts}*). At a lower temperature (18 °C), Gal80 is active and represses Gal4-mediated transcription (Figure 2A). However, at higher temperatures (25–29°C), Gal80^{ts} becomes inactive, allowing Gal4 to drive transgene expression (McGuire et al., 2004). To validate the *Gal80^{ts}* system with the ED driver, we raised flies carrying *Luna-Gal4, UAS-nls-RFP*, and *Gal80^{ts}* at 18 °C. At this temperature, *Gal80^{ts}* repressed Gal4, and no *nls-RFP* expression was detected. Upon shifting the flies to 29 °C, we observed robust *nls-RFP* expression in the ED (Figure 6A), indicating activation of *Gal4* due to *Gal80^{ts}* inactivation. To determine how quickly Gal4 activity is repressed after returning to 18 °C, we used a *destabilized GFP (dsGFP)* reporter, which is rapidly degraded in the absence of *Gal4* activity, providing a readout of transient gene expression. Flies expressing *Luna-Gal4, UAS-dsGFP*, and *UAS-Reaper* were maintained at 18 °C and showed no GFP signal. After shifting to 29 °C, GFP expression appeared in the anterior region of the ED after 32 hours, with no expression in the posterior ED. We then shifted the animals back to 18 °C to assess the time required for Gal4 repression following *Gal80^{ts}* reactivation. We observed that within 24 hours, GFP fluorescence was completely lost, indicating detectable repression of Gal4 and degradation of *dsGFP* (Figure 6B).

Based on our initial observations using the *Gal4/Gal80^{ts}* system with *dsGFP* and *nls-RFP* reporters, we chose to shift *Luna-Gal4/UAS-ReaperGal80^{ts}* animals from 18 °C to 29 °C on the day of eclosion (DOE) for 32 hours to induce transient damage (Figure 2A). As the ED is a post-mitotic tissue with secretory cells that undergo endoreplication for the first 2 days post-eclosion,

we chose to induce damage on the day of eclosion, during the window of endogenous endoreplication. Upon activation of *Reaper*, we observed caspase-induced apoptosis in cells located in the anterior ED, marked by the presence of multiple pyknotic nuclei labeled with DAPI (Figure 2B). In contrast, no pyknotic nuclei were observed in the posterior region within 32h of *Reaper* induction (Figure 6D), indicating region-specific ablation. We observed a similar pattern with an antibody against cleaved Death caspase-1 (DCP-1), which marks cells undergoing proteolytic cleavage during apoptosis (Figure 6D) as well as a *Drice*-Based Sensor GFP (*DBS-GFP*) which is a read-out for caspase-mediated cleavage of substrates (Baena-Lopez et al., 2018) (Figure 6C, 6E). The anterior ED contains larger secretory cells with higher ploidy levels of 16-32C, while the middle and posterior ED contain smaller secretory cells with lower ploidies of 8-4C. We speculate that the increased Gal4 copy number and expression level in the anterior ED preferentially induces apoptosis with this limited activation window.

Using this damage paradigm, we observed that 100% of animals exhibited loss of secretory cells in the anterior region of the ejaculatory duct (Figure 6F). We also confirmed that cell loss could be completely suppressed by co-expression of the baculoviral apoptosis inhibitor *UAS-P35* with *UAS-Reaper* (Hay et al., 1994). Interestingly, organs co-expressing *UAS-P35* with *UAS-Reaper* appeared indistinguishable from control animals without Reaper, suggesting that apoptosis-induced proliferation does not take place in this tissue (Figure 7) (Perez-Garijo et al., 2004; Perez-Garijo et al., 2009). Thus, our system efficiently induces partial ablation of the ED through cell loss via caspase-induced apoptosis.

After inducing *UAS-Reaper*, we shifted the animals back to 18 °C to repress *Reaper* expression via $Gal80^{ts}$ and maintained them at this temperature for 10 days to observe tissue response to damage (Figure 2A). Remarkably, we observed substantial recovery of the ED 10 days post-ablation. Cells were no longer DCP1-positive, consistent with the resolution of apoptosis (Figure 2C and Figure 6E). We next quantified the area of the ED following damage and recovery. We measured the overall area of the ED for a subset of animals immediately after Reaper-induced damage and found it to be significantly reduced compared to controls (Figure 2D, 2E). In the animals after a 10-day recovery without Reaper expression, we observed near-normal tissue size (Figure 2D). As our damage paradigm induces cell and tissue loss in 100% of animals, we interpret

this to be evidence of significant restoration of both organ mass and epithelial integrity in this postmitotic and terminally differentiated tissue (Figure 2E).

4.3.3 The ED undergoes compensatory cellular hypertrophy (CCH) in response to cell loss.

The loss of anterior secretory cells led to organ shrinkage during the damage phase. To assess whether this affected the basally located muscle layer, we labeled the tissue with Phalloidin to visualize F-actin filaments. We observed no breach or disruption of the muscle fibers following secretory cell loss (Figure 2F). By contrast, epithelial septate junctions visualized using Fas III staining, were severely disrupted immediately after damage (Figure 2F). After 10 days of recovery at 18 °C septate junctions were restored and appeared normal (Figure 2G).

While we observe cell loss and cell death in 100% of animals immediately after damage, the degree of cell loss is variable. In cases where cell loss was mild, we observed enlarged epithelial cells with normal or near normal nuclear sizes, suggestive of cellular growth without increased ploidy. However in cases where many secretory cells were lost, the remaining cells appeared to undergo compensatory cellular hypertrophy (CCH) with enlarged nuclei, indicative of an increase in cellular ploidy (Tamori and Deng, 2013; Tamori and Deng, 2014) (Figure 2G). We quantified recovery by measuring cell size, nuclear area, and the total number of cells/nuclei in the ED immediately after damage and after 10 days of recovery (Figure 3). For each ED, we quantified at least 20 secretory cells and plotted the individual cell size distributions across conditions. When we plotted the average cell size per ED, we found that the mean cell size was significantly larger post-recovery compared to controls (Figure 3A). Notably, three EDs post-recovery showed secretory cell sizes approximately three times larger than those observed in both control and post-damage conditions. The nuclear area was also significantly larger in both damaged and 10-day post-recovery EDs compared to controls (Figure 3B). Thus, the secretory cells of the ED are capable of significant growth after mild cell loss in addition to compensatory cellular hypertrophy (CCH) in response to severe cell loss to restore lost tissue mass.

To quantify the ploidy/DNA content of the cells in the anterior region, we measured the integrated DAPI intensity from the polyploid nuclei of secretory cells, normalized to diploid cells of the innervated muscle layer within the same tissue. We observed that the ploidy of the ED immediately post-damage was significantly reduced compared to controls (Figure 3C), consistent with loss of the anterior-most, highest ploidy ED cells. This resulted in an increased number of 8C and 16C

cells in the anterior region immediately post-damage (compared to 32C in controls). By contrast, after 10 days of recovery at 18°C, we found that cellular ploidies in the anterior region were nearly fully restored (Figure 3G), with the reappearance of many 32C cells in the anterior ED. We confirmed these results using flow cytometry, showing the loss of the highest ploidy cells immediately after damage with substantial restoration of 32C cells after recovery (Figure 3D, 3H). Notably the effect on ploidy in the flow cytometry assay is muted compared to the imaging quantifications because the flow assay uses nuclei isolated from the entire duct, while our imaging ploidy measurements reveal differences that are specific to the anterior region of the ED, where the most severe cell loss occurs. As a whole, these findings support that an increase in cellular ploidy accompanies the observed CCH following damage and recovery.

To visualize DNA synthesis during CCH, we fed the animals EdU immediately after the 32-hour damage period and throughout the timepoints of recovery. Tissues were dissected at Day 2, Day 5, and Day 10 of recovery and stained for both EdU and phospho-Histone H3 (PH3 Ser10) to visualize DNA synthesis and detect any mitotic activity, respectively. At Day 5, we observed numerous EdU-positive cells, indicating active endocycling in the recovering ED (Figure 3E, middle panel). However, no PH3-positive cells were detected throughout the secretory and muscle layers of the ED. Control EDs (Figure 3E, top panel) showed no EdU-positive cells, consistent with our prior observations that the tissue exits endocycling by Day 3 post-eclosion under normal conditions (Ramesh et al., 2025). As a positive control for mitotic staining within each sample, we included *Drosophila* larval imaginal discs, which undergo robust mitotic proliferation and showed strong PH3 staining (Figure 3E, Figure 8B). By Day 5, despite significant endocycling, the anterior ED remained smaller than controls, but by Day 10, the ED tissue mass was fully restored with significant EdU labeling and no evidence of mitoses.

Our EdU labeling time course indicates that most endoreplication likely occurs between Days 2 - 4 of recovery (Figure 3F). This is equivalent to ~72-96 hours post-eclosion without damage, a time when the ED has normally exited the endocycle and is fully quiescent (Ramesh et al., 2025). This suggests that following secretory cell ablation during the post-eclosion endocycle, the remaining ED cells extend their endocycling window to complete additional damage-induced endocycles as

a compensatory mechanism. Following the compensatory endoreplication, the tissue eventually regains mass through increased cell growth.

To test whether secretory cell restoration in the ED could originate from other cell types in or near the ED, we performed G-TRACE labeling after induced damage using the *Luna-Gal*4 driver. G-TRACE (Gal4 Technique for Real-time and Clonal Expression) enables visualization of both real-time (RFP) and permanent Gal4-lineage driven expression (GFP) (Evans et al., 2009). The *Luna-Gal4* driver used here is specific to the secretory cells of the ED in the male reproductive system and is active in the ED secretory cells from 1 day prior to eclosion throughout adulthood (Ramesh et al., 2025). We reasoned that if *Luna-Gal4* negative cells, possibly from the muscle layer or other nearby cell types, contribute to ED restoration through differentiation into the ED fate and subsequently turn on *Luna-Gal4* expression only after damage, their window of Gal4 expression prior to $Gal80^{TS}$ restoration would be very brief, resulting in temporally delayed and therefore limited expression of RFP (and possibly GFP) compared to resident ED cells that experience Gal4 activity immediately following the temperature-dependent inactivation of Gal80. This would be expected to result in much weaker expression of RFP, or possibly RFP "current" positivity without GFP "past" expression immediately after damage in non-resident derived cells. When we express G-TRACE under the control of *Luna-Gal4* with or without *UAS-Reaper*, we observe that all secretory cells in the ED co-express both GFP and RFP, immediately after damage (Figure 8E). This suggests that no new or alternative cell types contribute to the secretory cell population during damage. To validate this during the recovery phase, we analyzed tissues 10 days post-damage and again, found no weakly expressing or GFP-/RFP- cells, indicating that all remaining secretory cells originated from the pre-existing Gal4-positive lineage (Figure 8E). These findings strongly suggest that tissue mass recovery occurs exclusively within the Luna-Gal4-expressing lineage of differentiated secretory cells, without the involvement of stem or progenitor cells.

Perfect regeneration restores tissue mass, patterning, composition and function after cell loss, while tissues with few or no progenitors or stem cells may undergo "imperfect" regenerative mechanisms which may fail to restore cell numbers and tissue pattern, but can aid in restoring tissue or organ function as occurs in the mammalian liver (Cordero-Espinoza and Huch, 2018) . To test whether the CCH we observe in the ED restores male fertility, we performed fertility assays

on males during damage as well as after recovery. In brief, we crossed males expressing *UAS-Reaper* to Canton-S virgin females at a male-to-female ratio of 1:8, either at 29 °C to sustain Reaper-induced damage during mating or after 10 days of recovery at 18 °C. Males with damaged EDs produced significantly fewer offspring compared to controls (Figure 3I), and we observed sperm trapped within damaged EDs, indicating that the damaged organ was unable to function (Figure 8C).

By contrast, recovered males showed significantly improved fertility (Figure 4D) and lacked sperm entrapped within the ED lumen, indicating that the tissue had recovered function. Thus, the post-mitotic ED is capable of partial functional regeneration following transient loss of anterior secretory cells.

4.3.4 Cell cycle plasticity is required for ED regeneration.

Thus far, our damage induction paradigm begins killing secretory ED cells on the day of eclosion, when these cells are still actively undergoing endocycling. However, this window of cell cycle plasticity closes by 48-72h post eclosion, when nearly all secretory ED cells exit the endocycle and become quiescent. To test whether active endocycling is required for ED recovery after damage, we induced ED cell death on Day 3 post-eclosion by shifting the males to 29 °C for 32 hours to activate Reaper expression (Figure 4A). We observed ablation of secretory cells from the anterior ED, with noticeable shrinkage of the anterior region compared to controls (Figure 4B). This loss of cells also disrupted epithelial cell-cell junctions, as indicated by Fas III staining. We then shifted the damaged males back to 18 °C for 10 days to allow for recovery. However, the tissue was unable to exhibit the level of recovery we observed when damage was induced on the day of eclosion. The anterior ED remained smaller, and although some compensatory cellular hypertrophy (CCH) was observed, cell junctions were not fully restored (Figure 4C). Even after 10 days, the tissue remained small, with obvious loss of tissue mass. We saw no significant difference in cell size or recovery of cell density after 10 days of recovery (Figure 4E, 4F).

To test the endocycling response to damage at this later stage of adulthood, we fed EdU to males immediately after damage induction on Day 3, and allowed them to recover at 18 °C for 10 days. Tissues were then dissected on Day 10 post-recovery. We observed a higher number of EdU-positive cells in the Reaper group compared to controls (Figure 4G). However, the number of EdU-positive cells in response to damage induced on day 3 was substantially lower than that observed

after damage on the day of eclosion. This suggests that the limited window of endocycling on day 3 may limit tissue recovery. Consistent with this, we observed a loss of higher-ploidy (32C) cells immediately after damage (Figure 4H), and these high-ploidy cells did not recover even after 10 days (Figure 4I). Together, these results highlight that the early endoreplication window is likely to be essential for the regenerative capacity of post-mitotic ED secretory cells following transient damage.

We previously showed that morphology of the ED correlates with cellular ploidy, such that the largest volume region in the anterior ED contains the highest ploidy cells, while the thinner posterior region contains cells of lower ploidy (Ramesh et al., 2025). Our observation that the highest ploidy cells in the anterior are preferentially eliminated by UAS-Reaper expression and are restored by compensatory cellular hypertrophy of more posterior cells through additional endocycling suggests this process accompanies significant organ remodeling. Consistent with organ remodeling after damage, we see induction of MMP1 secretion, which is resolved by 10 days of recovery (Figure 9). Other examples of compensatory cellular hypertrophy are triggered by a local alteration of tissue tension and function by accelerating the endocycle which then completes on time (Tamori and Deng, 2013). Instead, our data in the adult ED suggests this organ responds to a threshold level of cell loss to prolong the window of cell cycle plasticity to enable CCH to improve regenerative capacity. Future work will be needed to understand the signaling pathways that determine the window of cell cycle plasticity in the newly eclosed adult ED and how cell loss and damage extends this window.

4.4 Materials and methods

4.4.1 Drosophila husbandry

All the flies for constitutive Reaper expression for experiments in Figure 1 and Figure 5 were housed at room temperature (23°C) on a Bloomington Cornmeal food recipe without crowding (<50 animals per vial). For the damage and recovery paradigm with $Gal80^{ts}$, flies were housed at 18°C in the same media and shifted to 29°C for 32hrs for the activation of UAS-Reaper and shifted back to 18°C for the recovery. All the male flies used in all the experiments are virgins except for fertility assays. We used the fly lines Luna-Gal4 (BDSC#63746), UAS-Reaper (BDSC#5824),

Luna-Gal4 recombined with UAS-*nlsRFP* (BDSC#8546), UAS- Destabilized GFP (provided by D. McKay Lab, UNC Chapel Hill), GTRACE (BDSC#28280) and *Tubulin*-Gal80^{ts} (BDSC#7017).

4.4.2 ED dissection, fixation, and Immunostaining

Drosophila male EDs were dissected in 1X Phosphate buffered Saline (PBS), the dissected EDs were immediately transferred to an Eppendorf containing 1ml of 4% Paraformaldehyde (PFA) in 1X PBS to fix the tissues for 30 minutes under continuous rocking. Fixed EDs were rinsed twice using 0.1% Triton-X +1× PBS for 10 minutes each wash. Fixed EDs were permeabilized with 1% Triton-X+1X PBS for 30 minutes on a rocker. Permeabilized tissues were blocked with PAT (1X PBS, 0.1% Triton X-100, 1% BSA) for 10 min. Tissues were resuspended in primary antibody freshly diluted in PAT at an appropriate concentration (below) and incubated overnight at 4ºC on a rocker. Tissues were then washed these tissues with 1XPBS 0.1% Triton X-100, 3 times 10 min. prior to incubation with secondary antibody in PBS-T (1× PBS + 0.1% bovine serum albumin + 0.3% Triton-X (PBT)-X, + 2% Normal Goat Serum (NGS)) for 4h at room temperature. Secondary antibodies were diluted to 1:2000. EDs were washed thrice with 1X PBS 0.1% Triton-X after the secondary antibody incubation for 10 minutes each wash. For actin staining we added 2 drops of Actin Red 555 in 1ml of PBS and incubated the EDs for 30 mins and washed twice with 10 mins each wash to remove unbound stain and incubated the EDs in DAPI 1µg/ml for 15 minutes to stain the DNA. EDs were washed with 1× PBS + 0.1% Triton-X after the DAPI staining and mounted in vectashield (Vector Labs). Tissues were mounted by creating a spacer between the slides and coverslip with double-sided tape or one layer of clear nail polish. The list of antibodies used is in the following table with their dilutions.

Table 4.1 Antibody and the dilutions used

Antibody	**Source**	**Catalog numbers**	**Dilutions Used**
Mouse Anti-Myosin	Developmental Studies Hybridoma Bank	MF 20	1:500
Actin Red 555	Thermo Fisher Scientific	R37112	2 drops/ml
Mouse Anti-Fas III	Developmental Studies Hybridoma Bank	7G10	1:500

Rat Anti-Elav	Developmental Studies Hybridoma Bank	7E8A10	1:100
Rabbit Anti-Phospho Histone3 Serine 10 (PH3)	Millipore	06-570	1:500
Rabbit Cleaved Drosophila Dcp-1	Cell Signaling Technology	9578S	1:1000
DAPI-DNA Dye	Sigma-Aldrich	D9542	1:1000
Alexa Fluor Goat 488 anti-mouse	Invitrogen	A11029	1:2000
Alexa Fluor 568 goat anti-mouse	Invitrogen	A11031	1:2000
Alexa Fluor 568 goat anti-rat	Invitrogen	A11077	1:2000
Alexa Fluor Goat 633 anti-mouse	Invitrogen	A21052	1:2000
Mouse MMP1 catalytic domain	Developmental Studies Hybridoma Bank	5H7B11-s, 3B8D12-s, 3A6B4-s	1:10

4.4.3 5-Ethynyl-2-deoxyuridine (EdU) feeding and labeling

To capture the endoreplication in ED secretory cells after inducing the damage, we fed the animals immediately after the 32hrs of 29°C damage with an EdU solution made with 1mM EdU, 10% Sucrose, and blue food coloring (5µl/ml). We visually verified uptake of the EdU by the presence of food color in the abdomen. In cornmeal agar food vial, a Whatman paper was wetted with EdU solution (250µl in each vial). Flies were allowed to feed on this solution for 10 days during the recovery. The Whatman paper was replaced with a new one with a freshly made EdU solution every 2 days to prevent contamination due to the presence of sucrose. EDs were dissected at different time points during recovery when fed on EdU and proceeded with fixing, permeabilizing, and iclick-it reaction. We used Click-IT Plus EdU AlexaFluor-555 or 488 (Thermo Fisher C10638). We quantified the total number of EdU positive secretory cells by using the cell counter plugin in ImageJ Fiji.

4.4.4 Confocal imaging

EDs for all the experiments were imaged using a Leica SP8 Confocal microscope with 40X objective. Some of ED's 10X and 20X magnification images were imaged using Leica SP5 Confocal microscope and Leica DMI6000B epifluorescence system.

4.4.5 Area measurements

For the ED area measurement ED image was captured in one frame using a Leica SP5 Confocal microscope with 10X objective. The images were opened in Fiji Imagej software and obtained the maximum Z projection of the stacks of the image. Manually using the free hand selection tool the area around the ED was drawn from the Anterior end of the ED where the AG, Seminal vesicles are connected to the posterior end of the ED where it connects to the EB. Now the area around the ED was measured by clicking Analyze and then Measure. These area values were plotted using the Graph pad Prism.

For measuring the Secretory cell size using Fiji ImageJ we drew the area around the Fas III cell-cell junction staining of each cell using the free hand selection tool in the anterior region of ED and measured the area of each cell. For measuring the area of nuclei of secretory cells in the anterior region we took the maximum Z- projections of DAPI staining images and measured area for nuclei in the anterior region of ED.

4.4.6 Ploidy/DAPI intensity measurements

All the ED DAPI images were obtained without saturating the DAPI using a Leica SP8 confocal microscope. Images were exported in Tiff format and opened in Fiji Imagej. The maximum projection of the stacks of DAPI-stained images was obtained. We have observed that the basally located nuclei in the external muscle layer of the ED are diploid by flow cytometry. We used these diploid muscle nuclei of ED to normalize the measurements and to calculate the haploid nuclei intensity. We measured the background intensity by drawing the region of interest (ROI) in the background region of the images. After the background subtraction ROI was manually drawn around the DAPI-stained nuclei of Diploid and polyploid secretory cells. Measured the Raw integrated Intensity of both diploid and secretory cells polyploid nuclei. We measured around 30 secretory cell polyploid nuclei and 10 diploid nuclei from muscle for each ED and We calculated the corrected fluorescence intensity from each nucleus raw integrated intensity, by subtracting the average background intensity. The intensity of the haploid nuclei DNA was calculated by taking

the average of the diploid nuclei intensity and dividing it by half. We used this as a reference of haploid nuclei with DNA content of 1C. Based on these haploid nuclei we estimated the DNA content of polyploid secretory cell nuclei. For Figures 4F we directly scored the DNA content without binning. For all other DNA content/ploidy measurements we plotted the after the following binning-2N (1.9-2.9), 4N (3.0-6.9), 8N (7-12.9), 16N (13.0-24.9), 32N (>24.9).

4.4.7 Fertility Assay

Virgin males were used to set up the fertility assay in all the mentioned figures. For the fertility assay showed in figure 1 we used 2-3 day old virgin males expressing reaper and control were crossed to Canton S females. We used a ratio of 1:8 (Male: Female) to set up the fertility assay in each vial and allowed them to mate for 3 days in 25°C incubator. The total number of the pupae and the offspring eclosed were counted and plotted as the result of fertility. For each genotype we performed the fertility assay with 15 animals in each trial and repeated it three trials. For the fertility assay with Gal80ts Reaper presented in Figure 4 we performed the fertility assay at two different temperatures. (i)For the post damage fertility test after the animals of both control and Gal80ts Reaper underwent 32hrs 29°C damage and they were mated with virgin Canton S females with a ratio of 1:8 (Male:Female) in each vial in 29°C incubator to keep the damage on and allowed to mate for six days where we flipped them to fresh vial every two days. The total number of pupae were counted and plotted. (ii) For Day 10 post recovery after damage we performed the fertility assay after the 10 days of the recovery. The males were crossed to virgin Canton S females with a ratio of 1:8 (Male:Female) in each vial and allowed to mate in 18°C incubator for 6 days with every two days flipping and finally we counted the total number of pupae.

4.4.8 Flow cytometry

Nuclei from the ED were isolated post dissection in S2 media (Thermofisher #21720024) with 10%Fetal Bovine Serum (Cytiva # SH30396.02HI) and 1% Pen-strep antibiotic solution. We used 25-30 intact EDs for the nuclear extraction per sample. We briefly spun the tissues to settle, S2 media was removed, then 1ml of Lysis Buffer (10mM Tris HCl-pH 7.4, 10mM NaCl, 3mM MgCl2, 0.1% NP40) was added and the sample was transferred to a Dounce homogenizer placed

on ice. To release the nuclei we homogenized the tissues with 20 strokes of loose Dounce pestle and allowed the tissue to rest on ice for 5 minutes. Following this we homogenized with tight Dounce pestle for 40 strokes. We triturated the tissue 15 times with a silanized fire-polished glass Pasteur pipette (BrainBits). This homogenate was filtered through 100 microns filter mesh, followed by 40 micron filter mesh to remove debris and unlysed tissue. To this homogenate 100µl of S2 media was added to stop the lysis reaction. This filtrate was centrifuged at 800 rcf for eight minutes at 4°C. Removed the supernatant and added 200µl of S2 media to the nuclei pellet with and incubated on ice for 5 minutes. To this additional 800µl of S2 media was added and centrifuged for eight minutes at 800 rcf, 4°C, supernatant was removed and the pellet was resuspended in 200µl S2 media with Vybrant DyeCyle Violet (Invitrogen #V35003) at a ratio of 1:100 and allowed to incubate on ice for 5 minutes, after the incubation to this 800µl of S2 media was added and centrifuged at 800rcf for eight minutes at 4°C. The supernatant was removed and resuspended the pellet in 1ml of S2 media, gently vortexed, and run on an Attune NxT Flow Cytometer.

4.4.9 Software and data analysis

We used Fiji ImageJ to analyze all the data. We used GraphPad Prism software to perform statistical significance in each graph plotted in the figures. The tests used to run the significance are mentioned in the figure legends.

4.5 Acknowledgements

We thank Dr. Allison Box and members of the Buttitta Lab for helpful discussions regarding this project. We also thank Dr. Jill Haenfler and the lab of Dr. Josie Clowney for assistance with male courtship assays. N.R. was supported in part by a U. Michigan MCDB Edwards fellowship. Work in the Buttitta Lab is supported by NIH R35GM149273 and NIH P01CA093900. Stocks obtained from the Bloomington Drosophila Stock Center (NIH P40OD018537) were used in this study. Several antibodies used in this study were obtained from the Developmental Studies Hybridoma Bank (DSHB), created by the NICHD of the NIH and maintained at The University of Iowa, Department of Biology, Iowa City, IA 52242. We used FlyBase (most recently release FB2025_02,

released April 17, 2025) to find information on Drosophila gene sequences, phenotypes, and gene functions (Ozturk-Colak et al., 2024).

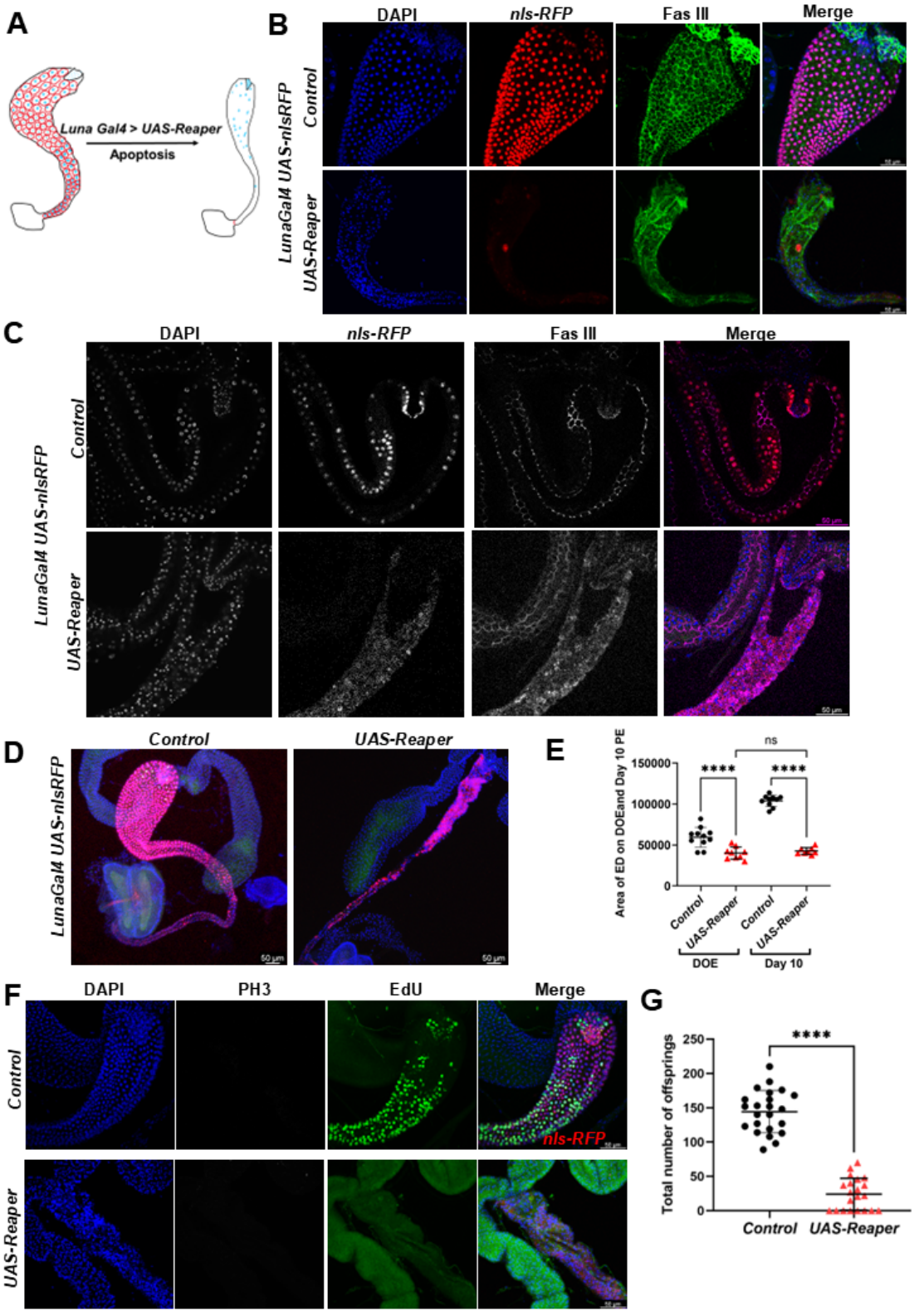


Figure 4.1: Reaper expression induces apoptosis in Drosophila ejaculatory duct (ED) secretory cells.

(A) Schematic illustration showing targeted expression of Reaper in the secretory cells of the ED using Luna-Gal4, leading to cell death.
(B) Confocal images of control and constitutive Reaper-expressing EDs at Day 10 post-eclosion, visualized using UAS-nls-RFP to confirm Gal4-driven expression. Tissues are immunolabeled with Fasciclin III (FasIII) and counterstained with DAPI. Images represent maximum Z-projections of individual channels and merged images. Scale bar: 50 μm.
(C) Single optical section images of control and Reaper-expressing EDs on Day 0 post-eclosion (DOE). In control tissues, secretory cells are localized apically, surrounding the hollow lumen. In Reaper-expressing EDs, secretory cells appear extruded apically into the lumen, indicating apoptosis-induced delamination of secretory cells. Tissues are stained with FasIII. Scale bar: 50 μm.
(D) Confocal image of the entire male reproductive tract, highlighting the reduced size of the ED upon Reaper expression using Luna-Gal4, with ED-specific expression confirmed by UAS-nls-RFP. Scale bar: 50 μm.
(E) Quantification of ED area on Day 0 and Day 10 post-eclosion in control and Reaper-expressing EDs. EDs expressing Reaper show a significant reduction in tissue area compared to controls (n = 9).
(F) Confocal images of the ED with constitutive Reaper expression and control fed with EdU to capture the S- phase DNA synthesis and immune stained with mitotic marker PH3. The tissue is counter stained with DNA marker DAPI (Blue)
(G) Quantification of male fertility in control and Reaper-expressing animals. Males with ablated secretory cells (Reaper expression) produce significantly fewer offspring, with some individuals producing no progeny, indicating compromised fertility.

Statistical analysis:
(E) One-way ANOVA with multiple comparisons between Day 0 and Day 10 for control vs. Reaper. $P<0.0001$ ****.
(F) Unpaired two-tailed t-test. $P<0.0001$ ****.

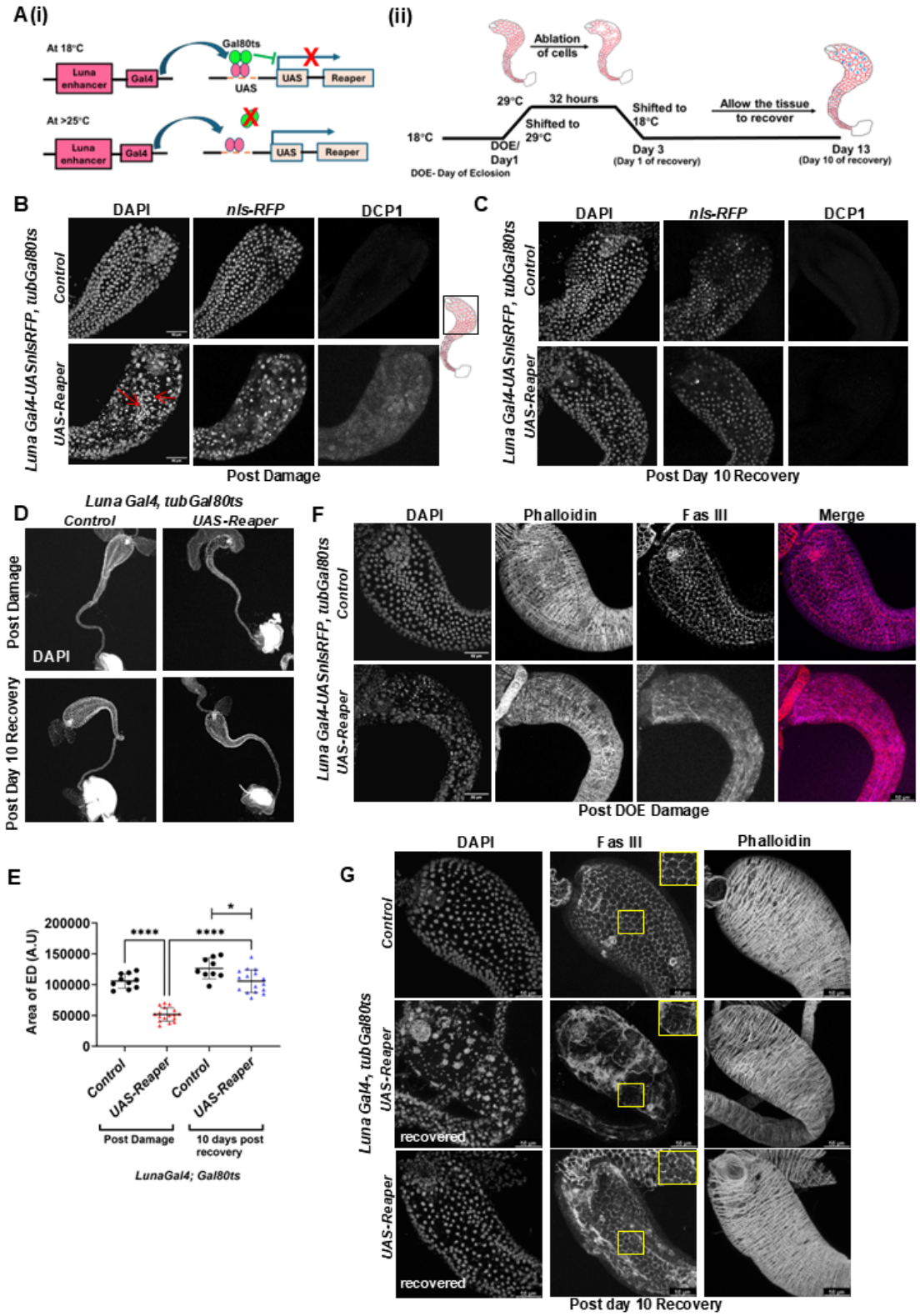


Figure 4.2: Transient Reaper expression using temperature-sensitive Gal80 system enables ablation and recovery of ejaculatory duct (ED) secretory cells in anterior region

(A)(i) Schematic diagram illustrating the use of the temperature-sensitive Gal80^{ts} system to control the Luna-Gal4-mediated expression of Reaper in ED secretory cells.
(ii) Illustration of the ED damage and recovery paradigm: Flies are reared at 18°C to suppress Gal4 activity via Gal80^{ts} . On the day of eclosion, flies are shifted to 29°C for 32 hours to induce Gal4 activity and express Reaper, leading to targeted ablation of secretory cells in the anterior ED. Flies are then returned to 18°C for 10 days to allow tissue recovery.
(B) Confocal images of the anterior region of the ED immediately after 32 hours of damage induction at 29°C. UAS-nls-RFP confirms Gal4 expression in secretory cells. Reaper-expressing EDs show numerous pyknotic nuclei (indicated by red arrows), characteristic of apoptosis. Tissues are stained with DCP-1 (cleaved death caspase-1) to mark caspase activation and apoptosis and counterstained with DAPI. Scale bar: 50 μm.
(C) Confocal images of the anterior ED from both control and Reaper groups after 10 days of recovery post-damage. Reaper-expressing EDs show structural recovery and absence of DCP-1 staining, indicating that apoptotic cell death has ceased. Nuclei are counterstained with DAPI. Scale bar: 50 μm.
(D) Confocal images of whole EDs from control and Reaper-expressing animals immediately post-damage and after 10-day recovery (10× magnification). Reaper EDs show reduced tissue size following damage and restoration of size after recovery. Scale bar: 50 μm.
(E)Quantification of ED area in control and Reaper-expressing tissues immediately post-damage and after 10-day recovery. Reaper-expressing EDs show a significant reduction in area post-damage and a partial to full recovery of area after 10 days.
(F) Confocal images of the anterior region of the ED immediately after 32 hours of damage induction at 29°C using the Gal80^{ts} system. Both control and Reaper-expressing EDs were stained with Phalloidin (muscle layer), FasIII (cell-cell junctions), and DAPI (nuclei). Reaper EDs exhibit structural disruption and altered epithelial organization. Scale bar: 50 μm.
(G)Confocal images of the anterior ED after 10-day recovery. Tissues were stained with Phalloidin, FasIII, and DAPI. The middle row represents partial recovery, showing enlarged nuclei and cells, indicative of compensatory cellular hypertrophy (CCH). The bottom panel shows full recovery of ED morphology. Insects show zoomed views of FasIII-labeled cell-cell junctions in recovered EDs, highlighting restoration of epithelial structure.

Statistical analysis:
(E) One-way ANOVA with multiple comparisons between Every column for control vs. Reaper. $P<0.0001$ ****.

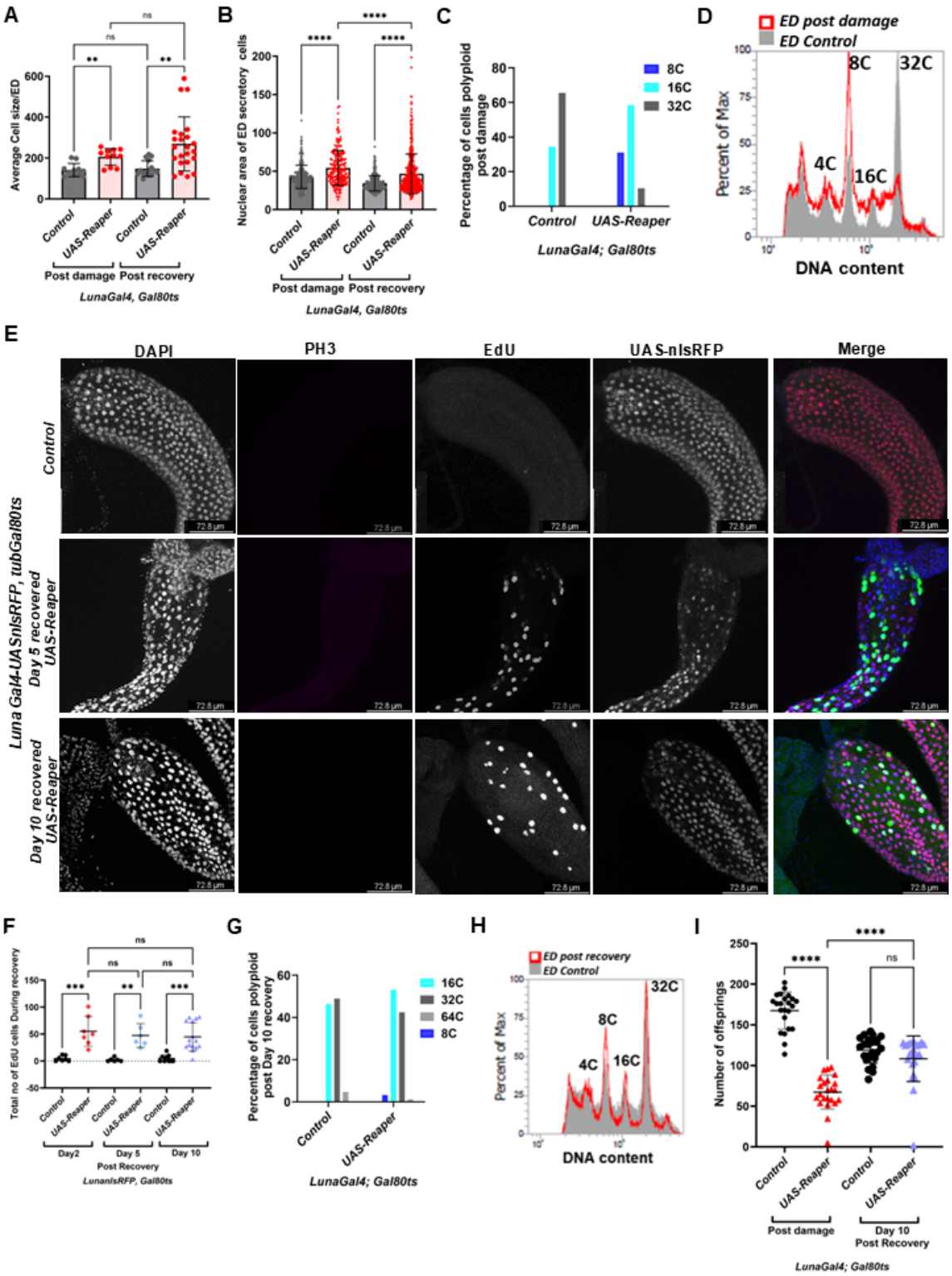


Figure 4.3: Endoreplication in the ED during recovery restores ploidy, tissue mass and supports functional regeneration

(A) Quantification of average secretory cell size per ED. Each dot represents the mean cell size per animal calculated from the individual secretory cell area from the anterior region of ED in control, damaged (post 32-hour Reaper induction), and recovered (Day 10 post-damage), showing consistent trends across biological replicates.
(B) Quantification of nuclear area of ED secretory cells in the anterior region of both control and Reaper-expressing EDs immediately after damage and after Day 10 recovery. Each dot represents the area of an individual nucleus. Reaper EDs show a significant increase in nuclear area compared to controls in both conditions, indicating nuclear hypertrophy.
(C) Quantification of DNA content/ploidy in secretory cells of the anterior ED, measured by DAPI intensity, immediately after 32 hours of Reaper-induced damage. Compared to controls, Reaper EDs show a decrease in high-ploidy (32C) cells and an increase in lower-ploidy (8C) cells, indicating loss of polyploid cells due to ablation.
(D) Flow cytometric analysis of nuclear ploidy in control and Reaper-damaged EDs immediately after 32 hours of damage. Grey peak represents control ED nuclei; red peak corresponds to Reaper EDs, showing a shift towards lower ploidy levels.
(E) Confocal micrographs of the anterior region of the ED in Control, Day 5 Reaper-recovered, and Day 10 Reaper-recovered animals. Animals were fed EdU immediately after damage to label S-phase cells, and tissues were stained and imaged at the indicated recovery time points to detect EdU incorporation and PH3-positive (mitotic) cells in secretory cells. We did not see any PH3 positive mitotic cells during the recovery. Scale bar: 50 μm.
(F) Quantification of EdU-positive secretory cells in control and Reaper EDs at Day 2, Day 5, and Day 10 post-damage. Reaper EDs shows a significantly higher number of EdU+ cells during the recovery period, indicating active endoreplication.
(G) Quantification of DNA content/ploidy in the anterior secretory cells of control and Reaper EDs after Day 10 recovery, showing that Reaper EDs regains high-ploidy (32C) cells, suggesting restoration of ploidy through endoreplication.
(H) Flow cytometric analysis of nuclear ploidy in control and Reaper EDs after Day 10 recovery. Grey peak shows control ploidy profile; red peak shows the Reaper ED nuclei post-recovery, demonstrating restoration of high-ploidy peaks, consistent with regeneration.
(I) Quantification of male fertility in control and Reaper-expressing animals. Fertility was assessed under two conditions:
Damaged ED: Mating was performed immediately following 32 hours of Reaper induction at 29°C, representing animals with ablated secretory cells.
Recovered ED: Mating was conducted 10 days post-recovery at 18°C after transient Reaper expression.
Reaper-expressing males exhibited significantly reduced fertility immediately after damage. However, fertility was restored following the 10-day recovery period, indicating functional restoration of the ED secretory cells.

Statistical analysis:

One-way ANOVA with multiple comparisons between Every column for control vs. Reaper. P<0.0001 ****.

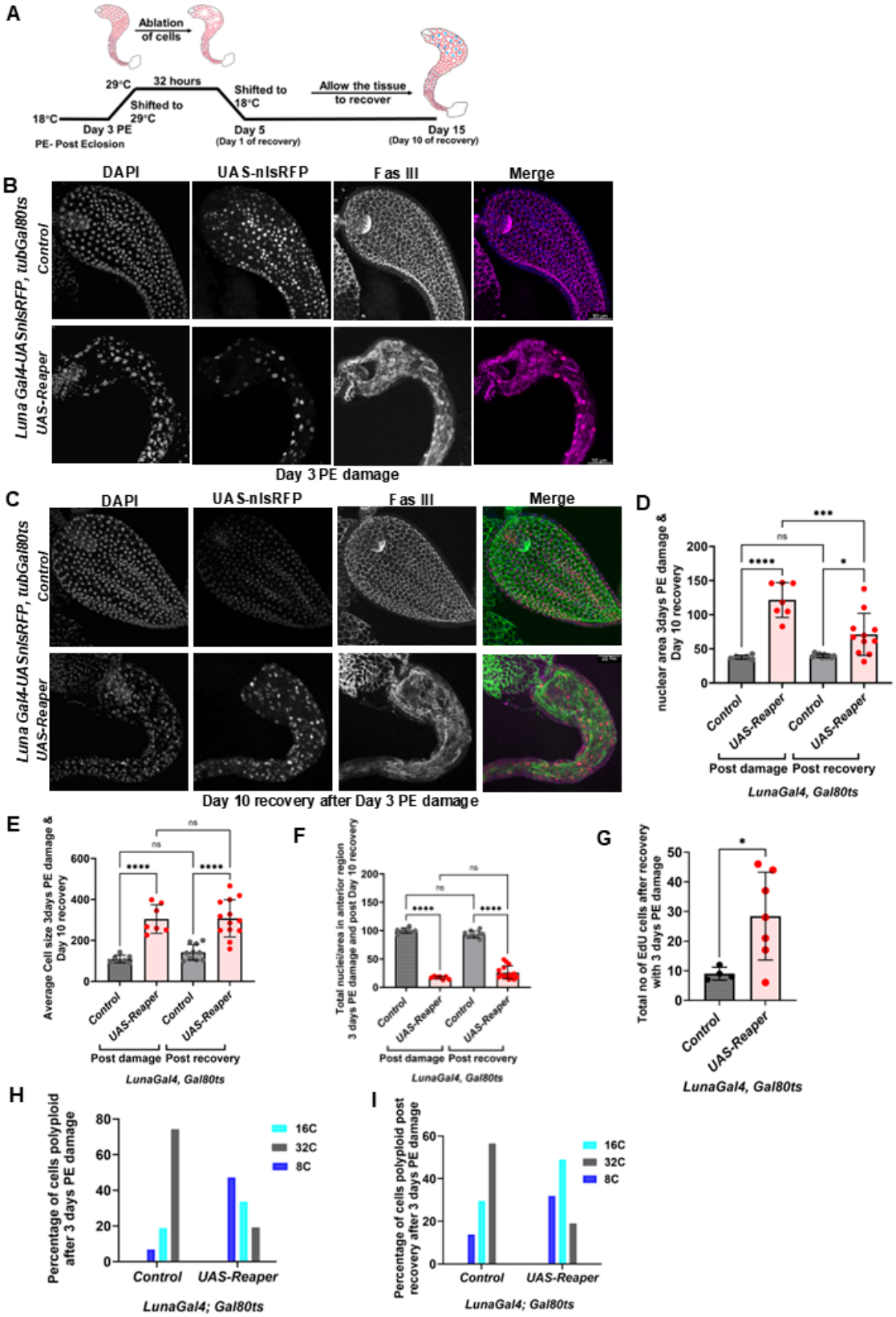


Figure 4.4: Inducing damage during the early endoreplication window is essential for optimal recovery of ED secretory cells

(A) Schematic of the damage and recovery paradigm. Flies were reared at 18°C to suppress Gal4 activity via $Gal80^{ts}$. On Day 3 post-eclosion, flies were shifted to 29°C for 32 hours to activate Luna-Gal4 and induce Reaper expression, leading to selective ablation of secretory cells in the anterior region of the ejaculatory duct (ED). Flies were then returned to 18°C for 10 days to allow recovery.
(B) Confocal images of the anterior ED region immediately after 32 hours of damage induction on Day 3 post-eclosion. EDs were stained with FasIII (green, cell-cell junctions) and DAPI (blue, nuclei). Reaper-expressing EDs show disruption of epithelial integrity, reduced cell number, and loss of organized junctions. Scale bar: 50 μm.
(C) Confocal images of the anterior ED region 10 days post-damage after Day 3 induction. EDs stained with FasIII (green) and DAPI. Partial recovery of ED morphology is observed in Reaper-expressing animals. Scale bar: 50 μm.
(D) Quantification of nuclear area of secretory cells in control and Reaper-expressing EDs, immediately after Day 3 damage and following Day 10 recovery. Each dot represents the average nuclear area per ED. Nuclear size increases in Reaper EDs post-damage and remains enlarged during recovery, consistent with compensatory cellular hypertrophy.
(E) Quantification of average cell size of secretory cells in control, Reaper-damaged (Day 3), and Reaper-recovered EDs (Day 10). Reaper EDs shows a significant increase in average cell size during damage and recovery, suggesting hypertrophic growth.
(F) Quantification of total nuclei per unit area in the anterior ED of control and Reaper-expressing animals. A significant reduction in cell number is observed in Reaper EDs post-damage, with partial recovery by Day 10.
(G) Quantification of EdU-positive secretory cells in control and Reaper-recovered EDs (damage induced on Day 3). EdU incorporation indicates that endoreplication is active during recovery. Reaper EDs show significantly increased EdU-positive cells compared to control, suggesting reactivation of endocycling to restore lost ploidy.
(H) Quantification of DNA content (ploidy) in anterior ED secretory cells of control and Reaper-expressing animals, immediately after 32 hours of damage induction on Day 3 post-eclosion, based on DAPI intensity measurements. Reaper-expressing EDs show a significant reduction in high-ploidy (32C) cells and a corresponding increase in lower-ploidy (8C) cells, indicating the selective loss of mature polyploid secretory cells due to apoptotic ablation.
(I) Quantification of DNA content (ploidy) in anterior secretory cells of control and Reaper EDs 10 days post-recovery following Day 3 post eclosion damage. While control EDs maintain a normal distribution of high-ploidy cells, Reaper EDs fails to fully restore the 32C population, indicating incomplete recovery when damage is induced during the late endocycling window.
Statistical analysis
(G) Unpaired two-tailed t-test. $P<0.0001$ ****.
(D, E, F, G) One-way ANOVA with multiple comparisons between Day 0 and Day 10 for control vs. Reaper. $P<0.0001$ ****.

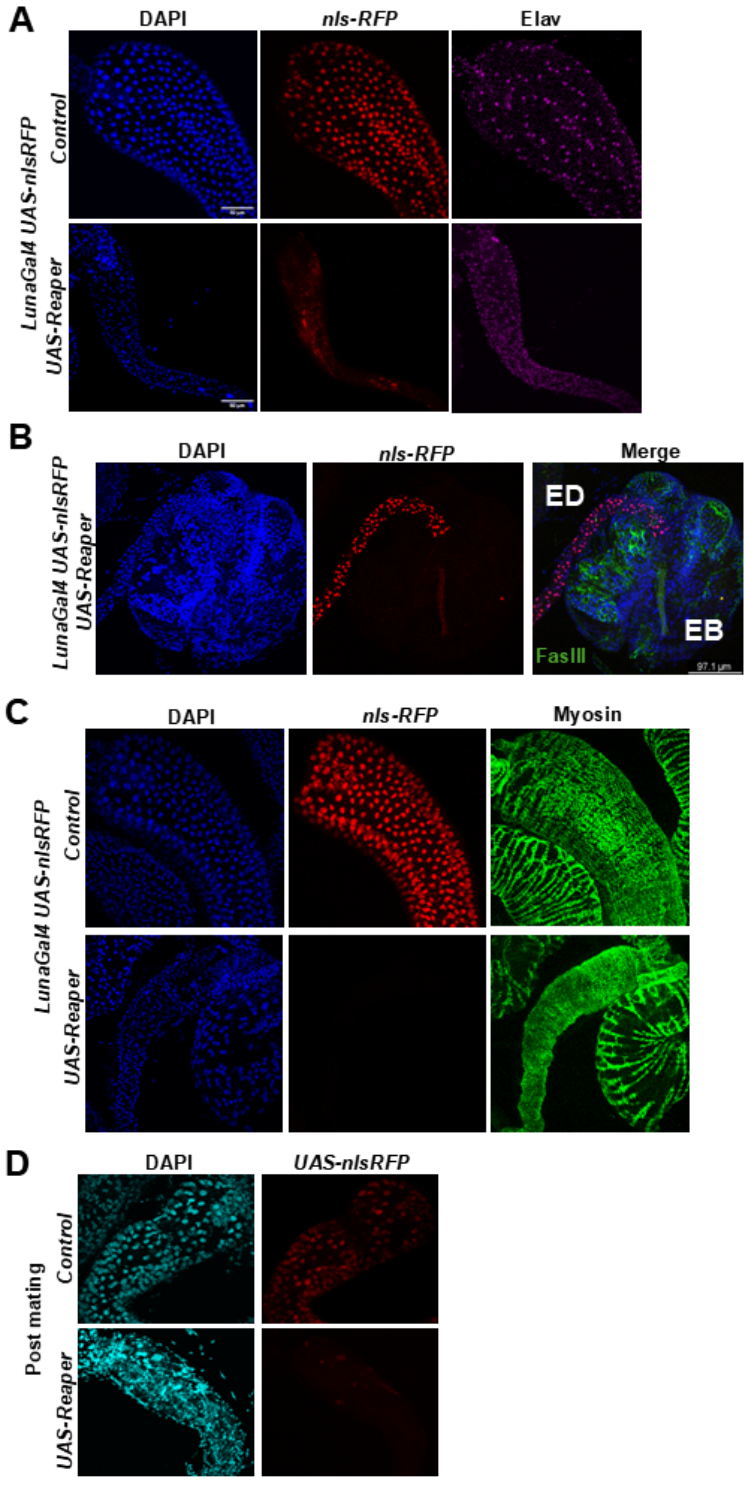


Figure 4.5: Constitutive expression of Reaper in ED

(A) Confocal images of EDs constitutively expressing Reaper and UAS-nls-RFP in secretory cells. To validate Gal4 activity, nls-RFP (Red) was expressed under UAS control. Tissues were

immunostained with Elav (Magenta), a neuronal/muscle nuclear marker. In Reaper-expressing EDs, complete ablation of secretory cells is evident, with only Elav-positive nuclei (neuronal/muscle) remaining, confirming selective loss of secretory cells.
(B) Confocal images of the posterior ED and ejaculatory bulb (EB) in control and Reaper-expressing flies. In Reaper EDs, nls-RFP–labeled secretory cells are observed being extruded apically through the EB.
(C) Confocal images of control and Reaper-expressing EDs stained with Myosin (Green) to label muscle fibers. Despite ablation of secretory cells, the muscle layer remains intact, indicating the specificity of Reaper-induced apoptosis to the epithelial cell population.
(D) Confocal images of the ED post-fertility assay in control and Reaper-expressing flies. In the Reaper EDs (lower panel), sperm accumulation is observed within the duct, suggesting impaired ejaculatory function due to secretory cell loss and tissue dysfunction.

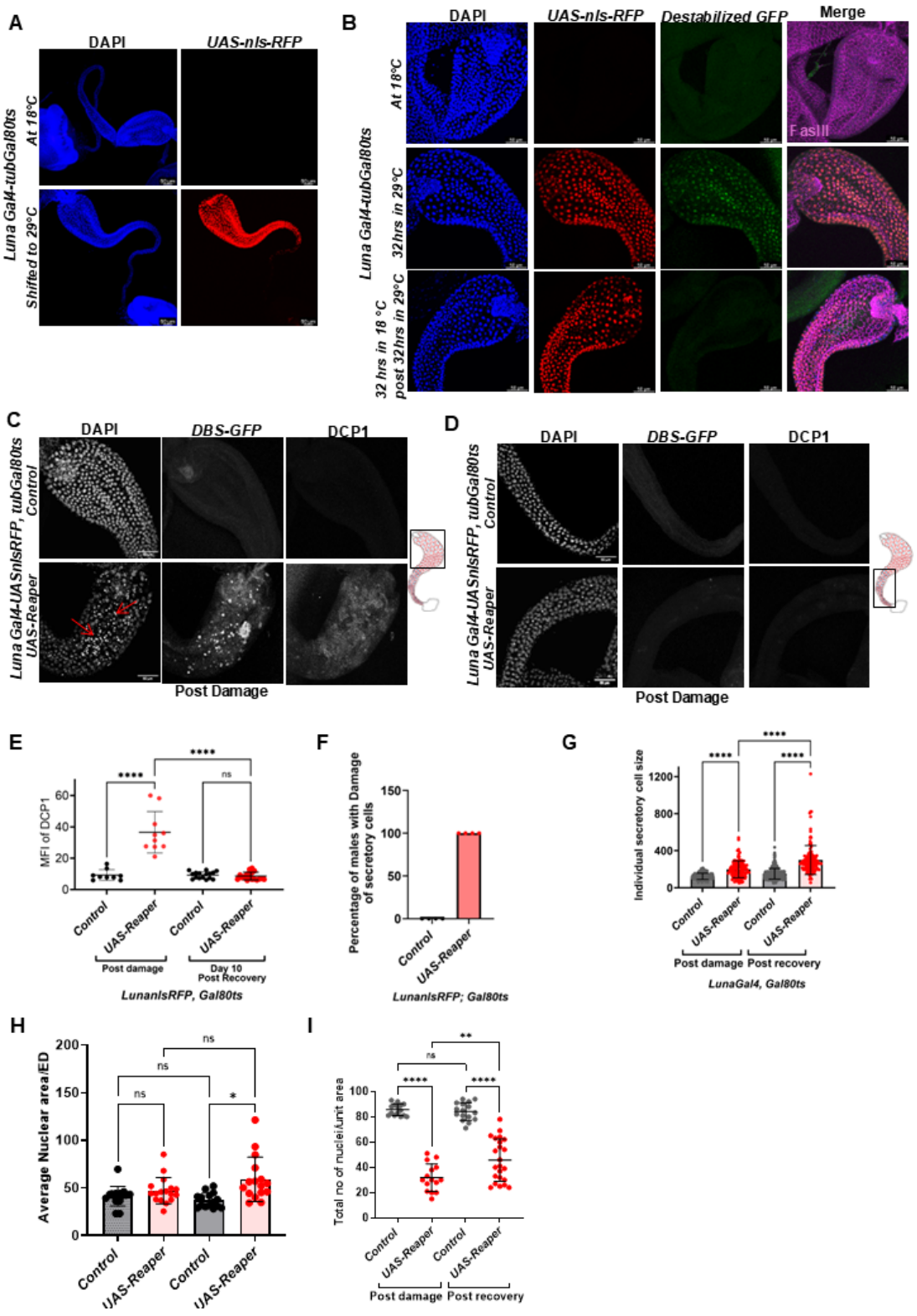


Figure 4.6: Temporal expression of Reaper in ED

(A) Confocal images of EDs showing temperature-dependent regulation of Luna-Gal4 by Gal80^{ts}. At 18°C (top panel), nls-RFP expression is suppressed, indicating Gal80^{ts} effectively blocks Gal4

activity. Upon shifting to 29°C (bottom panel), nls-RFP is robustly expressed in the ED, confirming activation of Luna-Gal4 upon Gal80^{ts} inactivation.
(B) Confocal images show *dsGFP* expression (reporting Luna-Gal4 activity) in EDs at different time points. At 18°C (top row), there is no *dsGFP* expression. After 32 hours at 29°C (middle row), *dsGFP* is detected in the anterior region of ED, confirming *Gal4* activation. Upon returning to 18°C, *dsGFP* signal disappears within 24 hours (bottom row), validating the kinetics of Gal80^{ts}-mediated repression.
(C) Confocal images of anterior EDs from control and Reaper-expressing flies after 32 hours at 29°C. In controls (top row), there is no signal from the *DBS-GFP* sensor or DCP-1 staining. In Reaper EDs (bottom row), strong *DBS-GFP* fluorescence and DCP-1 signal are detected, confirming caspase-mediated apoptosis in the anterior region of secretory cells.
(D) Confocal images of posterior region of ED from control and Reaper-expressing animals after 32 hours at 29°C. Both DBS-GFP and DCP-1 signals are absent in this region, demonstrating that Reaper-induced cell death is localized to the anterior ED.
(E) Quantification of mean fluorescence intensity of DCP-1 staining in EDs immediately after damage and after 10 days of recovery. Damaged EDs show significantly increased DCP-1 levels compared to controls, while no signal is detected after recovery.
(F) Quantification of the percentage of EDs that underwent secretory cell ablation following Reaper induction. Based on the presence of pyknotic nuclei, reduced ED size, and reduced secretory cell number per unit area, 100% of EDs exhibited damage.
(G) Quantification of individual secretory cell area from the anterior ED region in control, damaged (post 32-hour Reaper induction), and recovered (Day 10 post-damage) EDs. Each dot represents the area of a single secretory cell. Reaper-expressing EDs show a significant increase in cell size immediately after damage. Recovered EDs also display larger cell sizes compared to controls and damaged tissues, consistent with CCH.
(H) Average nuclear area per ED, calculated from the data in (i). Each dot represents the mean nuclear size per ED, supporting the observation of nuclear hypertrophy in damaged and recovered tissues.
(I) Quantification of the total number of nuclei per unit area in the anterior region of control and Reaper-expressing EDs, immediately after damage and post-Day 10 recovery. Reaper-expressing EDs show a reduction in nuclear density, consistent with cell loss and compensatory hypertrophy rather than proliferation during recovery.

Statistical analysis

(E) Descriptive percentage; 100% animals showed damage.
(E, G, H, I) One-way ANOVA with multiple comparisons between Day 0 and Day 10 for control vs. Reaper. $P<0.0001$ ****.

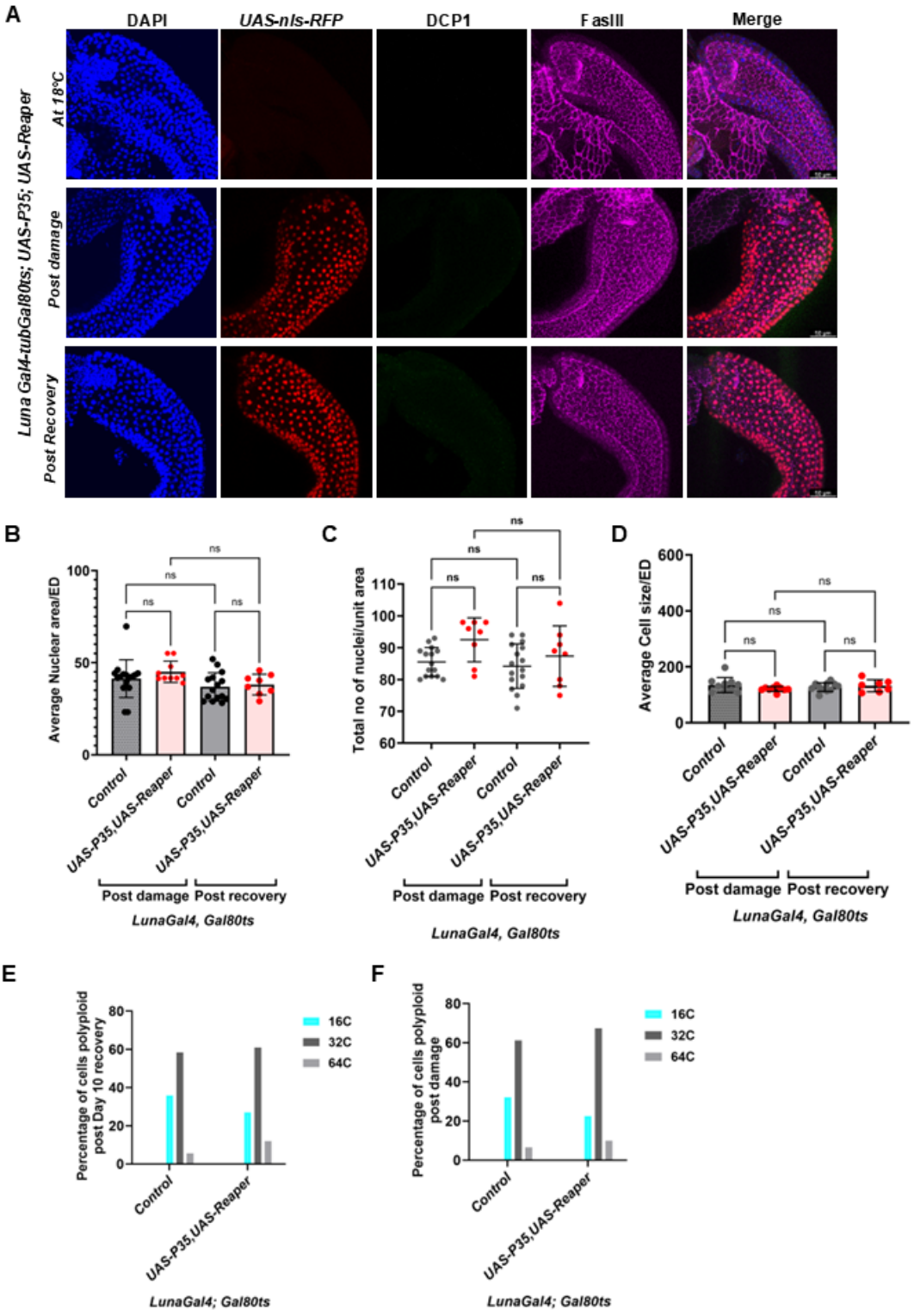


Figure 4.7: Temporal expression of reaper in ED in the presence of UAS-P35

(A) Confocal images of ED with the transient expression of Reaper using Gal80^{ts} showing the absence of damage of secretory cells with the *UAS-P35* expression that blocks the apoptosis. We

did not see any damage of secretory cells in ED with the reaper and UAS-p35 after inducing the 32hrs damage at 29°C (Middle panel). After Day 10 post recovery paradigm we did not see any further difference in the ED. DCP1 staining was absent in the presence of UAS-P35 in ED.
(B) Quantification of nuclear area of secretory cells in control and UAS-p35 Reaper-expressing EDs, immediately after 32hrs of damage paradigm and following Day 10 recovery paradigm. Each dot represents the average nuclear area per ED. We did not observe any significant increase in the nuclear area of ED of control and UAS-P35, Reaper expressing ED.
(C) Quantification of total nuclei per unit area in the anterior ED of control and UAS-p35, Reaper-expressing EDs both with the damage and recovery paradigm.
(D) Quantification of average cell size of secretory cells in control, UAS-p35 Reaper-expressing EDs. There is no significant difference in the cell size of ED in both control and UAS-p35 Reaper with both damage and recovery paradigm.
(E) Quantification of the ploidy of ED secretory cells in the anterior region of control EDs and UAS-p35 Reaper immediately after the 32hrs damage paradigm.
(F) Quantification of the ploidy of ED secretory cells in the anterior region of control EDs and UAS-p35 Reaper after the recovery paradigm.
Statistical analysis
(B, C, D) One-way ANOVA with multiple comparisons between Day 0 and Day 10 for control vs. Reaper. $P<0.0001$ ****.

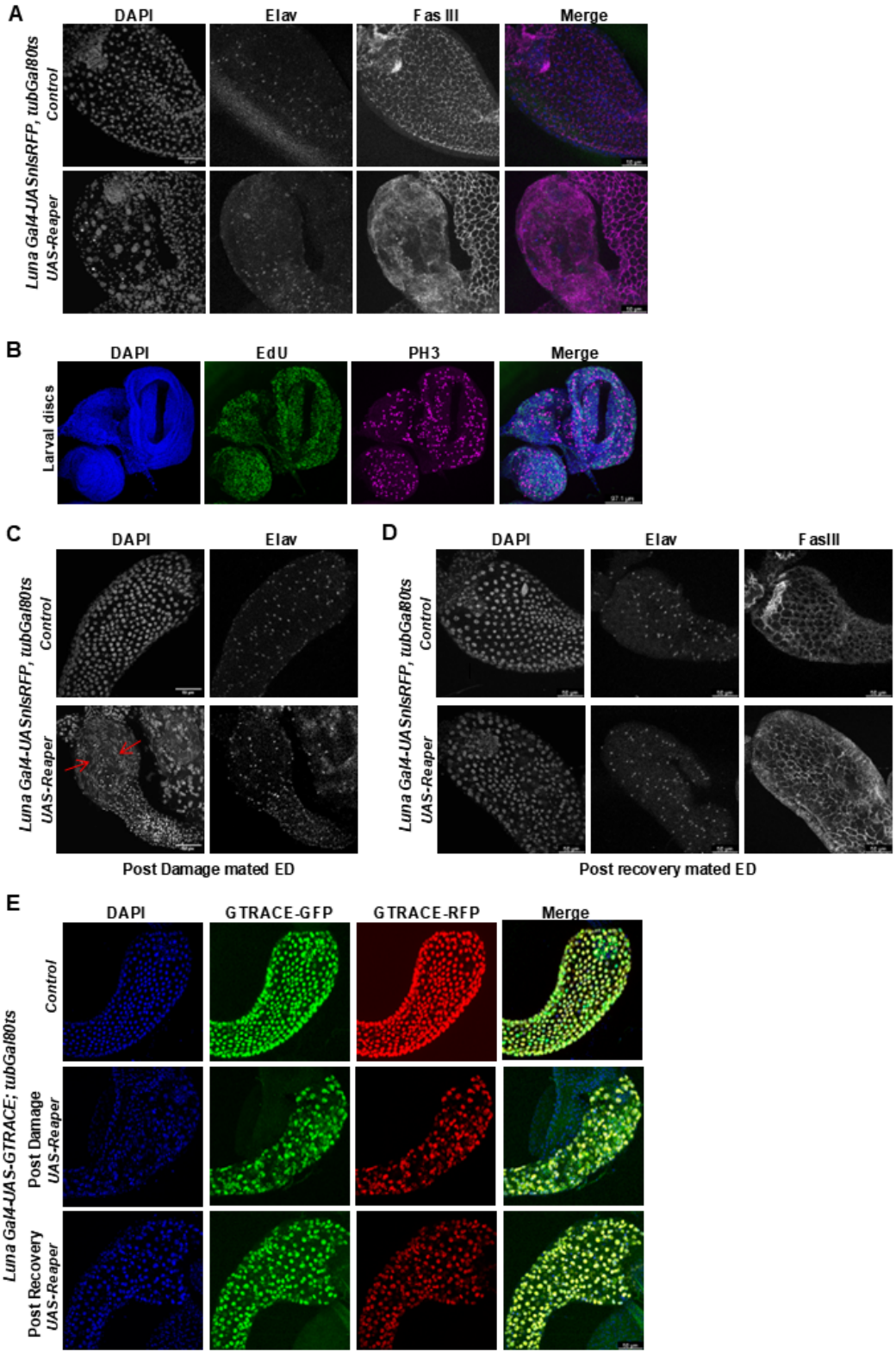


Figure 4.8: Different staining during ED damage and GTRACE expression

(A) Confocal images of anterior region ED stained with Elav, FasIII and DAPI of the control and the Reaper-induced ED with the $Gal80^{ts}$ control system post recovery.
(B) Confocal images of larval imaginal discs stained with PH3 in red, EdU in green used as a positive control for the PH3 positive mitosis and nuclei stained by DAPI (blue).
(C) Confocal images of the ED post-fertility assay in control and Reaper-expressing flies immediately after 32hrs of damage. In the Reaper EDs (lower panel), sperm accumulation is observed within the duct, suggesting impaired ejaculatory function due to secretory cell loss and tissue dysfunction.
(D) Confocal images of the ED post-fertility assay in control and Reaper-expressing flies allowed to mate post day 10 recovery.
(E) Confocal images of ED expressing GTRACE in both control and Reaper under the control of $Gal80^{ts}$ post damage and post day 10 recovery.

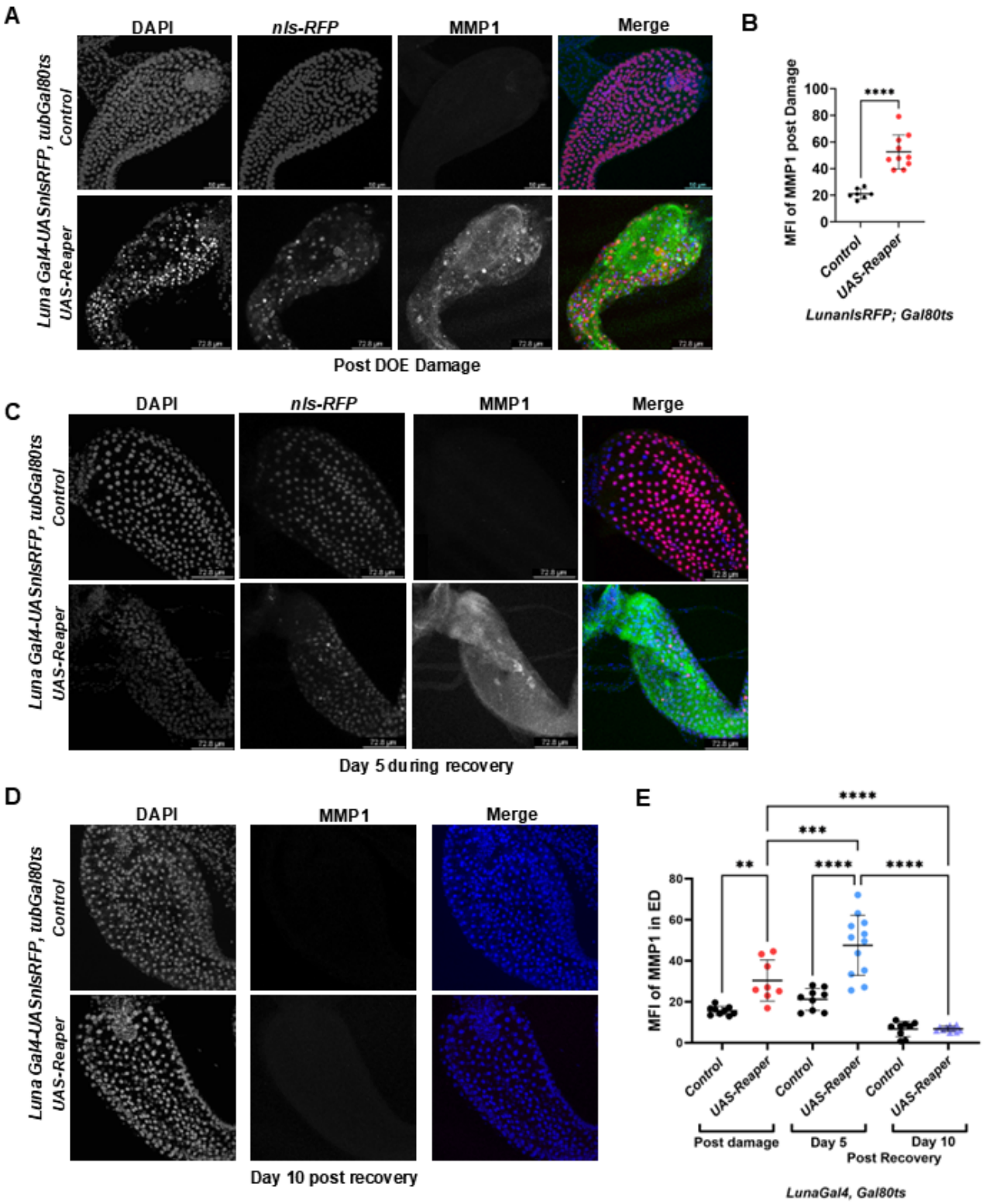


Figure 4.9: MMP1 is upregulated during ED damage and recovery

(A) Confocal images of the anterior region of the ED immediately after 32 hours of transient damage induction in control and Reaper-expressing animals. Tissues were stained with Matrix

Metalloprotease-1 (MMP1) antibody, which is known to be upregulated during tissue damage and repair. MMP1 (green), nls-RFP (magenta), and DAPI (blue). Reaper EDs show strong MMP1 signal compared to controls. Scale bar: 72.8 μm.
(B) Quantification of mean fluorescence intensity (MFI) of MMP1 in control and Reaper EDs immediately post-damage. MMP1 levels are significantly elevated in Reaper-expressing EDs compared to controls.
Statistical test: Unpaired t-test, **P < 0.0001, ****.
(C) Confocal images of the anterior ED on Day 5 post-damage in control and Reaper-expressing animals, stained with MMP1. MMP1 levels remain elevated in the Reaper EDs, consistent with ongoing tissue remodeling. MMP1 (green), nls-RFP (magenta), DAPI (blue). Scale bar: 72.8 μm.
(D) Confocal images of the anterior ED on Day 10 post-damage. MMP1 signal is absent in both control and Reaper-recovered EDs, indicating that tissue remodeling is complete by this stage. MMP1 (green), DAPI (blue). Scale bar: 72.8 μm.
(E) Quantification of MMP1 mean fluorescence intensity in control and Reaper EDs across three time points: immediately post-damage, Day 5 recovery, and Day 10 recovery. MMP1 levels are significantly increased after damage and during Day 5 recovery but return to baseline by Day 10.
Statistical analysis:
(B) Unpaired two-tailed t-test. P<0.0001 ****.
(E) One-way ANOVA with multiple comparisons between Day 0 and Day 10 for control vs. Reaper. P<0.0001 ****.

4.6 Bibliography

Baena-Lopez, L. A., Arthurton, L., Bischoff, M., Vincent, J. P., Alexandre, C. and McGregor, R. (2018). Novel initiator caspase reporters uncover previously unknown features of caspase-activating cells. *Development* 145.

Cordero-Espinoza, L. and Huch, M. (2018). The balancing act of the liver: tissue regeneration versus fibrosis. *J Clin Invest* 128, 85-96.

Date-Ito, A., Kasahara, K., Sawai, H. and Chigusa, S. I. (2002). Rapid evolution of the male-specific antibacterial protein andropin gene in Drosophila. *J Mol Evol* 54, 665-670.

de Morree, A. and Rando, T. A. (2023). Regulation of adult stem cell quiescence and its functions in the maintenance of tissue integrity. *Nat Rev Mol Cell Biol* 24, 334-354.

Edgar, B. A., Zielke, N. and Gutierrez, C. (2014). Endocycles: a recurrent evolutionary innovation for post-mitotic cell growth. *Nat Rev Mol Cell Biol* 15, 197-210.

Evans, C. J., Olson, J. M., Ngo, K. T., Kim, E., Lee, N. E., Kuoy, E., Patananan, A. N., Sitz, D., Tran, P., Do, M. T., et al. (2009). G-TRACE: rapid Gal4-based cell lineage analysis in Drosophila. *Nat Methods* 6, 603-605.

Hay, B. A., Wolff, T. and Rubin, G. M. (1994). Expression of baculovirus P35 prevents cell death in Drosophila. *Development* 120, 2121-2129.

Imamura, M., Haino-Fukushima, K., Aigaki, T. and Fuyama, Y. (1998). Ovulation stimulating substances in Drosophila biarmipes males: their origin, genetic variation in the response of females, and molecular characterization. *Insect Biochem Mol Biol* 28, 365-372.

Lavecchia, A. M., Pelekanos, K., Mavelli, F. and Xinaris, C. (2022). Cell Hypertrophy: A "Biophysical Roadblock" to Reversing Kidney Injury. *Front Cell Dev Biol* 10, 854998.

Losick, V. P. (2016). Wound-Induced Polyploidy Is Required for Tissue Repair. *Adv Wound Care (New Rochelle)* 5, 271-278.

Lung, O., Kuo, L. and Wolfner, M. F. (2001). Drosophila males transfer antibacterial proteins from their accessory gland and ejaculatory duct to their mates. *J Insect Physiol* 47, 617-622.

McGuire, S. E., Mao, Z. and Davis, R. L. (2004). Spatiotemporal gene expression targeting with the TARGET and gene-switch systems in Drosophila. *Sci STKE* 2004, pl6.

Ozturk-Colak, A., Marygold, S. J., Antonazzo, G., Attrill, H., Goutte-Gattat, D., Jenkins, V. K., Matthews, B. B., Millburn, G., Dos Santos, G., Tabone, C. J., et al. (2024). FlyBase: updates to the Drosophila genes and genomes database. *Genetics* 227.

Perez-Garijo, A., Martin, F. A. and Morata, G. (2004). Caspase inhibition during apoptosis causes abnormal signalling and developmental aberrations in Drosophila. *Development* 131, 5591-5598.

Perez-Garijo, A., Shlevkov, E. and Morata, G. (2009). The role of Dpp and Wg in compensatory proliferation and in the formation of hyperplastic overgrowths caused by apoptotic cells in the Drosophila wing disc. *Development* 136, 1169-1177.

Ramesh, N. A., Box, A. M. and Buttitta, L. A. (2025). Post-eclosion growth in the Drosophila ejaculatory duct is driven by Juvenile hormone signaling and is essential for male fertility. *Dev Biol* 519, 122-141.

Richmond, R. C., Gilbert, D. G., Sheehan, K. B., Gromko, M. H. and Butterworth, F. M. (1980). Esterase 6 and reproduction in Drosophila melanogaster. *Science* 207, 1483-1485.

Ryoo, H. D., Bergmann, A., Gonen, H., Ciechanover, A. and Steller, H. (2002). Regulation of Drosophila IAP1 degradation and apoptosis by reaper and ubcD1. *Nat Cell Biol* 4, 432-438.

Sandu, C., Ryoo, H. D. and Steller, H. (2010). Drosophila IAP antagonists form multimeric complexes to promote cell death. *J Cell Biol* 190, 1039-1052.

Shu, Z., Row, S. and Deng, W. M. (2018). Endoreplication: The Good, the Bad, and the Ugly. *Trends Cell Biol* 28, 465-474.

Sturm, S., Dowle, A., Audsley, N. and Isaac, R. E. (2021). Mass spectrometric characterisation of the major peptides of the male ejaculatory duct, including a glycopeptide with an unusual zwitterionic glycosylation. *J Proteomics* 246, 104307.

Susic-Jung, L., Hornbruch-Freitag, C., Kuckwa, J., Rexer, K. H., Lammel, U. and Renkawitz-Pohl, R. (2012). Multinucleated smooth muscles and mononucleated as well as multinucleated striated muscles develop during establishment of the male reproductive organs of Drosophila melanogaster. *Dev Biol* 370, 86-97.

Takemori, N. and Yamamoto, M. T. (2009). Proteome mapping of the Drosophila melanogaster male reproductive system. *Proteomics* 9, 2484-2493.

Tamori, Y. and Deng, W. M. (2013). Tissue repair through cell competition and compensatory cellular hypertrophy in postmitotic epithelia. *Dev Cell* 25, 350-363.

---- (2014). Compensatory cellular hypertrophy: the other strategy for tissue homeostasis. *Trends Cell Biol* 24, 230-237.

Xia, H., Li, X., Gao, W., Fu, X., Fang, R. H., Zhang, L. and Zhang, K. (2018). Tissue repair and regeneration with endogenous stem cells. *Nature Reviews Materials* 3, 174-193.

Chapter 5 Conclusions and Future Directions

5.1 Conclusions

The *Drosophila* male ED is an organ of the male reproductive system that is involved in the secretion of antimicrobial peptides, seminal fluid proteins, and acts as a conduit for the mixing of sperm, seminal fluid proteins, and other secretions from male reproductive tissues before transferring to the female during copulation. This thesis examined the cell cycle status of the secretory cells of the ED. Prior research on the ED had largely been restricted to descriptive methods like proteomic analyses, primarily because of the absence of a tissue-specific Gal4 driver to enable targeted genetic manipulation specifically in the ED. In this thesis, we demonstrate that the Luna-Gal4 driver provides effective ED-specific UAS-driven gene expression, allowing for the manipulation of hormonal signaling, protein synthesis, and cell cycle pathways in the adult ED. Thus, my work lays the foundation for future research on the ED.

In Chapter 2 I explored the basis of the post-eclosion organ growth in the *Drosophila* ED. My major findings demonstrate that the ED secretory epithelial cells remain post-mitotic after eclosion and throughout adulthood, but they retain the ability to undergo endocycles, a variant cell cycle lacking mitosis during the first 3 days of adulthood, leading to cells with DNA content/ploidy between 8C-32C and thereby increasing organ size. This growth is tightly correlated with the ED's functional output, where higher ploidy directly translates to greater protein synthesis, which is crucial for male fertility. We confirmed this by genetically compromising endoreplication in ED cells, which resulted in reduced ploidy, reduced organ size, diminished production of seminal proteins, and a significant decline in male reproductive success. My work also revealed that the early adult endocycling and post-mitotic growth of the ED is promoted, at least in part, by the JH signaling pathway. Furthermore, I show that the mTOR signaling pathway intersects with the cell cycle pathway, as the inhibition of mTOR signaling leads to a reduction in endocycling and cellular ploidy. As we saw, reduced endocycling occurred when the mTOR was severely knocked down.

These results demonstrate that in the postmitotic ED there in an interplay between mTOR signaling, endocycle progression and the optimal secretory and fertility function of the ED.

In chapter 3, we have optimized the nuclear isolation protocol to isolate the polyploid nuclei from the male reproductive system (ED + AG) and introduced a high-throughput flow cytometry protocol that fundamentally improves how we quantify polyploid nuclei. The traditional microscopy-based DNA content measurements were labor-intensive, low-throughput, and often lacked the resolution to detect subtle ploidy changes. This method is sensitive to measuring changes in chromosome numbers including aneuploidy, which can be difficult to detect using the image analysis method. This flow cytometry method can rapidly analyze thousands of nuclei in a single run, enabling detection of small but quantitative differences in nuclear DNA content that would be easily missed by conventional imaging techniques. This protocol allowed us to resolve distinct ploidy populations in these post-mitotic tissues with a high degree of accuracy. By applying the assay across multiple *Drosophila* species, we further demonstrated its robustness and discovery potential. Notably, these interspecific ploidy differences measured by flow cytometry were consistent with prior DAPI-intensity imaging data, underscoring the accuracy of both methods. This work bridges an important technological gap and opens the way for deeper exploration of endocycle regulation and function in the male reproductive system, which has been understudied compared to the female organs.

Chapter 4 of the thesis establishes the *Drosophila* ejaculatory duct as a new model for post-mitotic tissue regeneration. We show conclusively that an organ composed of differentiated, polyploid cells is capable of substantial restoration of function after significant cell loss. Endoreplication-driven compensatory cellular hypertrophy emerges as a central mechanism enabling this recovery in ED secretory cells. We observed that there is a narrow window after eclosion (adult emergence) during which ED cells retain the plasticity to extend their ability to undergo endocycling and initiate regeneration. Under normal conditions, these cells undergo several endocycles in the first 2–3 days of adult life to attain high ploidy, after which they permanently exit the cell cycle and become quiescent. Correspondingly, our injury experiments demonstrated that age is a significant factor in determining regenerative outcomes. When cell loss was induced in relatively young adults (just after the normal endocycles reduce in frequency), the tissue was able to temporarily extend its endocycle program to replace or recover organ mass and significantly restore fertility. In contrast, later cell loss, after most cells have exited endocycling, resulted in greatly diminished

organ recovery. We rigorously confirmed this by inducing cell loss after the ED fully exited the endocycle (after day 4 post-eclosion) and observed that the capacity for functional regeneration was lost. These observations demonstrate that the timing of endocycle exit is a critical factor that limits the organ's ability to regenerate. This is consistent with many studies in proliferative tissues where exit from a mitotic cycle limits regenerative capacity.

My results presented in Chapter 2 strongly suggest that JH signaling plays a crucial role in early endocycling, growth, and development of the ED. Additionally, as shown in Figure 1.4, the levels of JH are highest in adult males on the day of eclosion and decrease by day 2 and thereafter. Thus, developmental stage and age-dependent changes, for instance, changes in hormonal JH signaling, likely constrain the window of regenerative competence in this post-mitotic tissue. This again aligns with work in mitotic tissues where hormonal signaling changes limit regenerative capacity (Jaszczak JS, Halme A, 2016). Further work will be required to investigate the precise transcriptional targets of the JH signaling pathway involved in the recovery of the ED cells after damage.

5.2 Future experiments

Altogether, the work presented here establishes that the post-eclosion growth and development of post-mitotic ED is due to endoreplication driven in part by JH signaling. This foundational work on the ED organ brings with it the exciting opportunity for many future studies. This section outlines possible future research directions arising from this study and proposes experiments that could help to elucidate answers.

5.2.1 What are the regulatory factors limiting endocycle progression?

Our observations suggest ED cells normally stop endoreplicating at a maximum of ~32C DNA content, and many cells, mostly in the posterior organ, stop at ploidies of 16C and 8C. Even under strong proliferative drivers, such as overexpression of direct G1-S phase regulators, the maximum ED ploidy reached was 64C. This indicates there may be a physiological limit to the extent of endoreplication in these cells. Future work should investigate what intrinsic or extrinsic signals enforce this limit. One approach is to examine the expression of cell-cycle regulators around the time ED cells exit the endocycle (by day 3). Transcriptomic profiling, by RNA sequencing, could help us to identify the upregulated inhibitors (for instance, CDK/cyclin inhibitors or checkpoint proteins) that coincide with endocycle termination. We can do this experiment at different time

points. We can extract the RNA from ED secretory cells on Day 1/DOE when we see rapid endocycling in these cells, Day 2, and Day 3 post eclosion when the cells exit the endocycling. We can use *Canton.S* flies crossed to Luna Gal4 as a control, and UAS-CycE/Cdk2 crossed to Luna Gal4. The virgin males can be collected, and we can extract RNA from the dissected EDs on the first three days post eclosion and perform RNA sequencing. We already know some of the candidate genes likely to be regulated, such as Rbf, Dacapo, Geminin, APC/C components, and replication licensing factors that are activated and degraded for the oscillations of the endocycles. We will know if any of these are transcriptionally upregulated to stop the progression of endocycling beyond 32C in control and 64C in the CycE/Cdk2 expressing flies. Further work will also be needed to examine their protein levels since post-transcriptional regulation is a major factor in the control of these genes. In chapter 2 we saw that endoreplication could be blocked prematurely when we overexpressed Rbf, Dacapo, and the replication licensing factor Geminin. This suggests these factors may regulate endocycle exit. But we don't know if any of these factors are upregulated to limit endocycling beyond 32C or 64C.

5.2.2 Can we make cell cycle exit reversible in ED cells?

The secretory epithelium of the ED exits endoreplication largely by Day 2 and completely by Day 3 post-eclosion. As shown in Chapter 2, these ED cells were able to undergo only one additional round of endoreplication upon overexpression of CycE/Cdk2 or CycD/Cdk4, resulting in cells with a DNA content of 64C, but not beyond. This additional round of endoreplication occurs when the cells overexpress CycE/Cdk2 during late pupal and early adult development. What we have not yet tested is whether these cells can be induced to re-enter endocycling after exiting it on Day 3. To perform this experiment, we can cross UAS-CycE/Cdk2 or UAS-CycD/Cdk4 with Luna-Gal4; $Gal80^{ts}$ and maintain the cross at 18 °C to repress Gal4 activity. Virgin males can be collected on the day of eclosion (DOE) and aged at 18 °C for six days, during which the ED exits endocycling. These flies can then be shifted to 29 °C to activate CycE/Cdk2 expression in ED cells. We can subsequently feed the flies with EdU to assess whether the ED cells re-enter the cell cycle and undergo endocycles after having previously exited them.

We can also test whether these CycE/Cdk2-overexpressing EDs are capable of entering mitosis after having exited mitosis. We have preliminary evidence that some ED cells underwent polyploid mitoses on Day 2 when overexpressing CycE/Cdk2, and also when co-overexpressing CycE and String (Figure 5.1), and we did not see any multinucleated cells. String is a *Drosophila* Cdc25c

homolog that plays an important role in activating Cyclin B/Cdk1, which promotes progression through M phase (Edgar, Lehman, and O 1994; Schaeffer et al. 2004). This represents the first evidence of polyploid mitosis in ED cells, as no mitotic activity was observed in control animals. These findings suggest that ED cells can undergo polyploid mitosis when overexpressing mitotic drivers. The effects of polyploid mitoses on the protein production and epithelial barrier functions of the ED remain to be examined. It will be interesting to determine whether the organ remodels cell-cell junctions and extracellular matrix to maintain barrier function in the presence of mitoses. To further test whether ED cells can re-enter mitosis after fully exiting endocycling by Day 3 post-eclosion, we can use flies maintained at 18 °C expressing CycE/Cdk2 or CycE/String under Luna-Gal4; Gal80^{ts} control, and shift them to 29 °C. We can then stain the EDs for phospho-histone H3 (PH3), a marker for mitosis. Additionally, we can stain nuclear Lamin and septate junction markers to identify the mitotic stage of these cells. Polyploid mitosis has so far been observed during Drosophila hindgut development (Fox, Gall, and Spradling 2010) and in certain cancers (Matsumoto et al. 2021; Wang and Tamori 2024). Mostly, polyploid mitosis has resulted in chromosome instability and leads to the loss of a few chromosomes by misregulation (Sansregret, Vanhaesebroeck, and Swanton 2018; Targa and Rancati 2018). It also triggers tumor initiation and is observed during hepatocyte regeneration (Matsumoto et al. 2021; Gandarillas et al, 2019).Thus, these experiments will help determine whether the ED can serve as a model for studying polyploid mitosis in a developmentally post-mitotic tissue. This will help us determine if this polyploid mitosis is beneficial. Hence, it can be a new model to study polyploid mitosis and study the factors involved in it.

5.2.3 Identifying regional-specific genes in the ED

As shown in Chapter 2, ED cells exhibit ploidy levels ranging from 4C to 32C, with the anterior region containing the highest ploidy (32C), along with some 16C nuclei; the anterior-mid region contains 16C and 8C nuclei, and the posterior region predominantly harbors 8C and 4C nuclei. This distribution of ploidy correlates with the tissue volume in each respective region, with the anterior cells containing a larger lumen than the more posterior cells. However, the reason for this ploidy variation along the ED anterior-posterior (A-P) axis remains unknown. This raises several key questions: (i) what pathways pattern the AP-axis of the ED, (ii) how is this patterning mechanistically coupled to the cell cycle to regulate ploidy, and (iii) can we identify regional specific molecular markers and promoters to enhance studies of this tissue and its patterning.

It is unclear whether gene expression profiles differ among ED cells of distinct ploidy. To date, there is no available information on ploidy-enriched transcripts that might underlie functional differences among larger, polyploid cells. Furthermore, chromatin accessibility may also vary with ploidy in ED cells. Investigating these possibilities, potentially with spatial single-cell transcriptomics that retains information about ploidy status, could reveal whether highly polyploid nuclei possess unique chromatin states or exhibit different regulatory element accessibility compared to their lower-ploidy counterparts. Therefore, obtaining single-cell transcriptomic profiles across different ploidy levels and identifying the associated open or closed promoter regions would be highly informative.

In Chapter 3, we optimized a methodology for efficient isolation of individual secretory cell nuclei from the ED, stratified by ploidy. This protocol can now be employed to isolate ED nuclei for image-based single-cell RNA sequencing (scRNA-seq) and ATAC-seq (assay for transposase-accessible chromatin). We propose to use the ICELL8 (Takara) single-cell system, which utilizes 5,184 nanowells to distinguish between wells containing single cells versus multiple cells. ED nuclei can be labeled with DAPI or another DNA stain and visualized using fluorescence imaging. A key advantage of the ICELL8 platform is its nanowell-specific barcoding capability, which enables tracking of sequencing data back to individual nuclei selected for DNA content analysis. Nuclei can be chosen based on size, shape, and integrity prior to downstream applications.

Using the ICELL8 system, we can perform multi-omic profiling, such as parallel RNA-sequencing and ATAC-seq on individual ED nuclei. The imaging step allows for visual confirmation of single nuclei in nanowells before library preparation, and DAPI staining can be used to estimate DNA content and thereby determine the ploidy of each nucleus. This approach would enable the generation of a transcriptomic atlas of ED secretory cells correlated with their ploidy levels.

Once transcriptomes associated with specific ploidy classes are identified, they can be further validated using spatial transcriptomics and high-resolution gene expression imaging techniques, such as RNA fluorescence in situ hybridization (RNA-FISH). When combined with ploidy mapping, these approaches could link nuclear DNA content with spatial localization and functional gene expression. For example, if certain secretory genes are predominantly expressed in the anterior, high-ploidy region of the ED versus the posterior, lower-ploidy region, spatial transcriptomic data would allow for the identification of region-specific gene regulatory programs.

5.2.4 Identifying the downstream targets of Juvenile Hormone signaling

In Chapter 2, we established that endocycling and polyploidy in ED cells are dependent on Juvenile Hormone (JH) signaling. While JH acts as a master regulator of post-eclosion growth in the ED, the molecular effectors that link JH signaling to S-phase entry remain to be identified. Future studies could employ transcriptomic analysis such as RNA sequencing of ED tissue under altered JH signaling conditions to pinpoint genes whose expression correlates with endocycle induction. For this, EDs from control flies and those with knockdowns of *Gce* and *Met* the nuclear receptors mediating JH signaling can be compared.

Based on analogies to other systems, likely downstream targets include DNA replication factors that directly activate replication licensing machinery, such as *Mcm4*, *Mcm7*, and *Cdc6* (Baumann et al. 2010; Goodman and Cusson 2011; Jindra, Palli, and Riddiford 2013; Li, Jia, and Li 2019; Reyhaneh Ojani, Zhu, and Glenda Gillaspy Igor V Sharakhov Zachary B Mackey 2016; Riddiford 2012*;* Wu et al. *2020;* Zhang, Li, and Liu *2022)*. It would be valuable to determine if similar targets are induced by JH in Drosophila ED cells. Once these targets are identified, functional validation can be performed using the Luna-Gal4 driver to knock down suspected JH-responsive genes or to rescue JH signaling defects via overexpression of those genes to assess whether endoreplication and organ growth can be modulated. Identifying the gene network downstream of JH will help clarify how a hormonal signal orchestrates a cell cycle program in a post-mitotic tissue and may also reveal intersection points with other regulatory pathways.

Furthermore, in Chapter 2, we showed that JH is sufficient to drive additional endocycling in tissues where this process is blocked by stabilized Geminin. Additionally, the ectopic addition of JH was able to overcome the blockade of endocycling in the ED caused by overexpression of the CyclinE/Cdk2 inhibitor Dacapo. These results suggest that the critical targets of JH signaling likely function downstream of canonical G1–S regulators and act at the level of replication licensing or DNA synthesis. This experiment involved dissecting EDs immediately after eclosion, incubating them for one hour in media containing JH, and observing that tissues with inhibited endocycling were able to re-enter the endocycle in the presence of JH. We can identify the direct targets of the JH signaling by performing BrU sequencing. Bromouridine labeling and sequencing (BrU-Seq) is based on metabolic pulse-chase labeling of RNA using bromouridine (BrU). In BrU-Seq, recently labeled RNAs are sequenced to reveal spans of nascent transcription in the genome. Bru-Seq maps nascent RNA transcripts using bromouridine tagging. Active RNA polymerase synthesizes RNA in the presence of Br-UTP. Tagged RNA transcripts are immunoseparated from total RNA using

magnetic beads coated with anti-BrdU antibodies. The captured RNA transcripts are eluted and fragmented before synthesis of cDNA strands via RT and PCR amplification. The resultant cDNA strands are prepared for sequencing using an Illumina TruSeq RNA Library Prep Kit (Paulsen et al. 2014). For the experiment in Chapter 2, where we ectopically add JH under the blocked endoreplication state, we can add Br-UTP in both control and Stabilized Geminin overexpressed ED. This labels the nascent RNAs that are transcribed due to the JH signaling will be labelled with Br-UTP. We can further isolate the RNA from the ED cells and separate the RNA that is Br-UTP labelled, elute, and sequence. Thus, this method will provide the direct targets of JH signaling when compared with the transcriptome profile of ED without ectopic JH addition.

5.2.5 Does blocking endoreplication prevent recovery of the ED from cell loss?

In Chapter 4, we observed that when ED cells were induced to undergo damage on the day of eclosion (DOE), they responded by undergoing endoreplication, in addition to compensatory cellular hypertrophy (CCH), to restore tissue size. It would be valuable to rigorously determine whether endocycling is indeed essential for organ functional recovery. To test this, we can block S-phase DNA synthesis in ED cells during the damage and recovery periods. If the organ fails to significantly recover tissue mass or fertility function under these conditions, it would definitively prove endocycling is essential for ED organ regeneration following damage.

We can inhibit endocycling by overexpressing either stabilized Geminin or Dacapo. As shown in Chapter 2, overexpression of stabilized Geminin or Dacapo in ED cells prematurely blocked endocycling, leading to decreased ploidy. Stabilized Geminin is particularly useful because, once expressed, it is resistant to degradation and can effectively block endocycling during the damage response. To implement this, flies expressing stabilized Geminin, Luna-Gal4, Gal80^{ts}, and Reaper can be maintained at 18°C. On Day 1 post-eclosion, virgin flies can be shifted to 29°C for 32 hours to induce both stabilized Geminin expression and Reaper-mediated cell death. This would simultaneously trigger ED cell damage and inhibit endocycling. The flies can then be returned to 18°C to allow for recovery in the continued presence of stabilized Geminin. During this recovery period, the flies can be fed EdU to label any endocycling events. Finally, we can dissect the flies on Day 10 to assess whether the damaged ED tissue has recovered and whether endoreplication occurred during the regeneration process.

We can also use an alternative strategy to block endocycling in ED cells by feeding flies Hydroxyurea (HU). HU is a drug that induces cell cycle arrest by inhibiting ribonucleotide

reductase (RNR), the enzyme complex responsible for converting NDPs to dNDPs, which are necessary for the synthesis of dNTPs (Koç et al. 2004; Shaw et al. 2024). By depleting dNTP pools, HU starves DNA polymerase at replication forks, thereby stalling DNA replication. HU treatment has been shown to reduce purine dNTP pools in various mammalian cells. In *Drosophila* adult brains, HU feeding has successfully blocked DNA synthesis(Koç et al. 2004). We can prepare a 10 mg/ml HU solution in 50% sucrose and mix it with food dye to confirm ingestion. This concentration has been tested in the Buttitta lab and does not induce HU toxicity (Damschroder et al. 2024). The HU solution, along with 1 mg/ml EdU, can be applied to a filter paper placed on top of Bloomington cornmeal food inside a vial. Reaper flies raised at 18°C can then be transferred to this HU-containing food on the day of eclosion. It typically takes 6–8 hours for the HU to reach the ED on the day of eclosion (DOE). The flies can then be shifted to 29°C to induce ED cell damage for 32 hours while they continue feeding on the HU food. Afterward, they can be returned to 18°C to allow recovery, still on HU food. On Day 10 post-recovery, the flies can be dissected to assess whether the ED cells recovered and underwent endocycling. This experiment will help us to understand if endocycling is involved in the recovery of the ED cells.

5.2.6 Can ectopic or prolonged JH signaling activity improve or extend the recovery of the ED from cell loss?

Since Juvenile Hormone (JH) is involved in the endocycling of ED cells, we wanted to test whether feeding flies with JH would enhance their recovery after damage. In control *Drosophila* males, the titer of JH is highest on the day of eclosion (DOE) and decreases by day 2 and further by day 3 post-eclosion. Our damage paradigm is performed on DOE, when JH signaling is still elevated. However, by the time the flies are shifted back for recovery, they are three days old, and JH levels are significantly reduced. Additionally, in an RNA-seq experiment conducted on the accessory gland (AG) post-damage and during recovery, we observed a significant downregulation of *jheh2*, an enzyme involved in the catabolism of JH. This suggests that JH signaling may remain active during AG cell regeneration. We aim to test whether JH feeding during the recovery phase enhances tissue regeneration and increases endocycling activity. This would help us determine if JH can extend the endocycling window and promote better recovery outcomes. To do this, we can pre-feed flies with JH on DOE and then subject them to the 32-hour damage paradigm described in Chapter 4. Following the damage phase, the flies would continue to receive JH during the 10-

day recovery period. EdU can be included along with JH during recovery to quantify any increase in endocycling due to JH exposure.

We can also test whether JH signaling is involved in the recovery of ED cells following damage by knocking down the JH signaling receptors Gce and Met during the damage phase. In Chapter 2, we showed that knocking down these receptors in ED cells on the day of eclosion significantly reduced endocycling and lowered ploidy levels.

To assess whether recovery depends on JH signaling mediated by these nuclear receptors, we can examine the regenerative capacity of ED cells after inducing damage while simultaneously knocking down Gce and Met. If ED cells fail to recover under these conditions, it would strongly suggest that JH signaling is essential for the regeneration of ED cells.

Collectively, these experiments can help clarify the role of Juvenile Hormone (JH) and its nuclear receptors in facilitating damage and recovery in the ED. They may also shed light on whether this tissue possesses a developmental timing mechanism that influences its regenerative potential, similar to what has been observed in other systems.

5.2.7 What signaling pathways transmit information about organ damage or cell loss to trigger endocycling of the remaining ED cells?

One of the key downstream targets of JNK signaling in *Drosophila* is Matrix Metalloproteinase 1 (MMP1), which is known to be activated during wound healing and contributes to tissue repair (Stevens and Page-McCaw 2012). To investigate whether MMP1 is induced in response to ED secretory cell death, we performed MMP1 immunostaining on EDs immediately after damage induction. We observed a marked increase in MMP1 protein levels in the damaged EDs, whereas MMP1 was undetectable in the control (undamaged) EDs as shown in Chapter 4. MMP1 staining was elevated immediately after damage and Day2 to Day 5 of recovery and by Day 10 of recovery MMP1 staining was no longer detectable, suggesting that MMP1 expression and by inference JNK signaling, resolves after day 5 during recovery. In the context of secretory cell ablation in the ejaculatory duct (ED), we observed apical extrusion of the damaged cells. These cells are normally connected to one another through cell–cell junction proteins and may also be anchored to the basal membrane via integrins. Upon induction of apoptosis and subsequent ablation, these connections must be dismantled to allow extrusion and tissue remodeling. Altogether this data suggests that JNK signaling is activated in response to cell loss in the ED, resolves after tissue recovery, and its target, MMP1 induction, may play an important role in this process.

To investigate additional genes or pathways involved in postmitotic regeneration of ED cells, we can perform RNA sequencing in the ED cells immediately after the damage and on Day 3, Day 6 and Day 10 of recovery. RNA -seq will help us understand the genes induced by cell loss as well as the genes that may be involved in the regeneration of the ED. Knowing gene expression changes over time may allow us to elucidate the pathways that could be involved in the regeneration of ED, since many transcriptional targets of key signaling pathways are known in *Drosophila*. We can compare all these three responses with the already known wound healing/injury response (Lee and Miura 2014; Mace, Pearson, and Mcginnis 2005.; Morata, Shlevkov, and Pérez-Garijo 2011; Steller 2008; Zheng et al. 2017), regeneration response (Ahmed-De-Prado and Baonza 2018; Guerin, Kha, and Tseng 2021; Harris et al. 2020a; Bergmann, Steller, 2010), and cell cycle effectors activated during regeneration (Øvrebø and Edgar 2018; Smith-Bolton et al. 2009) in wing discs and other mitotic tissues of *Drosophila*. Comparing our data in the ED with regeneration genes that are already known in the literature could provide us with information on the pathways that are active during the damage, regeneration, and the effectors of the regeneration in ED. We will validate the involvement of specific regeneration genes and pathways by knocking them down during ED recovery from damage.

It has often been observed that the same gene can be used both during development and regeneration, but they are activated by different events for example during development genes gets activated by development signals, during regeneration the same genes are activated by damage-induced signals (Harris 2022; Suzuki and Ochi 2020). These signals for gene activation are different in different types of tissues (Sun et al. 2022), and can act through different regulatory elements, such as damage-specific regulatory elements often termed tissue regeneration enhancer elements (TREEs) or Damage-responsive, maturity silenced (DR-MS) elements (Harris et al, 2020; Thompson et al, 2020). To identify whether such damage-specific elements are used in the postmitotic ED, we can perform ATAC seq in ED during the damage and regeneration. The chromatin accessibility during damage and regeneration of postmitotic tissue has not been studied, and whether damage response elements are used in a non-mitotic context is completely unknown. By performing the ATAC seq at the same time points at which we perform RNA sequencing we can compare the results of both RNA seq and ATAC seq results and characterize the responses during damage and regeneration of ED cells. Once we get the ATAC seq results we will compare the open chromatin complex of the genes during damage and regeneration of ED with the open

chromatin complex of the damage and regeneration response elements in wing discs of *Drosophila* (Cao et al. 2022; Harris et al. 2020), fins & heart regeneration in zebra fish (Cao et al. 2022; Thompson et al. 2020; Yang et al. 2020) that re-enter into the cell cycle to undergo regeneration of cells post-injury.

5.2.8 Does polyploid mitosis in the ED aid or hinder recovery from cell loss?

In Chapter 4, we did not observe any ED cells undergoing mitosis during recovery; instead, we observed only endocycling. However, as shown in Figure 5.1, ED cells are capable of entering polyploid mitosis when overexpressing CycE/Cdk2 or CycE/String. Polyploid mitosis is a highly unusual cell cycle, which usually is accompanied by multinucleation. However, we do not observe bi-nucleate or multinucleate ED cells. This suggests the polyploid mitosis in this tissue involves cytokinesis, which may compromise the ED barrier epithelium. We can investigate whether mitoses enhances recovery by providing more cells, or hinders it by compromising the organ barrier function by promoting mitosis during regeneration in the ED. To explore this, we can apply the same damage and recovery paradigm described in Chapter 5, but with overexpression of CycE/Cdk2 and CycE/String during the recovery window. EDs can be dissected every 6 hours during the recovery phase immediately following damage to monitor for mitotic events. Additionally, flies can be fed by EdU during recovery to label DNA synthesis. Together, these experiments will help assess whether the ED can be used as a model to study polyploid mitosis during tissue regeneration.

5.2.9 How does damage and recovery impact nascent protein synthesis in the ED?

In Chapter 2, we observed that tissues with compromised endocycling and ploidy exhibited significantly reduced levels of nascent protein synthesis, as measured using the OPP assay. We can apply this assay to assess whether EDs show decreased protein synthesis immediately after cell loss and increased synthesis following regeneration.

To do this, we can perform the OPP protein synthesis assay using the same concentration and incubation duration as before, immediately after 32 hours of damage. The results can then be compared with undamaged controls to determine whether protein synthesis is reduced in damaged ED cells. We can also perform the OPP assay after 10 days of recovery and quantify the data to assess whether there is a significant increase in protein synthesis compared to the post-damage state. If accurate measurements of protein synthesis can be obtained at both post-damage and post-

recovery, this assay could serve as a valuable tool for evaluating the extent of ED cell recovery and the functional restoration of the tissue following injury.

Overall, this thesis establishes the *Drosophila* ejaculatory duct as a powerful new model to study how post-mitotic, polyploid cells contribute to tissue growth, function, and regeneration. Through genetic, hormonal, and cell cycle manipulations, we show that ED secretory cells undergo developmentally timed endocycles regulated by Juvenile Hormone signaling. These findings not only identify juvenile hormone as a critical upstream regulator of DNA replication in the male reproductive tract, but also establish the ED as a genetically tractable system to dissect how ploidy state, tissue patterning, and age collectively shape regenerative outcomes and fertility function in post-mitotic epithelia. In the regeneration field, perfect regeneration gets all the attention, but there are alternate mechanisms of regeneration that restore organ size and organ function that are imperfect. Imperfect regeneration does not perfectly restore the original tissue morphology or cell number, but does restore organ mass and function. This type of imperfect regeneration is what we observed in the ED. For post-mitotic tissues like the mammalian heart, this may be the only option to regenerate. Thus the *Drosophila* ED will be a valuable model to identify gene expression regulatory networks used during imperfect regeneration in post-mitotic tissues.

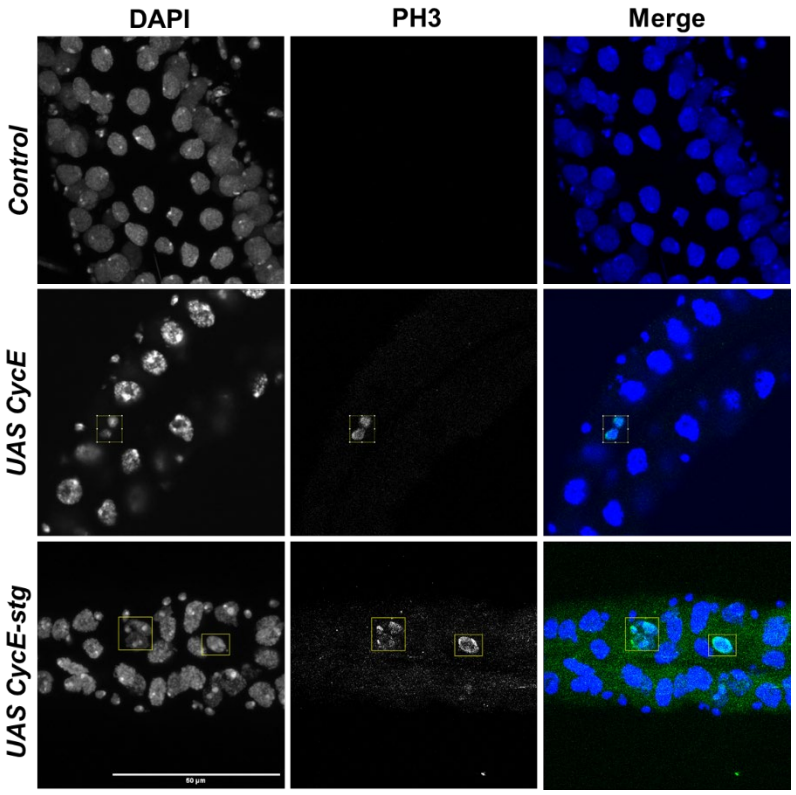


Figure 5.1: ED labelled with DAPI and PH3 expressing the indicated cell cycle regulators. PH3 labeling overlapping with DAPI indicates evidence of polyploid mitoses.

5.3 Bibliography

Ahmed-De-Prado, Sara, and Antonio Baonza. 2018. 'Drosophila as a Model System to Study Cell Signaling in Organ Regeneration'. *BioMed Research International* 2018.

Baumann, Aaron, Joshua Barry, Shaoli Wang, Yoshihiro Fujiwara, and Thomas G. Wilson. 2010. 'Paralogous Genes Involved in Juvenile Hormone Action in Drosophila melanogaster'. *Genetics* 185(4):1327–36. doi:10.1534/genetics.110.116962.

Cao, Yingxi, Yu Xia, Joseph J. Balowski, Jianhong Ou, Lingyun Song, Alexias Safi, Timothy Curtis, Gregory E. Crawford, Kenneth D. Poss, and Jingli Cao. 2022. 'Identification of Enhancer Regulatory Elements That Direct Epicardial Gene Expression during Zebrafish Heart Regeneration'. *Development (Cambridge)* 149(4). doi:10.1242/dev.200133.

Damschroder, Deena, Jenny Sun, Katherine O. McDonald, and Laura Buttitta. 2024. 'Cell Cycle Re-Entry in the Aging *Drosophila* Brain'.

Edgar, Bruce A., Dara A. Lehman, and Patrick H. O. 1994. *Transcriptional Regulation of String (Cdc25): A Link between Developmental Programming and the Cell Cycle*.

Fox, Donald T., Joseph G. Gall, and Allan C. Spradling. 2010. 'Error-Prone Polyploid Mitosis during Normal Drosophila Development'. *Genes and Development* 24(20):2294–2302. doi:10.1101/gad.1952710.

Gandarillas A, Sanz-Gómez N, Freije A. 2019. Polyploidy and the mitosis path to epidermal cell fate. *Cell Cycle*. Feb;18(3):359-362. doi: 10.1080/15384101.2019.1568766.

Goodman, W. G., and M. Cusson. 2011. 'The Juvenile Hormones'. Pp. 310–65 in *Insect Endocrinology*. Elsevier.

Guerin, Dylan J., Cindy X. Kha, and Kelly Ai Sun Tseng. 2021. 'From Cell Death to Regeneration: Rebuilding After Injury'. *Frontiers in Cell and Developmental Biology* 9.

Harris, Robin E. 2022. 'Regeneration Enhancers: A Field in Development'. *American Journal of Physiology - Cell Physiology* 323(5):C1548–54.

Harris, Robin E., Michael J. Stinchfield, Spencer L. Nystrom, Daniel J. McKay, and Iswar K. Hariharan. 2020a. 'Damage-Responsive, Maturity-Silenced Enhancers Regulate Multiple Genes That Direct Regeneration in Drosophila'. *ELife* 9:1–26. doi:10.7554/eLife.58305.

Harris, Robin E., Michael J. Stinchfield, Spencer L. Nystrom, Daniel J. McKay, and Iswar K. Hariharan. 2020b. 'Damage-Responsive, Maturity-Silenced Enhancers Regulate Multiple Genes That Direct Regeneration in Drosophila'. *ELife* 9:1–26. doi:10.7554/eLife.58305.

Harris, Robin E., Michael J. Stinchfield, Spencer L. Nystrom, Daniel J. McKay, and Iswar K. Hariharan. 2020c. 'Damage-Responsive, Maturity-Silenced Enhancers Regulate Multiple Genes That Direct Regeneration in Drosophila'. *ELife* 9:1–26. doi:10.7554/eLife.58305.

Jaszczak JS, Halme A. 2016. Arrested development: coordinating regeneration with development and growth in Drosophila melanogaster. *Curr Opin Genet Dev*. Oct;40:87-94. doi: 10.1016/j.gde.2016.06.008.

Jindra, Marek, Subba R. Palli, and Lynn M. Riddiford. 2013. 'The Juvenile Hormone Signaling Pathway in Insect Development'. *Annual Review of Entomology* 58:181–204.

Koç, Ahmet, Linda J. Wheeler, Christopher K. Mathews, and Gary F. Merrill. 2004. 'Hydroxyurea Arrests DNA Replication by a Mechanism That Preserves Basal DNTP Pools'. *Journal of Biological Chemistry* 279(1):223–30. doi:10.1074/jbc.M303952200.

Lee, Won Jae, and Masayuki Miura. 2014. 'Mechanisms of Systemic Wound Response in Drosophila'. Pp. 153–83 in *Current Topics in Developmental Biology*. Vol. 108. Academic Press Inc.

Li, Kang, Qiang Qiang Jia, and Sheng Li. 2019. 'Juvenile Hormone Signaling – a Mini Review'. *Insect Science* 26(4):600–606.

Mace, Kimberly A., Joseph C. Pearson, and William Mcginnis. 2005. *An Epidermal Barrier Wound Repair Pathway in Drosophila Is Mediated by Grainy Head*. https://www.science.org.

Matsumoto, Tomonori, Leslie Wakefield, Alexander Peters, Myron Peto, Paul Spellman, and Markus Grompe. 2021. 'Proliferative Polyploid Cells Give Rise to Tumors via Ploidy Reduction'. *Nature Communications* 12(1). doi:10.1038/s41467-021-20916-y.

Morata, Ginés, Evgeny Shlevkov, and Ainhoa Pérez-Garijo. 2011. 'Mitogenic Signaling from Apoptotic Cells in Drosophila'. *Development Growth and Differentiation* 53(2):168–76.

Øvrebø, Jan Inge, and Bruce A. Edgar. 2018. 'Polyploidy in Tissue Homeostasis and Regeneration'. *Development (Cambridge)* 145(14).

Paulsen, Michelle T., Artur Veloso, Jayendra Prasad, Karan Bedi, Emily A. Ljungman, Brian Magnuson, Thomas E. Wilson, and Mats Ljungman. 2014. 'Use of Bru-Seq and BruChase-Seq for Genome-Wide Assessment of the Synthesis and Stability of RNA'. *Methods* 67(1):45–54. doi:10.1016/j.ymeth.2013.08.015.

Reyhaneh Ojani, Pathway, Jinsong Zhu, and Chair E. Glenda Gillaspy Igor V Sharakhov Zachary B Mackey. 2016. *Molecular Mechanisms Underlying Juvenile Hormone (JH) Signaling*.

Riddiford, Lynn M. 2012. 'How Does Juvenile Hormone Control Insect Metamorphosis and Reproduction?' *General and Comparative Endocrinology* 179(3):477–84.

Sansregret, Laurent, Bart Vanhaesebroeck, and Charles Swanton. 2018. 'Determinants and Clinical Implications of Chromosomal Instability in Cancer'. *Nature Reviews Clinical Oncology* 15(3):139–50.

Schaeffer, Valerie, Cassandra Althauser, Halyna R. Shcherbata, Wu-Min Deng, and Hannele Ruohola-Baker. 2004. 'Notch-Dependent Fizzy-Related/Hec1/Cdh1 Expression Is Required for the Mitotic-to-Endocycle Transition in Drosophila Follicle Cells'. *Current Biology* 14:630–36. doi:10.1016/j.

Bergmann A, Steller H. 2010. Apoptosis, stem cells, and tissue regeneration. *Sci Signal*. Oct 26;3(145):re8. doi: 10.1126/scisignal.3145re8.

Shaw, Alisa E., Jackson E. Whitted, Mattias N. Mihelich, Hannah J. Reitman, Adam J. Timmerman, and Grant D. Schauer. 2024. 'Revised Mechanism of Hydroxyurea Induced Cell Cycle Arrest and an Improved Alternative'.

Smith-Bolton, Rachel K., Melanie I. Worley, Hiroshi Kanda, and Iswar K. Hariharan. 2009. 'Regenerative Growth in Drosophila Imaginal Discs Is Regulated by Wingless and Myc'. *Developmental Cell* 16(6):797–809. doi:10.1016/j.devcel.2009.04.015.

Steller, H. 2008. 'Regulation of Apoptosis in Drosophila'. *Cell Death and Differentiation* 15(7):1132–38.

Stevens, Laura J., and Andrea Page-McCaw. 2012. 'A Secreted MMP Is Required for Reepithelialization during Wound Healing'. *Molecular Biology of the Cell* 23(6):1068–79. doi:10.1091/mbc.E11-09-0745.

Sun, Fei, Jianhong Ou, Adam R. Shoffner, Yu Luan, Hongbo Yang, Lingyun Song, Alexias Safi, Jingli Cao, Feng Yue, Gregory E. Crawford, and Kenneth D. Poss. 2022. 'Enhancer Selection Dictates Gene Expression Responses in Remote Organs during Tissue Regeneration'. *Nature Cell Biology* 24(5):685–96. doi:10.1038/s41556-022-00906-y.

Suzuki, Nanoka, and Haruki Ochi. 2020. 'Regeneration Enhancers: A Clue to Reactivation of Developmental Genes'. *Development Growth and Differentiation* 62(5):343–54.

Targa, Altea, and Giulia Rancati. 2018. 'Cancer: A CINful Evolution'. *Current Opinion in Cell Biology* 52:136–44.

Thompson, John D., Jianhong Ou, Nutishia Lee, Kwangdeok Shin, Valentina Cigliola, Lingyun Song, Gregory E. Crawford, Junsu Kang, and Kenneth D. Poss. 2020. 'Identification and Requirements of Enhancers That Direct Gene Expression during Zebrafish Fin Regeneration'. *Development (Cambridge)* 147(14). doi:10.1242/DEV.191262.

Wang, Yuqing, and Yoichiro Tamori. 2024. 'Polyploid Cancer Cell Models in Drosophila'. *Genes* 15(1).

Wu, Zhongxia, Qiongjie He, Baojuan Zeng, Haodan Zhou, and Shutang Zhou. 2020. 'Juvenile Hormone Acts through FoxO to Promote Cdc2 and Orc5 Transcription for Polyploidy-Dependent Vitellogenesis'. *Development (Cambridge)* 147(18). doi:10.1242/dev.188813.

Yang, Hongbo, Yu Luan, Tingting Liu, Hyung Joo Lee, Li Fang, Yanli Wang, Xiaotao Wang, Bo Zhang, Qiushi Jin, Khai Chung Ang, Xiaoyun Xing, Juan Wang, Jie Xu, Fan Song,

Iyyanki Sriranga, Chachrit Khunsriraksakul, Tarik Salameh, Daofeng Li, Mayank N. K. Choudhary, Jacek Topczewski, Kai Wang, Glenn S. Gerhard, Ross C. Hardison, Ting Wang, Keith C. Cheng, and Feng Yue. 2020. 'A Map of Cis-Regulatory Elements and 3D Genome Structures in Zebrafish'. *Nature* 588(7837):337–43. doi:10.1038/s41586-020-2962-9.

Zhang, Xiaoshuai, Sheng Li, and Suning Liu. 2022. 'Juvenile Hormone Studies in Drosophila melanogaster'. *Frontiers in Physiology* 12.

Zheng, Qian, Ai Ying Ma, Lei Yuan, Ning Gao, Qi Feng, Nathalie C. Franc, and Hui Xiao. 2017. 'Apoptotic Cell Clearance in Drosophila melanogaster'. *Frontiers in Immunology* 8(DEC).